E.S.R. SPECTRA OF Mn^{2+} IN POWDERS

by

P. T. Dobney, B.Sc.

A Thesis

Submitted for the Degree of

Doctor of Philosophy

in the

Physics Department,

University of Adelaide.

March, 1969.

DECLARATION

The text of this thesis, except where due reference is made, describes the original and personal work of the author. The studies were done on a part-time basis, whilst the author was employed as a Lecturer in the School of Physics, South Australian Institute of Technology.

No material contained in this thesis has been submitted for a degree or diploma in this or any other University.

P. T. Dobney.

March, 1969.

SUMMARY.

During investigations of the X-band microwave spectrum of Mn^{2+} ions adsorbed on bacterial cells, weak doublets were noticed between the main ($\Delta m = o$) hyperfine lines. Similar doublets had been reported in the spectrum of Mn^{2+} adsorbed on inorganic ion-exchangers, which at the commencement of this work had not adequately been explained. These doublets were tentatively assigned as forbidden ($\Delta m = \pm 1$) transitions, and investigations to test this hypothesis were carried out. Initially it was found that there was poor agreement between the experimentally determined line positions of these doublets and line positions calculated using simple non-angular expressions. When angular dependent terms were taken into account, utilizing a method used by Bleaney and Rubins to explain splitting of hyperfine lines observed from a plasticine sample, agreement between theory and experiment could be obtained for the spectrum of the adsorbed Mn^{2+} ion.

Investigation of spectra from powdered samples containing Mn^{2+} in sites of large axial crystal fields then showed that the original theory of Bleaney and Rubins was unable to even qualitatively explain features of spectra observed. Because of this, exact methods were used to predict the intensity variations of allowed and forbidden transitions with angle between the crystal field axis and the applied static field, and interpretation of all powder spectra was then obtained.

The effect of rhombic crystal field symmetry on powder spectra was then considered, and it is shown that certain component lines of powder spectra are preferentially broadened, and as well, splitting of hyperfine lines can occur.

During the search for suitable samples, materials were obtained which produced Mn^{2+} spectra previously not reported.

Finally a technique is reported which, when refined, could enable investigations of central ($M = \frac{1}{2} \rightarrow M = -\frac{1}{2}$) transitions without the complication of overlapping fine structure, and enable identification of component lines in overlapping spectra.

ACKNOWLEDGEMENTS.

The author would like to thank -

Dr. S. G. Tomlin - for the encouragement to start, and for his patient supervision of, this work.

Mr. G. Troup - for his friendly and learned advice, and for making available to this author, facilities in the Physics Department of Monash University.

Mr. D. McColl, Curator of the Geology Department's Museum, University of Adelaide - for the supply of mineral specimens.

Miss H. Barrow - who prepared the diagrams.

Mr. G. Haskard, Past Head of the School of Physics, Mr. C. G. Wilson, Head of the School of Physics, and Dr. S. I. Evans, Director, S.A. Institute of Technology - for permission to start and continue these studies.

My colleagues in the School of Physics, S.A. Institute of Technology - who carried a larger load because of these studies.

My wife - for her help in every way.

CONTENTS

		Page
CHAPTER I : THE SPECTRUM OF ADSORBED Mn^{2+}		
1.1	Introduction	1
1.2	Crystal Field Symmetry for the Adsorbed Mn^{2+} Ion	2
1.3	Experimental Line Positions and Spacings	3
1.4	Previous Attempts to Explain Shifts	5
1.5	Averaging Over Random Orientations	6
CHAPTER II : THE SPIN HAMILTONIAN FOR TRIGONAL AND RHOMBIC SYMMETRY		
2.1	The Crystal Field Potential for Trigonal Symmetry	9
2.2	Transformations at Operator Equivalents	11
2.3	Transformation of Crystal Field Terms to Zeeman Diagonal System	13
2.4	Rhombic Component of the Crystalline Field	14
2.5	Operator Equivalents	15
2.6	The Fine Structure Hamiltonian	16
CHAPTER III : EXPRESSIONS FOR LINE POSITIONS		
3.1	Line Positions for Fine Structure	19
3.2	Hyperfine Structure	20
3.3	Second Order Corrections to Line Positions	20
3.4	Third Order Corrections	22
3.5	Line Positions Including Third Order Corrections	26
CHAPTER IV : TRANSITION PROBABILITIES		
4.1	Transition Probabilities by Second Order Perturbation - Axial Fields	28
4.2	Relative Intensity in Powder Spectra	31

Page

4.3 Transition Probabilities by Second Order Perturbation - Rhombic Fields 34

4.4 Intensity Variations Using Computer Diagonalization of the 36 x 36 Energy Interaction Matrix 34

CHAPTER V : LINE POSITIONS IN POWDER SPECTRA

5.1 Line Shifts Using Bleaney and Rubins' Method 37

5.2 Application to the (Mn^{2+}) Powder Spectrum from Calcite 39

5.3 Explanation of Observed Line Shifts in Adsorbed Mn^{2+} Spectra 40

5.4 The Calculation of Parameters from Powder Spectra 41

5.5 Line Shifts due to Line Shape Functions 44

5.6 Parameters for the Adsorbed Mn^{2+} Spectrum 49

5.7 The Determination of the Parameter 'A' from Powder Spectra Using Non-Angular-Dependent Expressions 52

5.8 Failure of Theory to Explain Features of Other Observed Spectra 53

CHAPTER VI : TRANSITION PROBABILITIES - BIR'S METHOD

6.1 Introduction 55

6.2 General Theory 55

6.3 Components of the Effective Field for Trigonal Symmetry 61

6.4 Calculation of $\mu = \cos \alpha_{MM'}$ 64

6.5 Discussion 65

6.6 Intensity Variations for Rhombic Crystal Field 67

CHAPTER VII : INTERPRETATION OF OTHER AXIAL POWDER SPECTRA

7.1 Introduction 68

7.2(a) Apatite : Transition Probabilities in Single Crystals 69

" (b) " Explanation of Features of the Powder Spectrum 69

" (c) " Single Crystal Spectra and Annealing Experiments 72

Page

7.3(a) Scheelite : Transition Probabilities 75

" (b) " Powder Spectrum 76

7.4 Dolamite : Single Crystal and Powder Spectra 78

7.5 Ankerite : Single Crystal and Powder Spectra 79

7.6 Summary of Theory for Axial Spectra 80

CHAPTER VIII : THE EFFECT OF RHOMBIC CRYSTAL FIELD SYMMETRY

8.1 Introduction 83

8.2 The Effect of Random Orientation 84

8.3 Discussion 86

8.4 Interpretation of the Mg (Mn^{2+}) $SO_4.7H_2O$ Powder Spectrum 88

8.5 Mn^{2+} in Tremolite 89

8.6 Mn^{2+} in Cordierite 92

8.7 Mn^{2+} in Pectolite 95

8.8 The Powder Spectrum of $NH_4Mg(SO_4)_2(Mn^{2+})$ 96

CHAPTER IX : THE SPECTRUM FROM CEMENT AND CEMENT COMPONENTS 98

CHAPTER X : A MODULATION TECHNIQUE

10.1 General Theory 100

10.2 Applications 102

CONCLUSIONS 105

APPENDICES

A : INTENSITY VARIATIONS FOR CUBIC CRYSTAL FIELD SYMMETRY

A1. Introduction

A2. Intensity Variations Using Perturbation Methods

A3. Intensity Variations for Cubic Field Symmetry Using Bir's Method.

B : THIRD ORDER PERTURBATION CALCULATIONS

C : THE OPERATOR EQUIVALENT FOR Y_4^1

D : THE SPIN OPERATORS T_2^0 , T_2^1 , T_2^2

E : EXPERIMENTAL DETAILS

F : Mn^{2+} SPECTRA FROM OTHER MINERALS

BIBLIOGRAPHY AND REFERENCES

CHAPTER I

The Spectrum of Adsorbed Mn^{2+}

1.1 Introduction.

The ion-exchange properties of bacterial cells is a well known phenomenon (Dubos 1949), and electro-negative cells washed in Manganese solutions readily take up Mn^{2+} ions.

The X-band microwave spectrum recorded from a sample of E.Coli washed in 0.01 N $MnCl_2$, is shown in fig. 1.1, and may be compared with an E.S.R. spectrum from Mn^{2+} adsorbed on the ion-exchange resin Amberlite IR-120(H), fig. 1.2. The observed spectra are seen to consist of six broad hyperfine lines ($\Delta m = 0$, $M = \frac{1}{2} \longrightarrow M = -\frac{1}{2}$) between which can be observed five pairs of broad weak lines. These broad doublets, observed in the spectrum of adsorbed Mn^{2+}, were originally identified as 'fine structure' by Faber and Rogers (1959). Although fine structure is observable in certain Mn^{2+} powder spectra (Kasai 1962, Bleaney & Rubins 1961) it seemed unlikely to this author that the doublets observed in the spectrum of adsorbed Mn^{2+} were fine structure. In Mn^{2+} powder spectra, fine structure lines, if observed, should also appear outside the central hyperfine sextet ($M = \frac{1}{2}$), whereas the weak lines observed in the spectra shown, all lie inside the central sextet. These weak lines were then tentatively assigned as forbidden transitions ($\Delta m = \pm 1$) and investigations carried out to test this hypothesis. Identification of the weak doublets which are observable in the spectrum of

N.B. The numbers running across this and other chart recordings shown, are inch markings, and do not refer to lines in spectra.

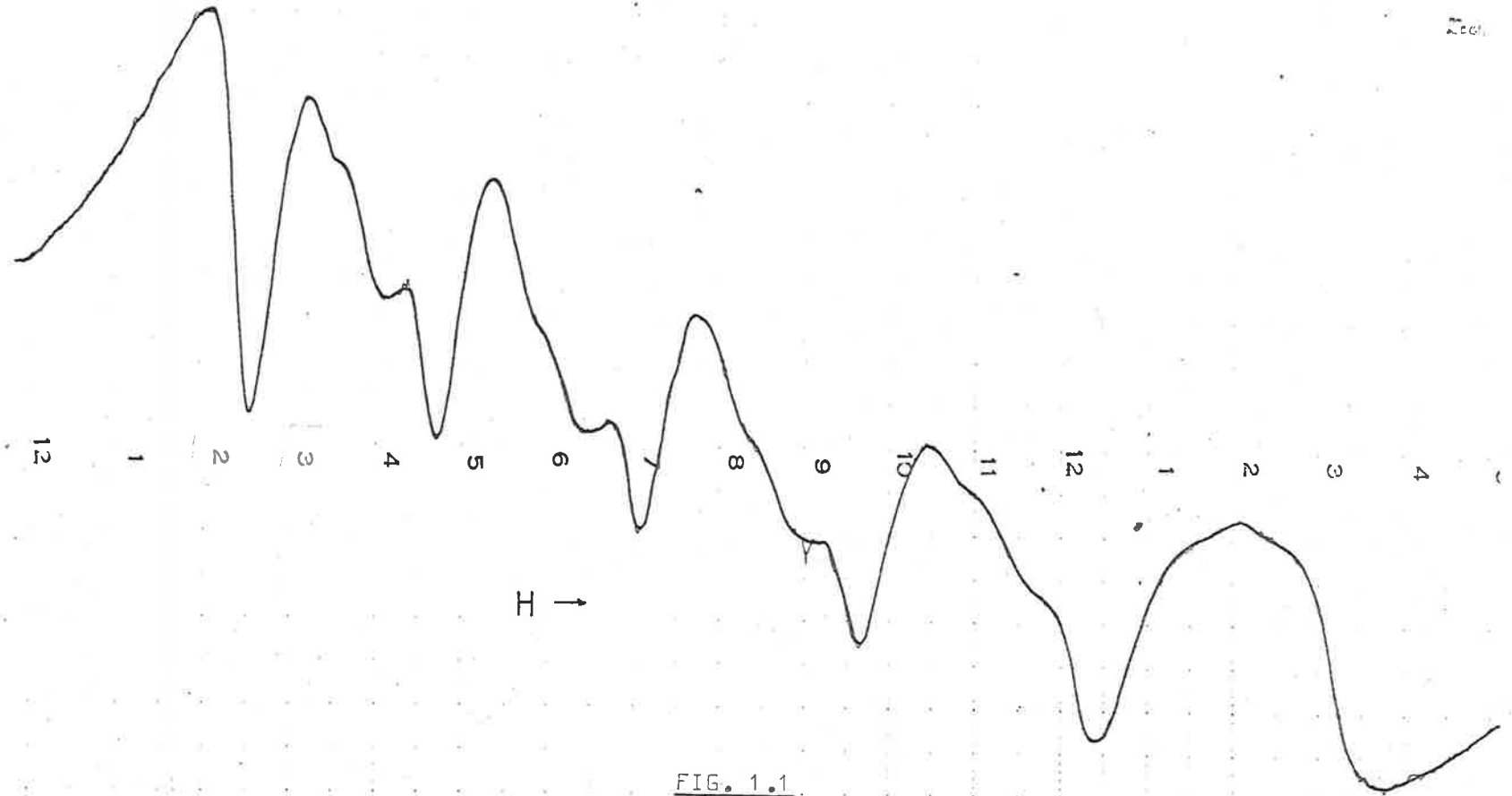

FIG. 1.1

Mn^{2+} Adsorbed on E.Coli cells

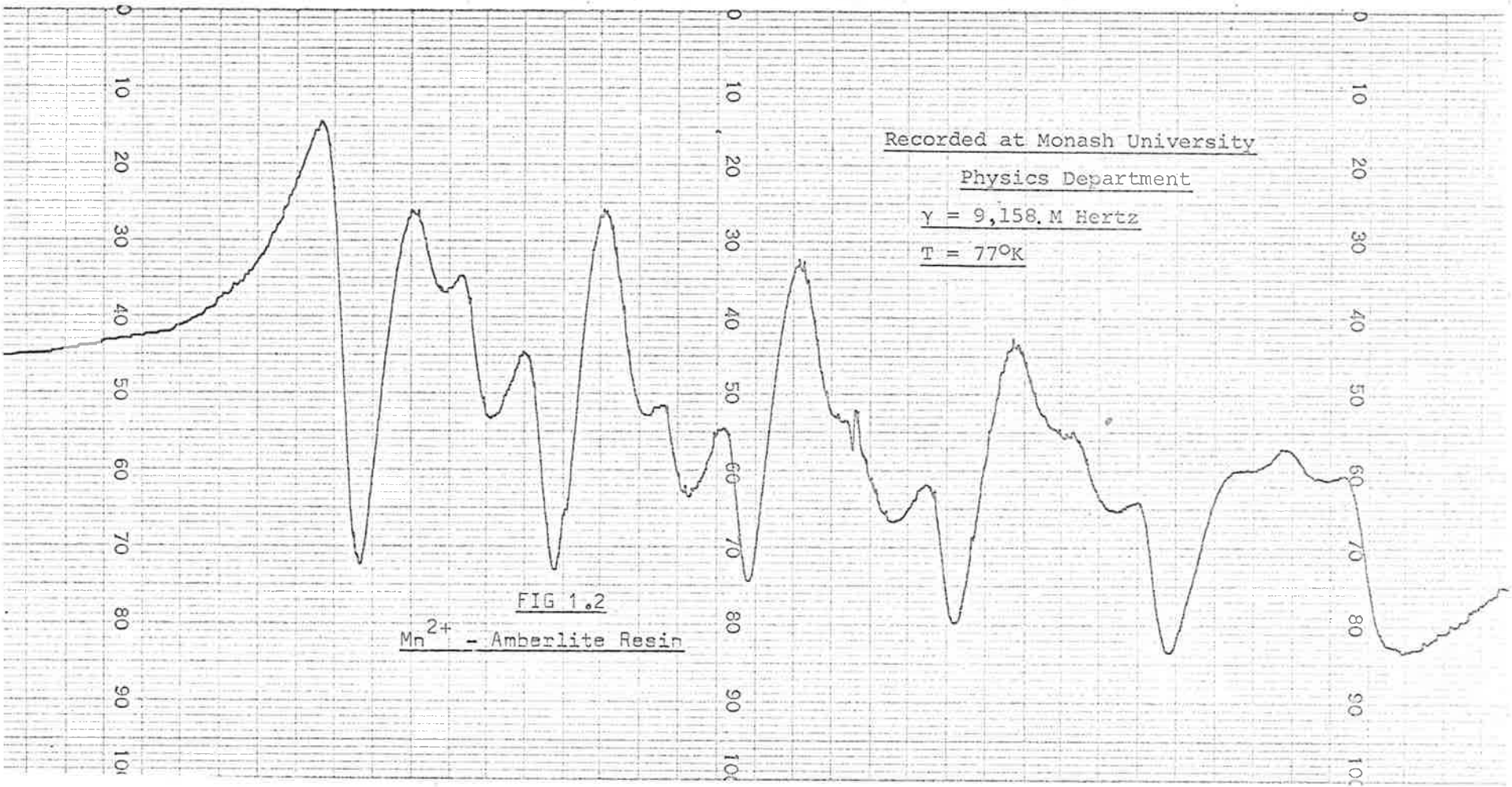

FIG 1.2

Mn^{2+} - Amberlite Resin

adsorbed Mn^{2+}, as forbidden transitions, was made by Nicula et al (1965) on the basis of line position measurements. The analysis used in this work does differ, however, from that used by Nicula et al (who have used incorrect expressions for line positions, as shown later). The analysis used to explain features in the adsorbed Mn^{2+} spectrum may also be extended to obtain an interpretation of Mn^{2+} powder spectra in general.

1.2 Crystal Field Symmetry For The Adsorbed Mn^{2+} Ion.

Forbidden transitions have been observed when the Mn^{2+} ion is in either a site of cubic or axial crystal field symmetry. (See for example Lyons and Kedzie 1966.) In acqueous solution the Mn^{2+} ion is surrounded by six hydrated water molecules, and neglecting perturbations, might be expected to occupy a site of cubic crystal field symmetry. It is shown in appendix A that the relative intensity of forbidden transitions of Mn^{2+} ions in a site of cubic field symmetry is proportional to the square of the cubic field parameter "a". Title (1963) has presented evidence that this parameter is small when the hyperfine parameter A is large, which is the case experimentally for the adsorbed ion. Because of the relatively large measured intensity of the doublets, we must then consider that the adsorbed Mn^{2+} ion is in a site of axial or rhombic crystal field symmetry, which may be due to distortion of the surrounding hydrated cage of water molecules, due to the adsorption process.

1.3 Experimental Line Positions and Spacings.

For powder spectra the parameters A and g (or $H_o = h\nu_o/g\beta$) may be determined approximately by a fit between experimental line positions, or field differences between adjacent lines, and non-angular dependent expressions (Faber & Rogers 1959, Wolga & Tseng 1964). For field differences between adjacent resonances, Wolga & Tseng (1964) have given the following expressions:-

$$H_A(m) = -\left[A - \frac{15A^3}{4H_o^2}\right] + \left[\frac{A^2}{2H_o}\right].\left[2m-1\right] \qquad (1.1)$$

$$H_F(m) = -\left[\frac{25A^3}{2H_o^2}\right].\left[2m-1\right] + \frac{17A^2}{2H_o} + 2g_N H_o \qquad (1.2)$$

A best fit between field spacings for allowed transitions observed in the adsorbed Mn^{2+} spectrum, fig. 1.2, and spacings calculated, using equations (1.1) is obtained for :-

$$A = -97.3 \text{ Oe}$$

$$H_o = 3,270 \text{ Oe}$$

m	Experiment	Theory
-3/2	90.5 ($\pm$ 1.0) Oe	91.2 Oe
-1/2	93.4 " "	94.0 "
1/2	97.0 " "	97.0 "
3/2	100.7 " "	99.9 "
5/2	102.9 " "	102.8 "

If these values of the parameters are then used to calculate spacing for forbidden doublets, using equation (1.2), the following results are obtained -

m	Experiment	Theory
-3/2	23.5 ($\pm$1.0) Oe	22.8 Oe
-1/2	24.5 " "	24.9 "
1/2	26.0 " "	27.1 "
3/2	27.0 " "	29.2 "
5/2	28.0 " "	31.4 "

The poor agreement between theoretical and experimental spacings would then seem to indicate that simple non-angular expressions are insufficient for the description of the experimentally determined line positions for the adsorbed Mn^{2+} spectra. As well, theoretical line positions for single crystal spectra also predict that forbidden doublets should lie midway between allowed ($M = \frac{1}{2}$, $\Delta m = 0$) transitions. Experimentally it is found that the doublets observed in adsorbed Mn^{2+} spectra are shifted towards the high field side relative to the midpoint between allowed transitions, with the relative shift increasing with field. Similar shifts have been reported for forbidden doublets observed in powder specimens containing Mn^{2+} (Waldner 1962, Odenhal 1963).

1.4 Previous Attempts to Explain Shifts.

Wolga and Tseng (1963) considered the possible effect of variations of line positions due to random orientation of the crystal field axis in the crystalites comprising a powder sample, relative to the applied static magnetic field, using an averaging method, and concluded that for a value of D = 50 Oe, no large relative shifts between lines should occur. Their conclusion is however suspect for two reasons, firstly, their apparent incorrect derivation of higher-order corrections using perturbation methods, and secondly, by following through the calculations suggested by these authors, it is apparent that they have failed to weight the function they averaged, when considering forbidden transitions, to take into account the $\sin^2 2\theta$ angular variation of intensity observed for low values of D.

Waldner (1962) and Nicula et al (1965) have also considered the effect of random orientation, using as an average shift the weighted function:-

$$H = \int_0^{\frac{\pi}{2}} H(\theta).\sin\theta.I(\theta).d\theta$$

where $H(\theta)$ is the variation of line position with angle between the Z axis of the crystal field and the direction of the applied magnetic field, and $I(\theta)$ is the angular variation of line intensity. Relative shifts of forbidden doublets were predicted using this averaging method. As explained later, however, these authors have used incorrect expressions for $H(\theta)$.

If an average is to be taken, the following may be considered.

1.5 Averaging Over Random Orientations.

Suppose $H = H(\theta)$ is the predicted field at which resonance occurs, and the directions of the crystal field axes are randomly oriented with respect to the direction of the static field. To maintain continuity with angles defined in the next chapter, we may consider, alternatively, that the crystal axes are fixed in space and the static field direction is randomly oriented with respect to these axes. The probability that the field direction will lie in the solid angle dw,

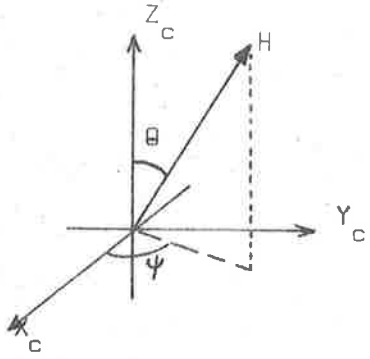

about the direction θ,ψ, as shown, is

$$\frac{dw}{4\pi} = \frac{\sin\theta \, d\theta \, d\psi}{4\pi}$$

The probability that the field direction will lie between θ and $\theta + d\theta$, irrespective of ψ is then -

$$\int_{\psi=0}^{2\pi} \frac{\sin\theta \, d\theta \, d}{4\pi} = \frac{\sin\theta \, d\theta}{2}$$

If P(H) dH is the probability of transition occurring in the range H to H + dH, then P(H) dH is equal to the probability of θ lying in the θ to $\theta + d\theta$ range corresponding to the $H(\theta)$ function -

$$\text{i.e.} \quad P(H)dH = \frac{1}{2} \sin\theta \, d\theta$$

$$\text{or} \quad P(H) = \frac{1}{2} \sin\theta \, \frac{dH}{d\theta} ,$$

which may be referred to as the line shape factor. (Bersohn & Baird 1966.)

If the intensity varies as a function of H or θ, the intensity in the range H to H + dH is P(H) dH.I(H), and as -

$$I(H)dH = I(\theta)d\theta$$

the intensity in the range θ to $\theta + d\theta$, or H to $H + d\theta$ is then

$$P(H)dH.I(H) = \frac{I(\theta)\sin\theta\ d\theta}{2\frac{dH}{d\theta}}$$

The average or effective shift due to angular terms can then be taken as the first moment of $H(\theta)$

$$H = \frac{\int H(\theta)\ P(H)\ I(H)\ dH}{\int P(H)\ I(H)\ dH} = \frac{\int_0^{\frac{\pi}{2}} \frac{H(\theta)\ I(\theta)\ \sin\theta\ d\theta}{2\frac{dH}{d\theta}}}{\int_0^{\frac{\pi}{2}} \frac{I(\theta)\ \sin\theta\ d\theta}{2\frac{dH}{d\theta}}}$$

When this function is evaluated for both allowed and forbidden lines, shifts of forbidden lines relative to allowed transitions are predicted. Averaging methods are however unable to explain even qualitatively other features observed in some powder spectra, such as splitting of hyperfine transitions. As well, as shown in section 4.2, averaging methods may predict values which differ considerably from experimental results. An extension of the method used by Bleaney & Rubins (1961) to explain observed splitting of hyperfine lines observed in modelling clay, will predict the observed shifts of lines. In addition, the method enables an interpretation of all powder spectra, when intensity variations of allowed and forbidden transitions, computed by exact methods, are used.

Before describing how the Bleaney & Robins' method may be used to predict line shifts, etc., it is first necessary to derive expressions for line positions, correct to third order, for which considerable disagreement exists in the published literature. As well, it was felt necessary to test the relative effect of the so called cubic component of a crystal field on predicted intensity variations. For this purpose an electrostatic crystal field of trigonal symmetry is arbitrarily considered.

CHAPTER II

THE SPIN HAMILTONIAN FOR TRIGONAL AND RHOMBIC SYMMETRY

2.1 The Crystal Field Potential for Trigonal Symmetry.

The Spin Hamiltonian representing the interaction of a paramagnetic ion with an applied magnetic field, and with surrounding ions, may be written as:-

$$H = \underset{\sim}{S} \cdot \underset{\sim}{g} \cdot \underset{\sim}{H} + V_c \qquad (2.1)$$

where the first term represents the Zeeman interaction energy, and the second term the "crystalline" potential energy due to the electric field of the surrounding ions. V_c can be represented in the form:-

$$V_c = \sum_i -eV(x_i, y_i, z_i) \qquad (2.2)$$

where V is the potential of the crystal field and x_i, y_i, z_i are the coordinates of the i-th electron in the unfilled shell. By assuming that the wave functions of the paramagnetic ion and the surrounding ions do not overlap, the potential V satisfies Laplace's equation, and may be expanded in a series of Spherical Harmonics -

$$V = \sum_{l,m} A_l^m r^l Y_l^m (\theta, \phi) \qquad (2.3)$$

This expression may be considerably simplified by retaining only some of the terms. The Mn^{2+} ion has a $3d^5$ electron configuration, and when V_c is calculated with the aid of d-electron wave functions, the Y_l^m for which $l > 4$ will give matrix elements equal to zero (Al'tshuler & Kosyrev 1964). All terms in odd l may also be omitted as their matrix elements equal zero, since the electron wave functions are invariant under an inversion transformation. The term in $l = 0$

gives an additive constant which may be set to zero, and further simplification is obtained by considering the symmetry of the crystalline electric field at the site of the paramagnetic ion. For the case of trigonal symmetry, i.e. $V(\phi + 2m\frac{\pi}{3}) = V(\phi)$, the values of m must equal 0, ± 3, ± 6, ± 9 ..... since the ϕ dependence is determined by $e^{im\phi}$. The previous condition, $l = 4$, with $m = l, l-1, l-2, \ldots -l$, then gives the possible values for m as 0 and ± 3. The terms which are then applicable for the Mn^{2+} ion, in a crystal field of trigonal symmetry, are Y_2^0, Y_4^0 and $Y_4^{\pm 3}$, and we write:-

$$V_c = \Sigma -e \left(A_2^0 r^2 Y_2^0 + A_4^0 r^4 Y_4^0 + A_4^3 r^4 Y_4^3 + A_4^{-3} r^4 Y_4^{-3}\right) \qquad (2.4)$$

For a real potential, and with a choice of Spherical Harmonics such that $(Y_l^m)^* = (-1)^m Y_l^{-m}$, we must have $A_4^3 = -A_4^{-3}$. (c.f. Dorain 1958).

The matrix elements of V_c may now be calculated by direct integration using Wigner coefficients, or by expressing the Harmonics in cartesian coordinates which allow "operator equivalents" (Stevens 1952) to be calculated, which can then be used to obtain the matrix elements. The latter method will be used by this author.

If we assume that the Zeeman interaction $\beta \underset{\sim}{S}.\underset{\sim}{g}.\underset{\sim}{H}$ is much larger than the crystal field interaction it is convenient to use a co-ordinate system in which the Zeeman term is diagonal. If H is parallel to the Z axis of a coordinate system which has Eulerian angles (ψ, θ, ϕ) relative to the crystal system, then on the assumption

that the g factor is isotropic, the problem involves transformation of our Hamiltonian by rotation through (ψ,θ,ϕ). (Low 1960, Kikuchi and Matarrese 1960), and in practice the ϕ rotation is arbitrary and may be set equal to zero.

Under this transformation $\beta\underset{\sim}{S}.\underset{\sim}{g}.\underset{\sim}{H} \rightarrow g\beta S_z H$

The transformation of the crystal field terms may be accomplished by first converting them to their operator equivalents, which are functions of the spin operators S_z, S_+, S_-. Known transformations may then be applied to each of these operators, to obtain a transformed operator equivalent (Low 1960).

Alternatively, and with much less effort, one may use the fact that the operator equivalents, denoted by T_l^m, which are derived from the cartesian form of the Spherical Harmonics, possess the same transformation properties (Dorain 1958), as outlined in the next section.

2.2 Transformation of Operator Equivalents.

Following Hamermesh (1962) we denote the transformation by $R(\phi,\theta,\psi)$ where the transformation is described by -

1) A rotation through the angle ψ about the Z axis $\rightarrow$(X',Y',Z) axes

2) A rotation through the angle θ about the Y' axis $\rightarrow$(X",Y',Z') axes

3) A rotation through the angle ϕ about the Z' axis $\rightarrow$(X"',Y",Z') axes

with positive rotations defined by the right hand screw rule.

The same rotation is produced for a rotation about fixed axes in the order ϕ, then θ, then ψ.

Associated with the transformation is the operator O_R such that

$$O_R(\phi,\theta,\psi)\ T_1^m = \sum_{m'} T_1^{m'} D_1^{m'm}(\phi,\theta,\psi) \qquad (2.5)$$

where the $D_1^{m'm}(\phi,\theta,\psi)$ are matrix elements of the irreducible representation of the rotation group, given by :-

$$D_1^{m'm}(\phi,\theta,\psi) = e^{im'\phi} e^{im\psi} d_1^{m'm}(\theta)$$

$$d_1^{m'm}(\theta) = \sum_n \frac{(-1)^{m'-m+n}\sqrt{(1+m)!(1-m)!(1+m')!(1-m')!}}{(1+m-n)!(1-m'-n)!n!(n+m'-m)!}$$

$$.(\cos\theta/2)^{2l+m-m'-2n}(\sin\theta/2)^{m'-m+2n} \qquad (2.6)$$

and the range of the integer n in the summation, is determined by non-negative factorials in the denominator.

For our purpose, the final rotation ϕ is completely arbitrary, and may be set equal to zero.

Before (2.5) is used to transform the crystal field terms to the Zeeman diagonal system, we may first consider establishing a relationship between the coefficients A_4^o and A_4^3. This has been established by Kikuchi & Mataresse (1960) using an alternative transformation - the following, it is hoped, is a clearer exposition.

For a fourfold axis of symmetry the crystal field potential is given unambiguously by:-

$$V^4 = \frac{a}{15}\left[T_4^o + \sqrt{\frac{5}{14}}.(T_4^4 + T_4^{-4})\right] \qquad (2.7)$$

Kikuchi & Mataresse (1960)
Ballhausen (1962)
Cavenett (1964a, 1964b)

where 3a = zero field splitting. This expression contains no term

in T_4^{+1}. We may then transform the cubic potential expression referred to a threefold axis, to a fourfold axis, and equate the coefficient of T_4^1, derived from this transformation, to zero. From fig. 2.1, it may be seen that the transformation may be performed in two non-equivalent ways, viz. :-

a) a rotation about Z by $-\frac{\pi}{4}$, then a rotation of $-\cos^{-1}(\frac{1}{\sqrt{3}})$ about Y,

OR

b) a rotation about Z by $-\frac{\pi}{4}$, then a rotation of $+\cos^{-1}(\frac{1}{\sqrt{3}})$ about Y,

i.e. $R(-\frac{\pi}{4}, \pm\cos^{-1}(\frac{1}{\sqrt{3}}), 0)$

Performing the transformation we find -

$$O_R(-\tfrac{\pi}{4}, \pm\cos^{-1}(\tfrac{1}{\sqrt{3}}), 0)\left[A_4^0T_4^0+A_4^3(T_4^3-T_4^{-3})\right]\rightarrow(\sqrt{10}.A_4^0 \pm \sqrt{7}.A_4^3).T_4^1.e^{-i\pi/4}/18$$

whence :

$$A_4^3 = \pm\sqrt{\frac{10}{7}}.A_4^0 \qquad (2.8)$$

(The ambiguity of sign has been discussed by Kikuchi & Mataresse 1960)

Similarly: $O_R(-\frac{\pi}{4}, \pm\cos^{-1}(\frac{1}{\sqrt{3}}), 0)\left[A_4^0T_4^0 \pm\sqrt{\frac{10}{7}}(T_4^3-T_4^{-3})\right]\rightarrow -\frac{3}{2}A_4^0T_4^0$

and on equating with the coefficient of T_4^0 in equation (2.7),

$$A_4^0 = -\frac{2a}{45}.$$

2.3 Transformation of Crystal Field Terms to Zeeman Diagonal System.

As our crystal field potential we use:

$$V_c = DT_2^0 - \frac{2a}{45}\left[T_4^0 \pm\sqrt{\frac{10}{7}}.(T_4^3 - T_4^{-3})\right] \qquad (2.9)$$

where we have put $D = A_2^0$, and will be referred to as the axial field parameter.

For a general transformation by $R(0,\theta,\psi)$, we then obtain -

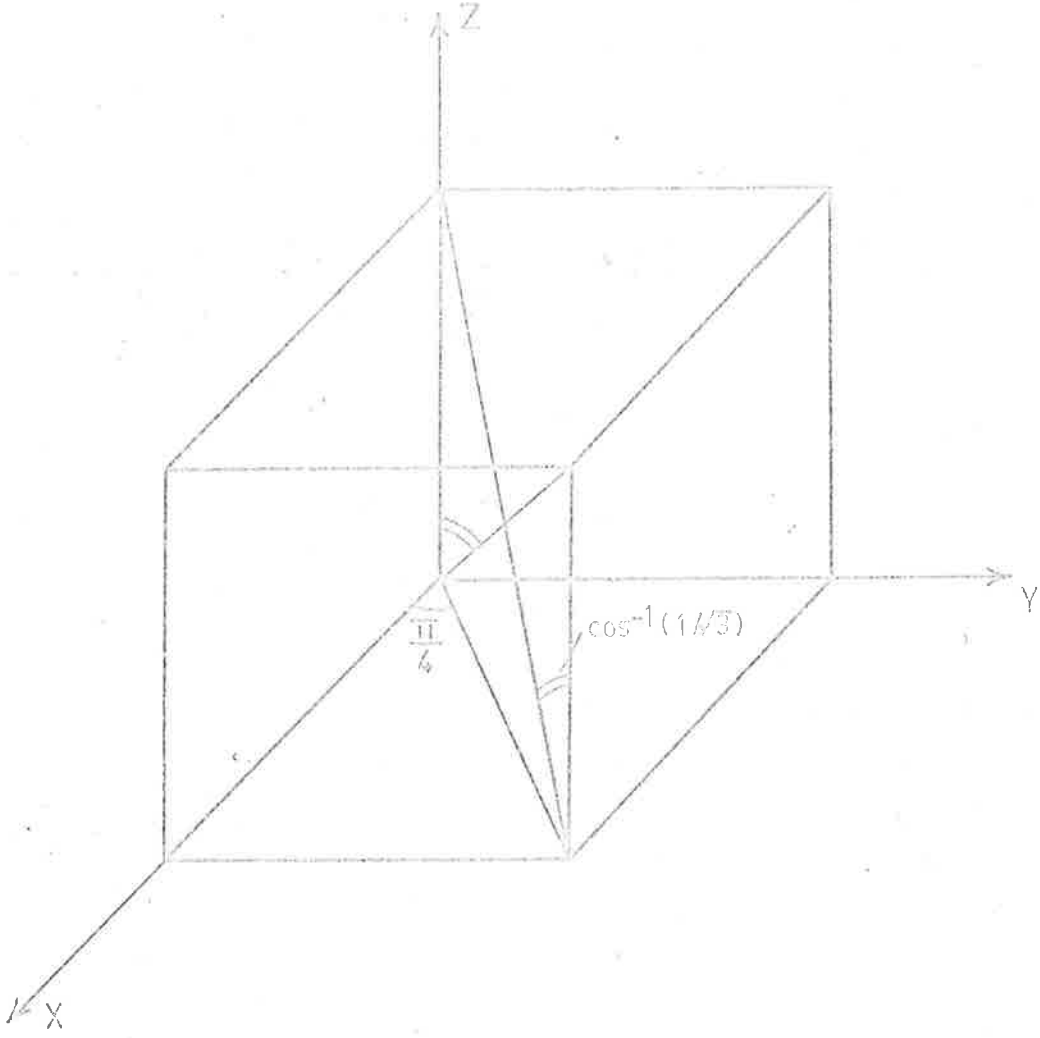

FIG. 2.1

$$D_R(D,\theta,\psi)\ V_c \longrightarrow$$

$$D\left[\frac{T_2^0}{2}(3\cos^2\theta-1) + T_2^1\left(-\frac{\sqrt{6}}{4}\sin 2\theta\right) + T_2^2\left(\frac{\sqrt{6}}{4}\sin^2\theta\right)\right]$$

$$-\frac{2a}{45}\left[\frac{T_4^0}{8}(35\cos^4\theta-30\cos^2\theta+3) \pm 20\sqrt{2}.\sin^3\theta\cos\theta\cos 3\psi\right)$$

$$+T_4^1.\left\{-\frac{\sqrt{20}}{32}\left[7\sin 2\theta\cos 2\theta + \sin 2\theta \mp 4\sqrt{2}\ (3\sin^2\theta\cos 3\psi - 4\sin^4\theta\cos 3\psi + i3\sin^2\theta\cos\theta\sin 3\psi)\right]\right\}$$

$$+T_4^2.\left\{\frac{\sqrt{10}}{8}\left[6\sin^2\theta - 7\sin^4\theta \pm 2\sqrt{2}\left\{2\cos^3\theta\sin\theta\cos 3\psi - i\,(3\sin^3\theta - 2\sin\theta)\sin 3\psi\right\}\right]\right\}$$

$$+T_4^3.\left\{-\frac{\sqrt{140}}{56}\left[7\sin^3\theta\cos\theta \mp \sqrt{2}\left\{\cos 3\psi(4\cos^2\theta + 4\sin^4\theta - 7\sin^2\theta) + i\sin 3\psi\ (4\cos\theta - 9\sin^2\theta\cos\theta)\right\}\right]\right\}$$

$$+T_4^4.\left\{\frac{\sqrt{70}}{112}\left[\sin^4\theta \mp 4\sqrt{2}\left\{\cos 3\psi\ (4\sin\theta\cos^3\theta + 3\sin^3\theta\cos\theta) + i\sin 3\psi\ (4\sin\theta - 3\sin^3\theta)\right\}\right]\right\}\Bigg] \qquad (2.10)$$

where for brevity we have listed only those terms which produce diagonal or above-diagonal matrix elements, noting that the resultant matrix is Hermitian

2.4 Rhombic Component of the Crystalline Field.

When the electrostatic crystal field at the site of a paramagnetic ion possesses rhombic symmetry, the energy interaction may be represented by the fine structure Hamiltonian (Al'tshuler & Kozyrev 1964).

$$H_c\ (\text{Rhombic}) = A_2^0T_2^0 + A_2^{\pm 2}T^{\pm 2} + A_4^0T_4^0 + A_4^{\pm 2}T_4^{\pm 2} + A_4^{\pm 4}T_4^{\pm 4} \qquad (2.11)$$

For the purpose required, the so-called cubic terms T_4^i will be neglected.

A trigonal or tetragonal field may be taken to be the sum of an axial field (represented by $A_2^o T_2^o$) and a cubic field (represented by terms in T_4^i). Similarly, it is convenient to regard a rhombic field as being equivalent to an axial field with a rhombic component (represented by $A_2^{\pm 2} T_2^{\pm 2}$). Transformation of this rhombic component to the Zeeman diagonal system then produces:-

$$D_R(0,\theta,\psi)A_2^2 T_2^{\pm 2} = A_2^2 \left[T_2^o . \frac{\sqrt{6}}{2} . \sin^2\theta \cos 2\psi \right.$$

$$+ \quad T_2^1 \left\{ \sin\theta \, (\cos\theta \cos 2\psi + i \sin 2\psi) \right\}$$

$$\left. + \quad T_2^2 \left\{ \frac{\cos 2\psi}{2} \, (\cos^2\theta + 1) + i \sin 2\psi \cos\theta \right\} \right] \qquad (2.12)$$

where again we list only terms which produce diagonal or above diagonal matrix elements.

2.5 Operator Equivalents.

The form of the operators used are listed below. T_2^o, T_2^1, T_2^2 and T_4^1 are derived from the Spherical Harmonics in appendices C and D. Others have been taken from the tables listed by Al'tshuler & Kosyrev (1964).

$$T_2^o = S_z^2 - \frac{1}{3} S(S+1)$$

$$T_2^{\pm 1} = \mp \frac{1}{\sqrt{6}} (S_z S_{\pm} + S_{\pm} S_z)$$

$$T_2^{\pm 2} = \frac{1}{\sqrt{6}} \; S_{\pm}^2$$

$$T_4^{0} = \frac{1}{8}\left[35\, S_z^4 - 30S(S+1)S_z^2 + 25\, S_z^2 - 6S(S+1) + 3S^2(S+1)^2\right]$$

$$T_4^{\pm 1} = \mp\sqrt{\frac{5}{8}}\left[S_{\pm} f_1(S_z) + f_1(S_z) S_{\pm}\right] \text{ with } f_1(S_z) = 7S_z^3 - 3S(S+1)S_z - S_z$$

$$T_4^{\pm 2} = \sqrt{\frac{5}{128}}\left[S_{\pm}^2 f_2(S_z) + f_2(S_z) S_{\pm}^2\right] \text{ with } f_2(S_z) = 7S_z^2 - S(S+1) - 5$$

$$T_4^{\pm 3} = \mp\sqrt{\frac{35}{64}}\left[S_{\pm}^3 S_z + S_z S_{\pm}^3\right]$$

$$T_4^{\pm 4} = \sqrt{\frac{35}{128}} \cdot S_{\pm}^4$$

2.6 The Fine Structure Hamiltonian.

Collecting all terms we use as our transformed Hamiltonian

$$\begin{aligned} H_c' = {} & g\beta H S_z + \sigma(S_z^2 - \tfrac{1}{3} S(S+1)) + \rho S_+^2 + \rho^* S_-^2 + \lambda(S_z S_+ + S_+ S_z) \\ & + \lambda^*(S_z S_- + S_- S_z) + \alpha(35\, S_z^4 - 30S(S+1)S_z^2 \\ & + 25 S_z^2 - 6S(S+1) + 3S^2(S+1)^2) \\ & + \beta(S_+ f_1(S_z) + f_1(S_z) S_+) + \beta^*(S_- f_1(S_z) + f_1(S_z) S_-) \\ & + \gamma(S_+^2 f_2(S_z) + f_2(S_z) S_+^2) + \gamma^*(S_-^2 f_2(S_z) + f_2(S_z) S_-^2) \\ & + \delta(S_+^3 S_z + S_z S_+^3) + \delta^*(S_-^3 S_z + S_z S_-^3) \\ & + \varepsilon\, S_+^4 + \varepsilon^*\, S_-^4 \end{aligned} \qquad (2.13)$$

For rhombic symmetry the following expressions are then used:-

$$\sigma = \frac{1}{2}\left[D(3\cos^2\theta - 1) + 3E \sin^2\theta\cos 2\psi \right] \qquad (2.14)$$

$$\rho = \frac{1}{4}\left[D \sin^2\theta + E (\cos 2\psi \cos^2\theta + \cos 2\psi) + 2iE\cos\theta\sin 2\psi \right] \qquad (2.15)$$

$$\lambda = \frac{1}{2}\sin\theta\left[\cos\theta (D - E\cos 2\psi) - iE\sin 2\psi \right] \qquad (2.16)$$

and we neglect all cubic terms, and have put $A_2^2 = E.\sqrt{6}/2$ to conform to the most common notation.

For trigonal symmetry we use:-

$$\sigma = \frac{D}{2}(3\cos^2\theta - 1) \qquad (2.17)$$

$$\rho = \frac{D}{4}\sin^2\theta \qquad (2.18)$$

$$\lambda = \frac{D}{4}\sin 2\theta \qquad (2.19)$$

$$\alpha = \frac{a}{1,440}(35\cos^4\theta - 30\cos^2\theta + 3 \pm 20.\sqrt{2}.\sin^3\theta\cos\theta\cos 3\psi) \qquad (2.20)$$

$$\beta = \frac{a}{576}\left[7\sin 2\theta\cos 2\theta + \sin 2\theta \mp 4\sqrt{2} .(3\sin^2\theta\cos 3\psi - 4\sin^4\theta\cos 3\psi + i3\sin^2\theta\cos\theta\sin 3\psi) \right] \qquad (2.21)$$

$$\gamma = \frac{a}{288}\left[6\sin^2\theta - 7\sin^4\theta \pm 2\sqrt{2}\left\{ 2\cos^3\theta\sin\theta\cos 3\psi - i .(3\sin^3\theta - 2\sin\theta)\sin 3\psi \right\} \right] \qquad (2.22)$$

$$\delta = \frac{a}{144}\left[7\sin^3\theta\cos\theta \mp \sqrt{2}\left\{ \cos 3\psi\ (4\cos^2\theta + 4\sin^4\theta - 7\sin^2\theta) + i \sin 3\psi\ (4\cos\theta - 9\sin^2\theta\cos\theta) \right\} \right] \qquad (2.23)$$

$$\varepsilon = \frac{a}{576}\left[\sin^4\theta \mp 4.\sqrt{2}\left\{\cos 3\psi(4\sin\theta\cos^3\theta + 3\sin^3\theta\cos\theta)\right.\right.$$

$$\left.\left. + i\sin 3\psi\,(4\sin\theta - 3\sin^3\theta)\right\}\right] \qquad (2.24)$$

CHAPTER III

EXPRESSIONS FOR LINE POSITIONS

3.1 Line Positions for Fine Structure.

To obtain an expression for the field intensity at which an induced transition may occur, which is often sufficient to describe the fine structure to the accuracy warranted, we need only consider diagonal terms in our Hamiltonian. The energy eigen values are then, for trigonal symmetry :-

$$E(M) = (M \mid H' \mid M)$$

$$= g\beta H.M + \frac{D}{2}(3\cos^2\theta - 1)\left[M^2 - \frac{S(S+1)}{3}\right]$$

$$+ \frac{a}{1,440}\left[35\cos^4\theta - 30\cos^2\theta + 3 \pm 20.\sqrt{2}.\sin^3\theta\cos\theta\cos 3\psi\right]$$

$$\cdot\left[35M^4 - 30S(S+1)M^2 + 25M^2 - 6S(S+1) - 3S^2(S+1)^2\right]$$

This expression is equivalent to that derived by Kikuchi & Mataresse (1960), noting that a rotation (ψ,θ) about OZ and then OY' is equivalent to a rotation $(\frac{\pi}{2} - \psi, \theta)$ about OZ and then OX', as these authors have used.

The expression for the eigen values derived by Dorain (1958) is considered by this author to be incorrect.

The resonance condition is then given by :-

$$\nu_o = g\beta H_o = E(M) - E(M-1)$$

For $\theta = 0$, we then obtain:-

$$H_{5/2} = H_o - 4D + \frac{4a}{3}$$

$$H_{3/2} = H_o - 2D - \frac{5a}{3}$$

$$H_{1/2} = H_o \qquad (3.1)$$

$$H_{-1/2} = H_o + 2D + \frac{5a}{3}$$

$$H_{-3/2} = H_o + 4D - \frac{4a}{3}$$

where the parameters D and "a" are now expressed in Oersted.

3.2 Hyperfine Structure.

When the nucleus possesses a non-zero spin, the Hamiltonian may be supplemented by : (Al'tshuler & Kosyrev 1964)

$$H_N = AS_zI_z + B(S_xI_x + S_yI_y) + \frac{Q}{2}\left[1_z^2 - \frac{1}{3}I(I+1)\right](3\cos^2\theta - 1) - g_N\beta_N HI_z$$

For the Mn^{2+} ion, A ≫ B (Ingram 1967) and putting $S_x = \frac{S_+ + S_-}{2}$, etc., we use -

$$H_N = AS_zI_z + \frac{A}{2}(S_+I_- + S_-I_+) + \frac{Q}{2}\left[I_z^2 - \frac{1}{3}I(I+1)\right](3\cos^2\theta - 1) - g_N\beta_N HI_z .$$

To first order the correction to the line positions is then

$$H = -Am$$

for the allowed $\Delta m = 0$ transitions, and

$$H = -\frac{A}{2}(2m-1)$$

for the $\Delta m = \pm 1$ forbidden transitions.

3.3 Second Order Corrections to Line Positions.

The corrections to the eigenstates are found to be :-

$$E^{(2)}_{Mm} = \sum_{M'm'}^{M' \neq M} \frac{(Mm|\,H'\,|\,M'm')(M'm|\,H'\,|\,Mm)}{E_{Mm} - E_{M'm'}}$$

$$= \frac{A^2}{2g\beta H_o}\left[\, m\left\{M^2 - S(S+1) + M(I+1) - m^2\right\}\right]$$

$$+ \frac{|\lambda|^2}{g\beta H_o}\left[\, 2M\left\{8M^2 - 4S(S+1) + 1\right\}\right]$$

$$+ \frac{|\rho|^2}{g\beta H_o}\left[\, 2M\left\{2S(S+1) - 2M^2 - 1\right\}\right]$$

where we have included only terms in D, E and A. The term in A^2 has been given by Bleaney & Rubins (1961), Folen (1962), Waldner (1962) and the terms including D, have been derived by Bleaney & Ingram (1951). From these terms the following correction to line positions is calculated:-

$$H = \frac{A^2}{2g\beta H_o}\left[m^2 - I(I+1) - m(2M-1)\right]$$

$$- \frac{2|\lambda|^2}{g\beta H_o}\left[24M(M-1) - 4S(S+1) + 9\right]$$

$$- \frac{2|\rho|^2}{g\beta H_o}\left[2S(S+1) - 6M(M-1) - 3\right]$$

For $M = +\frac{1}{2}$

$$H = \frac{A^2}{2g\beta H_o}\left(m^2 - \frac{35}{4}\right) + \frac{64|\lambda|^2}{g\beta H_o} - \frac{32|\rho|^2}{g\beta H_o} \qquad (\Delta m = 0)$$

$$= \frac{A^2}{2g\beta H_o}\left(m^2 - m + \tfrac{1}{4}\right) + \frac{64|\lambda|^2}{g\beta H_o} - \frac{32|\rho|^2}{g\beta H_o} \qquad (\Delta m = +1)$$

(3.2)

$$= \frac{A^2}{2g\beta H_o} \cdot \left(m^2 - m - \frac{67}{4}\right) + \frac{64|\lambda|^2}{g\beta H_o} - \frac{32|\rho|^2}{g\beta H_o} \qquad (\Delta m = -1)$$

To second order, for rhombic symmetry, agreement is obtained with the expressions derived by Morigaki et al (1958) and Kasai (1962). Brovetto et al (1953), Takeda (1967) and Bir (1964) list various different expressions which are considered incorrect by this author.

3.4 Third Order Corrections.

Third order perturbation calculations, relevant to the Mn^{2+} ion in a site of axial crystal field symmetry, have been carried out by a number of authors (Bleaney & Rubins 1961, Waldner 1962, Folen 1962, Wolga & Tseng 1964, Nicula et al 1965, Odenhal 1963), with remarkably little agreement between the expressions derived. In an attempt to resolve which, if any, of the expressions was correct, the calculation was carried out by this author, the full calculation being set out in appendix B.

The general form of the degenerate perturbation solution may be derived from expressions listed by Condon and Shortley (1951), viz. -

$$E_3(M,m) = \sum_{M'm'}^{M' \neq M} (Mm|H'|M'm') \left\{ a^{M'm'} \middle| 2^{Mm} \right\} \qquad (3.3)$$

$$\left\{ a^{M'm'} \middle| 2^{Mm} \right\} = - \frac{(M'm'|H'|Mm)(Mm|H'|Mm)}{(E_{M'} - E_M)^2}$$

$$- \sum_{M''m''} \frac{(M'm'|H'|M''m'')\left\{ a^{M''m''} \middle| 1^{Mm} \right\}}{(E_{M'} - E_M)} \qquad (3.4)$$

$$\left\{a^{Mm}\middle|1^{Mm}\right\} = 0 \qquad (3.5)$$

$$\left\{a^{M"m"}\middle|1^{Mm}\right\} = \frac{(M"m"|H'|Mm)}{E_M - E_{M"}} \qquad (M"\neq M) \qquad (3.6)$$

$$\left\{a^{Mm"}\middle|1^{Mm}\right\} = \sum_{M"'m"'}^{M"'\neq M} \frac{(Mm"|H'|M"'m"')(M"'m"'|H'|Mm)}{(E_M - E_{M"'})(E_{Mm} - E_{Mm"})} \qquad (3.7)$$

$$(m"\neq m)$$

Substituting (3.4) in (3.3) produces:-

$$E_3(M,m) = \sum_{M'm'}^{M'\neq M} \frac{(Mm|H'|M'm')(M'm'|H'|Mm)(Mm|H'|Mm)}{(E_{M'} - E_M)^2}$$

$$- \sum_{M'm'}^{M'\neq M} \sum_{M"m"} \frac{(Mm|H'|M'm')(M'm'|H'|M"m")\left\{a^{M"m"}\middle|1^{Mm}\right\}}{(E_{M'} - E_M)} \qquad (3.8)$$

If equation (3.6) is now substituted directly in (3.8), the expression listed and used by Waldner (1962) and Nicula et al (1965) is obtained. This substitution is not correct, however, as (3.6) is defined strictly for $M"\neq M$, whereas the summation $\sum_{M"m"}$ in (3.8) or (3.4) involves a summation over all M" (and m"), including $M"=M$. The correct expression for the third order perturbation may be found by writing this summation as -

$$\sum_{M"m"} \frac{(M'm'|H'|M"m")\left\{a^{M"m"}\middle|1^{Mm}\right\}}{(E_{M'} - E_M} = \frac{(M'm'|H'|Mm)\left\{a^{Mm}\middle|1^{Mm}\right\}}{(E_{M'} - E_M)}$$

$$+ \sum_{m"}^{m"\neq m} \frac{(M'm'|H'|Mm")\left\{a^{Mm"}\middle|1^{Mm}\right\}}{(E_{M'} - E_M)} + \sum_{M"m"}^{M"\neq M} \frac{(M'm'|H'|M"m")\left\{a^{M"m"}\middle|1^{Mm}\right\}}{(E_{M'} - E_M)}$$

(3.9)

Substitution of (3.5), (3.6) and (3.7) in this expansion of the summation then produces:-

$$E_3(M,m) = -\sum_{M'm'}^{M'\neq M} \frac{(Mm|H'|M'm')(M'm'|H'|Mm)(Mm|H'|Mm)}{(E_{M'}-E_M)^2}$$

$$-\sum_{M'm'}^{M'\neq M}\sum_{M''m''}^{M''\neq M} \frac{(Mm|H'|M'm')(M'm'|H'|M''m'')(M''m''|H'|Mm)}{(E_{M'}-E_M)(E_M-E_{M''})}$$

$$-\sum_{M'm'}^{M'\neq M}\sum_{m''}^{m''\neq m}\sum_{M'''m'''}^{M'''\neq M} \frac{(Mm|H'|M'm')(M'm'|H'|Mm'')(Mm''|H'|M'''m''')(M'''m'''|H'|Mm)}{(E_{M'}-E_M)(E_M-E_{M'''})(E_{Mm}-E_{Mm''})} \qquad (3.10)$$

The first two terms only in this expression are given by Waldner (1962) and Nicula et al (1965).

Performing the calculation, using (3.10), the following is then derived for the third order correction to the eigenvalues, where we list only terms involving both quantum numbers m & M, which contribute to the expression for line positions of the central hyperfine transitions.

$$E_3(M,m) = \left[\frac{D\sin 2\theta}{4g\beta H_o}\right]^2 \frac{Am}{M}\left[(M^2-S(S+1))^2-M^2\right]$$

$$+\left[\frac{D\sin^2\theta}{4g\beta H_o}\right]^2 2AMm\left[2M^2+1-2S(S+1)\right]$$

$$+\frac{DA^2}{8(g\beta H_o)^2}.(3\cos^2\theta-1).\Big[\{S(S+1)-M(M+1)\}.\{I(I+1)-m(m-1)\}.(2M+1)$$

$$-\{S(S+1)-M(M-1)\}.\{I(I+1)-m(m+1)\}.(2M-1)\Big]$$

$$+\frac{A^3}{(2g\beta H_o)^2}\Big[\{S(S+1)-M(M+1)\}\{I(I+1)-m(m-1)\}\{m-M-1\}$$

$$+\{S(S+1)-M(M-1)\}\{I(I+1)-m(m+1)\}\{M-m-1\}\Big] \qquad (3.11)$$

Comparing this expression with those derived by other authors we find :-

1) Complete agreement is obtained with the expressions derived by Odenhal (1963) and de Wijn and van Balderen (1967).

2) The first term in this expression is the resultant of terms derived from the single, double and triple summations in the perturbation calculation. As shown in the appendix we find for this term in $AD^2\sin^2 2\theta$:-

a) $\Sigma \rightarrow -\left[\frac{D\sin 2\theta}{4g\beta H_o}\right]^2 . AMm\Big[(2M+1)^2\{S(S+1)-M(M+1)\}+(2M-1)^2\{S(S+1)-M(M-1)\}\Big]$

which is the expression given by Waldner;

b) $\Sigma + \Sigma\Sigma \rightarrow \left[\frac{D\sin 2\theta}{4g\beta H_o}\right]^2 Am\Big[(2M+1)^2\{S(S+1)-M(M+1)\}-(2M-1)^2\{S(S+1)-M(M-1)\}\Big]$

which is the expression given by Nicula et al;

c) $\Sigma\Sigma\Sigma \rightarrow 18\left[\frac{D\sin 2\theta}{4g\beta H_o}\right]^2 \frac{Am}{M}\left[M^2-S\left(\frac{S+1}{3}\right)\right]^2$

which is the expression originally given by Bleaney & Rubins (1961). This term, as these authors have stated, is the most important term (in magnitude).

3) As shown in the appendix, terms in $\frac{D^3}{H^2}$, which are functions of only one quantum number (M) are also obtained, but these terms do not contribute to the expression for line positions for $(M = +\frac{1}{2} \longrightarrow M = -\frac{1}{2})$.

4) The third order corrections for the case of rhombic symmetry ($E \neq o$) may be derived from the above equations (3.11) by substituting -

$\sigma = \frac{1}{2}\left[D(3\cos^2\theta - 1) + 3E\sin^2\theta\cos 2\psi \right]$ for $\frac{D}{2}(3\cos^2\theta - 1)$ etc.

3.5 Line Positions Including Third Order Corrections.

From the expression for third order corrections to energy levels obtained in the previous section, corrections to the expressions for line positions may be obtained. Performing these calculations and collecting all terms we obtain the following expressions for line positions:-

$$\Delta m = o : \quad H = H_o - Am + \frac{A^2}{2H_o}(m^2 - \tfrac{35}{4}) - \frac{A^3 m}{2H_o^2}(m^2 - \tfrac{65}{4}) + H_1(A,D,Q,\theta,m) \qquad (3.12)$$

$$\Delta m = +1 \ (\text{HIGH FIELD}) : \quad H = H_o - \frac{A}{2}(2m-1) + \frac{A^2}{2H_o}(m^2 - m + \tfrac{1}{4}) - \frac{A^3}{4H_o^2}(2m-1)(m^2 - m + \tfrac{73}{4})$$
$$+ \gamma H_o + H_2(A,D,Q,\theta,m) \qquad (3.13)$$

$$\Delta m = -1 \ (\text{LOW FIELD}) : \quad H = H_o - \frac{A}{2}(2m-1) + \frac{A^2}{2H_o}(m^2 - m - \tfrac{67}{4}) - \frac{A^3}{4H_o^2}(2m-1)(m^2 - m - \tfrac{195}{4})$$
$$- \gamma H_o + H_3(A,D,Q,\theta,m) \qquad (3.14)$$

where the parameters are all expressed in oersted, $\gamma = \frac{g_N \beta_N}{g\beta}$, and the $H_i(A,D,Q,\theta,m)$ are angular dependent terms, which for convenience we write as :-

$$H_i = E_i(3\cos^2\theta - 1) + F_i(\sin^2 2\theta) + G_i \sin^4\theta \qquad (i = 1,3) \qquad (3.15)$$

	E_i	F_i	G_i
i=1 ($\Delta m=0$)	$\frac{-4DA^2m}{H_o^2}$	$\frac{4D^2}{H_o} - \frac{36AD^2m}{H_o^2}$	$\frac{-2D^2}{H_o} + \frac{2AD^2m}{H_o^2}$
i =2 ($\Delta m=+1$)	$\frac{-Q}{2}(2m-1)$	$\frac{4D^2}{H_o} \frac{-18AD^2}{H_o^2}(2m-1)$	$\frac{-2D^2}{H_o} \frac{+AD^2}{H_o^2}(2m-1)$
i=3 ($\Delta m=-1$)	$\frac{Q}{2}(2m-1)\frac{-4DA^2}{H_o^2}(2m-1)$	$\frac{4D^2}{H_o} \frac{-18AD^2}{H_o^2}(2m-1)$	$\frac{-2D^2}{H_o} \frac{+AD^2}{H_o^2}(2m-1)$

N.B. The term H_o in expressions derived by perturbation methods is an approximation for the field at which resonance occurs. Better agreement between theory and experiment was obtained substituting :-

$$H_o - Am \qquad (\Delta m = 0)$$

$$H_o - \frac{A}{2}(2m-1) \qquad (\Delta m = \pm 1)$$

for H_o, in the denominators of expressions. This substitution is used in all future calculations of line positions for axial spectra.

CHAPTER IV

TRANSITION PROBABILITIES

4.1 Transition Probabilities by Second Order Perturbation - Axial Fields.

The theory of the variation of intensity of the forbidden ($\Delta m = \pm 1$) transitions was first considered by Friedman and Low (1960). The expression derived by these authors predicted a $\sin^2 2\theta$ variation in intensity of the forbidden transitions, which for small values of D is observed experimentally (see later), but could not account for the observed variation of intensity with the applied static field. An expression for the intensity variations was finally obtained by Bleaney & Rubins (1961) which predicted the $\sin^2 2\theta$ variation, and a $\frac{1}{H}$ variation with applied static field.

A derivation of the expression given by Bleaney & Rubins is now outlined to illustrate the general method, which will be used later to derive a correct expression for the intensity variation in the case of cubic crystal field symmetry. (Appendix A)

The transition probability describing the transition from a state $\Phi_{M,m}$, to a higher state $\Phi_{M',m'}$, is given by -

$$I \propto \left| (\Phi_{M'm'} \mid S' \mid \Phi_{M,m}) \right|^2 \qquad (4.1)$$

where S' is a spin operator which reflects the polarization of the inducing R.F. field. For linear polarization in the Y direction of the crystal axis, which is the case experimentally

$$S' \propto (S_+ + S_-) \qquad \text{(Shulz-Dubois 1959)}$$

To obtain an expression for the intensity we first expand the $|\Phi_{M,m}\rangle$ as a linear combination of zero-order wave functions, i.e. -

$$|\Phi_{M,m}\rangle = \sum_{M'',m''} a^{M''m''}_{M,m} |M'',m''\rangle$$

whence -

$$I \propto \left| (\Sigma a^{M'',m''}_{M',m'})^{*} (M'',m'' | (S_+ + S_-)(\Sigma a^{M'',m''}_{M,m} | M'',m'' \rangle \right|^2 \qquad (4.2)$$

The coefficients $a^{M'',m''}_{M',m'}$ in the expansion of the perturbed wave function may be calculated to second order in perturbation theory, using the general expression given by Condon & Shortley (1951), which in our present notation may be written:-

$$|\Phi_{M,m}\rangle = |M,m\rangle + \sum_{m' \neq m} \sum_{M'' \neq M} \sum_{M''m''} \frac{\langle Mm' | H' | M''m'' \rangle \langle M''m'' | H' | Mm \rangle . | Mm' \rangle}{(E_M - E_{M''})(E_{Mm} - E_{Mm'})} \qquad (4.3)$$

For our perturbation Hamiltonian we use:-

$$H' = \frac{D}{2}\left[S_z^2 - \frac{1}{3}S(S+1) \right].(3\cos^2\theta - 1) + \frac{D}{4}\left[S_z(S_+ + S_-) + (S_+ + S_-)S_z \right].\sin 2\theta$$

$$+ \frac{D}{4}\left[S_+^2 + S_-^2 \right]\sin^2\theta + AS_zI_z + \frac{A}{2}(S_+I_- + S_-I_+) \qquad (4.4)$$

For the operators in this expression, the possible terms in the summation are:-

$$\frac{\langle M,m+1 | S'_+ | M-1,m+1 \rangle . \langle M-1,m+1 | S'_- I'_+ | M,m \rangle . | M,m+1 \rangle}{(E_M - E_{M-1})(E_{M,m} - E_{M,m+1})}$$

$$\frac{\langle M,m+1 | S'_- I'_+ | M+1,m \rangle . \langle M+1,m | S'_+ | M,m \rangle . | M,m+1 \rangle}{(E_M - E_{M+1})(E_{M,m} - E_{M,m+1})}$$

$$\frac{(M,m-1|\ S'_-\ |M+1,m-1)(M+1,m-1|\ S'_+I'_-\ |Mm)\ .\ |M,m-1)}{(E_M-E_{M+1})(E_{M,m}-E_{M,m-1})}$$

$$\frac{(M,m-1|\ S'_+I'_-\ |M-1,m)(M-1,m|\ S_-|Mm)\ .\ |M,m-1)}{(E_M-E_{M-1})(E_{M,m}-E_{M,m-1})} \qquad (4.5)$$

where $S'_+ = \frac{D}{4}\left[(S_zS_+ + S_+S_z)\right]\sin 2\theta$ etc.

Taking $E_M = g\beta H_o M$ and $E_{M,m} = g\beta H_o M + AMm$ as approximations, we then obtain:-

$$|\Phi_{M,m}) = |M,m) + C_1|M,m+1) + C_2|M,m-1) \qquad (4.6)$$

where $C_1 = \frac{D\sin 2\theta\{S(S+1) - 3M^2\}\{I(I+1) - m(m+1)\}^{\frac{1}{2}}}{4g\beta H_o M}$

and $C_2 = \frac{-D\sin 2\theta\{S(S+1) - 3M^2\}\{I(I+1) - m(m-1)\}^{\frac{1}{2}}}{4g\beta H_o M}$

Forbidden transitions occur between states $(M,m) \longrightarrow (M-1, m\pm1)$, and for the $\Delta m = +1$ transitions, the transition probability is then:-

$$I_F \propto \left|(\Phi_{M,m}|(S_+ + S_-)|\Phi_{M-1,m-1})\right|^2 \qquad (4.7)$$

For the expansion of $|\Phi_{M-1,m-1})$ we obtain:-

$$|\Phi_{M-1,m-1}) = |M-1,m-1) + C_3|M-1,m) + C_4|M-1,m-2)$$

where $C_3 = \frac{D\sin 2\theta\{S(S+1) - 3(M-1)^2\}\{I(I+1)-m(m-1)\}^{\frac{1}{2}}}{4g\beta H_o(M-1)}$ (4.8)

and $C_4 = \frac{-D\sin 2\theta\{S(S+1)-3(M-1)^2\}\{I(I+1)-(m-1)(m-2)\}^{\frac{1}{2}}}{4g\beta H_o(M-1)}$ (4.9)

Substituting in the expression for the intensity we then obtain:-

$$I_F \propto \Big| (M,m| + C_1^*(M,m+1| + C_2^*(M,m-1|)(S_+ + S_-)(|M-1,m-1) + C_3|M-1,m) + C_4|M-1,m-2) \Big|^2$$

$$= \Big| F_-(M)(C_2+C_3) \Big|^2 \text{ where } F_-(M) = \Big[S(S+1) - M(M-1) \Big]^{\frac{1}{2}} \qquad (4.10)$$

Substituting for the coefficients C_2 and C_3 we find:-

$$I_F \propto \left[F_-^2(M) \left[\frac{3D\sin 2\theta}{4g\beta H_o} \right]^2 \left[1 + \frac{S(S+1)}{3M(M-1)} \right]^2 \Big[I(I+1) - m(m-1) \Big] \right] \qquad (4.11)$$

For the allowed transition $(M,m) \longrightarrow (M-1,m)$ we obtain in a similar manner:-

$$I_A \propto \left[F_-(M) \left\{ 1 + \left[\frac{D\sin 2\theta}{4g\beta H_o} \right]^2 \frac{\{S(S+1) - 3M^2\}\{S(S+1) - 3(M-1)^2\}}{M(M-1)} \{2[I(I+1) - m^2]\} \right\} \right]^2 \qquad (4.12)$$

For $D \ll H_o$, $I_A \propto F_-^2(M)$, and for the intensity of the forbidden transitions relative to the allowed transitions, we thus obtain the expression derived by Bleaney & Rubins:-

$$\left[\frac{3D\sin 2\theta}{4g\beta H_o} \right]^2 \left[1 + \frac{S(S+1)}{3M(M-1)} \right]^2 \Big[I(I+1) - m(m-1) \Big] \qquad (4.13)$$

4.2 Relative Intensity in Powder Spectrum.

Bleaney & Rubins (1961) have stated that for the purpose of estimating the magnitude of the parameter D, using the relative intensity of forbidden to allowed transitions observed in a powder spectrum, the $\sin^2 2\theta$ term in equation (4.13) should be replaced by 8/15. A value of $|D| = 125$ Oe was then calculated by these authors for the measured

relative intensity observed in the Mn^{2+} spectrum from a sample of modelling clay (plasticine).

The manufacturers (under licence) in Australia, of Harbutt's plasticine (Bellco Ltd., Melbourne), kindly provided this author with samples of the ingredients used in the manufacture of this material. The component responsible for the Mn^{2+} spectrum was found to be powdered calcite. If we assume that the Mn^{2+} spectrum from the plasticine sample used by Bleaney & Rubins, was also due to Mn^{2+} in calcite, ($|D|$ = 81 Oe, Hurd et al 1954), the computed value of $|D|$ = 125 Oe from the plasticine sample spectrum is then seen to be in error by $\sim$50%. Fig. 4.1 shows a spectrum recorded from a powdered sample of Magnesite ($MgCO_3$), from which a value of $|D| \sim 130$ Oe was obtained from the relative intensities of forbidden to the first allowed transition (m = -5/2), using the Bleaney & Rubins' expression for a powder spectrum. From single crystal measurements, however, a value of $|D|$ = 85.5 Oe has been obtained (Vinokurov et al 1961), and once again a value of the parameter $|D|$, larger by $\sim$50% than the single crystal determination, is obtained from powder measurements. An even larger relative error was found in a similar determination of 'D' from the spectrum of powdered $Zn(Mn^{2+})CO_3$, fig. 4.2. From the relative intensity of forbidden lines observed in this spectrum, a value of $|D| \sim 90$ Oe was obtained. From single crystal measurements however, $|D|$ = 44 Oe (Burley 1964).

It must then be assumed that the determination of the axial splitting parameter D, by applying the expression for the relative

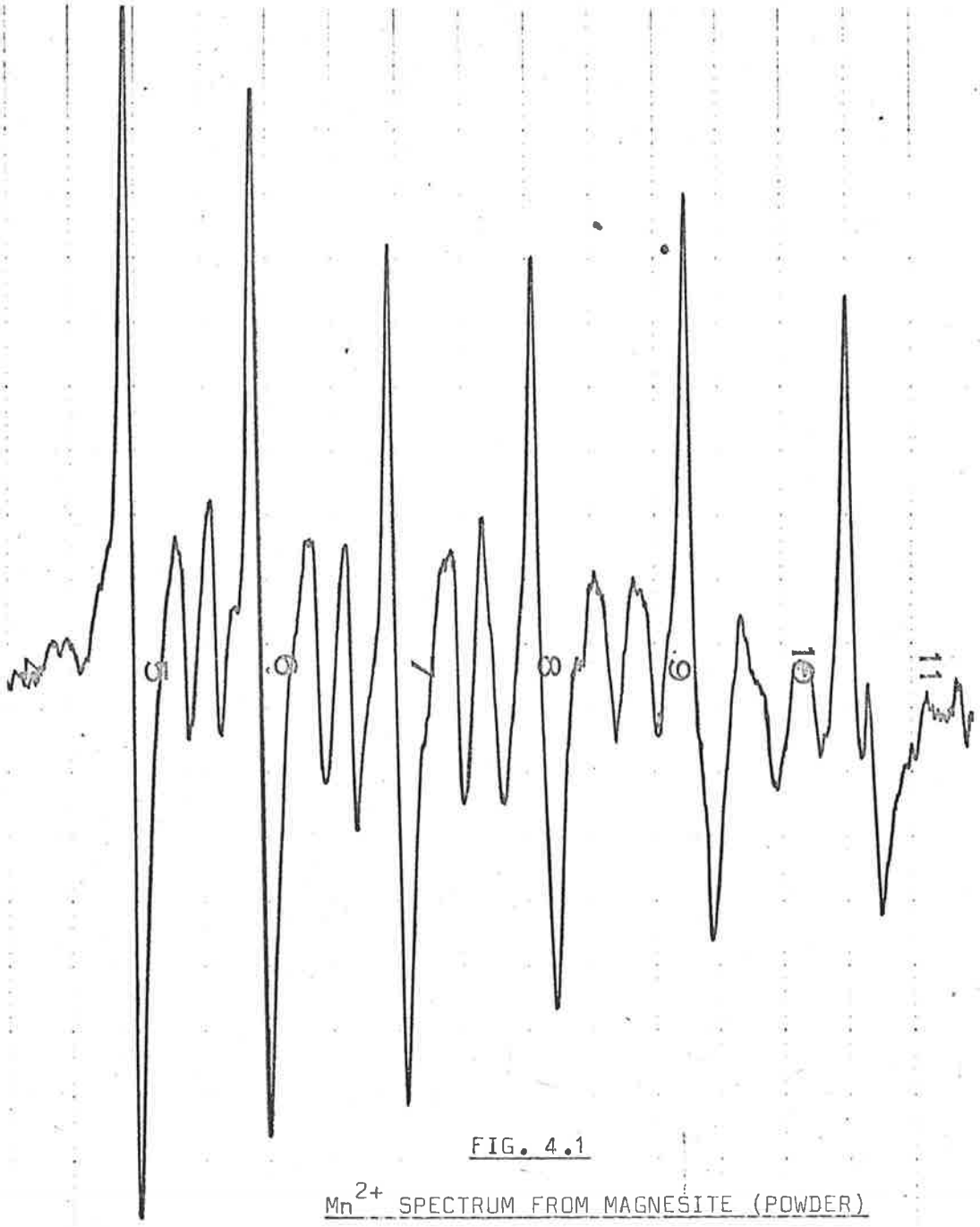

FIG. 4.1

Mn^{2+} SPECTRUM FROM MAGNESITE (POWDER)

X-BAND : ROOM TEMPERATURE

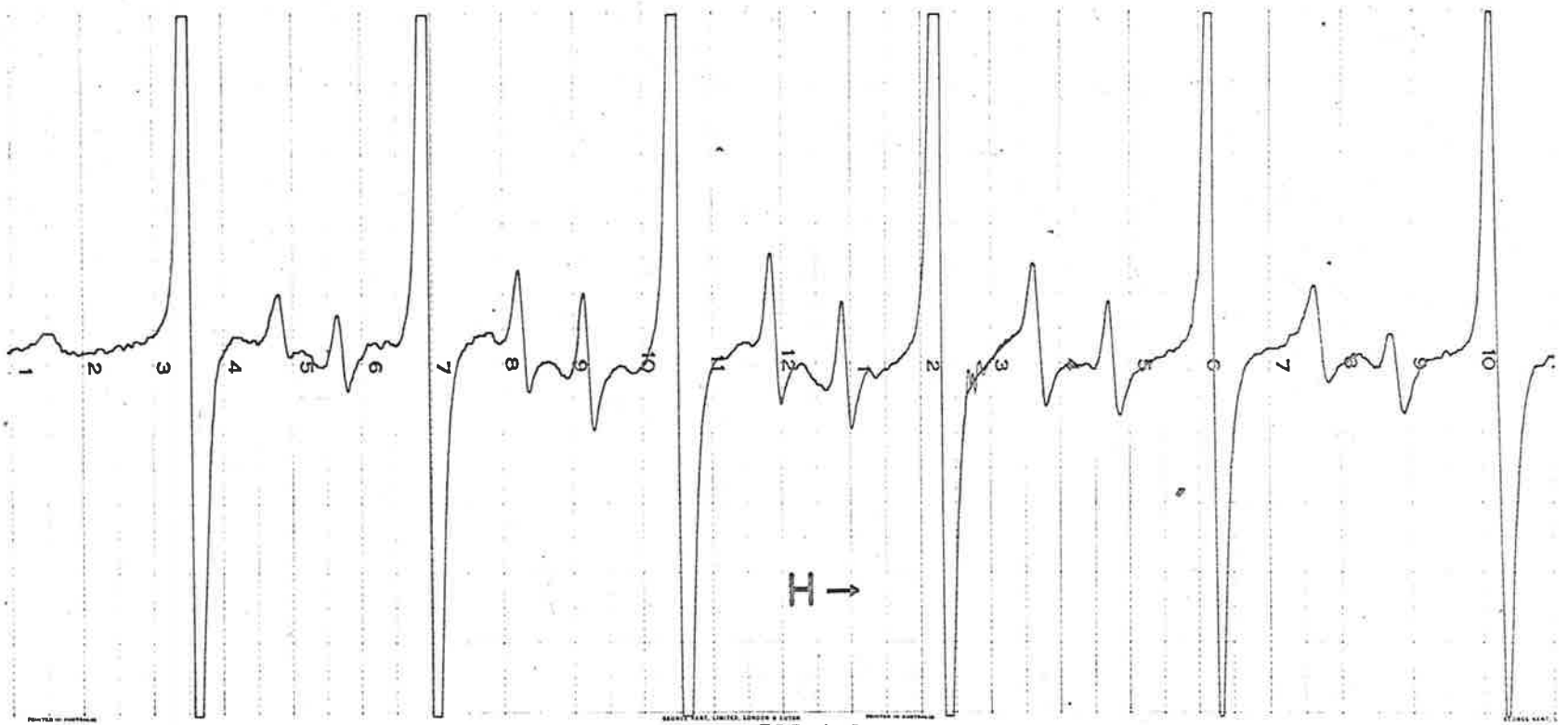

FIG.4.2

Mn^{2+} SPECTRUM FROM SMITHSONITE (POWDER)

X-BAND : ROOM TEMPERATURE

intensity of forbidden transitions in a powder spectrum, given by Bleaney & Rubins (1961), to experimentally determined values, may produce relatively large errors. The expression derived by these authors for the relative intensity observed in single crystal spectra, equation (4.13), does however predict values which are in reasonable agreement with experiment, for the Mn^{2+} spectrum observed from crystalline calcite. For this spectrum, the predicted intensity ratios of forbidden to allowed transitions, in the central group ($M = \frac{1}{2}$) of lines at X-band, and $\theta = 45^{o}$, as determined from (4.13) with D = 81 Oe, H = 3,300 Oe, are approximately :-

m =	$\underline{-3/2}$	$\underline{-1/2}$	$\underline{1/2}$
Relative Intensity	1 : 5.2	1 : 3.2	1 : 2.9

From the spectrum shown by Ursu et al (1966), corresponding experimental ratios of

1 : 4.2 1 : 3.2 1 : 3.1

are obtained.

It would then appear that the relatively large error in the determination of 'D' from powder spectra, is due to the substitution of 8/15 for $\sin^2 2\theta$ in (4.13). The factor of 8/15 was obtained by Bleaney & Rubins by an averaging method. The failure of this averaging process to produce a factor which would enable reasonable agreement to be obtained between the theoretical expression and experimental values of relative intensities in powder spectra, would then seem to cast a doubt on similar averaging methods used to predict relative shifts of line positions in powder spectra. (Nicula et al 1965, Waldner 1962.)

4.3 Transition Probabilities by Second Order Perturbation - Rhombic Fields.

When the electrostatic crystalline field possesses rhombic symmetry, the analogous expression for the relative intensity of the forbidden transitions may be found by substitution of $|\lambda|$ for $\frac{D\sin 2\theta}{4}$, viz. :-

$$\left[\frac{3|\lambda|}{g\beta H}\right]^2 \left[1 + \frac{S(S+1)}{3M(M-1)}\right]^2 \left[I(I+1)-m(m-1)\right] \qquad (4.14)$$

with $$|\lambda| = \frac{\sin\theta}{2}\left[\cos\theta(D-E\cos 2\psi) + iE\sin 2\psi\right]$$

4.4 Intensity Variations Using Computer Diagonalization of the 36 x 36 Energy Interaction Matrix.

When off-diagonal terms in the energy matrix $(M'',m''|\,H\,|M',m')$ are no longer small compared to diagonal elements, perturbation methods are no longer accurate, and exact methods are necessary to calculate (say) the coefficients of the zero-order wave functions in the expansion of perturbed wave functions.

Suppose $E_{M,m}$ denotes the eigenvalue of the eigenstate $|\Phi_{M,m}\rangle$

i.e. $$H\,|\Phi_{M,m}\rangle = E_{M,m}|\Phi_{M,m}\rangle \qquad (4.15)$$

Substitution of the expansion in terms of zero-order functions, multiplication by $(M'',m''|$, and integration, then allows us to write:-

$$\sum_{M'm'} A^{M'm'}_{Mm}\,(M''m''|\,H\,|M''m') - E_{M,m}(M''m''|M'm') = 0 \qquad (4.16)$$

or:-

$$A^{1}_{Mm}\left[(1|H|1)-E_{M,m}\right] + A^{2}_{Mm}(1|H|2) + A^{3}_{Mm}(1|H|3) + \ldots\ldots$$

$$\ldots\ldots + A^{36}_{M,m}(1|H|36) = 0$$

$$A^{1}_{Mm}(2|H|1) + A^{2}_{M,m}\left[(2|H|2)-E_{M,m}\right] + A^{3}_{M,m}(2|H|3) + \ldots\ldots$$

$$\ldots\ldots + A^{36}_{M,m}(2|H|36) = 0$$

$$\vdots \qquad\qquad\qquad\qquad \vdots$$

$$A^{1}_{Mm}(36|H|1) + \ldots\ldots + A^{36}_{M,m}\left[(36|H|36)-E_{M,m}\right] = 0 \quad \ldots\ldots$$

(4.17)

With modern digital computers the (36 x 36) energy interaction matrix $(M''m''|H|M'm')$ may be readily diagonalized to find the eigenvalues $E_{M,m}$. Substitution of a particular eigenvalue in equations (4.17) above, then enable the coefficients $A^{M'm'}_{Mm}$ to be found. In practice one coefficient A^{Mm}_{Mm} is set equal to unity, and the other coefficients expressed in terms of A^{Mm}_{Mm}. Any 35 of the 36 simultaneous equations may then be solved to find these coefficients.

Noting that the operators S_+ and S_- only link states $(M\pm1)$ and (M), and that $S^{\pm}|M,m) = F^{\pm}(M)|M\pm1,m)$, the intensity of a forbidden transition may then be written:-

$$I \propto \left| \left[\sum_{M''m''} A^{M'',m''*}_{M+1,m+1} (M'',m'') \right] (S_+ + S_-) \left[\sum_{M'm'} A^{M',m'}_{M,m} (M',m') \right] \right|^2$$

$$= \left| \sum_{M''m''} A^{M''m''*}_{M+1,m+1} \left[A^{M''+1,m''}_{M,m} F_+(M''+1) + A^{M''-1,m''}_{M,m} F_-(M''-1) \right] \right|^2 \qquad (4.18)$$

where $F_{\pm}(M) = \left[S(S+1) - M(M \pm 1) \right]^{\frac{1}{2}}$

The intensity variation for the central forbidden doublet, for D = 81 Oe, obtained using the method described above, is shown in figure 4.3. As described in Chapter VI, the computations necessary to obtain intensity variations may be reduced by a factor of $\sim 10^3$, using a method described by Bir (1964).

N.B.

The vertical scale in fig. 4.3 is completely arbitrary. The absolute values computed for the forbidden transition intensity by this method would have to be normalized, using the $\theta = 0^\circ$ value obtained in a similar manner for allowed transitions.

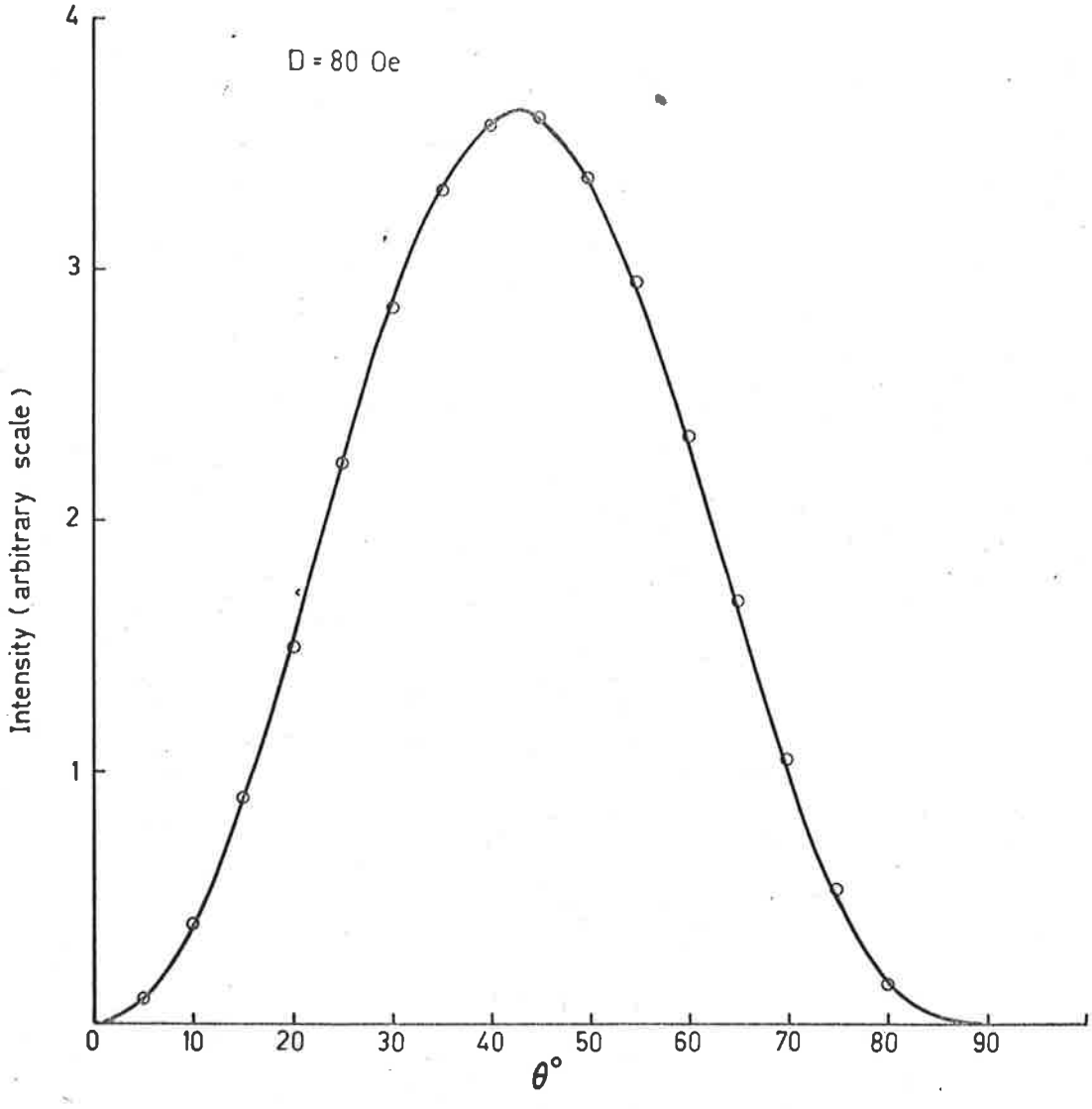

Intensity of forbidden transition by computer diagonalization.
(36 x 36 Matrix)

FIG. 4.3

CHAPTER V

Line Positions in Powder Spectra.

5.1 Line Shifts Using Bleaney and Rubins' Method.

Having derived required expressions, we are now in a position to return to the problem of line shifts, etc., observed in powder spectra.

The observed splitting of the $\Delta m = o$ hyperfine lines observed from Mn^{2+} in a sample of powdered calcite ($CaCO_3$) has been adequately explained by Bleaney and Rubins (1961) by considering extreme values of the intensity function -

$$I'(\theta) = \frac{\sin\theta\, I(\theta)}{2\frac{dH}{d\theta}} \qquad (5.1)$$

For the forbidden transitions we may use, for values of $|D|$ less than about 100 Oe (as shown later), the intensity variation with angle -

$$I_F(\theta) \propto \sin^2 2\theta \qquad (5.2)$$

and for the same range of D, we assume that for the allowed transitions -

$$I_A(\theta) = \text{constant.} \qquad (5.3)$$

Using $$H_i = E_i(3\cos^2\theta - 1) + F_i\sin^2 2\theta + G_i\sin^4\theta \quad (i = 1,3)$$

$$\frac{dH_i}{d\theta} = \sin 2\theta(U_i + V_i\sin^2\theta) \qquad (5.4)$$

where $U_i = 4F_i - 3E_i$

$V_i = 2G_i - 8F_i$ where E_i, F_i and G_i are defined in section 3.5.

We then have for our intensity or line shape functions for allowed and forbidden transitions by substitution of (5.2), (5.3) and (5.4) in (5.1) :-

$$I'_A(\theta) \propto \frac{1}{\cos\theta(U_i + V_i\sin^2\theta)}$$

$$I'_F(\theta) \propto \frac{\sin\theta\sin2\theta}{U_i + V_i\sin^2\theta}$$

For allowed transitions, extreme values occur for $\theta = \frac{\pi}{2}$ and $\theta = \arcsin\sqrt{\frac{-U_i}{V_i}}$, and for the forbidden transitions we have one extreme value at $\theta = \arcsin\sqrt{\frac{-U_i}{V_i}}$, which corresponds approximately to $\theta \sim 40^\circ$, and will be referred to as $\theta \sim 40^\circ$ peaks in the later discussion. Typical intensity or line shape functions are shown plotted in fig. 5.1.

$\theta = \arcsin\sqrt{\frac{-U_i}{V_i}}$ is a turning point (or maximum) of the $H(\theta)$ versus θ curve. The physical significance of the peak corresponding to this value of θ is that for resonance in the range $H(\theta \sim 40^\circ)$ to $H \pm dH$, there is a much larger number of spins contributing to the resonance, compared with another general range (except $H(\theta = 90^\circ)$ to $H \pm dH$).

The shift in the line position from that calculated using only non-angular dependent expressions, can now be evaluated by substitution

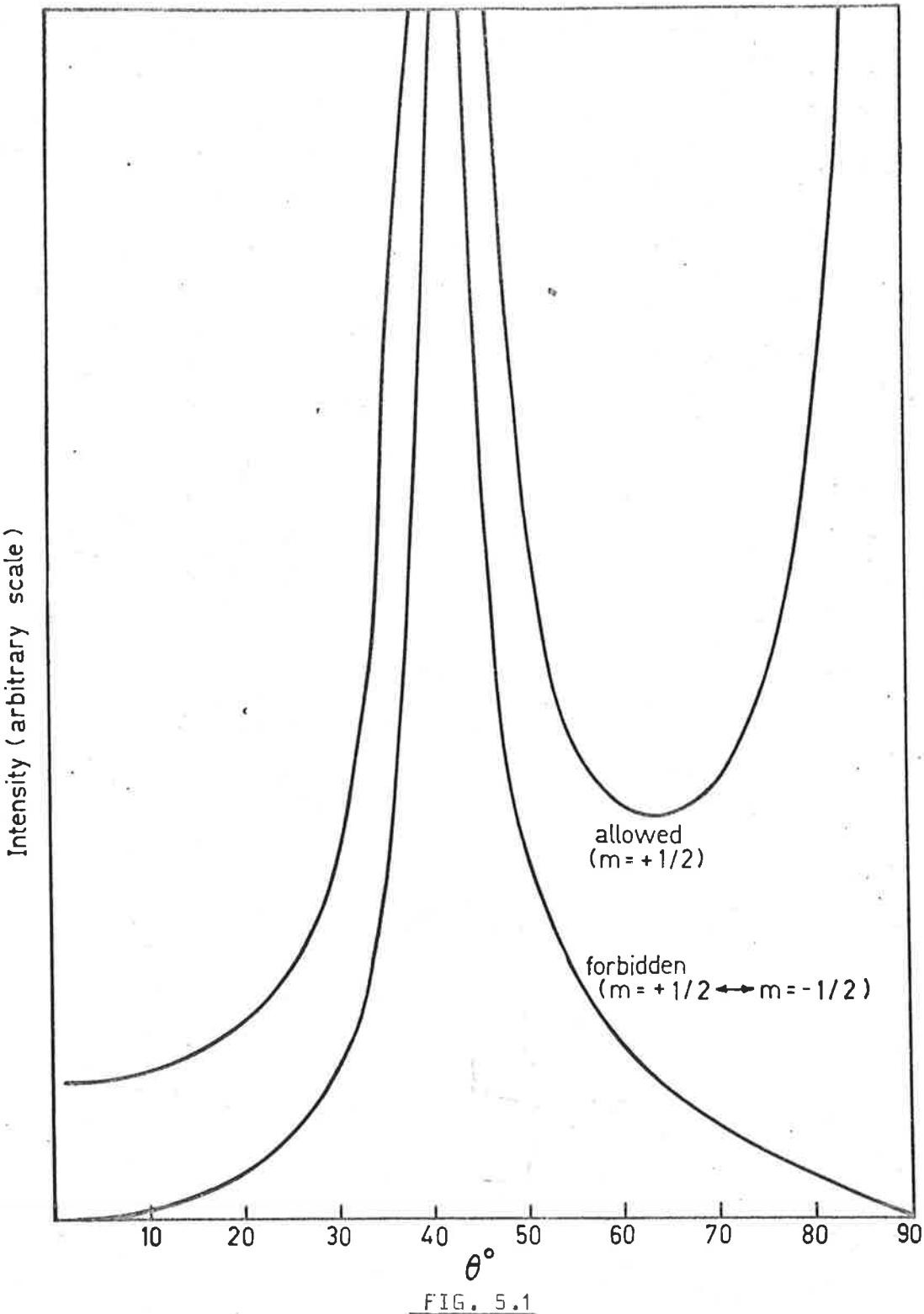

FIG. 5.1

Intensity functions for powder samples. D = -80, A = -94

of the value of θ for a maximum, in the appropriate angular dependent expression $H_i(\theta)$.

5.2 Application to the (Mn^{2+}) Powder Spectrum from Calcite.

As a test of the theory we may first consider in more detail the powder spectrum of Mn^{2+} in powdered calcite, for which the appropriate parameters are A = -94Oe, D = -81Oe and g = 2.0 (approximately). (Hurd, Sachs and Hershberger (1954), Mataresse (1961)) Experimentally determined variations of intensity with angle between the crystal axis and the applied static magnetic field, are shown in fig. 5.2. These intensity variations were obtained using a natural calcite crystal (picked from crushed marble), which was slightly strained (as evidenced by Laue backscatter photographs). In this, and other strained crystals, such as $CaWO_4$ discussed later, the outer sextets of hyperfine lines are so broadened, that away from $\theta = 0^o$, observations of the central transitions are not obscured as the crystal is rotated in the applied magnetic field (fig. 5.3). For these outer transitions ($M = \pm 5/2 \longleftrightarrow M = \pm 3/2$ and $M = \pm 3/2 \longleftrightarrow M = \pm 1/2$) the field position at which resonance occurs is much more angular dependent than field positions for the central transitions, and variations in the direction of the crystal field axis throughout the ionic sites in the crystal due to strains, would thus produce much greater broadening of the outer transitions, than for the central resonances. With the assumption that observed intensity variations for a strained crystal do not differ greatly from those in an

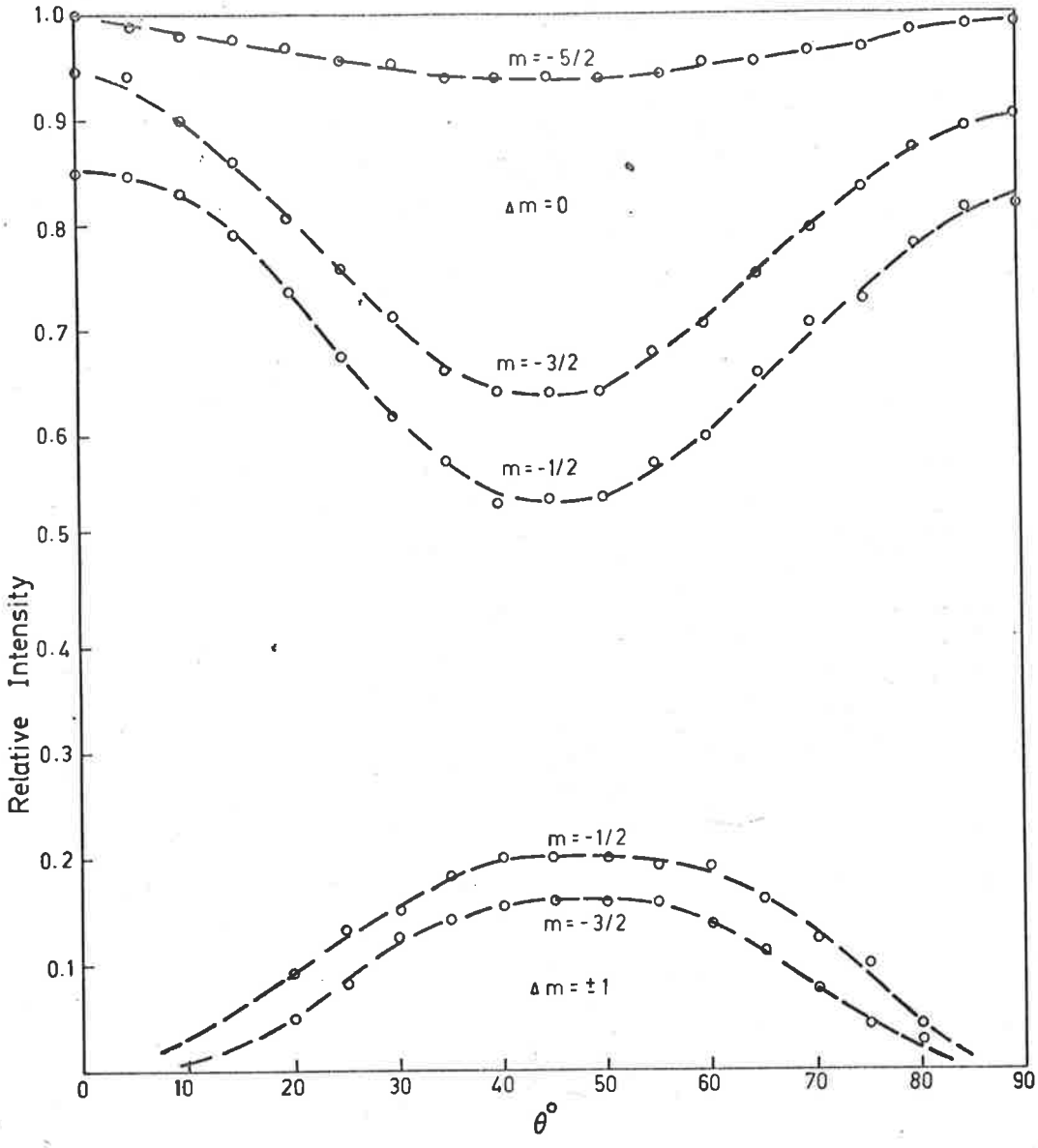

Experimental intensity variations for M = 1/2 transitions in calcite. (strained crystal. X - band; room temperature)

FIG. 5.2

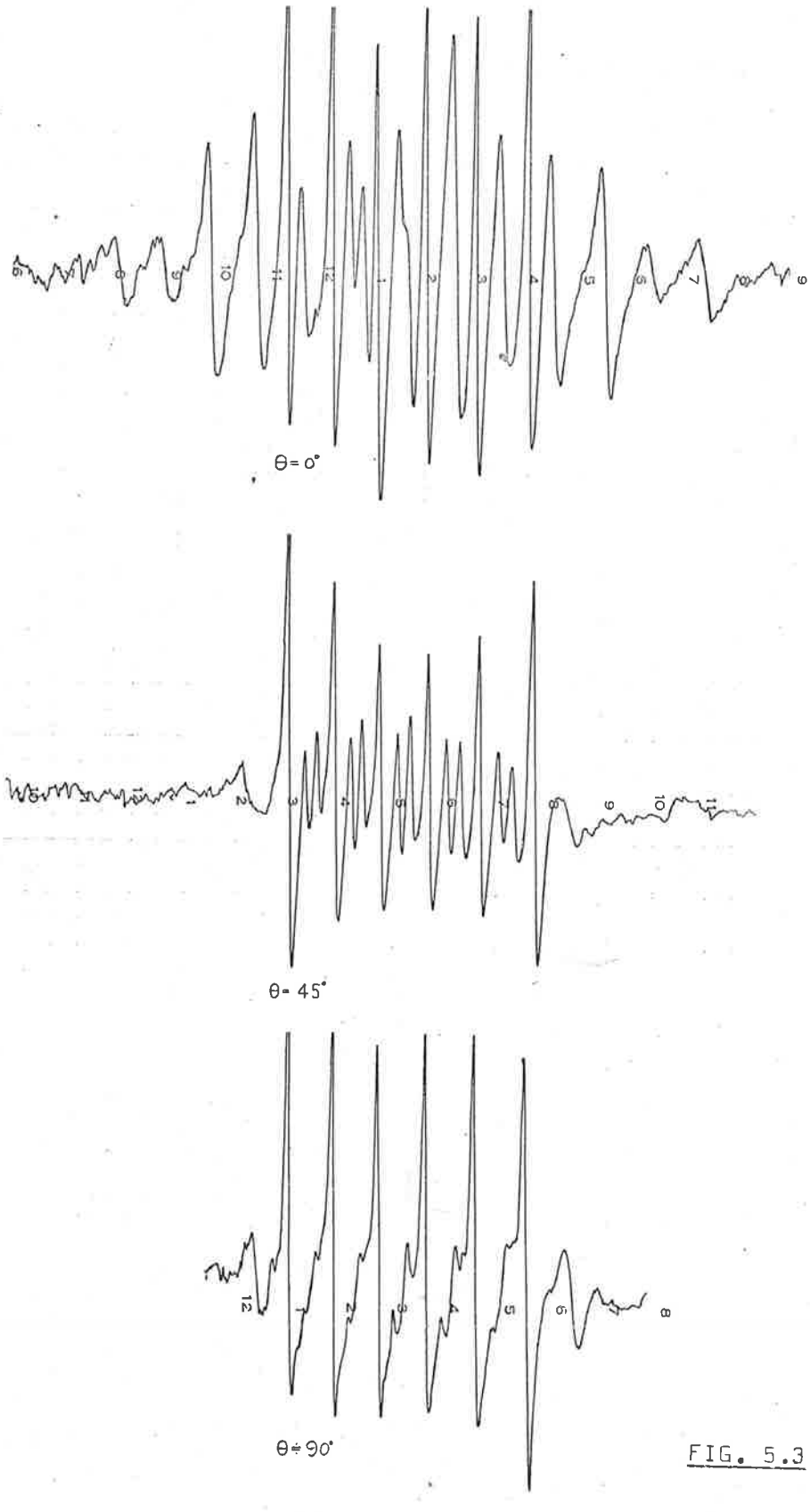

FIG. 5.3

unstrained crystal, our previous assignment of a $\sin^2 2\theta$ variation for forbidden transitions, and constant intensity for the allowed transitions is qualitatively (at least) justified. (Quantitatively the assumption of constant intensity for $\Delta m = 0$ lines is not justified.)

The predicted shifts for the forbidden transitions and components of the split allowed transitions, using the method described in the previous section, are shown in fig. 5.4.

From these calculated shifts we could thus expect:-

1) The spacings between the low field ($\theta = 90^\circ$) components of the split allowed transitions should be slightly less ($\sim$0.2 Oe) than spacings predicted using non-angular expressions.

2) Spacings between high-field ($\theta \sim 40^\circ$) components should be wider ($\sim$2 Oe) than predicted by the non-angular expression.

3) The forbidden doublets should be approximately midway between the High-field components of the allowed transitions.

Fig. 5.5 shows a spectrum recorded from powdered calcite. By comparison with spacings calculated using non-angular expressions, and by observation, it is readily seen that predictions 1-3 are confirmed experimentally.

5.3 Explanation of Observed Line Shifts in Adsorbed Mn^{2+} Spectra.

The observed shifts of the forbidden doublets relative to the mid points between the allowed transitions in the adsorbed ion spectrum, and other powder spectra mentioned earlier and now readily

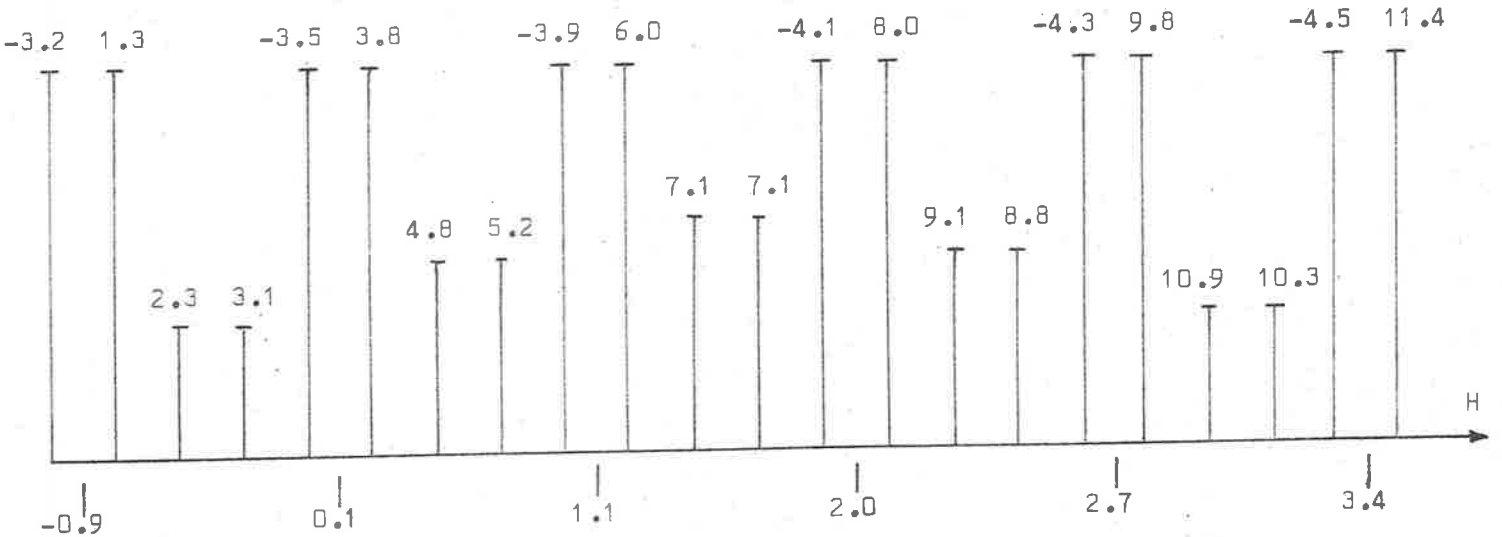

FIG. 5.4 : Shifts of Lines in Powder Spectra from Positions Calculated Using Non-Angular Expressions (Oe)

D = -81 Oe, A = -94 Oe, H_o = 3300 Oe, Q = 0

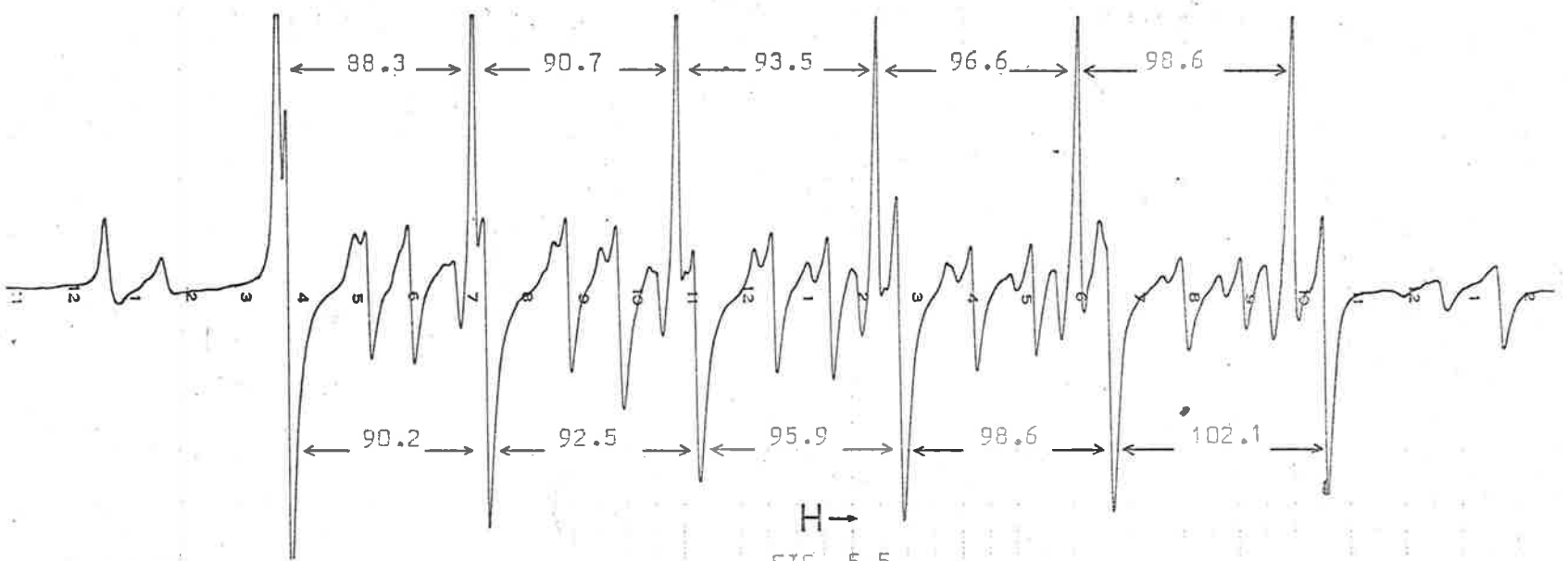

FIG. 5.5

SPACINGS CALCULATED (NON-ANGULAR EXPRESSION) :	88.3	91.0	93.7	96.4	99.1

explained. In a sample in which the lines are broadened by any mechanism, the component of each allowed transition may be so broad that only a single resonance for each allowed transition will be observed. The centre of this observed line will lie approximately midway between the centres of each unresolved component, and from fig. 5.4 we can readily see that the forbidden transitions will then be shifted towards the high field side of the spectrum more than the observed allowed transitions, with the relative shift between forbidden doublets and allowed lines increasing with field, as is observed experimentally. Experimentally this is also found for the spectrum of a powdered sample of calcite which contains a higher percentage of Mn^{2+} than the calcite sample which produced the spectrum discussed earlier. For this heavily doped sample, fig. 5.6, the lines are dipolar broadened, no splitting of the allowed transitions is observed, and forbidden doublets are seen to be shifted towards the high field side relative to the allowed transitions.

5.4 The Calculation of Parameters from Powder Spectra.

To further test the theory presented, a computer programme was written to evaluate parameters by a best-fit between theoretical and experimental line positions, using an iterative least squares method described by Marriage (1965).

The following assumptions were made:-

1. The position of lines in a powder spectrum are given by equations (3.12), (3.13) and (3.14),

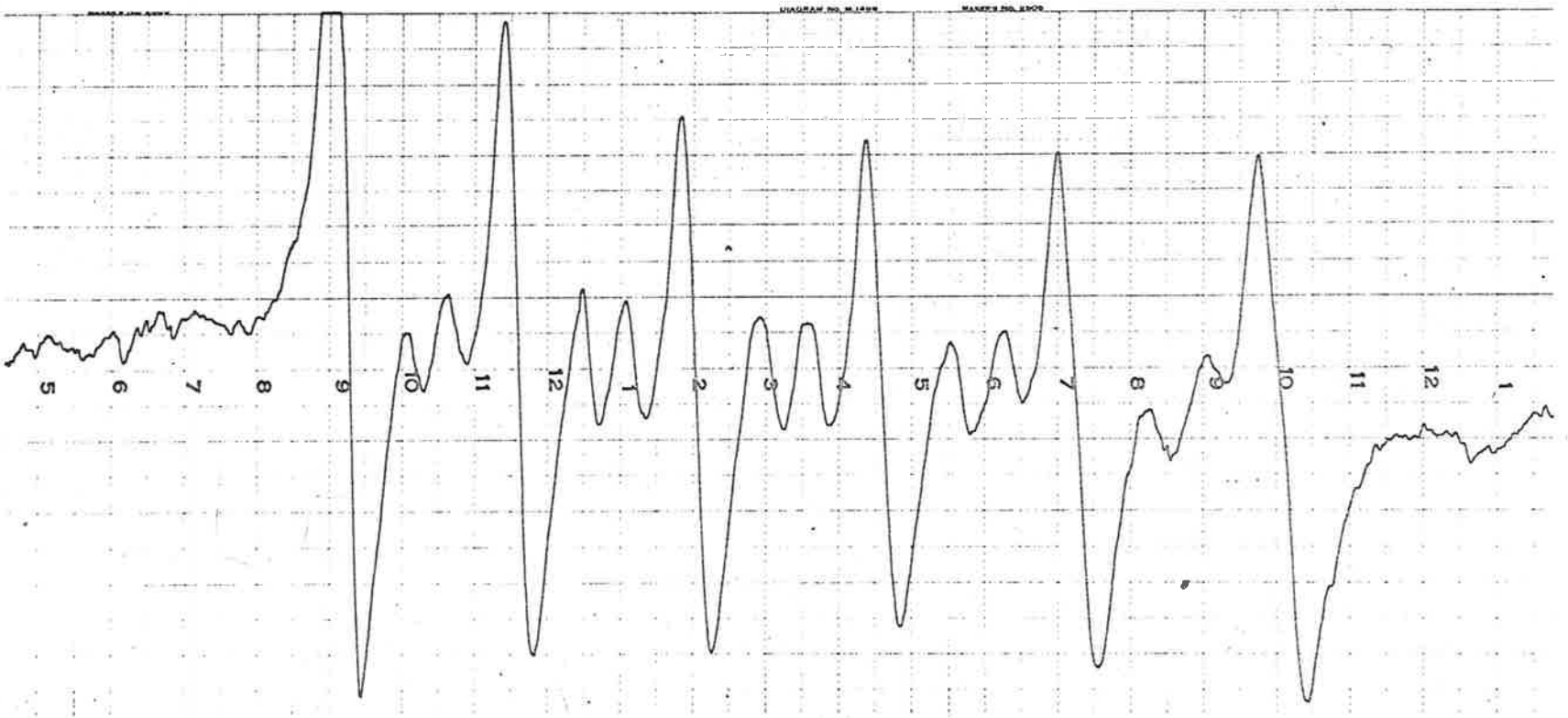

FIG. 5.6

Mn^{2+} IN POWDERED CALCITE

with $\theta = \pi/2$ and arc sin $\sqrt{\frac{-U_i}{V_i}}$ for allowed components, and

θ = arcsin $\sqrt{\frac{-U_i}{V_i}}$ for forbidden transitions.

2. When allowed components are broadened into a single observable line, the centre of this broadened line is at the mid-point of centres of the components.

The programme was tested on the broadened calcite powder spectrum shown previously in fig. 5.6. A best fit was obtained for the following value of parameters -

Powder		Single Crystal
A = 94.3 Oe		A = 94.0 Oe
D = -75.8 "	c.f.	D = -81.0 "
Q = - 0.2 "		

The theoretical line positions and spacings obtained for these values of the parameters for this powder spectrum, and the experimentally determined values, are shown in table 5.1. The theoretical values are shown in brackets.

Table 5.1:

Experiment and Theoretical Line Positions and Spacings for Mn^{2+} in Powdered Calcite (X-Band-Room Temperature)

Line Spacings (Oe)		Line Positions (Oe)
		3,065.5 (3,064.3)
	36.0 (36.8)	
		3,101.5 (3,101.1)
88.4 (89.5)	20.7 (21.1)	
		3,122.2 (3,122.2)
	31.7 (31.6)	
		3,153.9 (3,153.8)
	37.3 (38.2)	
		3,191.2 (3,192.0)
91.8 (92.2)	23.1 (23.4)	
		3,214.3 (3,215.4)
	31.4 (30.6)	
		3,245.7 (3,246.0)
	39.6 (39.5)	
		3,285.3 (3,285.5)
94.6 (94.8)	25.4 (25.4)	
		3,310.7 (3,310.9)
	29.6 (29.9)	
		3,340.3 (3,340.8)
	41.8 (40.9)	
		3,382.1 (3,381.7)
97.8 (98.4)	26.6 (27.2)	
		3,408.7 (3,408.9)
	29.4 (29.3)	
		3,438.1 (3,438.2)
	43.1 (42.3)	
		3,481.2 (3,480.5)
100.2 (100.1)	28.5 (28.8)	
		3,509.7 (3,509.3)
	28.6 (29.0)	
		3,538.3 (3,538.3)

Better agreement between the parameters determined from this powder spectrum,and parameters determined by single crystal measurements, may be obtained however, if it is assumed that a small relative shift of lines may occur as outlined in the next section.

5.5 Line Shifts due to Line Shape Functions.

By previous theory, the line shape or intensity functions, used to predict peaks in powder spectra, have infinite values at certain points. In practice the value of the intensity at these points must be finite, and it could be expected that for (say) the allowed transitions the line shape functions would rise gradually to maxima at $\theta \sim 40^{\circ}$ and $\theta = 90^{\circ}$, as shown exaggerated in fig. 5.7, together with a line shape function drawn (qualitatively) as a function of field strength. The resultant shape of the absorption curve expected may then be calculated from the I'(H) function by assuming a line shape (Lorentzian or Gaussian generally), and summing the contributions at each point, of the Lorentzian or Gaussian lines (modulated by the appropriate value of the intensity function I'(H)) originating from all points at which resonance may occur. If this is done it is readily seen, as shown in fig. 5.8, that the maxima of the resultant absorption curve do not coincide with maxima of the intensity function I'(H), i.e., the peaks in a powder spectrum would be shifted from field positions corresponding to $\theta = 90^{\circ}$ and $\theta \sim 40^{\circ}$ by an amount determined by both the shape of

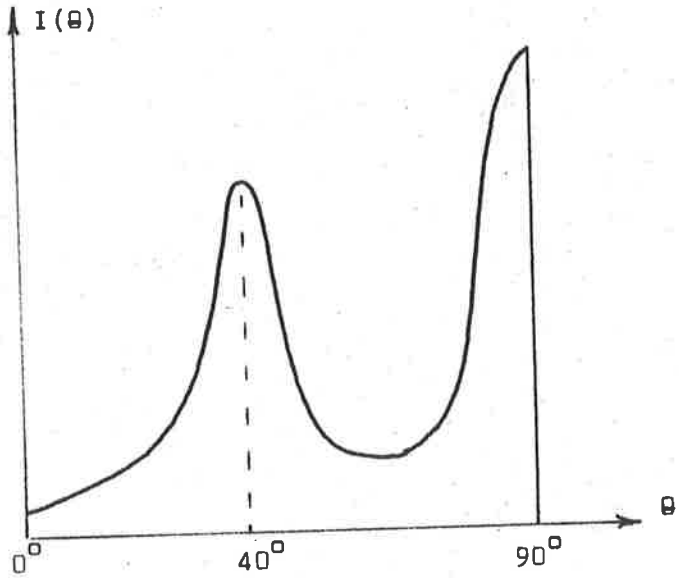

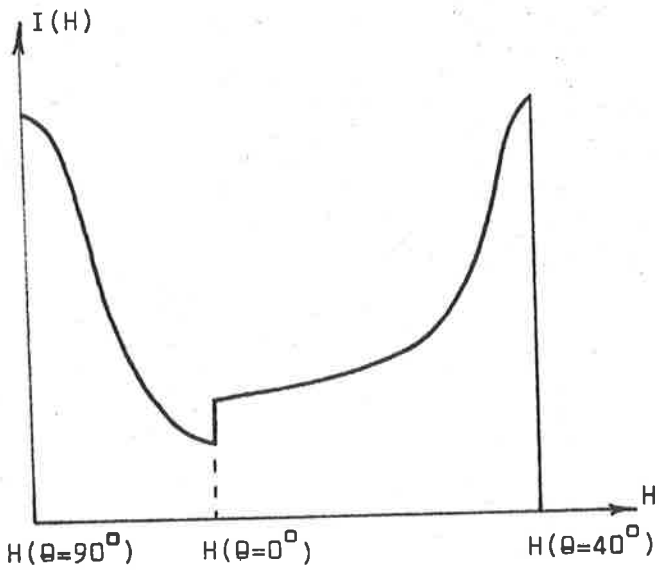

FIG.5.7

LINE SHAPE FUNCTIONS vs θ & H

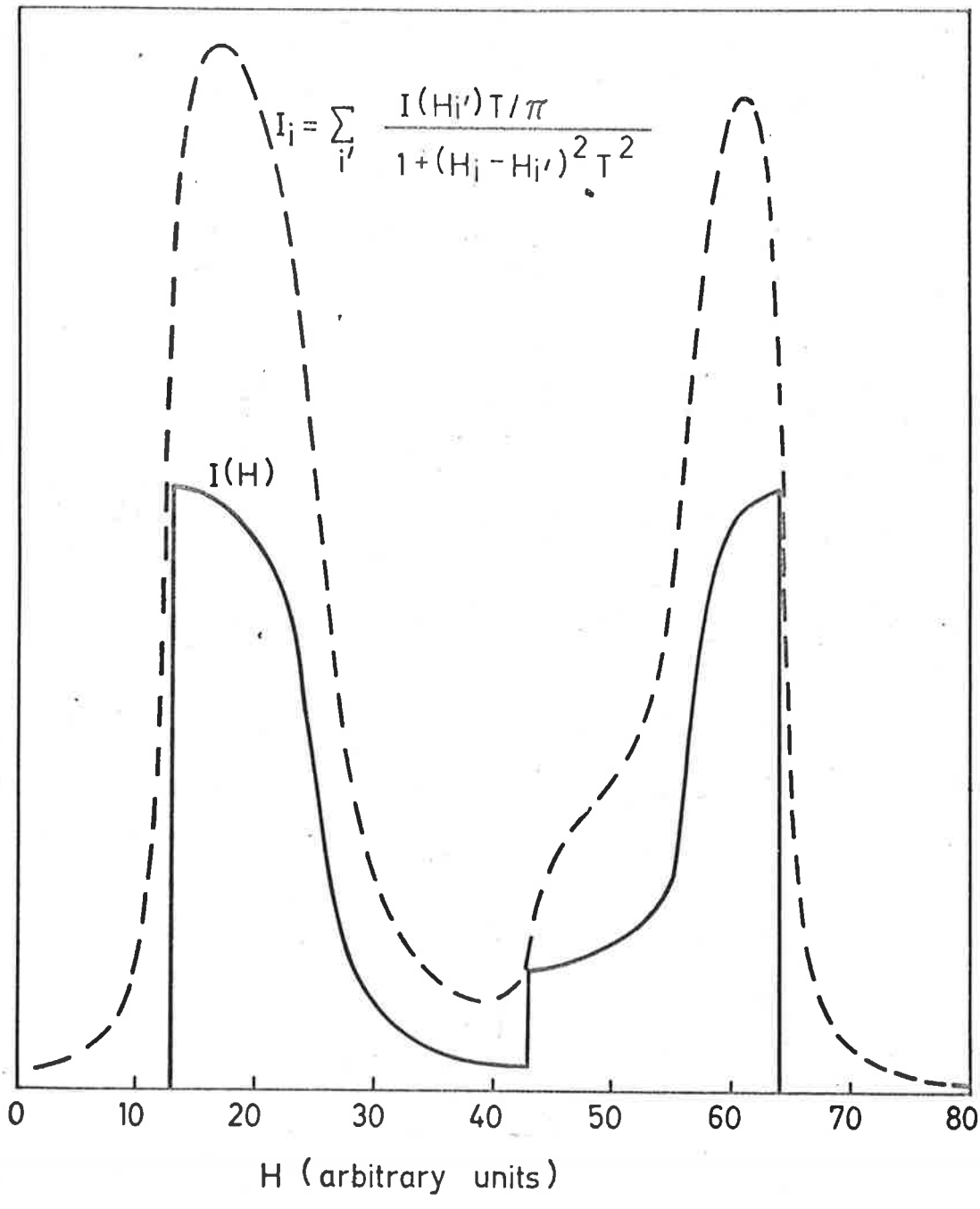
$I_j = \sum_{i'} \frac{I(H_{i'})T/\pi}{1+(H_j - H_{i'})^2 T^2}$
I(H)
0
10
20
30
40
50
60
70
80
H (arbitrary units)

FIG.5.8

the intensity or line shape function, and the natural line-widths of the resonance lines. From fig. 5.8 it may be seen that the $\theta \sim 40^{o}$ components would be shifted towards the low field side and $\theta = 90^{o}$ components shifted towards the high field side, by such a mechanism. We might then expect that the splitting of the allowed hyperfine lines in a powder spectrum, would be less than the field difference between turning points of the $H(\theta)$ variation. Experimentally this appears to be the case for the splitting of the hyperfine lines in the calcite spectrum shown earlier in fig. 5.5. Theoretically a field difference of 15.9 Oe between turning points of the $H(\theta)$ variation for the $m = {}^{+}5/2$ transitions, is predicted using line positions listed in section 3.5. Experimentally, a field difference of 15.3 ($\pm$ 1.0) Oe was found for turning points in the ($m = {}^{+}5/2$) line position observed, as a single crystal of calcite is rotated in the applied field. The measured splitting of the $m = {}^{+}5/2$ allowed transition in the calcite powder spectrum, shown in fig. 5.5, is found to be 14.3 ($\pm$ 1.0) Oe however, indicating a possible shift of powder lines of $\sim$0.5 Oe. Conversely, it might be expected that a determination of 'D' from observed splitting of allowed transitions in a powder spectrum, would yield of value of 'D' slightly lower than that obtained from single crystal measurements. It may be noted that Bleaney & Rubins calculated a value of $|D| = 70\text{-}80$ Oe from the splitting of allowed transitions observed in the spectrum of plasticine (calcite), which may be compared to the single crystal value, $|D| = 81$ Oe.

In a powder spectrum in which the $\theta \sim 40^{\circ}$ and $\theta = 90^{\circ}$ components of an allowed transition are broadened into a single line, the field position of this broadened line may not be shifted by this mechanism. The $\theta \sim 40^{\circ}$ forbidden doublets would, however, be shifted towards the low field side relative to the observed allowed transitions. If this were so, it would be expected that the parameter fitting method, described in the previous section would return values of parameters closer to single crystal values, if small positive increments were artificially added to each of the experimentally determined forbidden line positions, or a small equivalent negative shift included in the theoretical expression for forbidden line positions. Such was found to be the case.

As increments are added to each of the experimental forbidden line positions, shown in table 5.1, the values of the parameters A and D determined by the parameter fitting programme, decrease and increase, respectively.

The best fit between the values of parameters determined from single crystal measurements (A = - 94.0 Oe and D = - 81.0 Oe) and values determined from the calcite powder spectrum (A = - 94.2 Oe D = - 81.4 Oe) was obtained when an increment of 0.8 Oe was added to each of the forbidden line positions, e.g. 3102.3 Oe c.f. 3101.5 Oe, used for the first forbidden line position, etc.

As well, for this value of the increment, the sum of the squares of the differences of experimental and theoretical line

positions (denoted S) is smaller (4.09 Oe^2) than calculated when no increment has been added (4.58 Oe^2).

The parameter fitting programme was also applied to line positions given by Waldner (1962), for Mn^{2+} in powdered $MgAl_2O_4$. For this spectrum, however, the sign of the parameter 'D' is not known. The third-order corrections to line positions contain a term in DA^2/H_o^2, and the sign of this term, depends on the sign of 'D'. It was thus necessary to obtain best-fits for the parameters of this spectrum, for both negative and positive 'D'. Without the addition of increments to forbidden line positions, the following parameters were determined from the fourteen line positions listed by Waldner.

	D (+ ve)	D (- ve)
A =	-80.9 Oe	- 80.8 Oe
D =	52.3 "	- 52.0 "
Q =	0.17 "	- 0.12 "
S =	1.13 Oe^2	0.47 Oe^2

As evidenced by the relatively small values of S, an extremely good fit between theory and experiment is obtained.

Lower values of S were again obtained, however, by the addition of increments to forbidden line positions. The parameters corresponding to the minimum values of S, together with the corresponding increments, were:-

	D (+ ve)	D (- ve)
A =	- 80.6 Oe	- 80.8 Oe
D =	66.9 "	- 53.2 "
Q =	0.2 "	- 0.12 "
S =	0.76 Oe^2	0.46 Oe^2
Increments =	1.6 Oe	0.2 Oe

It must be noted, however, that the better agreement obtained for parameters obtained from single crystal measurements and powder spectra measurements, by the addition of a small increment to forbidden line positions in powder spectra, to compensate for a shift attributed to the line shape factor, may also be explained, if one of our original assumptions in section 5.4 is incorrect. It was there assumed that in a broadened spectrum,the line position for an observed allowed transition lies midway between the line positions of the broadened components. If the line position of an allowed transition in a broadened spectrum does in fact lie towards the high field side of the midpoint of line positions of the components, by a small amount, the spacings between forbidden and allowed lines would differ by this amount from that predicted, by the method described in the previous section. A small increment added to the measured forbidden line positions observed in the powder spectrum, would then produce closer agreement with single crystal parameters using the best-fit method described, with assumption (2) of section 5.4 taken to be valid.

A more detailed investigation of a comparison of line positions at turning points of the H(θ) variation observed with single crystals, and line positions in powder spectra, is planned in an attempt to clarify the mechanism(s) for this small relative shift of the forbidden doublets in powder spectra. The addition of small increments to the experimentally determined forbidden line positions does produce an increase of the parameter 'D' and a decrease of the parameter 'A' using the method described in the previous section. The values of these parameters determined using this method, without the addition of increments, may be taken as an indication of lower and upper limits of 'D', and 'A', respectively.

5.6 Parameters for the Adsorbed Mn^{2+} Spectrum.

Gorter (1932) has shown that the axial field parameter 'D' is positive when an ion site is surrounded by an octohedran of water molecules, which is the case for the adsorbed Mn^{2+} ion. The parameters then obtained for the spectrum of Mn^{2+} adsorbed on the ion-exchange resin shown in fig. 1.2, by the method previously described in section 5.4, were:-

$$A = -96.4 \text{ Oe}$$

$$D = 78.6 \text{ "}$$

$$Q = 0.8 \text{ "}$$

$$H_o = 3270.0 \text{ "}$$

A comparison of experimentally determined line positions and spacings, and corresponding values calculated for these values of the parameters, are shown in table 5.2. Theoretical values are shown in brackets.

Table 5.2:

Line Positions and Spacings for Mn^{2+} Adsorbed on Amberlite IR-120(H) Ion-Exchange Resin.

(X-Band : T = ~~90~~ 77 °K)

m	Line Spacings (Oe)		Line Positions (Oe)
-5/2			3,026.0 (3,025.1)
		37.0 (37.7)	
			3,063.0 (3,062.8)
	90.5 (91.5)	23.5 (23.8)	
			3,086.5 (3,086.6)
		30.0 (29.8)	
-3/2			3,116.5 (3,116.4)
		39.0 (39.1)	
			3,155.5 (3,155.5)
	93.4 (94.2)	24.5 (25.2)	
			3,180.0 (3,180.7)
		29.9 (29.9)	
-1/2			3,209.9 (3,210.6)
		41.0 (40.5)	
			3,251.0 (3,251.1)
	97.0 (97.0)	26.0 (26.6)	
			3,277.0 (3,277.7)
		29.9 (30.5)	
1/2			3,306.9 (3,307.6)
		43.6 (41.9)	
			3,350.5 (3,349.5)
	100.7 (99.8)	27.0 (27.9)	
			3,377.5 (3,377.4)
		30.1 (30.0)	
3/2			3,407.6 (3,407.4)
		43.6 (43.4)	
			3,451.0 (3,450.8)
	102.9 (102.6)	28.0 (28.8)	
			3,479.5 (3,479.7)
		31.0 (30.3)	
5/2			3,510.5 (3,510.0)

For these line positions, S = 4.2 Oe^2. A minimum of S occurs at 4.07 Oe^2 for a shift of the forbidden doublets of 0.7 Oe, with the following values of parameters:-

$$A = -96.2 \text{ Oe}$$

$$D = 83.4 \text{ "}$$

$$Q = 0.8 \text{ "}$$

$$H_o = 3270.0 \text{ "}$$

From the Bleaney & Rubins' expression, equation (4.13), a $\frac{1}{H}$ variation is predicted for the relative intensity of forbidden transitions. Fig. 5.9 shows the spectrum of Mn^{2+} adsorbed on Amberlite resin, recorded on the Q-band microwave spectrometer at the Department of Physics, Monash University, by courtesy of Mr. Gordon Troup. The doublets, which have a relatively large intensity in X-band spectra, are barely resolvable at the higher frequency.

The line positions of these doublets, and the intensity variation with applied frequency and magnetic field, are then adequately explained if these doublets are forbidden transitions, as originally postulated.

From the relative intensity of these forbidden doublets, a value of the parameter 'D' of $\sim \pm$ 100 Oe, is obtained by using the method of Bleaney & Rubins, discussed in section 4.2. This estimation of the parameter 'D' is then $\sim$ 25% larger than the value calculated from line positions. Other powder spectra were shown to predict values larger than single crystal values by > 50%. As

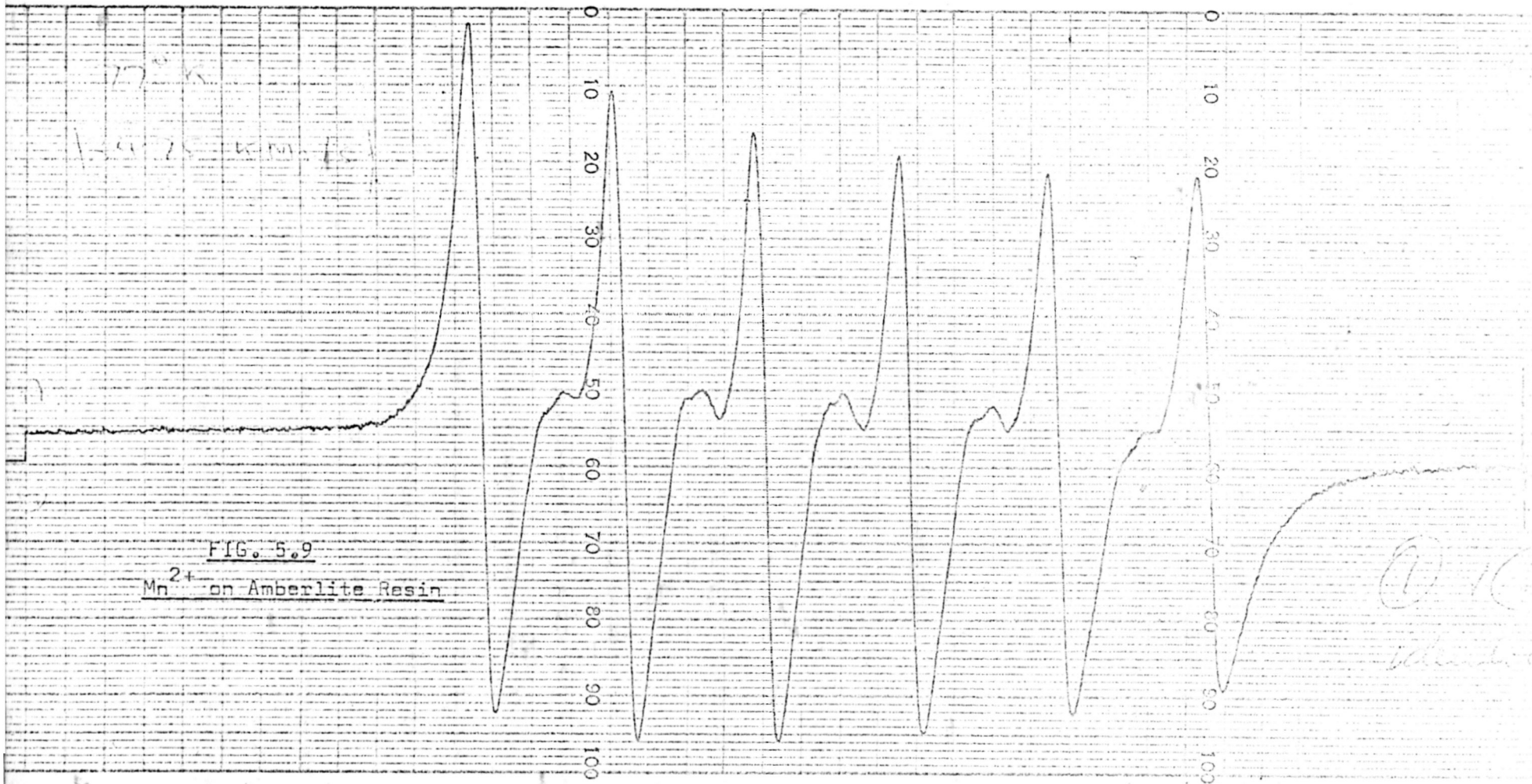

FIG. 5.9

Mn^{2+} on Amberlite Resin

ade in Australia by J. J. MILLER Ptg. Co. Melb.
Type 5A Maker's No. 735

shown later in section 8.3, a rhombic component of the crystal field may reduce the relative intensity of forbidden transitions in powder spectra. The overestimation of the parameter 'D' by only $\sim 25\%$, compared with the value obtained from line position measurements, may then be taken as a possible indication that a small rhombic component is present in the crystal field at the adsorbed Mn^{2+} ion site.

5.7 The Determination of the Parameter 'A' from Powder Spectra Using Non-Angular - Dependent Expressions.

From the predicted shifts shown in fig. 5.4, it may be seen that if the components of allowed transitions are broadened into a single observed peak, the centres of the measured allowed transitions will have field separations wider than those predicted or calculated using only non-angular expressions. Conversely, it could be expected, that if experimentally determined spacings between the observed allowed peaks, and non-angular theoretical expressions were used to calculate the magnitude of the hyperfine parameter 'A', a value of A larger by ~ 1 Oe than the value as determined by single crystal measurements would be obtained. Experimentally this is found for the broadened calcite powder spectrum shown in fig. 5.6, for which a value of A = - 95.4 Oe was determined using non-angular expressions. This value may be compared to the value of A = 94.0 Oe obtained from single crystal measurements (Hurd et al 1954), and the

value of A = -94.3 Oe obtained using the method described in section 5.4. Similarly, the value of A = -97.3 Oe, determined from experimental line positions of the adsorbed Mn^{2+} ion in section 1.3, is higher by $\sim$1 Oe, than the value obtained when angular terms and shifts are used, as given in the previous section.

5.8 Failure of Theory to Explain Features of Other Observed Spectra.

The theory of powder spectra as presented has only limited application, as a brief survey of spectra from available powder samples, containing Mn^{2+} in trace amounts, quickly showed. The theory of Bleaney & Rubins, as presented and applied to explain features of the powder spectra of Mn^{2+} in sites of electrostatic crystal field symmetry characterized by an axial field parameter |D| of less than $\sim$100 Oe, is unable to even qualitatively explain features observed in high-D Mn^{2+} powder spectra. For example, if we consider the powder spectrum of Mn^{2+} in apatite ($Ca_{10}(PO_4)_6(F,Cl)$), reported by Kasai (1962), we find that for the values of |D| $\sim$ 433 Oe, and |A| $\sim$ 96 Oe, obtained from single crystal measurements (Burley 1964), we should expect to find, using the Bleaney & Rubins' theory, a splitting of the allowed hyperfine lines of the order of hundreds of oersted. It is immediately seen, however, on inspection of the spectrum shown by Kasai, or the spectrum of a powdered sample of apatite from Erenfriedersdorf, fig. 5.10, which contains Mn^{2+} ion impurities, that no splitting of the allowed transitions is

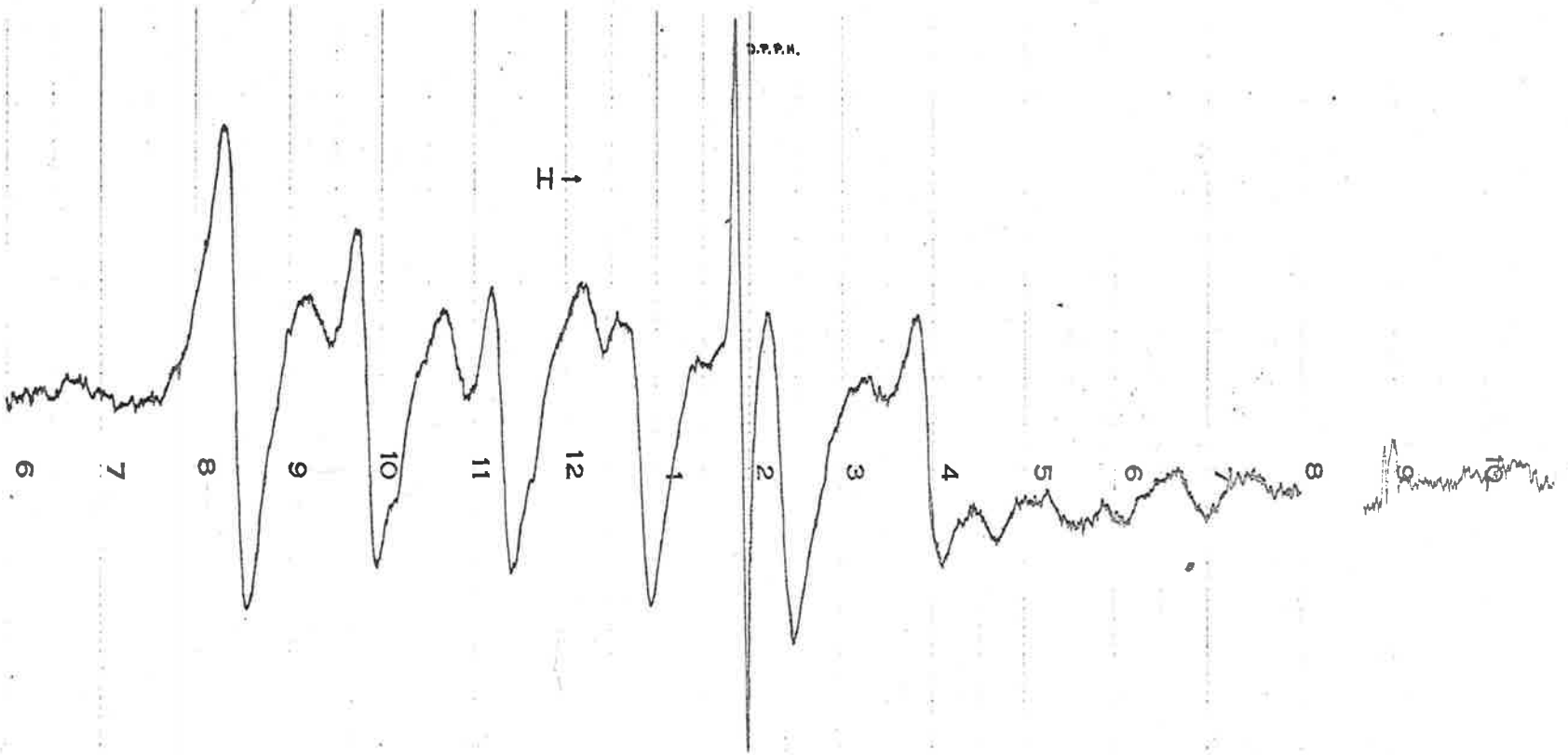

FIG. 5.10

Mn^{2+} SPECTRUM FROM POWDERED APATITE

observable at all. As well, no forbidden doublets are resolvable, whereas the simple expression for forbidden transition intensities derived by Bleaney & Rubins (1961) predicts, that for this value of D, the forbidden transitions would rival the allowed transitions in intensity. For intermediate values of the axial parameter D, the powder spectra are extremely complex. Fig. 5.11 shows the Mn^{2+} spectrum recorded from a powdered sample of Scheelite ($CaWO_4$), for which from single crystal measurements the Mn^{2+} ion is in a site for which $|D| \sim 150$ Oe (Lyons and Kedzie, 1966). For both spectra, complete line identification is not possible with any degree of certainty by existing theory. However, as will now be outlined, interpretation of all Mn^{2+} powder spectra is obtained when exact methods are used to predict intensity variations.

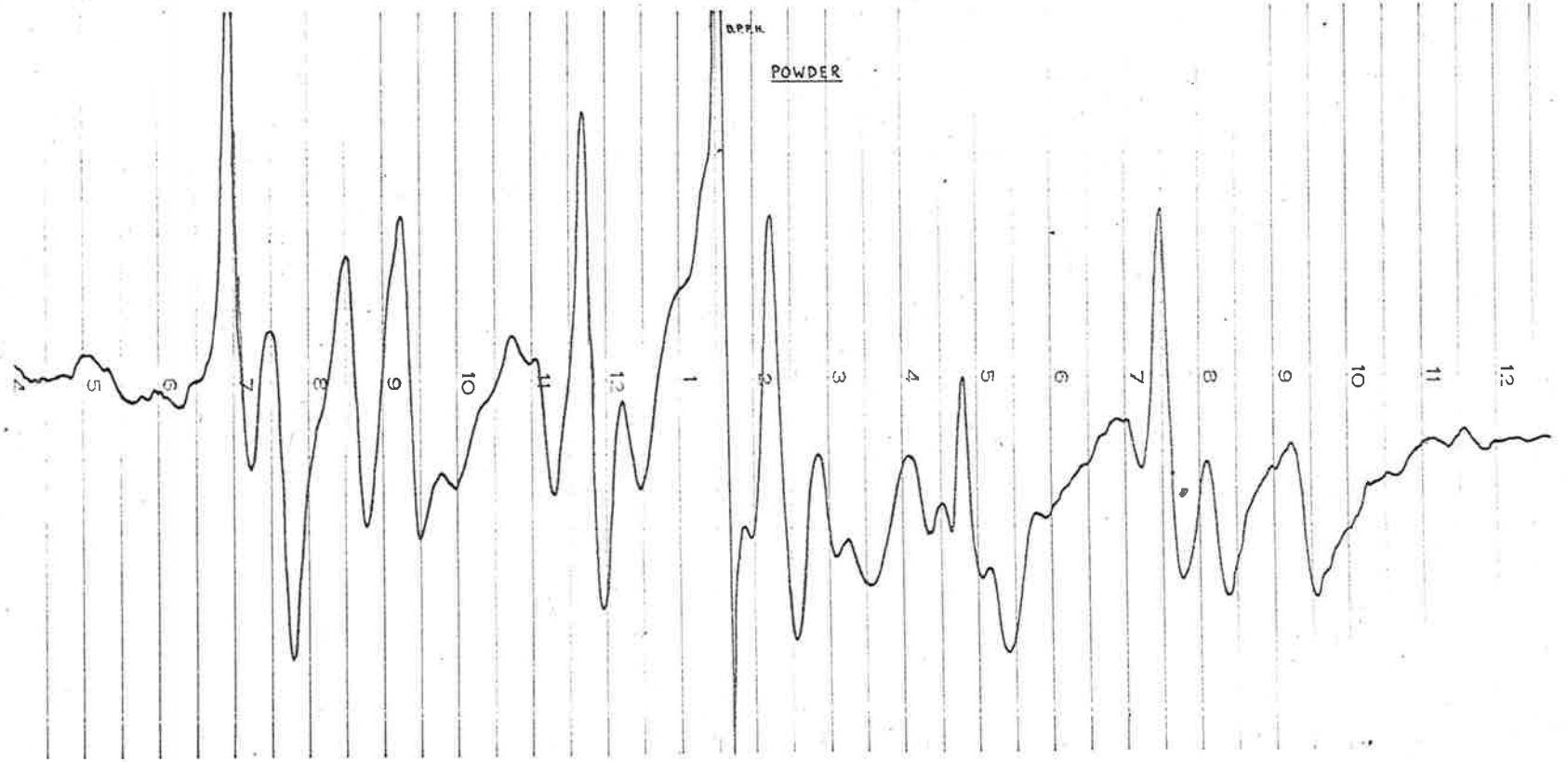

FIG. 5.11

Mn^{2+} SPECTRUM FROM POWDERED SCHEELITE

CHAPTER VI

TRANSITION PROBABILITIES - BIR'S METHOD.

6.1 Introduction

The expression for the variation of intensity of the forbidden transitions as derived by Bleaney & Rubins has only limited application, as acknowledged by these authors themselves. When the axial crystal field splitting is large, perturbation methods are no longer accurate enough, and it is necessary to use exact methods to obtain intensity variations, as outlined in section 4.4. Simplification of the computations necessary may be made by using a method given by Bir (1964).

The derivation of expressions, which enables a calculation of intensities for the case of trigonal symmetry, is now given, including terms in the parameter "a" which Bir has neglected because of their general smallness.

6.2 General Theory

Bir considered that when hyperfine interaction occurred, the direction of quantization for the nuclear spin was not the direction of the applied field, but instead the direction of the effective field due to the magnetic moment of the unpaired electron. This effective field was much larger than the applied field, and its direction depended on the electron state and the angle θ between the applied field and the axis of the crystalline field. The dependence of the effective field on the electron state, then led to

a non-orthogonality between the nuclear spin functions for different electron states, and the nuclear spin projections, which resulted in the $\Delta m = \pm 1$ transitions becoming allowed, with a corresponding reduction in the normal allowed transitions.

Bir considered that the eigenfunction $\Phi_{M,m}$, which diagonalized the Spin Hamiltonian, could be written as a product of electron and nuclear functions.

i.e. $$\Phi_{M,m} = \Psi_M \cdot \phi_m^{(M)} \qquad (6.1)$$

where Ψ_M is the eigenfunction which diagonalized the fine structure Hamiltonian, and $\phi_m^{(M)}$ were nuclear spin functions corresponding to an electron state, denoted (M). If ϕ_m^o represented eigenfunctions in the absence of a crystal field, the $\phi_m^{(M)}$ could be expressed as a linear combination

$$\phi_m^{(M)} = \sum_{m''} D_I^{mm''}(g^{(MH^o)})\, \phi_{m''}^o \qquad (6.2)$$

where the $D_I^{mm''}(g^{(MH^o)})$ were matrix elements of the irreducible representation of the rotation group of weight I = 5/2, and $g^{(MH^o)}$ is the transformation which rotates the direction of the effective field H^o in the absence of a crystal field, to the direction of the effective field H^M for a given electron state, when a crystal field was present at the site of the ion. The components of the field, H^M, could be found by calculating the expectation value of the electron spin in the state denoted (M).

i.e. $$H_\alpha^{(M)} = \frac{A}{g_N \beta_N} (\Psi_M | S_\alpha | \Psi_M) \qquad (\alpha = x,y,z) \qquad (6.3)$$

Bir then showed that the transition probability between states labelled (M,m) and (M',m') was proportional to the product of the square of the modulus of the matrix element of the electronic transition (which produced only small angular variations of intensity), and the square of the modulus of the product of the spin functions $\Phi_m^{(M)}$ and $\Phi_{m'}^{(M')}$, which was strongly angular dependent.

i.e. $$I \text{ (angular)} \propto \left| \Phi_m^{(M)} \Phi_{m'}^{(M')} \right|^2 \qquad (6.4)$$

Bir then derived -

$$I \propto \left| d_I^{mm'} (\mu_{MM'}) \right|^2 \qquad (6.5)$$

where the $d_I^{mm'} (\mu_{MM'})$ are known functions and $\mu_{MM'} = \cos \alpha_{MM'}$, with $\alpha_{MM'}$, the angle between the quantization axis of the nuclear spin for electronic states M and M'.

This expression for the intensity is correct for the transitions $M = \pm 5/2 \longleftrightarrow M = \pm 3/2$, and $M = \pm 3/2 \longleftrightarrow M = \pm \frac{1}{2}$, but is not strictly correct for the central hyperfine sextet ($M = \frac{1}{2} \longrightarrow M = -\frac{1}{2}$). This is shown most easily by considering axial symmetry, for which the effective field has components, using Bir's expressions, for a general angle θ between the applied field and the crystal field axis

$$\begin{aligned} H_x &\propto M^2 - \tfrac{1}{3} S(S+1) \\ H_y &= 0 \\ H_z &\propto M \end{aligned} \qquad (6.6)$$

The effective field directions for the (2S+1) electronic states, is then shown diagramatically in fig. 6.1. In the absence of a

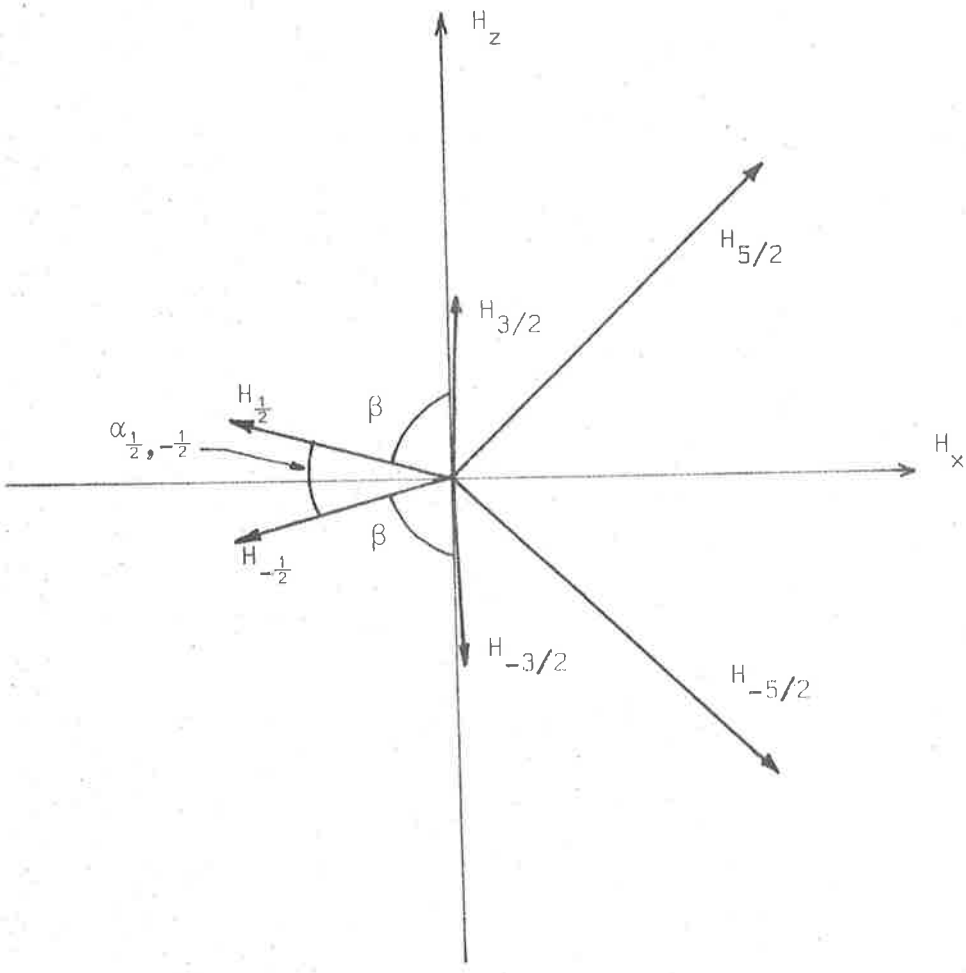
H_z
$H_{5/2}$
$H_{3/2}$
$H_{\frac{1}{2}}$
$\alpha_{\frac{1}{2},-\frac{1}{2}}$
β
H_x
β
$H_{-\frac{1}{2}}$
$H_{-3/2}$
$H_{-5/2}$

FIG. 6.1

crystal field the expectation values of S_x and S_y are zero, and hence H_x and H_y are both zero, and the direction of the effective field acting at the nucleus, is then parallel to the direction of the applied field for electronic states $M = +5/2, +3/2$ and $+\frac{1}{2}$, and antiparallel for $M = -\frac{1}{2}, -3/2$ and $-5/2$.

With our convention for positive rotation, defined in section 2.2, we then have for our expansions:-

$$\phi_m^{(+\frac{1}{2})} = \Sigma_{m''} D_I^{mm''}(g^{(+\frac{1}{2},H^o)})\, \phi_{m''}^{(o)} \quad \text{with} \quad g^{(+\frac{1}{2},H^o)} = +\beta$$

Similarly -

$$\phi_{m'}^{(-\frac{1}{2})} = \Sigma_{m''} D_I^{m'm''}(g^{(-\frac{1}{2},H^o)})\, \phi_{m''}^{(o)} \quad \text{with} \quad g^{(-\frac{1}{2},H^o)} = -\beta$$

Then -

$$I \propto \left| \Sigma_{m''} D_I^{mm''}(\beta)\, D_I^{m'm''}(-\beta) \right|^2 \quad \text{using} \quad \phi_m^o \phi_{m'}^o = \delta_{mm'}$$

$$= \left| \Sigma_{m''} d_I^{mm''}(\beta)\, d_I^{m'm''}(-\beta) \right|^2$$

$$= \left| \Sigma_{m''} d_I^{mm''}(\beta)\, d_I^{m''m'}(\beta) \right|^2 \quad \text{as} \quad d_I^{m'm''}(-\beta) = d_I^{m'',m'}(\beta)$$

$$= d_I^{mm'}(2\beta)^2 \quad \text{from the closure properties of the } d_I^{mm'}$$

From the diagram, $2\beta = \pi - \alpha_{\frac{1}{2},-\frac{1}{2}}$ whence:

$$I \propto \left| d_I^{mm'}(\pi - \alpha_{\frac{1}{2},-\frac{1}{2}}) \right|^2 \quad \text{or as a function of } \mu_{\frac{1}{2},-\frac{1}{2}} = \cos\alpha_{\frac{1}{2},-\frac{1}{2}}$$

$$I \propto \left| d_I^{mm'}(-\mu_{\frac{1}{2},-\frac{1}{2}}) \right|^2 \qquad (6.7)$$

The non-appearance of the negative sign in the general expression given by Bir for the transition probability, is compensated by the

non-appearance ofanegative sign, when $M = \frac{1}{2} \longrightarrow M = -\frac{1}{2}$, in his general expression for $\mu_{M,M'}$, as will be shown later.

For the functions $d_1^{mm'}(\mu)$, Bir has used the expressions listed by Gel'fand et al (1963), viz. :-

$$d_I^{m'm'}(\mu_{MM'}) = \frac{(-1)^{I-m}}{(I-m)!} \cdot \frac{i}{2}^{m'-m}_I \cdot \sqrt{\frac{(I-m)!(I+m')!}{(I+m)!(I-m')!}}$$

$$\cdot(1-\mu)^{\frac{-(m'-m)}{2}} \cdot(1+\mu)^{\frac{-(m'+m)}{2}} \cdot \frac{d}{d\mu}^{I-m'}_{I-m'}((1-\mu)^{I-m} \cdot (1+\mu)^{I+m})$$

For continuity, we will use the equivalent expression defined in section 2.2

$$d_I^{mm'}(\mu_{MM'}) = \sum_n (-1)^{m'-m+n} \sqrt{\frac{(I+m)!(I-m)!(I+m')!(I-m')!}{n!(I+m-n)!(I-m'-n)!(n+m'-m)!}}$$

$$\cdot \frac{1+\mu}{2}^{\frac{2I-2n+m-m'}{2}} \cdot \frac{\mu-1}{2}^{\frac{2n+m'-m}{2}} \qquad (6.8)$$

For the $M = \frac{1}{2} \longrightarrow M = -\frac{1}{2}$ transitions, the intensities for allowed and forbidden lines are then :-

Allowed $(\Delta m = 0)$

m	$\pm 5/2$	$\pm 3/2$	$\pm \frac{1}{2}$
	$\left\| d_{5/2}^{5/2,5/2}(-\mu) \right\|^2$	$\left\| d_{5/2}^{3/2,3/2}(-\mu) \right\|^2$	$\left\| d_{5/2}^{\frac{1}{2},\frac{1}{2}}(-\mu) \right\|^2$

Forbidden ($\Delta m = \pm 1$)

m	$\pm 3/2 \leftrightarrow \pm 5/2$	$\pm\frac{1}{2} \leftrightarrow \pm 3/2$	$\frac{1}{2} \leftrightarrow -\frac{1}{2}$
	$\left\| d^{5/2,3/2}_{5/2}(-\mu) \right\|^2$	$\left\| d^{3/2,\frac{1}{2}}_{5/2}(-\mu) \right\|^2$	$\left\| d^{\frac{1}{2},\frac{1}{2}}_{5/2}(+\mu) \right\|^2$

where we have used $\left\| d^{m,m'}_{I}(\mu) \right\|^2 = \left\| d^{m',m}_{I}(\mu) \right\|^2$

and $\left\| d^{m,-m'}_{I}(\mu) \right\|^2 = \left\| d^{m,m'}_{I}(-\mu) \right\|^2$

For the expressions of interest we obtain using equation 6.8 :-

$$\left\| d^{5/2,5/2}_{5/2}(-\mu) \right\|^2 = \left(\frac{1-\mu}{2}\right)^5 \qquad (6.9\ a)$$

$$\left\| d^{3/2,3/2}_{5/2}(-\mu) \right\|^2 = \left(\frac{1-\mu}{2}\right)^3 \left(\frac{3+5\mu}{2}\right)^2 \qquad (6.9\ b)$$

$$\left\| d^{\frac{1}{2},\frac{1}{2}}_{5/2}(-\mu) \right\|^2 = \left(\frac{1-\mu}{2}\right)\left(\frac{5\mu^2+2\mu-1}{2}\right)^2 \qquad (6.9\ c)$$

$$\left\| d^{5/2,3/2}_{5/2}(-\mu) \right\|^2 = 5\left(\frac{1-\mu}{2}\right)^4 \left(\frac{1+\mu}{2}\right) \qquad (6.9\ d)$$

$$\left\| d^{3/2,\frac{1}{2}}_{5/2}(-\mu) \right\|^2 = \left(\frac{1-\mu}{2}\right)^2 (1+\mu)(1+5\mu)^2 \qquad (6.9\ e)$$

Note that the power of three is missing in the equivalent expression for (6.9 b), given by Bir & Sochava (1964), and the error has been duplicated by Manoogion (1968).

In the absence of a crystal field we have $\alpha\ \frac{1}{2},-\frac{1}{2} = \pi \rightarrow \mu = -1$. The intensity of the allowed transitions is then unity, i.e. no change with angular variation, and the probability of transition for $\Delta m = \pm 1$ is zero.

6.3 Components of the Effective Field for Trigonal Symmetry.

To derive an analytic expression for μ ($= \cos\alpha_{MM'}$), we must first derive expressions for the components of the effective field:-

$$H_\alpha^M = \frac{A}{g_N \beta_n} (\Psi_M | S_\alpha | \Psi_M) \quad (\alpha = x,y,z) \tag{6.10}$$

Expanding the Ψ_M in terms of zero-order eigenfunctions of S_z, we have:-

$$|\Psi_M) = |M) + a_M^{M+1} |M+1) + a_M^{M+2} |M+2) + a_M^{M-1} |M-1) + a_M^{M-2} |M-2) + \ldots$$

where by first-order perturbation theory

$$a_M^{M'} = \frac{(M | H' | M')}{E_M - E_{M'}} ,$$

and to first order in $(\frac{D}{H})$ it is only necessary to calculate

$$a_M^{M+1} \quad \text{and} \quad a_M^{M-1} .$$

As our perturbation Hamiltonian we use:-

$$H' = \lambda(S_z(S_+ + S_-) + (S_+ + S_-)S_z) + \beta(S_+ f(S_z) + f(S_z)S_+) + \beta^*(S_- f(S_z) + f(S_z)S_-)$$

where $\lambda = \frac{D\sin 2\theta}{4}$

$$\beta = \frac{a}{576} (7\sin 2\theta\cos 2\theta + \sin 2\theta \pm 4.\sqrt{2}(-4\sin^4\theta\cos 3\psi + 3\sin^2\theta\cos 3\psi + i3\sin^2\theta\cos\theta\sin 3\psi))$$

$$f(S_z) = 7S_z^3 - 3S(S+1)S_z - S_z$$

Then $$a_M^{M+1} = \frac{(\lambda(2M+1) + \beta^*(f(M+1) + f(M)))\, F_+(M)}{-g\beta H_o}$$

$$a_M^{M-1} = \frac{(\lambda(2M-1) + \beta(f(M-1) + f(M))\, F_-(M)}{g\beta H_o} \qquad (6.11)$$

where $F_-^+(M) = (S(S+1) - M(M^+-1))^{\frac{1}{2}}$ and we have taken $E_M = g\beta H_o M$ as an approximation.

The components of the effective field may now be calculated -

$$H_x^M = \frac{A}{g_N\beta_N}(\Psi_M \mid S_x \mid \Psi_M)$$

$$= \frac{A}{g_N\beta_N}\left[a_M^{*M-1}(M-1| + a_M^{*M+1}(M+1| + (M|\right](S_+ + S_-)/2$$
$$\cdot\left[|M) + a_M^{M+1}|M+1) + a_M^{M-1}|M-1)\right]$$

$$= \frac{A}{2g_N\beta_N}\left[a_M^{*M-1}F_-(M) + a_M^{M+1}F_-(M+1) + a_M^{*M+1}F_+(M)\right.$$
$$\left. + a_M^{M-1}F_+(M-1)\right]$$

$$= \frac{A}{2g_N\beta_N}\left[F_-(M)\left(a_M^{*M-1} + a_M^{M-1}\right) + F_+(M)\left(a_M^{*M+1} + a_M^{M+1}\right)\right]$$

$$= \frac{A}{2g_N\beta_N}\left[\frac{F_-^2(M)\cdot\left\{(2M-1)(\lambda^*+\lambda) + (f(M-1) + f(M))(\beta^*+\beta)\right\}}{g\beta H_o}\right.$$
$$\left.\frac{-F_+^2(M)\cdot\left\{(2M+1)(\lambda^*+\lambda) + (f(M+1) + f(M))(\beta^*+\beta)\right\}}{g\beta H_o}\right]$$

$$= \frac{A}{g_N\beta_N g\beta H_o}\left[F_-^2(M).\left\{(2M-1)\lambda + (f(M-1) + f(M))R(\beta)\right\} - F_+^2(M).\right.$$
$$\left.\cdot\left\{(2M+1)\lambda + (f(M+1) - f(M))R(\beta)\right\}\right] \qquad (6.12)$$

where $R(\beta)$ = real part of β, and $R(\lambda) = \lambda$.

For $M = +\frac{1}{2}$: $(2M-1) = f(M-1) + f(M) = 0$

$F_+^2(M) = 8$

$(2M+1) = 2$

$f(M+1) + f(M) = -30$,

$M = -\frac{1}{2}$: $(2M+1) = f(M+1) + f(M) = 0$

$F_-^2(M) = 8$

$(2M-1) = -2$

$f(M-1) + f(M) = +30$

and we obtain :-

$$H_x^{\frac{1}{2}} = H_x^{-\frac{1}{2}} = \frac{-16A\ (\lambda - 15R(\beta))}{g_N\beta_N g\beta H_o} \qquad (6.13)$$

Similarly -

$$H_y^M = \frac{A}{g_N\beta_N}(\psi_M|S_y|\psi_M) = \frac{A}{g_N\beta_N}(\psi_M|\frac{S_+ - S_-}{2i}|\psi_M)$$

and on substitution of the expansion of the ψ_M and reduction we obtain -

$$H_y^{\frac{1}{2}} = H_y^{-\frac{1}{2}} = \frac{-16A}{g_N\beta_N g\beta H_o}(-15I(\beta)) \qquad (6.14)$$

and

$$H_z^M = \frac{A}{g_N\beta_N}(\psi_M|S_z|\psi_M) = \frac{AM}{g_N\beta_N}$$

$$H_z^{\frac{1}{2}} = -H_z^{-\frac{1}{2}} = \frac{A}{2g_N\beta_N} \qquad (6.15)$$

6.4 Calculation of $\mu = \cos\alpha_{MM'}$

The cosine of the angle between the directions of the effective fields corresponding to electron states M & M' may be calculated in terms of the components, viz. :-

$$\mu = \frac{H_x^M H_x^{M'} + H_y^M H_y^{M'} + H_z^M H_z^{M'}}{\left[\left\{(H_x^M)^2 + (H_y^M)^2 + (H_z^M)^2\right\}\left\{(H_x^{M'})^2 + (H_y^{M'})^2 + (H_z^{M'})^2\right\}\right]^{\frac{1}{2}}} \quad (6.16)$$

For $D \ll H_o$ and 'a' $\ll H_o$, H_y^M and H_x^M are both $\ll H_z^M$ and we may use the Binomial approximation to reduce this expression to :-

$$\mu = \frac{H_z^M H_z^{M'}}{\left[(H_z^M)^2 (H_z^{M'})^2\right]^{\frac{1}{2}}}\left[1 - \frac{1}{2}\left\{\frac{H_x^M}{H_z^M} - \frac{H_x^{M'}}{H_z^{M'}}\right\}^2 - \frac{1}{2}\left\{\frac{H_y^M}{H_z^M} - \frac{H_y^{M'}}{H_z^M}\right\}^2\right] \quad (6.17)$$

For $M = \pm 5/2 \rightleftharpoons M = \pm 3/2$ and $M = \pm 3/2 \rightleftharpoons M = \pm \frac{1}{2}$,

$$\frac{H_z^M H_z^{M'}}{\left[(H_z^M)^2 (H_z^{M'})^2\right]^{\frac{1}{2}}} = +1$$

(as $H_z^M \propto M$, and noting that the denominator must be positive). For the transitions $M = \frac{1}{2} \longrightarrow M = -\frac{1}{2}$, however, this term = - 1 , and we obtain -

$$\mu = -\left[1 - \frac{1}{2}\left\{\frac{H_x^{\frac{1}{2}}}{H_z^{\frac{1}{2}}} - \frac{H_y^{\frac{1}{2}}}{H_z^{\frac{1}{2}}}\right\}^2 - \frac{1}{2}\left\{\frac{H_x^{-\frac{1}{2}}}{H_z^{-\frac{1}{2}}} - \frac{H_y^{-\frac{1}{2}}}{H_z^{-\frac{1}{2}}}\right\}^2\right] \quad (6.18)$$

Substituting for these components from (6.13), (6.14) and (6.15) we obtain -

$$\mu = -\left[1 - \frac{2,048}{(g\beta H_o)^2}\left\{\left[\lambda - 15R(\beta)\right]^2 + \left[15\ I(\beta)\right]^2\right\}\right]$$

$$= -\left[1 - \frac{2,048}{(g\beta H_o)^2}\left\{\left[\frac{D}{4}\sin 2\theta - \frac{15a}{576}\left\{7\sin 2\theta\cos 2\theta + \sin 2\theta \mp 4.\sqrt{2}(-4\sin^4\theta\cos 3\overset{\psi}{\wedge} + 3\sin^2\theta\cos 3\psi)\right\}\right]^2 + \left[\frac{15a}{276}.12.\sqrt{2}.\sin^2\theta\cos\theta\sin 3\psi\right]^2\right\}\right] \qquad (6.19)$$

6.5 Discussion.

Writing $\mu = -f(D,a,\theta,\psi)$ we find that for $a = 0$, $f(D,0,\theta,0)$ is identical with the expression for μ derived by Bir (for $M = \frac{1}{2} \longrightarrow M = -\frac{1}{2}$, and $E = 0$), and that identical expressions are obtained for intensity variations, i.e. -

Bir:

$$\mu = +f(D,0,\theta,0) \text{ and } I \propto \left|d_1^{mm'}(+\mu)\right|^2 = \left|d_1^{mm'}(f(D,0,\theta,0))\right|^2$$

This author:

$$\mu = -f(D,0,\theta,0) \text{ and } I \propto \left|d_1^{mm'}(-\mu)\right|^2 = \left|d_1^{mm'}(f(D,0,\theta,0))\right|^2$$

This double change of sign may be regarded as trivial, if the approximate expressions only, are used, in the calculation of intensity variations. When exact methods are used, however, to predict these variations for the $M = \frac{1}{2}$ transitions, this double change of sign must be taken into account.

Only first-order perturbation methods are necessary to derive the expression for μ and it would be expected that for values of $|D|$

which are not small compared with H, more exact treatment would be required. For $|D| > \sim 400$ Oe, we in fact find from this approximation, that at $\theta = 45^{o}$, the value of μ ($= \cos\alpha_{MM'}$) becomes greater than unity. Rather than derive expressions for μ, using higher orders of D/H, and higher order perturbation methods, an exact solution was then found. A computer programme was written which found all coefficients in the expansion of the perturbed wave function, by computer diagonalization of the 6 x 6 energy matrix for the fine structure, and values of μ were found by direct substitution of the calculated components of the effective field, in equation 6.16. The computed intensity variations by exact methods, for various values of parameters, are shown later in figures 7.1, 7.2, 7.5, 7.11 - 7.16.

As stated before, the number of calculations necessary to obtain predicted intensity variations by this method, are of the order of three orders of magnitude less than the number required using the method described in section 4.4. The total computer time required to obtain intensity variations for six lines, in the range $\theta = 0$ to $\theta = \pi/2$, at $2\frac{1}{2}^{o}$ intervals, was in fact less than one-half that required to obtain a single point of the intensity variation, by diagonalization of the 36 x 36 matrix, as described in section 4.4.

The effects on the predicted intensity variation of a forbidden transition, of variations in the parameter 'a' are shown in fig. 6.2.

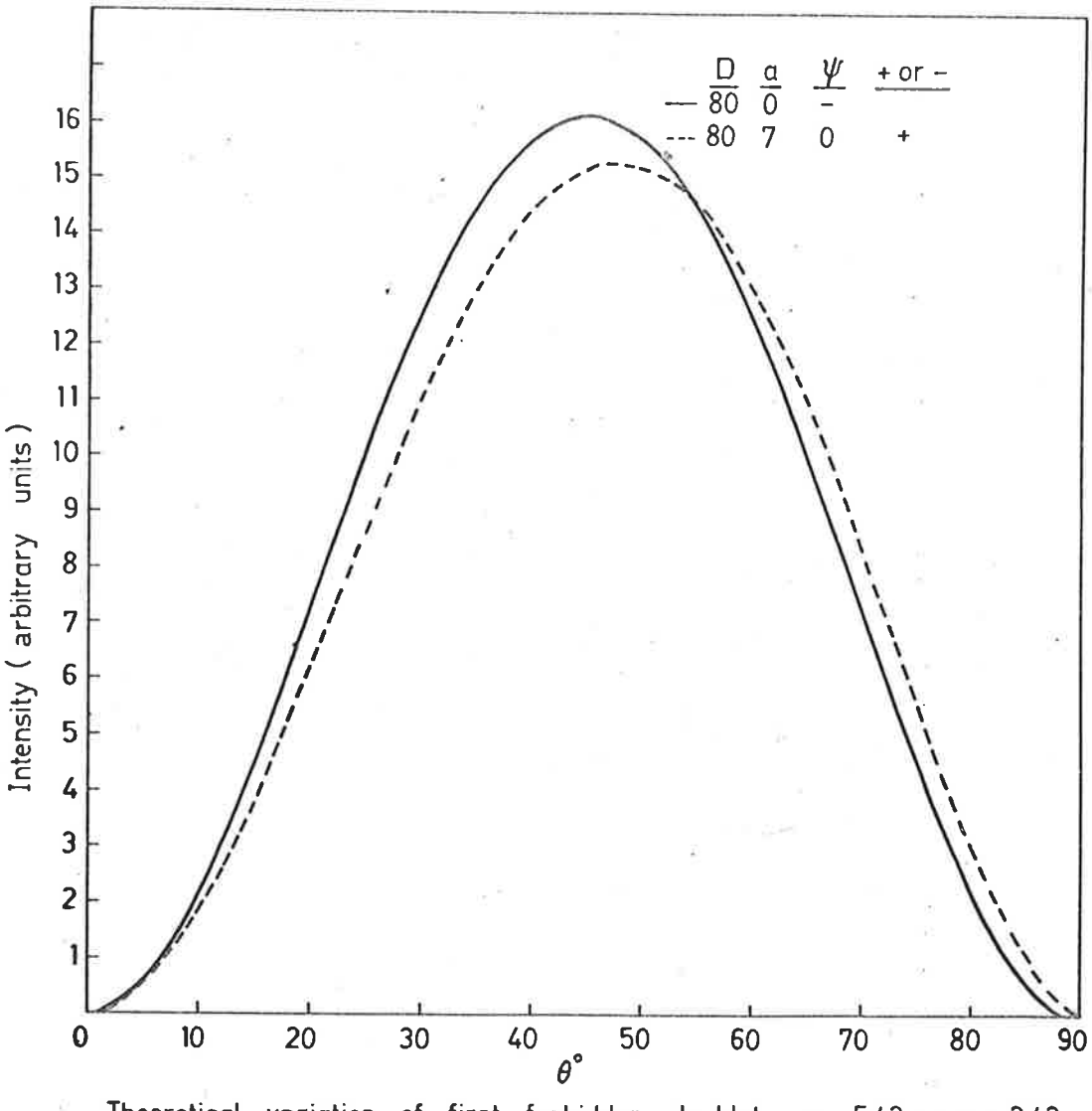

Theoretical variation of first forbidden doublet. $m = 5/2 \leftrightarrow m = 3/2$

FIG. 6.2

Qualitatively these variations may be taken as having no effect on the resultant intensity variation, but quantitatively, significant variation may occur if the "cubic" terms are neglected, for small values of D.

For the purpose of the following work, in which interpretation of powder spectra is mainly qualitative, the cubic terms will be neglected.

6.6 Intensity Variations for Rhombic Crystal Field.

For rhombic crystalline field symmetry we obtain:-

$$\mu = -\left[1 - \frac{2,048}{(g\beta H)^2} \cdot |\lambda|^2\right]$$

with $$|\lambda| = \frac{\sin\theta}{2}\left[\cos\theta(D-E\cos 2\psi) + iE\sin 2\psi\right]$$

CHAPTER VII

Interpretation of Other Axial Powder Spectra.

7.1 Introduction.

We have seen that features of some Mn^{2+} powder spectra are adequately explained using the intensity or line shape function:-

$$I'(\theta) = \frac{\sin\theta . I(\theta)}{2^{dH}/d\theta}$$

$$\text{and } I'(\theta) \propto \frac{I(\theta)}{\cos\theta(U_i+V_i\sin^2\theta)} \qquad (7.1)$$

where we have previously used -

$$I(\theta) \propto \sin^2 2\theta \qquad (\Delta m = \pm 1)$$

$$\text{and } I(\theta) = \text{constant} \qquad (\Delta m = 0)$$

Quantitatively, features of all axial powder spectra may be explained, by considering maxima of the line shape function, equation (7.1) above, using intensity variations $I(\theta)$, predicted using Bir's method.

For our interpretation we assume that the $I(\theta)$ variation modulates the $\frac{1}{\cos\theta(U_i+V_i\sin^2\theta)}$ function, which has finite values at $\theta = \pi/2$ and $\theta = \arcsin\sqrt{\frac{-U_i}{V_i}}$, $\sim 40^{o}$, rather than undefined values.

7.2(a) Apatite : Transition Probabilities in Single Crystals.

The intensity variations predicted, for allowed and forbidden transitions of the central hyperfine sextet, are shown in figures 7.1 and 7.2, using the exact methods described in section 6.5. Experimental verification of these predicted variations for all lines was not possible because of the overlap of outer transitions, and the rapid rise of $\Delta m = \pm 2$ (and possibly $\Delta m = \pm 3$) transitions, as the angle between the crystal axis and the applied static magnetic field was increased from zero. It was, however, possible to follow the variations of intensity for the first allowed line ($m = -5/2$) and the first forbidden transition ($m = -5/2 \rightarrow m = -3/2$) over a large range of angles for a single crystal of apatite from Erenfriedersdorf. These variations are shown in fig. 7.3, and by comparison with the predicted variations we obtain excellent qualitative agreement between theory and experiment. The experimental intensities near $\theta \sim 45^{o}$ are smaller than the predicted intensities. This would be expected, however, as overlapping by adjacent lines would produce a reduction in the observed peak to peak of the derivative of the absorption curve, which was taken as a measure of the intensity.

7.2(b) Apatite : Explanation of Features of the Powder Spectrum.

Assuming that for the other allowed and forbidden lines, for which intensity variations with rotation could not be followed,

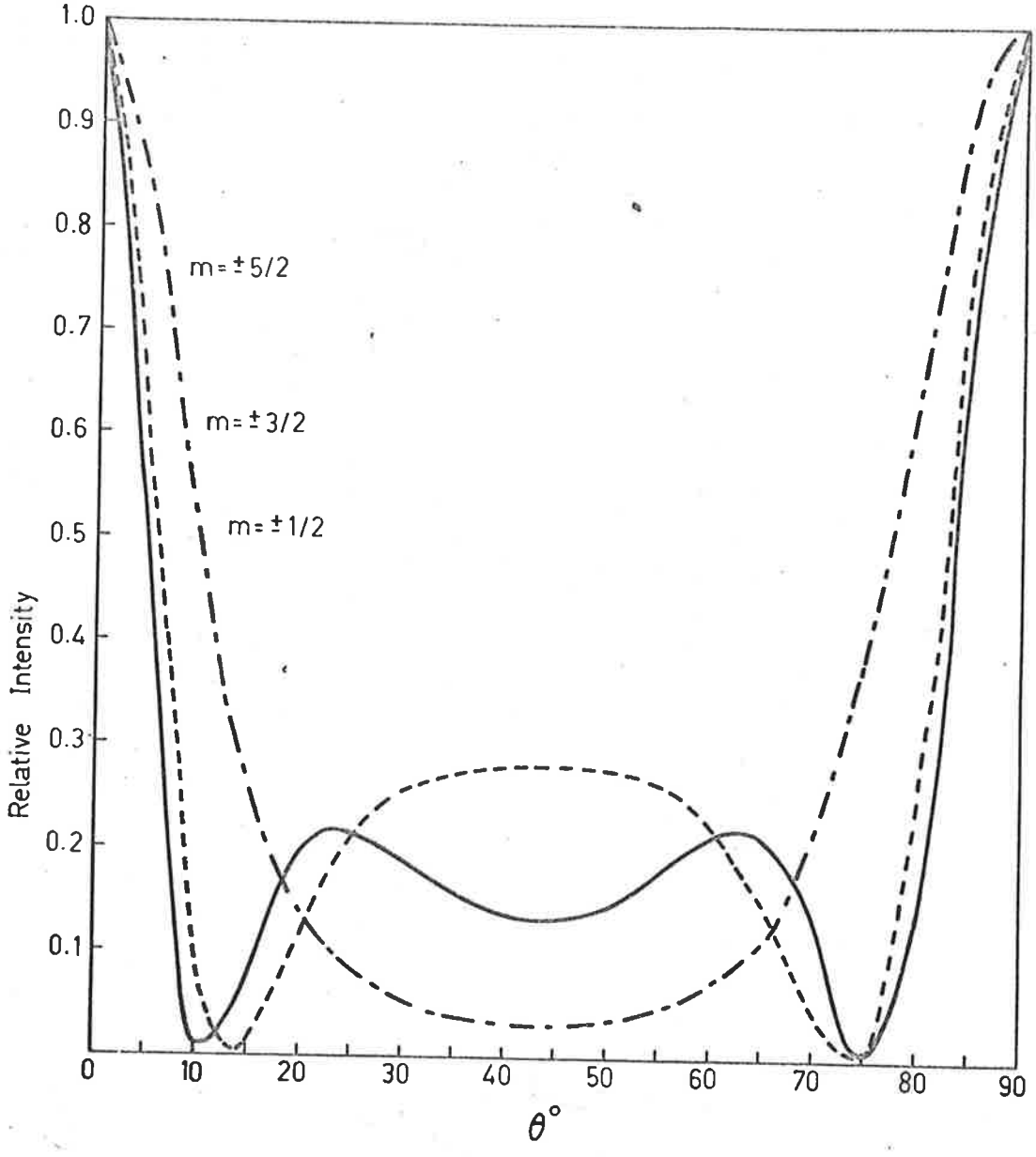

Predicted intensity of allowed transitions for apatite. D = 433 Oe
Computer diagonalization of (6 x 6) Matrix. (Bir's method)

FIG. 7.1

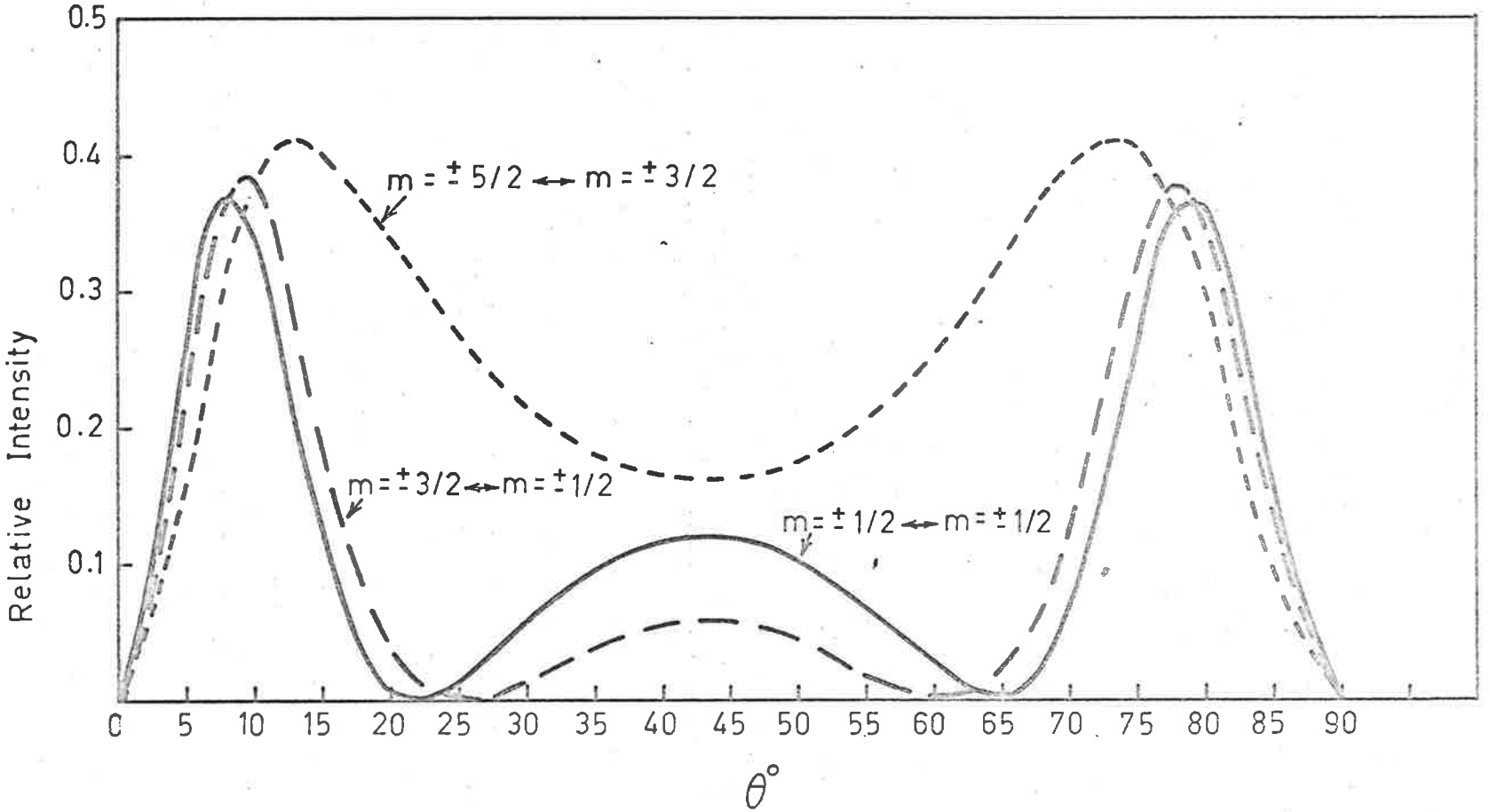

Predicted intensity variation of forbidden transitions for apatite. D = 433 Oe

FIG. 7.2

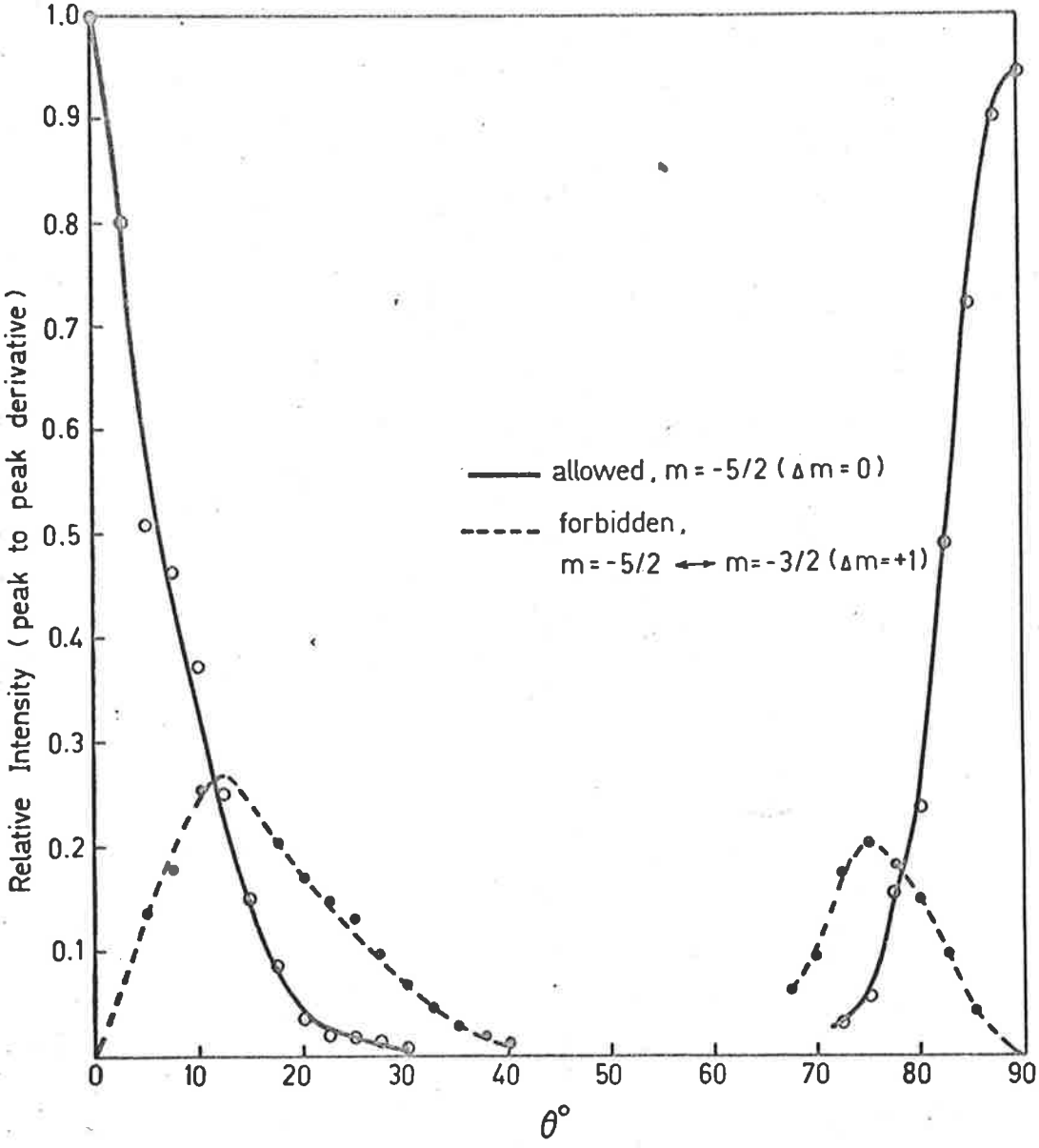

Experimental variations of intensity for Mn^{2+} in apatite.

FIG. 7.3

the intensity variations are as predicted, but with the measured peak to peak intensities smaller near $\theta \sim 45^{\circ}$ than shown in figs. 7.1 and 7.2, we may conclude that the intensities of all lines are very small near $\theta \sim 40 - 45^{\circ}$. When this modulation is applied to the function $\frac{1}{\cos\theta(U_i + V_i \sin^2\theta)}$ we could then expect that for a powder sample the $\theta \sim 40^{\circ}$ peaks predicted by this function would only be of very small intensity, and may not be observable. For the allowed transitions we could then expect only $\theta = 90^{\circ}$ peaks, i.e., in a powdered sample of apatite, we would not expect to observe splitting of the allowed transitions, as is observed for low D samples, and we would expect the observed line positions of these lines, to coincide approximately with line positions observed for a single crystal at $\theta = 90^{\circ}$. Such is the case for the apatite powder spectrum shown in fig. 5.10.

Kasai's (1962) assumption that the Mn^{2+} apatite powder spectrum corresponded to the $\theta = 90^{\circ}$ single crystal spectrum, in his determination of parameters, is therefore justified. It may be noted that Kasai has used only second order calculations in his analysis which predict equal angular shifts for each hyperfine line. Third order terms predict unequal angular shifts for the central hyperfine lines, and as shown previously in section 5.2, predict that the spacings between adjacent allowed hyperfine lines, at $\theta = 90^{\circ}$, is less than the spacings calculated using only second order terms.

Conversely it would be expected that if the hyperfine parameter A (or $A_{//}$ and $A_{\perp}$) was determined by fitting experimental $\theta = 90^{o}$ line positions from a powder spectrum, to theoretical terms containing only up to second order corrections, a value of A lower than that obtained from single crystal measurements would be obtained. This could then explain why Kasai's determined values ($A_{//} = 94.4$, $A_{\perp} = 92.4$) are slightly lower than values obtained from single crystal measurements ($A_{//} = 95.0$, $A_{\perp} = 92.6$: Ohkubo (1963); $A_{//} = 96.2$, $A_{\perp} = 95.5$: Burley (1964); $A_{//} = 96\ (\pm 1)$, $A_{\perp} = 93\ (\pm 1)$: Vinokurov et al (1964 b)).

For the forbidden transitions, the modulation by $I(\theta)$ produces a small broad peak in the intensity function at $\theta \sim 70^{o} - 80^{o}$. It could then be expected, that in the powder spectrum, the forbidden doublets, possibly broadened into a single broad resonance, could be observed at line positions corresponding to $\theta \sim 70^{o} - 80^{o}$, or 20 - 30 Oe towards the high field side relative to the mid point between the allowed transitions. For the spectrum shown in fig. 5.10, such broad resonances are observed.

In the single crystal studies of apatite, a much weaker spectrum was observed underlying the main spectrum, fig. 7.4. This weaker spectrum has been reported by Vinokurov et al (1964 b) and Ohkubo (1963).

It has been assumed that the apatite powder spectrum discussed in this section was actually the spectrum due to the main ion site.

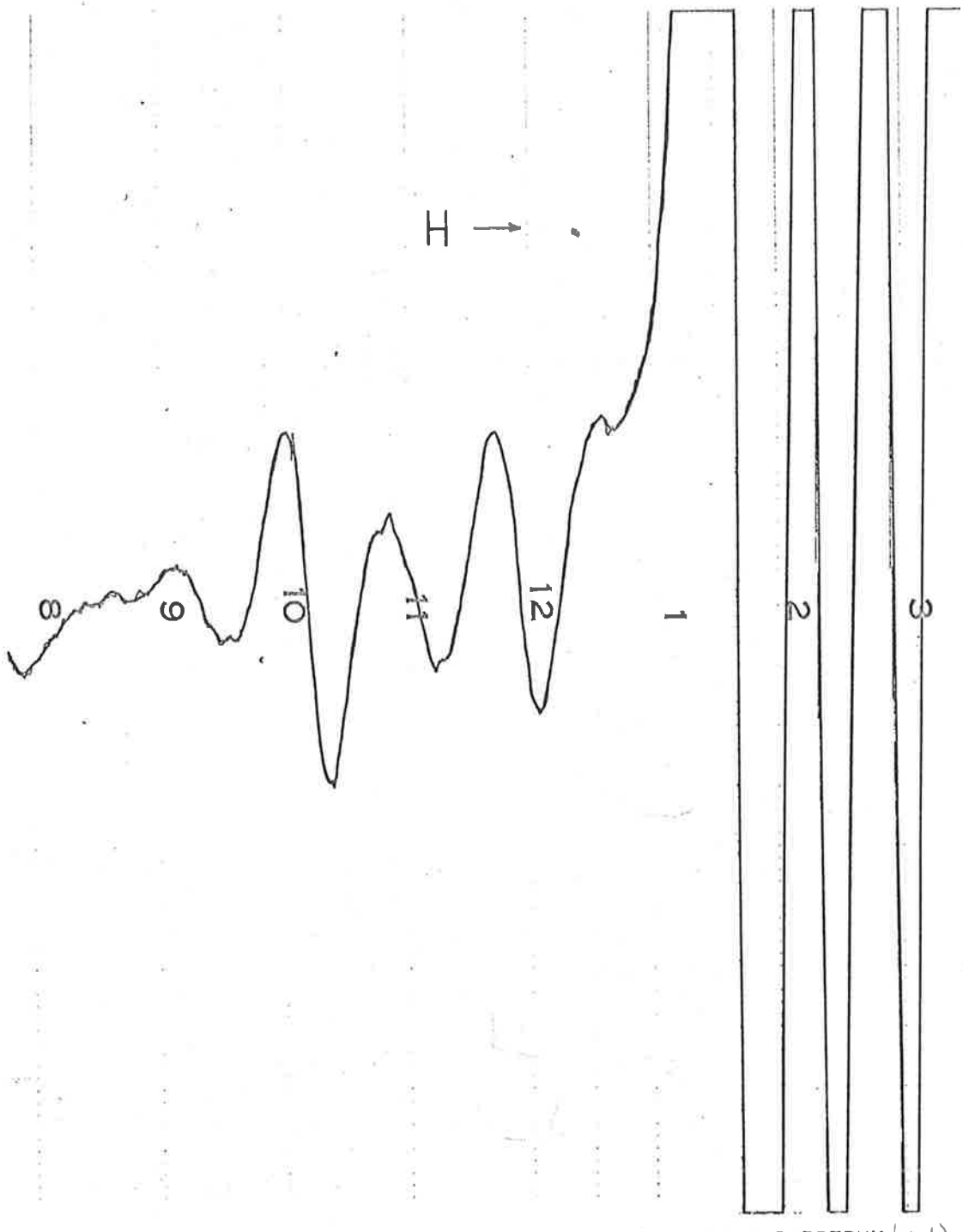

MAIN SPECTRUM ($M = \frac{1}{2}$)
($\theta = 0°$)

FIG. 7.4

As shown later in sections 7.4 and 8.4, if two or more non-equivalent Mn^{2+} ion sites exist in a material, the features of a powder spectrum may be dominated by the site of lower axial crystal field splitting. This may occur, even though the single crystal Mn^{2+} spectrum of the lower 'D' ion site, may be of relatively small intensity, compared to the single crystal spectrum from Mn^{2+} ions in the higher 'D' site. Because of this, a brief investigation was carried out to verify that the apatite powder spectrum previously discussed, was in fact, due to the ion site which produces the main spectrum in single crystal studies.

7.2(c) Apatite - Single Crystal Spectra and Annealing Experiments.

There are two non-equivalent Ca-sites in the apatite crystal structure (St. Naray - Szabo 1930). The CaI site is on a trigonal symmetry axis in the centre of a slightly twisted prism of six oxygen atoms (point group symmetry C_3). In fluorapatite the CaII site is in a reflection plane containing an adjacent fluoride ion also in the reflection plane (point group symmetry C_{1h}). In the chlorapatite the halide lies on the same hexagonal screw axis as the fluoride, but between the reflection planes (Johnson 1962).

Butler and Jerome (1950), and Ouweltjes (1951), have concluded that the shift in the luminescence emission of Mn^{2+} with change of Cl^- and F^- composition, is evidence that the Mn^{2+} is in the CaII site. Narita (1961), however, has calculated the effect of change

in lattice constants on the emission spectrum of Mn^{2+} in halophosphates, assuming the manganese to be in the CaI site, and found that the calculated shift was in accord with the experimentally observed effect on the Mn^{2+} emission spectrum, of changing the $[Cl^-]/[F^-]$ ratio. Johnson (1962) has applied symmetry arguments to explain the observed spontaneous polarization of luminescence of single halophosphate crystals, and has concluded, that in fluorapatite the Mn^{2+} is predominantly in the CaI site, in chlorapatite the CaII site is preferentially occupied, and in mixed halides, including natural crystals, both sites are occupied. Kasai (1962), on the basis of the electrostatic symmetry at the two sites, concluded that the paramagnetic resonance of Mn^{2+} in powder synthetic apatite phosphors, was due to the Mn^{2+} ion occupying the more symmetric CaI site. Vinokurov et al (1964 b) have come to the same conclusion, for the more intense single crystal spectrum observed in natural apatite crystals. These authors reported observations of a much weaker spectrum underlying the main spectrum, which they attributed to Mn^{2+} ions in the CaII site. Ohkubo (1963) has published spectra from naturally occurring apatite crystals, showing this much weaker set of lines, which he also attributed to Mn^{2+} in the CaII site. The parameters for the Mn^{2+} spectrum, generally attributed to this ion occupying the CaI site, have been given by Burley (1964), Vinokurov et al (1964 b), Kasai (1962) and Ohkubo (1963). No parameters have yet been determined for the Mn^{2+} ion in the CaII site.

Johnson (1962) reported that E.S.R. observations of synthetic chlorapatite crystals containing Mn^{2+} impurities, indicated that this ion was in the CaII position. In reply to a letter by this author requesting the parameters for Mn^{2+} in the CaII site, Johnson (November, 1967) has stated that "due to large departures from stoichiometry resulting in many centres of the type studied by Piper et al (1965) having hyperfine interaction with the two Cl isotopes, the E.S.R. spectra of chlorapatite crystals are hopelessly complex" !

Apple and Ishler (1962) observed that the rate of cooling from elevated temperatures affected the structure and luminescence of calcium halophosphates with Sb and Mn. These authors proposed that very fast quenching ($\sim$sec) from high temperatures (800 - 1,000^{o}C), "freezes in" a more random distribution of Mn over the two Ca sites, whereas on slow-cooling, the Mn^{2+} tends to migrate to, and occupy, the CaI site, and suggested that E.S.R. measurements on annealed samples could help to substantiate or disprove their proposals.

Ohkubo (1963) reported that the weaker CaII - Mn^{2+} spectrum was reduced in intensity with annealing, which would seem to substantiate the proposal of Apple & Ishler (1962), that Mn^{2+} would migrate from CaII sites to CaI sites, with annealing. Quenching and annealing experiments were carried out by the author, using single crystals, but in all cases a large reduction of the intensity of the weaker spectrum was the only effect observed. This large

reduction of intensity of the weaker spectrum with quenching, would then seem to cast a doubt on the proposal of Apple & Ishler, if this weaker spectrum is due to Mn^{2+} in the CaII site.

No large reduction of the intensity of lines observed in Mn^{2+} apatite powder spectrum occurred with annealing. If the lines in the powder spectrum were due to Mn^{2+} ions, which produced the weaker spectrum in single crystal studies, these powder lines should be reduced in intensity with annealing or quenching. We may then conclude that lines in the powder spectrum discussed in the previous section, are, as originally assumed, due to Mn^{2+} in the ion site which produces the main spectrum in single crystal studies.

7.3(a) Scheelite : Transition Probabilities.

The existance of strained single crystals of $CaWO_4$ containing manganese for which only the central ($M = \frac{1}{2} \rightarrow M = -\frac{1}{2}$) transitions are observable (Lyons & Kedzie, 1966), enables the study of intensity variations of allowed and forbidden lines in the central transition, without the complication of overlapping fine structure. Natural crystals of $CaWO_4$ of unknown locality, which contained Mn^{2+}, and produced intensity variations similar to that described for the synthetic crystals, was found among specimens in the Geology Department of the University of Adelaide. Near $\theta = 0^o$, all fine structure in the Mn^{2+} spectrum was observable, but for θ greater than about 5^o, the fine structure was so broadened that observations of the

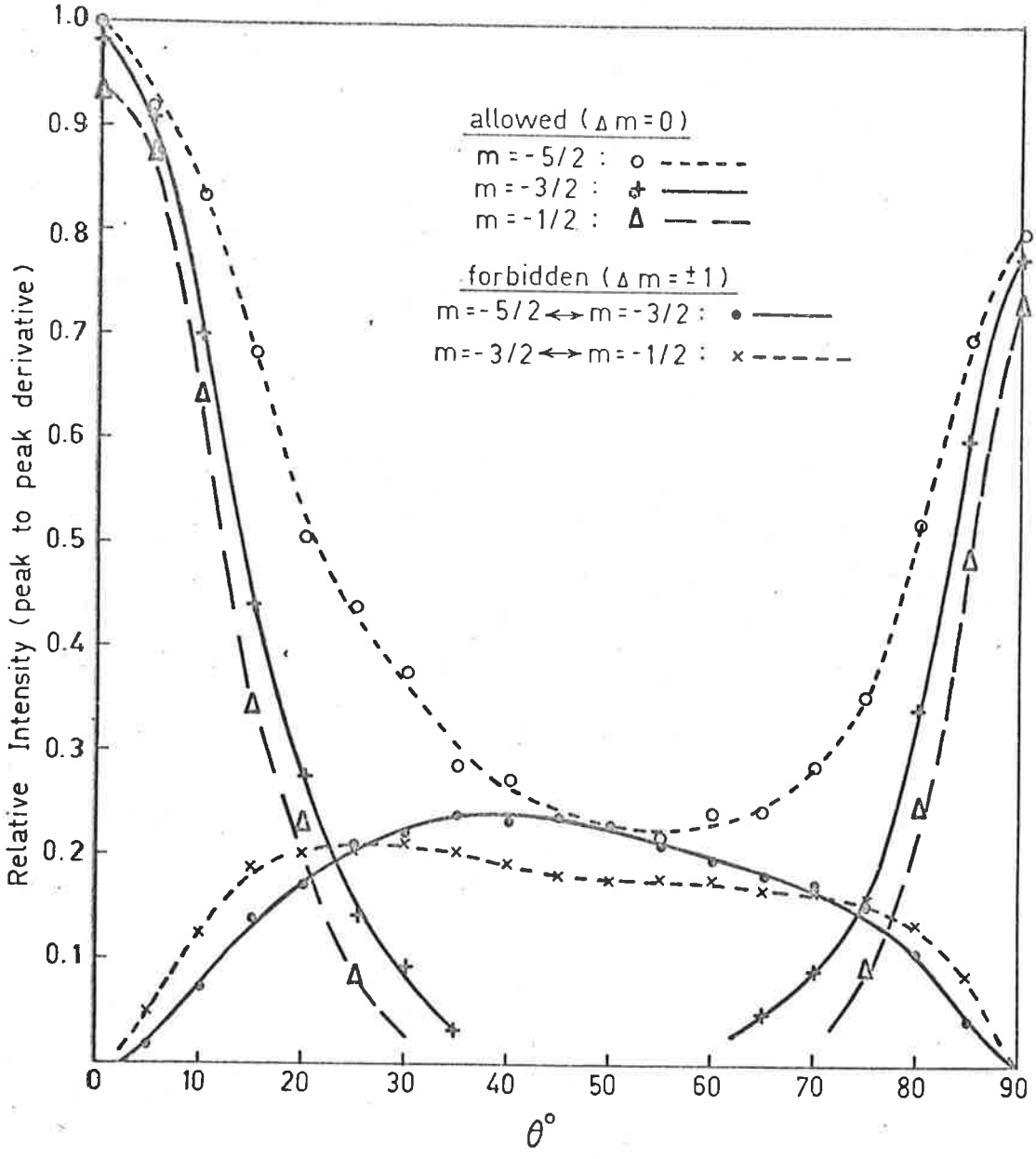

Experimental intensity variations for $CaWO_4 (Mn^{2+})$.
(X- band - room temperature)

FIG. 7.5

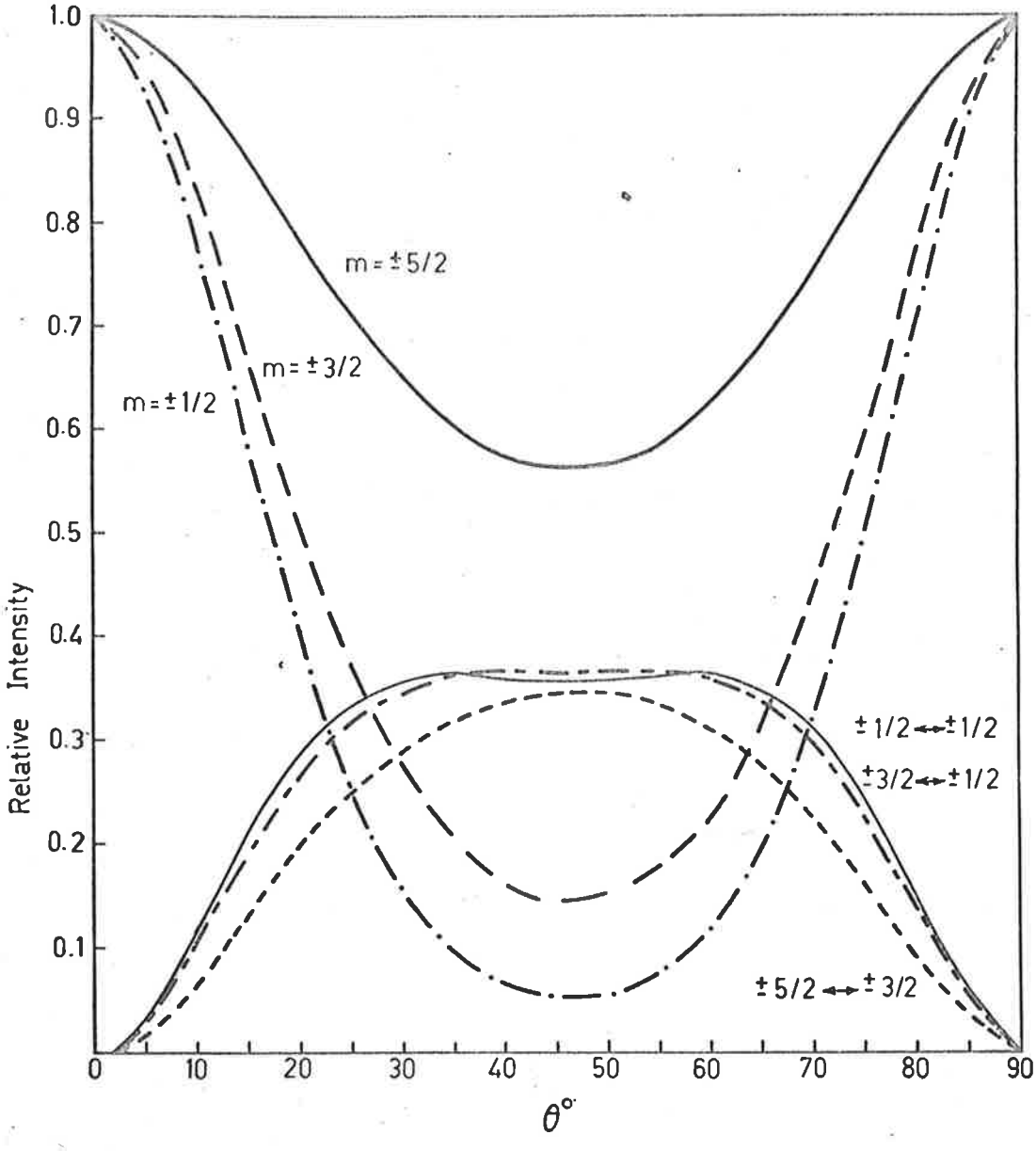

Intensity variations for allowed and forbidden transitions. Computer diagonalization. D = 150.0 Oe

FIG. 7.6

central structure were not hindered. Experimentally determined intensity variations obtained from this natural crystal are shown in fig. 7.5 and predicted variations shown in fig. 7.6.

Taking into account the reduction of observed intensity due to overlapping by adjacent lines, excellent agreement between experimental and theoretical variations is once again obtained.

The experimentally determined intensities were all taken relative to a D.P.P.H. signal. At certain angles between the Z crystal field axis of the tungstate crystal, and the applied field, this D.P.P.H. line overlapped the central forbidden lines of the tungstate spectrum. Because of this, the intensity variations of these forbidden lines were not fully determined.

7.3(b) Scheelite : Powder Spectrum.

For the allowed transitions it is seen from the predicted intensity variations shown, that at $\theta \sim 40^{\circ}$, the first ($m = -5/2$), and last ($m = +5/2$), of these transitions still have a relatively large intensity, whereas the other allowed lines ($m = \pm 3/2, \pm \frac{1}{2}$) are relatively weak.

We could thus expect that for the powder spectrum, the $\theta \sim 40^{\circ}$ peaks in the intensity function would be relatively large for the first and last allowed transitions, and relatively small for the central four allowed lines. Splitting of the allowed transitions would then be observed only for the $m = \pm 5/2$ resonances.

For the forbidden transitions ($\Delta m = \pm 1$), the intensity at $\theta \sim 40^{\circ}$ is relatively large, and the intensity variation could be approximated by a $\sin^2 2\theta$ variation. In the powder spectrum we would thus expect forbidden peaks corresponding to $\theta \sim 40^{\circ}$. These predictions, both for the allowed and forbidden transitions, are verified experimentally.

For this, and all other powder spectra from samples for which the Mn^{2+} ion is in a site of axial field symmetry, we could perhaps generalize, and state, that the resultant powder spectra can be regarded as the resultant of the single crystal spectra at $\theta = 90^{\circ}$ and $\theta \sim 40^{\circ}$. This is shown for the tungstate spectrum in fig. 7.7, where the powder spectrum, and $\theta = 90^{\circ}$ and $\theta \sim 40^{\circ}$ spectra from the strained single crystal, have been aligned using a D.P.P.H. marker, making possible a complete identification of major lines in this powder spectrum.

Line	Identification
1, 2	Split allowed transition ($m = -5/2, \Delta m = 0$)
3	Forbidden ($m = -5/2 \rightarrow m = -3/2$, $\Delta m = +1$)
4	Allowed ($m = -3/2$, $\Delta m = 0$) + Forbidden ($m = -3/2 \rightarrow m = -5/2$, $\Delta m = -1$)
5	Forbidden ($m = -3/2 \rightarrow m = -\frac{1}{2}$, $\Delta m = +1$)
6	Allowed ($m = -\frac{1}{2}$, $\Delta m = 0$) + Forbidden ($m = -\frac{1}{2} \rightarrow m = -3/2$, $\Delta m = -1$)
7	Allowed ($m = +\frac{1}{2}$, $\Delta m = 0$) + Forbidden ($m = -\frac{1}{2} \rightarrow m = +\frac{1}{2}$, $\Delta m = +1$)

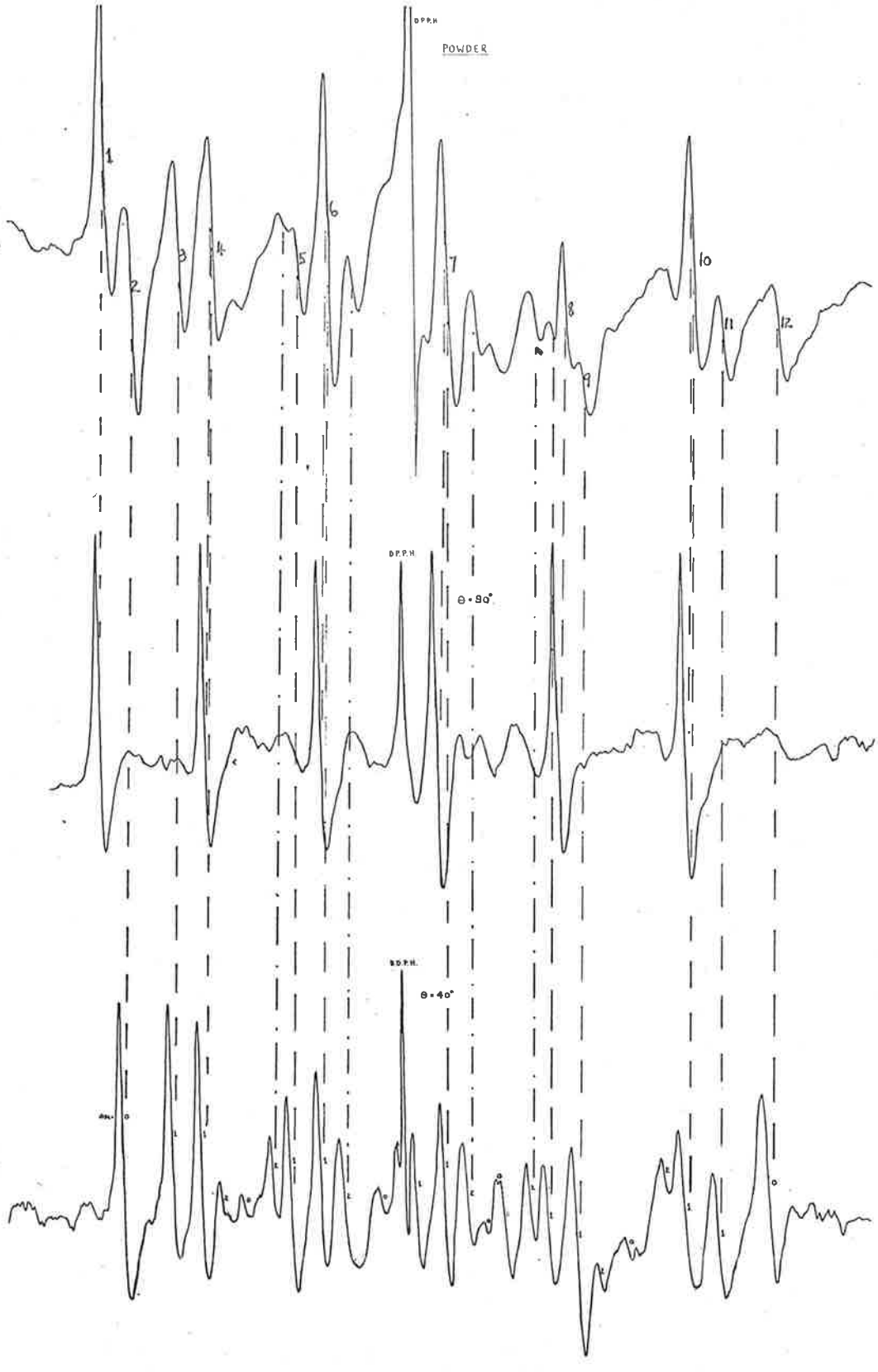

FIG. 7.7

8 Allowed ($m = 3/2$, $\Delta m = 0$)

9 Forbidden ($m = 3/2 \rightarrow m = \frac{1}{2}$, $\Delta m = -1$)

10 Allowed ($\theta = 90^{\circ}$ component) ($m = 5/2$, $\Delta m = 0$)

+ Forbidden ($m = 3/2 \rightarrow m = 5/2$, $\Delta m = +1$)

11 Forbidden ($m = 5/2 \rightarrow m = 3/2$, $\Delta m = -1$)

12 Allowed ($\theta \sim 40^{\circ}$ component) ($m = 5/2$, $\Delta m = 0$)

7.4 Dolamite : Single Crystal and Powder Spectra.

The spectrum of Mn^{2+} in dolamite, $CaMg(CO_3)_2$, has been reported by Vinokurov et al (1961). These authors reported the existance of two overlapping spectra, one characterised by $|D| = 150$ Oe, and the other of relatively small intensity by $D \sim 0$. The Mn^{2+} spectrum from a sample of powdered dolamite is shown in fig. 7.8, together with $\theta \sim 40^{\circ}$ and $\theta = 90^{\circ}$ single crystal spectra, the three spectra being aligned using a D.P.P.H. marker. (For this sample of dolamite, the outer fine structure also fell rapidly in intensity away from $\theta = 0^{\circ}$, enabling observation of the central hyperfine transitions.) Complete identification of the lines in the powder spectrum is then possible and it is seen that the major lines in the powder spectrum are due to the Mn^{2+} ion in the $D \sim 0$ site, which produced relatively weak lines in the single crystal spectra.

Transitions of the $|D| = 150$ Oe site are much more angular dependent than corresponding transitions of the $D \sim 0$ site. The powder spectrum of this $|D| = 150$ Oe site would then be spread over a much larger field region, with a corresponding larger reduction

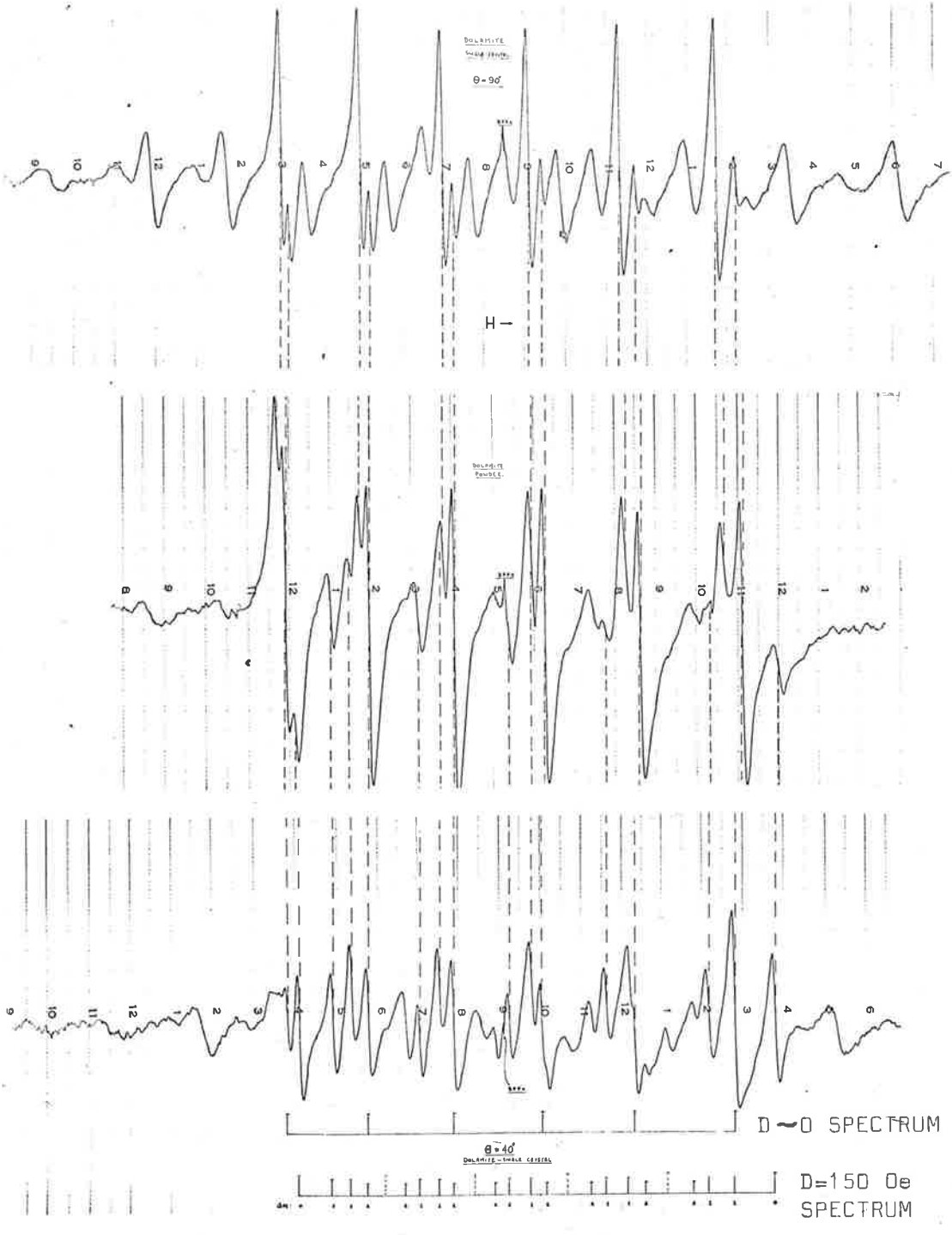

FIG. 7.8

in the observed peak to peak intensity, than would occur for the powder spectrum of the D ~ O site.

7.5 Ankerite : Single Crystal and Powder Spectra.

The spectrum of Mn^{2+} in ankerite, $Ca(Mg,Fe^{2+},Mn)(CO_3)_2$ has been reported by Vinokurov et al (1961). These authors, however, were unable to determine parameters accurately, due presumably to the broadness of the lines observed for the sample used, which they stated were broadened by an Fe - Mn dipolar interaction. The $\theta = 0^{o}$ spectrum from a single crystal of ankerite from Western Australia, obtained from Mineral Specimens Ltd., S.A., is shown in fig. 7.9. For this spectrum a best fit between experimentally determined line positions and theoretical line positions was obtained for the following values of parameters -

$$g = 2.00 \ (\pm 0.005)$$

$$A = -94.1 \ (\pm 0.5) \text{ Oe}$$

$$D = \pm 154 \ (\pm 5) \text{ Oe}$$

$$a = \mp 11 \ (\pm 5) \text{ Oe} \quad (T = 20^{o}\text{C}, \ = 9.17 \text{ Gc/s.})$$

The values of these parameters appear identical (within experimental error) with those determined by this author for dolomite. The spectrum of a powdered ankerite sample is shown in fig. 7.10 and appears to be just a broadened version of the dolamite powder spectrum (fig. 7.8). As the dolomite powder spectrum was shown to consist of two overlapping sets of lines, it is reasonable to assume, from a comparison of the powder spectra, that there are two sites available for Mn^{2+} ions in ankerite as well, with a weaker spectrum masked and unobservable in the single crystal observations.

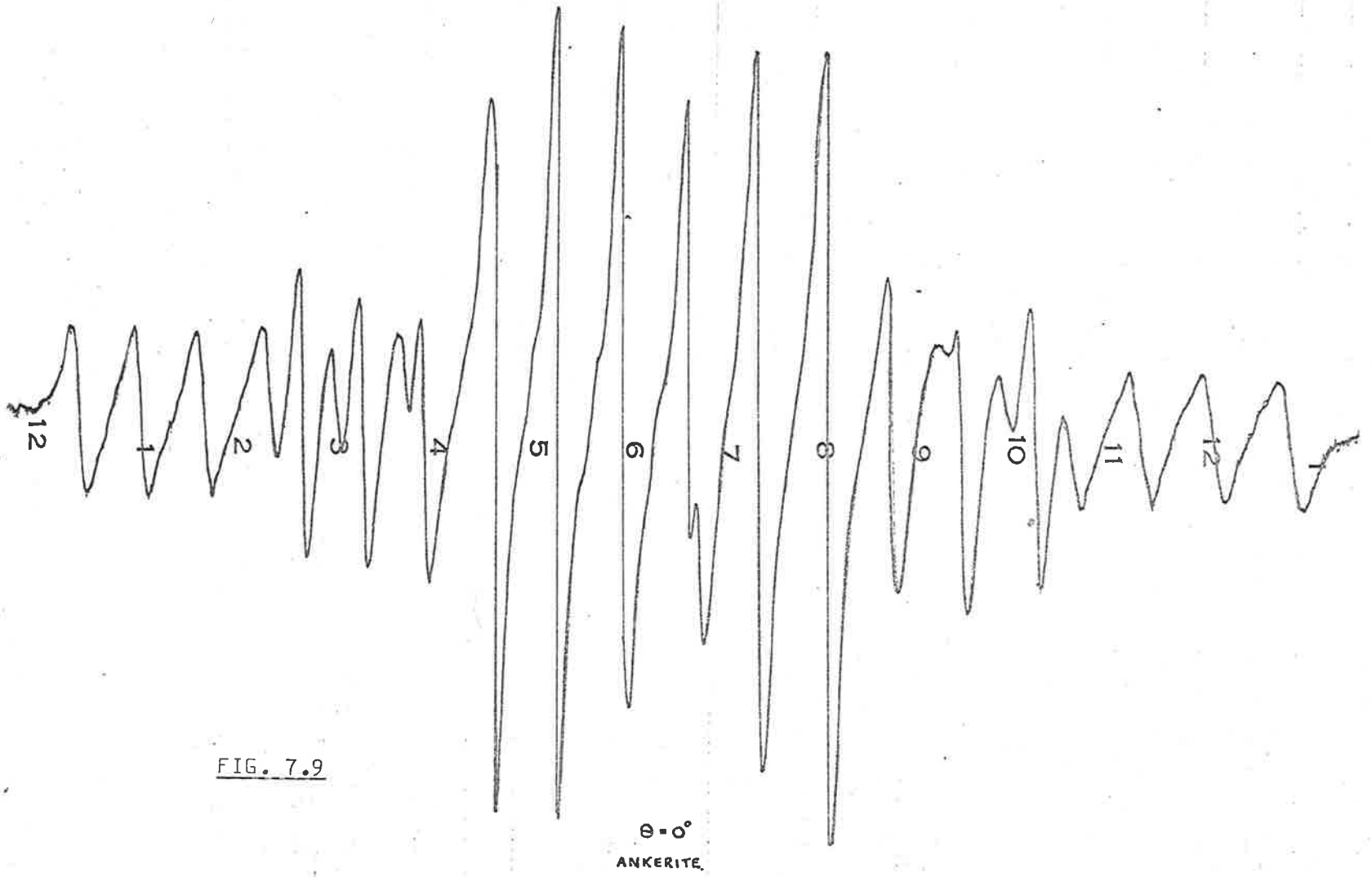

FIG. 7.9

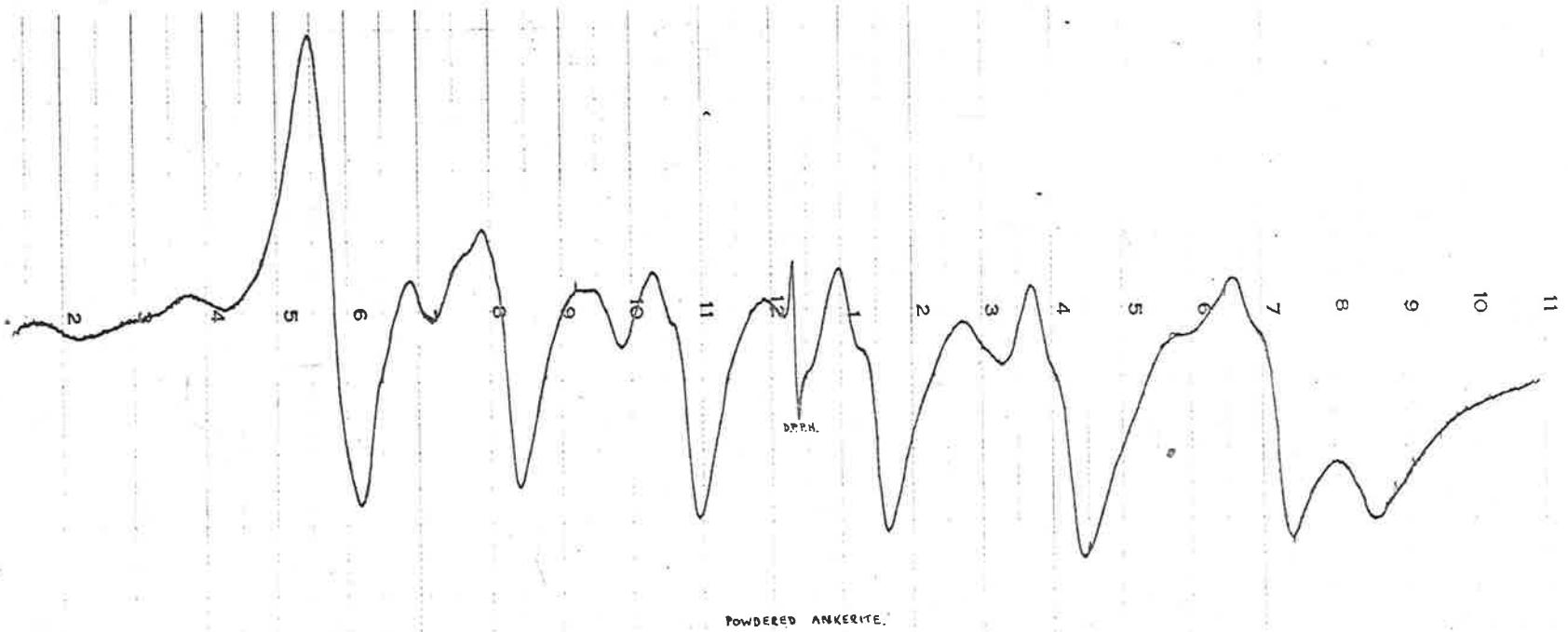

FIG. 7.10

7.6 Summary of Theory for Axial Spectra.

At this point we may summarize the theory of axial powder spectra as follows:-

1. For any value of the axial parameter 'D', a powder spectrum may be regarded qualitatively, as the sum of the $\theta = 90^{\circ}$ and $\theta \sim 40^{\circ}$ single crystal spectra.

2. For values of $|D| < \sim 100$ Oe, the intensity of all allowed transitions at $\theta \sim 40^{\circ}$ is relatively large, and a powder spectrum should consist of both $\theta = 90^{\circ}$ and $\theta \sim 40^{\circ}$ allowed peaks, which may be broadened into only a single observable line. Forbidden doublets should be observable (corresponding to $\theta \sim 40^{\circ}$), and in broadened spectra will appear shifted towards the high field side of the spectrum, relative to the observed allowed transitions.

3. An additional small relative shift of the forbidden doublets towards the low field side, may possibly be attributed to the line shape factor.

4. The determination of the parameter 'D', using the Bleaney and Rubins' expression for relative intensities in a powder spectrum, may be larger than the value determined from single crystal measurement by $> 50\%$ (for values of $|D| < \sim 100$ Oe). The method is not applicable for large values of $|D|$.

5. For $|D| \sim 150$ Oe, the intensities of only the first and last ($m = \pm 5/2$) allowed transitions might be sufficiently large, near $\theta \sim 40^{\circ}$, to have an effect on a powder spectrum. Doubling of only

these allowed lines may therefore be observable in a powder spectrum. $\theta \sim 40^{\circ}$ forbidden lines should be observable, but may be so shifted relative to the allowed $\theta = 90^{\circ}$ peaks, that overlap occurs. e.g. $CaWO_4$ powder spectrum, fig.5.11.

6. For $|D| = 250$ Oe and $|D| = 350$ Oe, predicted intensity variations are shown in figs. 7.11, 7.12, 7.13 and 7.14. From the variations for allowed transitions, it is seen that near $\theta \sim 40^{\circ}$ the transition probability is relatively small for all lines. In axial powder spectra of Mn^{2+} in sites for which $|D| \sim 250 - 350$ Oe, we might then expect that all $\theta \sim 40^{\circ}$ allowed components may be of relatively small intensity, compared with $\theta = 90^{\circ}$ peaks, and may not be observable. For forbidden transitions, the predicted intersity near $\theta \sim 40^{\circ}$ is relatively large for only the first and last pair of transitions ($m = \mp 3/2 \leftrightarrow m = \mp 5/2$), and only these pairs of lines may be observable in a powder spectrum. High-field lines have a larger variation of field position for resonance, as θ is varied, than low field lines. High field lines in powder spectra, are therefore broadened more than low field lines, and it might be expected that the low field forbidden doublet ($m = -3/2 \leftrightarrow m = -5/2$), would have a larger intensity than the high field doublet, ($m = +3/2 \leftrightarrow m = +5/2$), and may even be the only forbidden lines clearly discernable.

7. For larger values of 'D' (~ 450 Oe) the intensities of <u>all</u> transitions at $\theta \sim 40^{\circ}$ may be sufficiently small that peaks in a

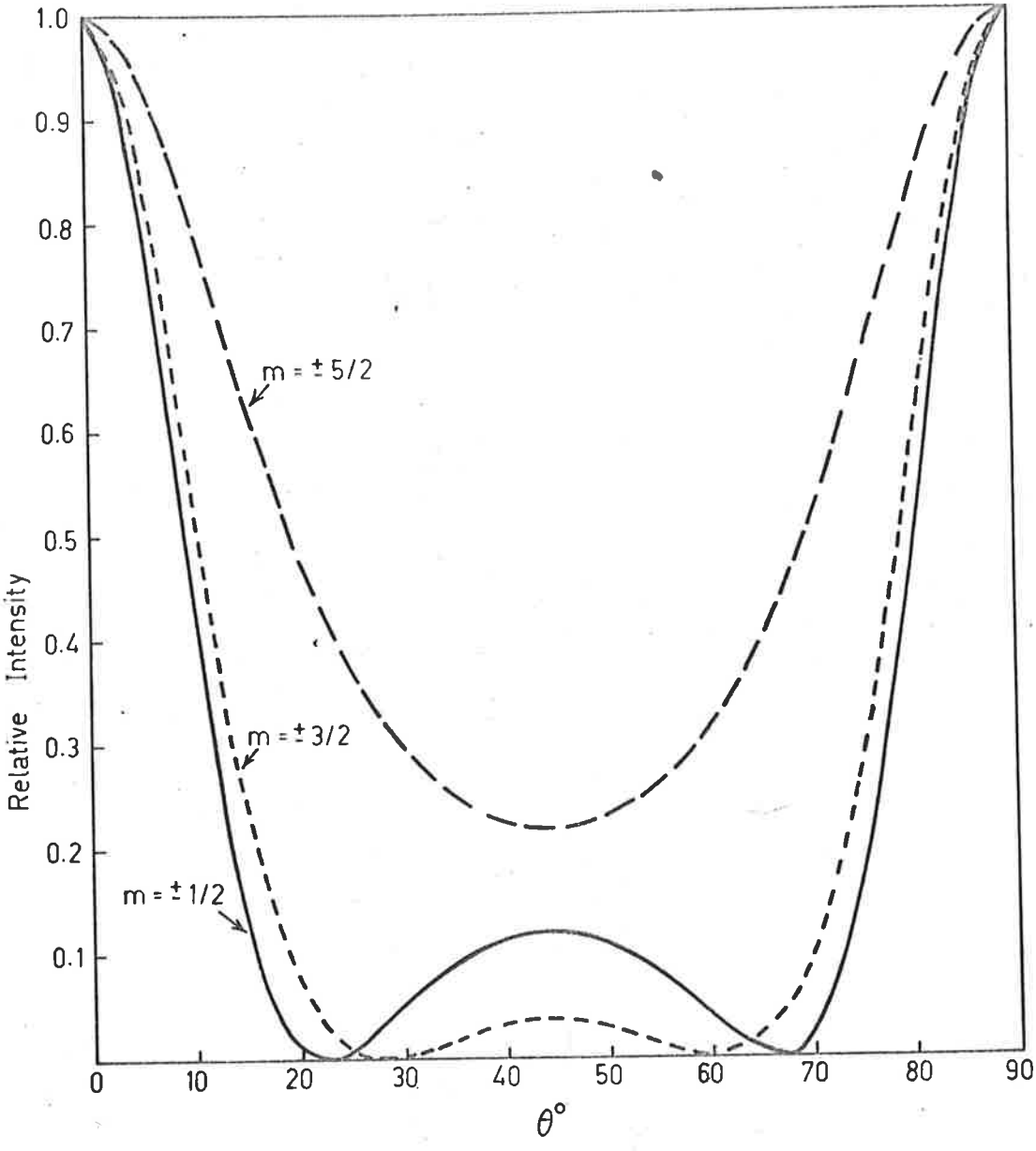

Predicted intensity variations — Allowed transitions D = 250 Oe

FIG. 7.11

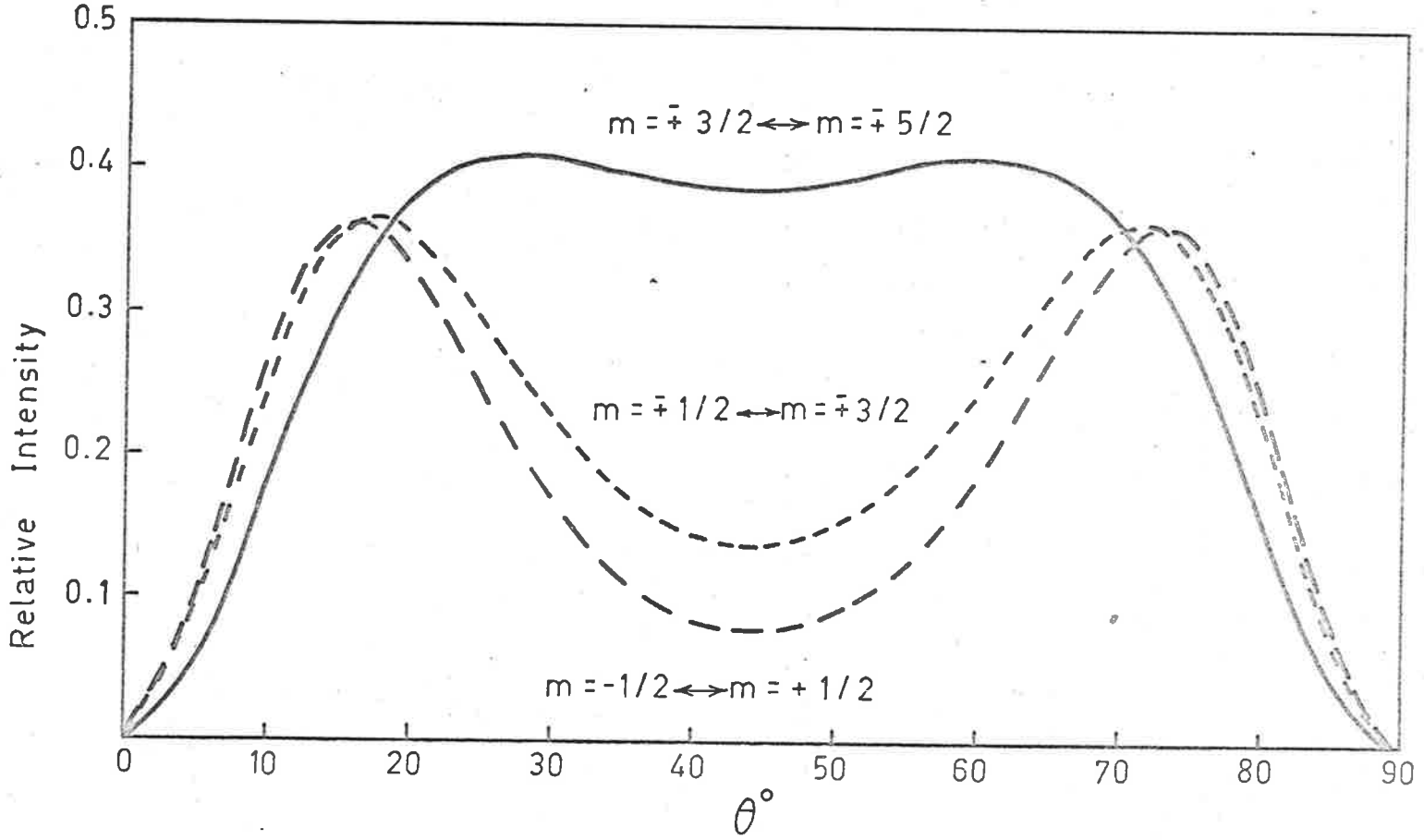

Predicted intensity variation — Forbidden transitions D = 250 Oe

FIG. 7.12

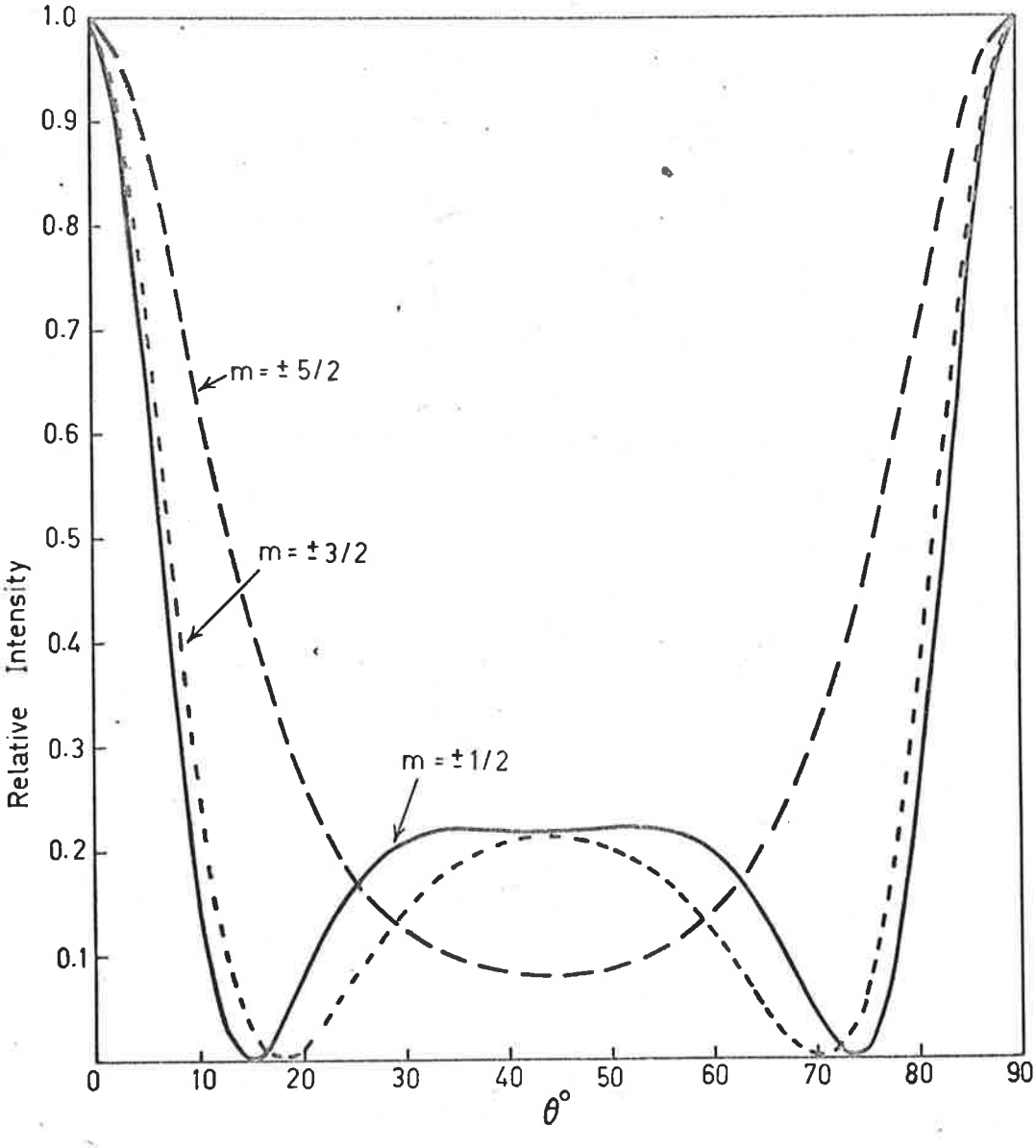

Predicted intensity variations — Allowed transitions D = 350 Oe

FIG .7.13

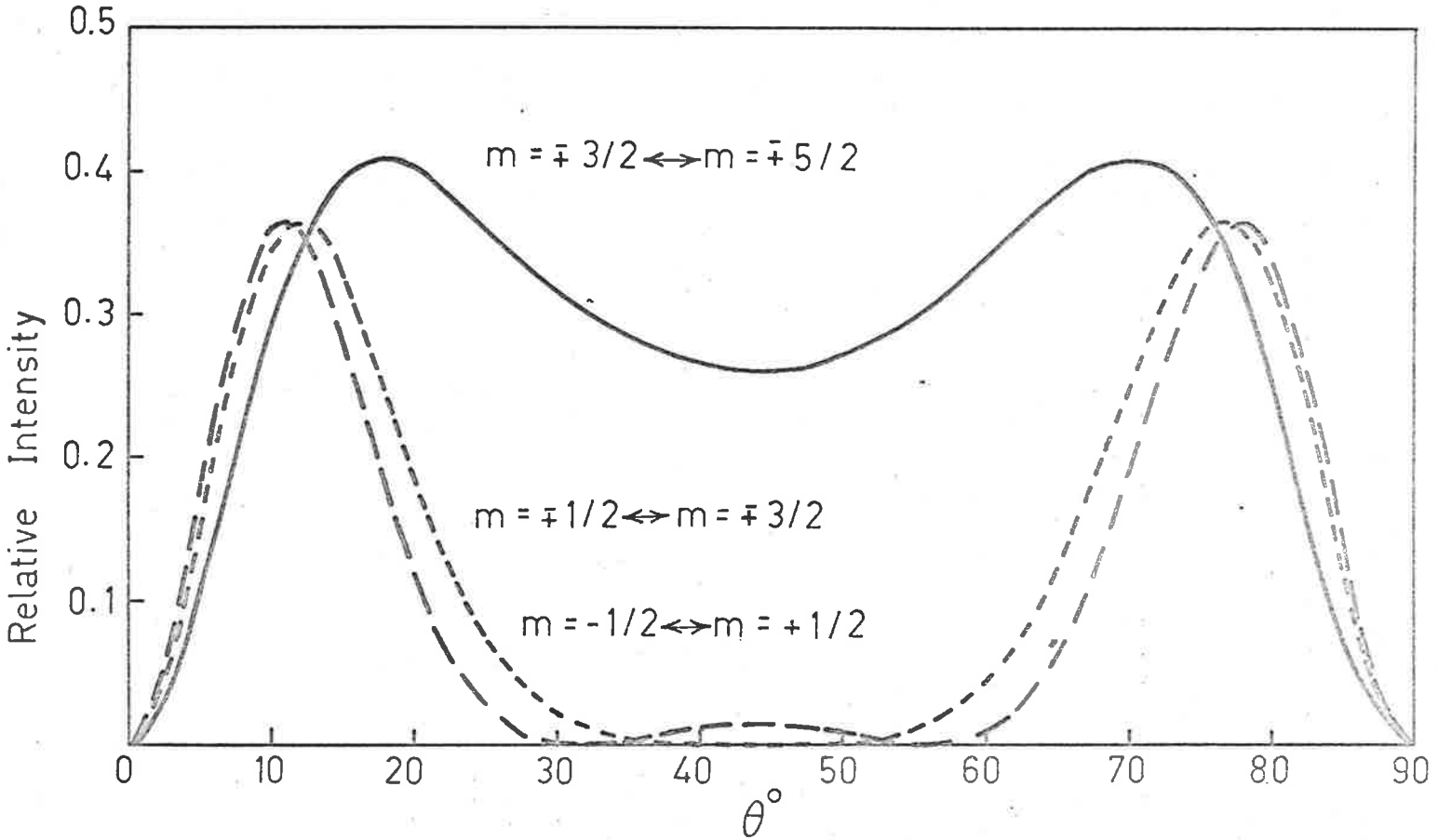

Predicted intensity variations — Forbidden transitions D= 350 Oe

FIG. 7.14

powder spectrum, corresponding to crystallites possessing this orientation, may not occur. The resultant powder spectrum then consists basically, of allowed transitions, corresponding to $\theta = 90^{o}$. e.g. Apatite powder spectrum, fig. 5.10.

8. Predicted intensity variations for $|D| = 876$ Oe are shown in figs. 7.15 and 7.16. From these, we may predict, that for values of 'D', of this order, $\theta = 90^{o}$ allowed peaks should still be the dominant feature of a powder spectrum.

It is of interest to compare the intensity variations, for $I = S = 5/2$, $|D| = 876$ Oe, calculated by Bir's method, with intensity variations for $I = 7/2$, $S = 3/2$, $|D| = 876$ Oe, shown by Bleaney and Rubins (1961), calculated by computer diagonalization of the 36 x 36 energy interaction matrix. For $m = \pm \frac{1}{2}$ ($\Delta m = 0$, $\Delta m = \pm 1$), the variations predicted by the two methods are qualitatively in agreement, as may be seen by a comparison of figs. 7.15 and 7.16, with fig. 3 of Bleaney and Rubins (1961).

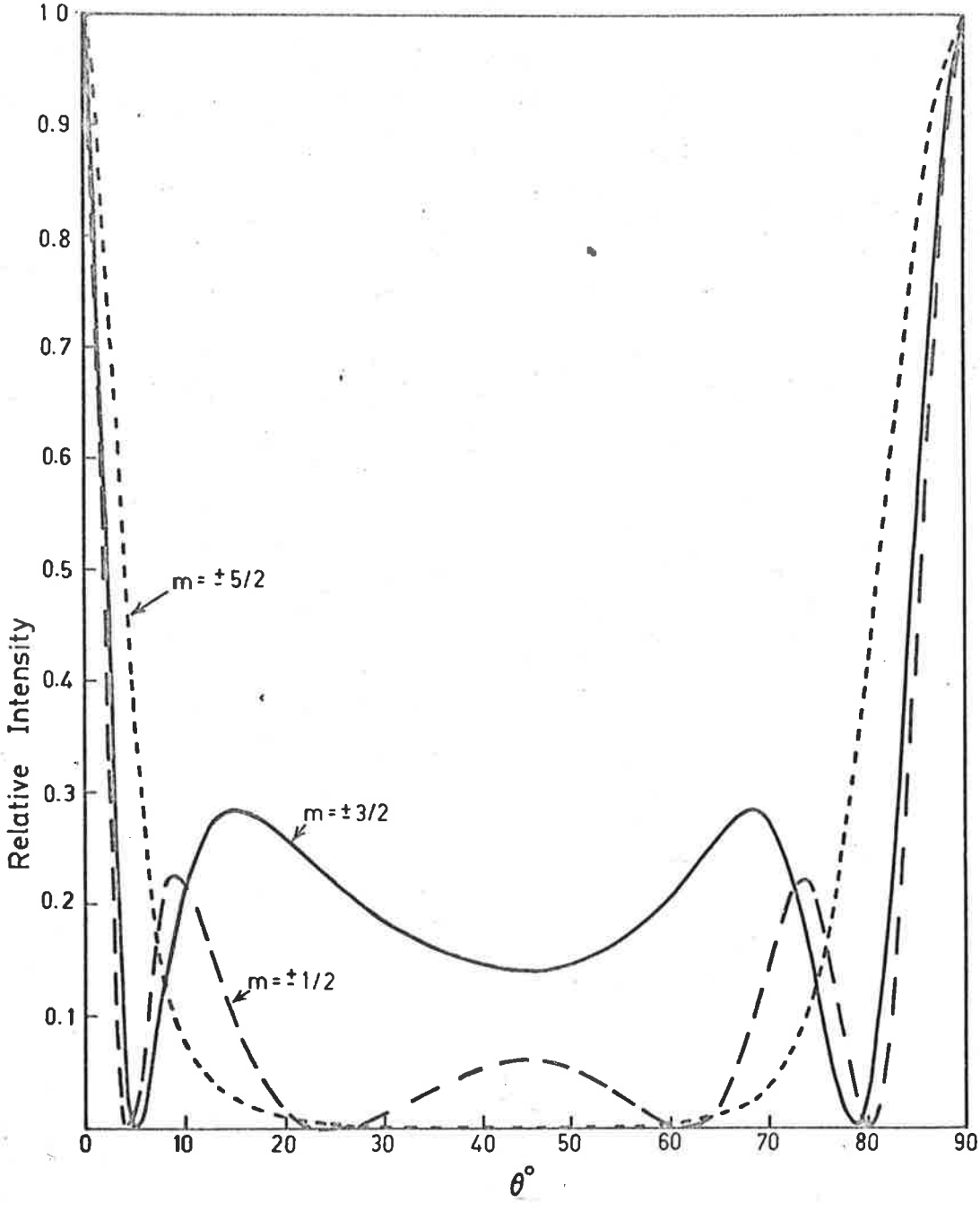

Predicted intensity variations — Allowed transitions
D = 876.0 Oe

FIG .7.15

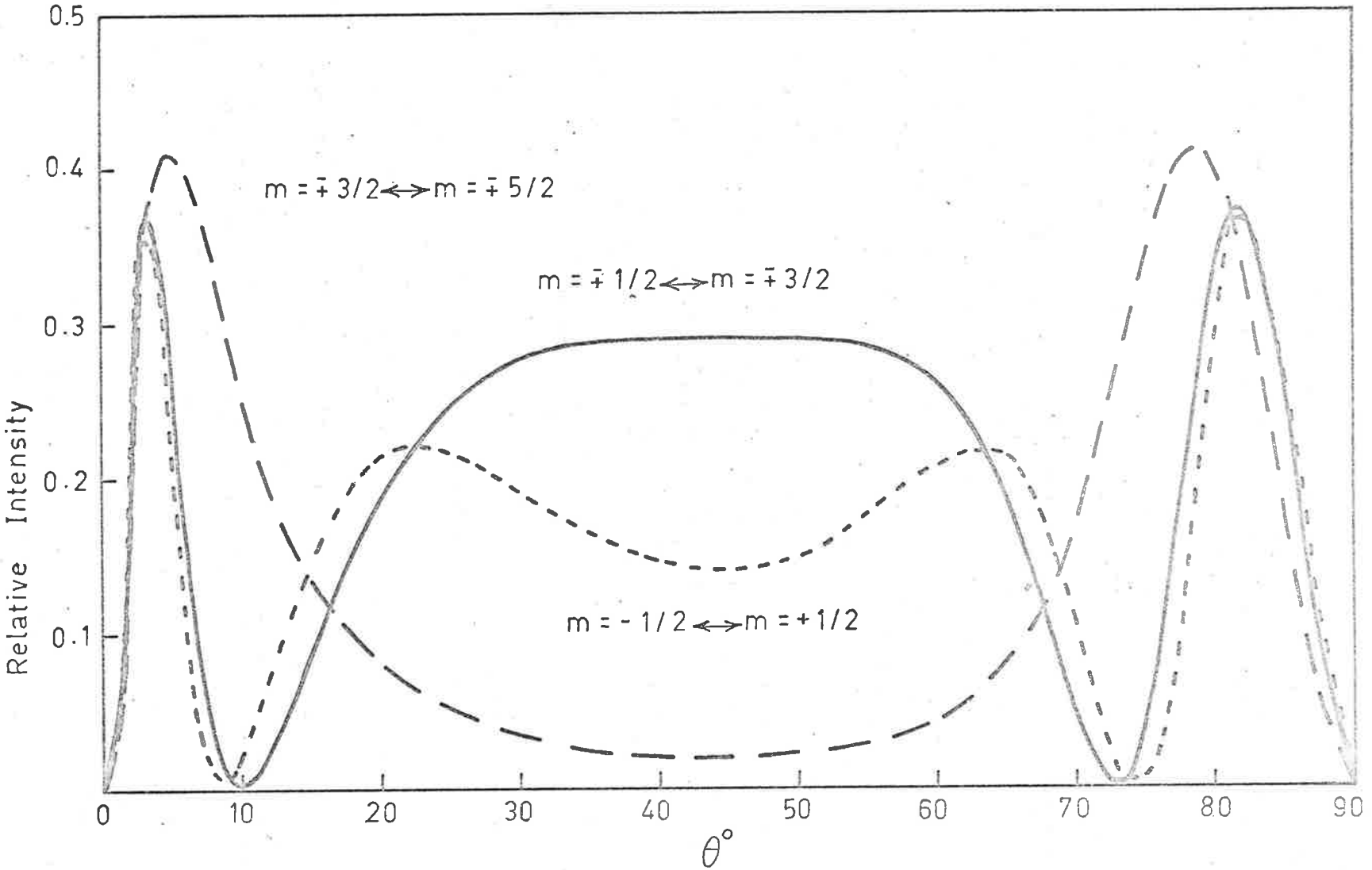

FIG. 7.16

Predicted intensity variations — Forbidden transitions D = 876.0 Oe

CHAPTER VIII

The Effect of Rhombic Crystal Field Symmetry

8.1 Introduction.

Hayashi and Ono (1953) have reported the existence of four non-equivalent Mn^{2+} ion sites in $MgSO_4.7H_2O$. These ion sites were characterized by the parameters A = - 94.7 Oe, D = 428 Oe, E~0. The Z axes of the crystal fields at these sites possessed direction cosines relative to the crystal axes a, b and c of ($\pm$ 0.282, 0.952, 0.122), ($\pm$ 0.282, 0.952, -0.122).

For this value of the parameter 'D', the theory presented above predicts that the spectrum from a powder sample of $MgSO_4.7H_2O$ (Mn^{2+}), should consist basically, of six $\theta = 90^{o}$ allowed lines. Contrary to this prediction, the spectrum obtained was extremely complex (fig. 8.1), which suggested that the published parameters were incorrect, and single crystal studies were then undertaken. Agreement with Hayashi and Ono was obtained for the magnitude of the parameter 'D', but a relatively large value of E(~80 Oe) was necessary to describe the observations that for rotation in the X-Y plane ($\theta = 90^{o}$), large variations of line positions and line intensities occurred. It was then postulated that the complexity of the $MgSO_4.7H_2O$ (Mn^{2+}) powder spectrum was due to the rhombic component of the crystal field, and the theory of such a component, and its effect on powder spectra, was then investigated.

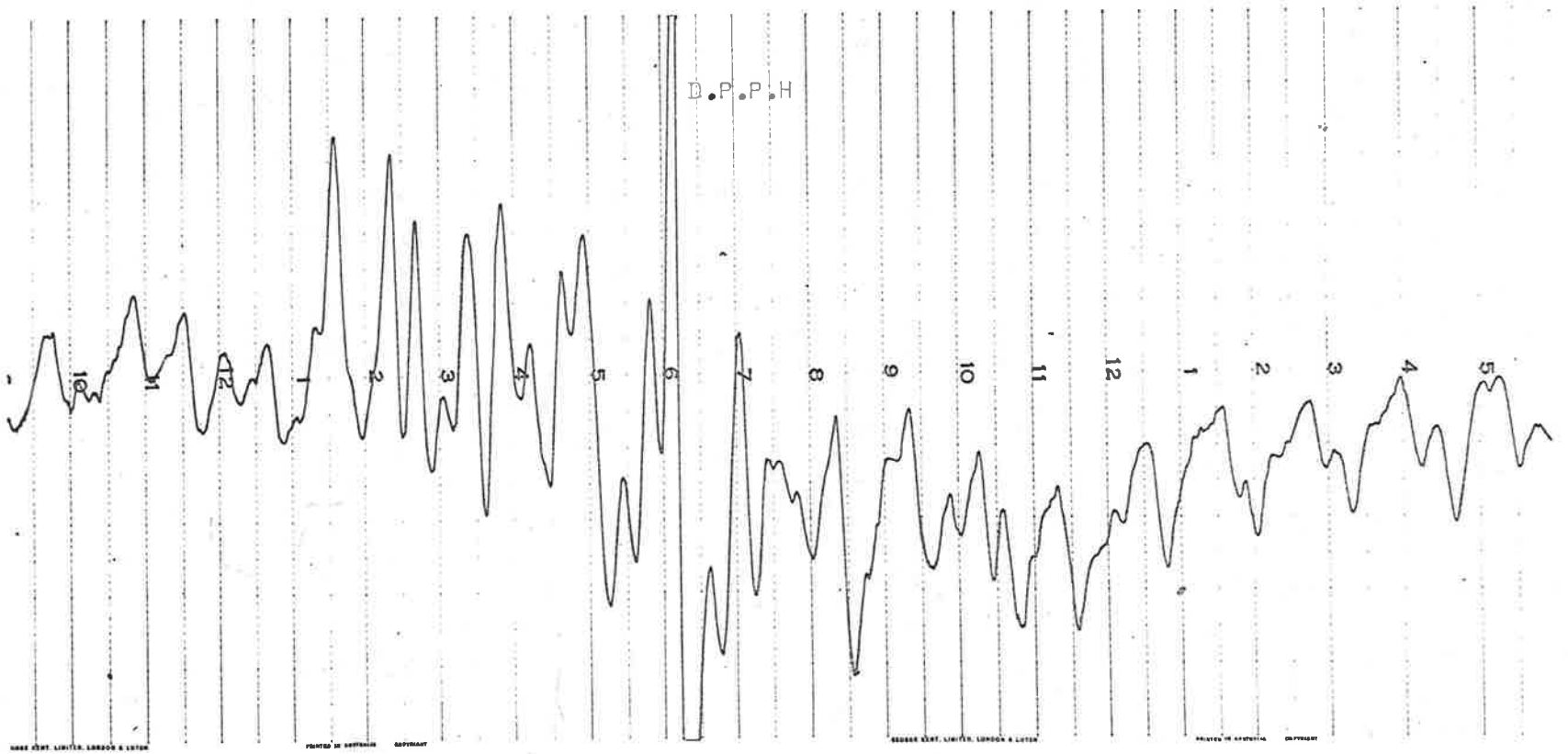

FIG . 8.1

Mn^{2+} SPECTRUM FROM POWDERED EPSOM SALT

It has been assumed by some authors that the only effect of a rhombic component of the crystalline field, on a spectrum from a powdered sample containing Mn^{2+}, is a broadening of lines. (Kasai 1962, de Wijn & Van Balderen 1967.) It will now be shown, however, that if a rhombic component exists -

a) the $\theta \sim 40^{\circ}$ components of the powder spectrum are preferentially broadened, compared to the $\theta = 90^{\circ}$ lines.

b) Splitting of the $\theta = 90^{\circ}$ lines may occur.

8.2 The effect of Random Orientation.

For a powder sample we have seen in section 1.5 that the probability of the direction of the applied field lying in the elementary solid angle dw, about the direction θ, ψ , is:-

$$\frac{\sin\theta d\theta d\psi}{4\pi} \qquad (8.1)$$

From the symmetry of the ψ variation, it then follows that for a given θ, the intensity or line shape function for the ψ variatior is:-

$$I'(\psi) \propto \frac{I(\psi)}{dH/d\psi}\Bigg|_{\theta = \text{cons}} = \frac{I(\psi)}{\partial H/\partial \psi} \qquad (8.2)$$

The angular variation of line positions for rhombic symmetry, may be derived from line positions for axial symmetry, given in section 3.5

Substituting -

$$\sigma = \frac{1}{2}\left[D(3\cos^2\theta - 1) + 3E\sin^2\theta\cos 2\psi\right] \quad \text{for} \quad \frac{D}{2}(3\cos^2\theta - 1)$$

$$|\lambda|^2 = \frac{1}{4}\left[\left\{\sin\theta\cos\theta(D-E\cos2\psi)\right\}^2 + \left\{E\sin\theta\sin2\psi\right\}^2\right]$$

$$\text{for}\left(D\sin2\theta\right)^2$$

$$|\rho|^2 = \frac{1}{16}\left[\left\{D\sin^2\theta + E(\cos2\psi\cos^2\theta + \cos2\psi)\right\}^2 + \left\{2E\cos\theta\sin2\psi\right\}^2\right]$$

$$\text{for}\ \left(\frac{D\sin^2\theta}{4}\right)^2$$

we obtain -

$$H_i(\theta,) = R_i\sigma + S_i.\lambda^2 + T_i.\rho^2 \qquad (8.3)$$

	R_i	S_i	T_i
$i = 1$ $(\Delta m = 0)$	$\frac{-8A^2m}{H_o^2}$	$\frac{64}{H_o} - \frac{576Am}{H_o^2}$	$\frac{-32}{H_o} - \frac{32Am}{H_o^2}$
$i = 2$ $(\Delta m = +1)$	-	$\frac{64}{H_o} - \frac{288A(2m-1)}{H_o^2}$	$\frac{-32}{H_o} - \frac{16A(2m-1)}{H_o^2}$
$i = 3$ $(\Delta m = -1)$	$\frac{-8A^2(2m-1)}{H_o^2}$	$\frac{64}{H_o} - \frac{288A(2m-1)}{H_o^2}$	$\frac{-32}{H_o} - \frac{16A(2m-1)}{H_o^2}$

Differentiation then produces:-

$$\frac{\partial H_i}{\partial\psi} = \sin2\psi\left[-3ER_i\sin^2\theta + S_i\left\{E\sin^2\theta\cos^2\theta(D-E\cos2\psi) + E^2\sin^2\theta\cos2\psi\right\}\right.$$

$$\left. + \frac{T_i}{4}\left\{4E^2\cos^2\theta\cos2\psi - E(\cos^2\theta+1)(D\sin^2\theta+E\cos2\psi(\cos^2\theta+1))\right\}\right] \qquad (8.4)$$

Extreme values of $\partial H/\partial\psi$ then occur at $\psi = 0$ and $\psi = 90^\circ$, and may occur at intermediate values depending on the magnitudes and relative signs of the various parameters.

For $I(\psi)$ we use the expression in Chapter VI, viz. -

$$I(\psi) \propto \left| d_I^{mm'}(-\mu_{\frac{1}{2}-\frac{1}{2}}) \right|^2$$

where the expression for μ $(= \cos\alpha_{\frac{1}{2}-\frac{1}{2}})$, when the crystal field possesses a rhombic symmetry, has been given in section 6.6 as:-

$$\mu = -\left(1 - \frac{2.048\,|\lambda|^2}{H_o^2}\right)$$

At this point we may note that for $E = 0$:-

$$|\lambda|^2 = D^2 \sin^2 2\theta / 16$$

but for $E \neq 0$, and $\theta = 90^o$:-

$$|\lambda|^2 = (2E)^2 \sin^2 2\psi / 16$$

and by comparison we may conclude that the $I(\psi)$ variations at $\theta = 90^o$, are similar to the $I(\theta)$, $(E = 0)$ variations, with $D = 2E$.

8.3 Discussion.

Typical values of $\frac{1}{\frac{\partial H}{\partial \psi}}$, $I(\psi)$ and $I'(\psi) \propto I(\psi)/\partial H/\partial \psi$ are shown qualitatively in fig. 8.2, and the $I'(\psi)$ variations, coupled with the spread of the lines, due to the ψ rotation, calculated from equations (8.3), shown in fig. 8.3. From this latter diagram it is seen that the spread of lines is greater for $\theta \sim 40^o$ than for $\theta = 90^o$. The observed intensity of a line in a powder spectrum generally decreases with an increase of the field region over which resonance may occur for the randomly oriented microcrystallites. It might therefore be expected, that, when Mn^{2+} ions are in a site

$1/(\partial H/\partial \psi)$ $I(\psi)$ $I(\psi)' = I(\psi)/(\partial H/\partial \psi)$

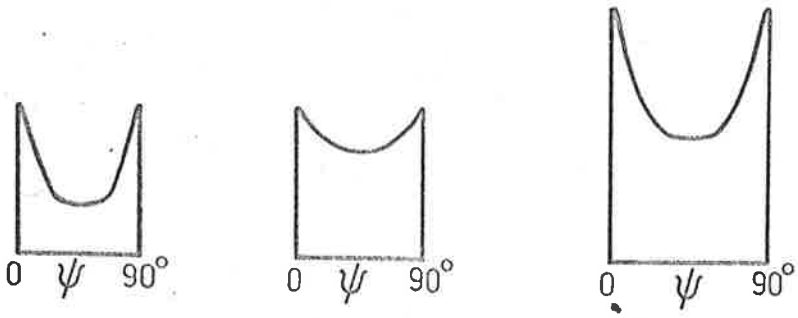

$\theta = 90°$ - allowed

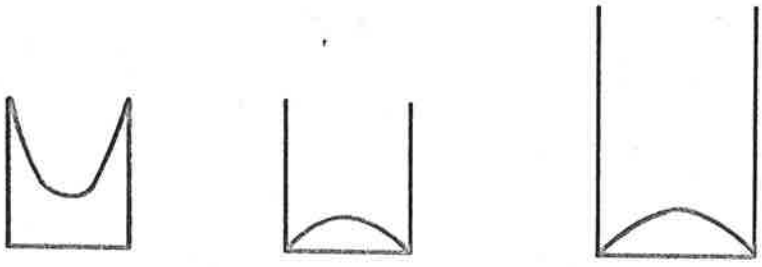

$\theta = 90°$ - forbidden

$\theta = 40°$ - allowed

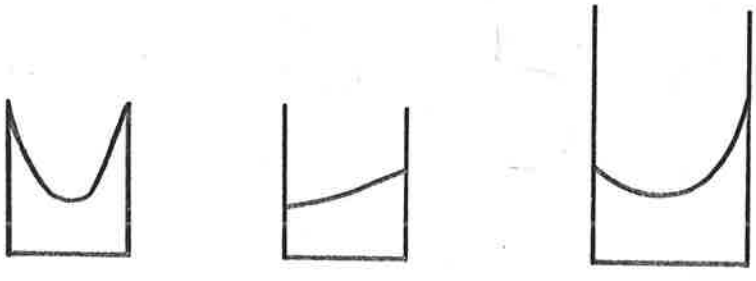

$\theta = 40°$ - forbidden

FIG. 8.2

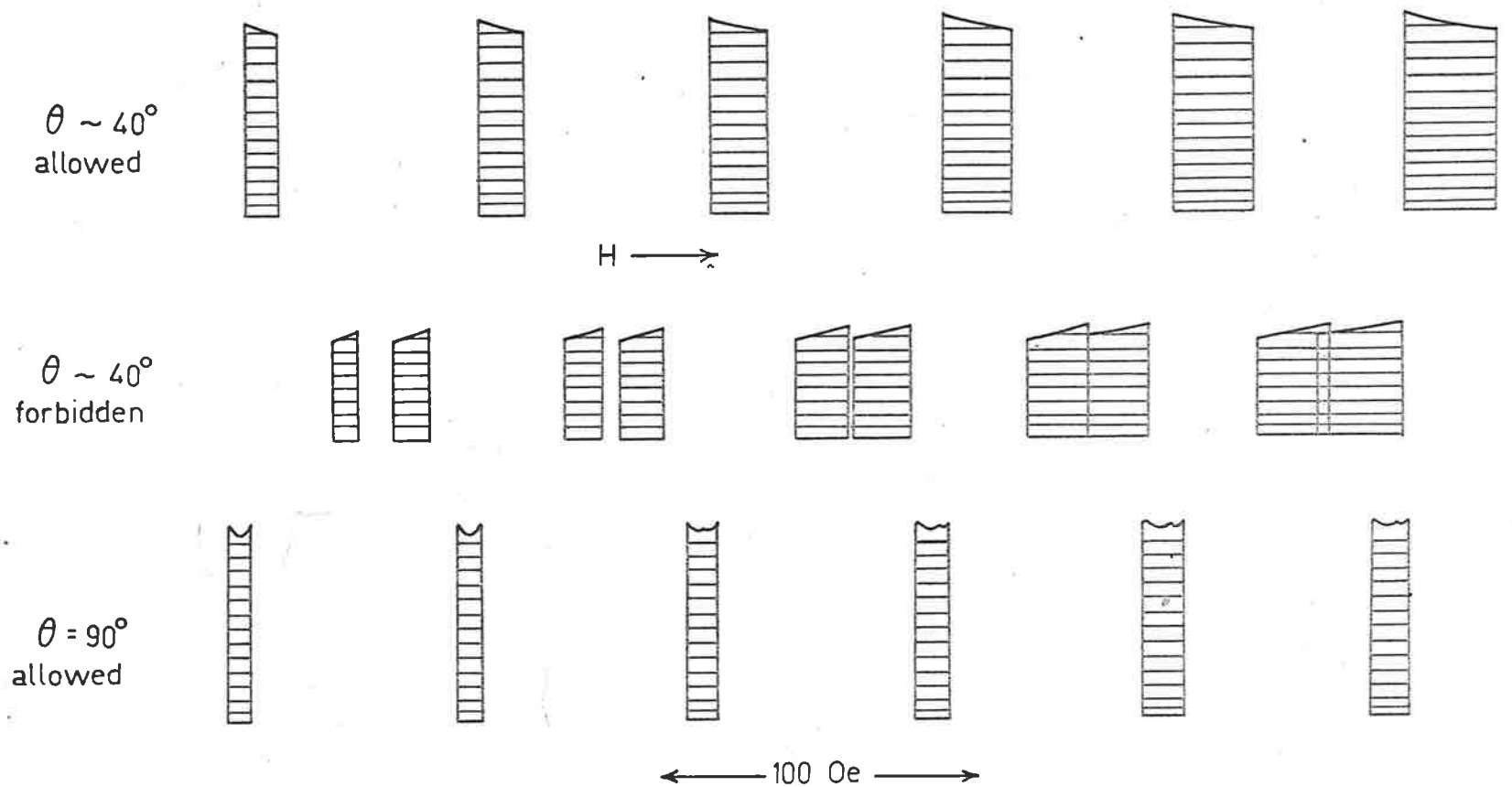

FIG. 8.3

Spread of lines in powder due to rhombic component.

of rhombic crystal field symmetry, ($E \neq 0$) the $\theta = 90^{\circ}$ allowed lines dominate the spectrum from a powdered sample. Such appears to be the case for the spectrum observed from a powdered sample of querched $NaCl(Mn^{2+})$, shown in fig. 8.4 for which the parameters listed in fig. 8.3 apply. (Morigaki et al, 1958) The magnitude of the parameter 'D' for this spectrum, is approximately the same as for the $CaWO_4$ spectrum, discussed in section 7.3. If a rhombic component broadened all lines of a powder spectrum equally, the powder spectrum of $NaCl(Mn^{2+})$ should then be a broadened edition of the tungstate powder spectrum. A comparison of these spectra shows that this is not so. The observed features of the chloride powder spectrum are explained however, if $\theta \sim 40^{\circ}$ components are preferentially broadened.

This preferential broadening could then introduce an underestimation of the parameter 'D' from a powder spectrum, using the Bleaney & Rubins' expression for relative intensities, derived purely for axial symmetry. The ratio of forbidden ($\theta \sim 40^{\circ}$) to allowed ($\theta \sim 40^{\circ}$ and $\theta = 90^{\circ}$) intensity would be smaller for $E \neq 0$, than for $E = 0$, for the same value of D. An underestimation of the parameter 'D' could then result if the Bleaney & Rubins' expression was then applied to the measured relative intensity observed in a 'rhombic' powder spectrum.

In the case of 'axial' powder spectra, forbidden doublets may not be relatively large for both very small ($D \sim 0$) and large

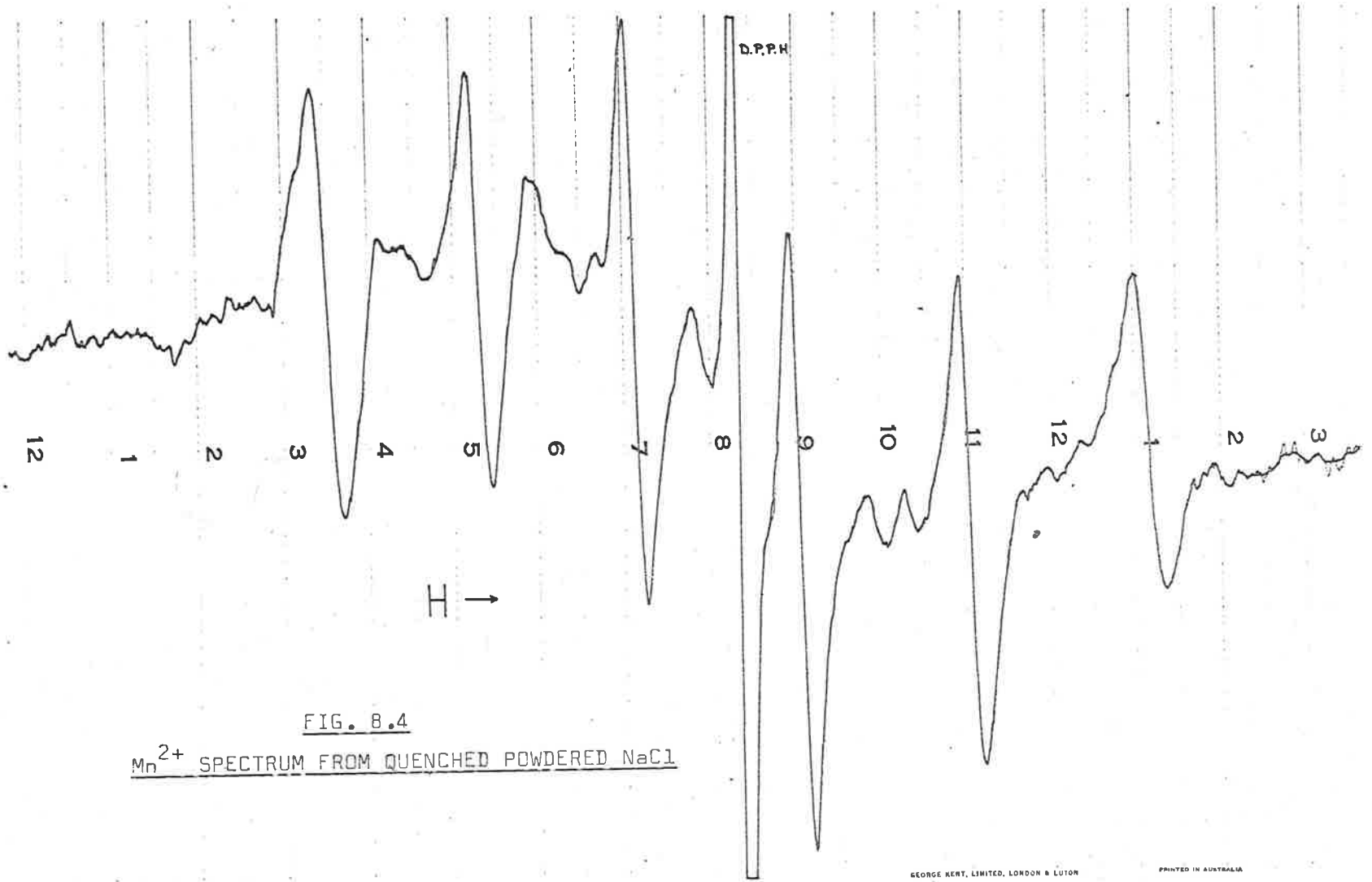

FIG. 8.4

Mn^{2+} SPECTRUM FROM QUENCHED POWDERED NaCl

(D ~ 400 Oe) values of D. For rhombic spectra these doublets may not be relatively large for all values of this parameter.

For |E| = 80 Oe, the computed intensity variations in the X-Y plane, for allowed transitions, are shown in fig. 8.4(a), and it is seen that the intensity of all lines is a maximum at $\psi = 0^{\circ}$ and 90° (i.e. H//OX and H//OY) and relatively small near $\psi = 45^{\circ}$. As $^{1}/\partial H/\partial\psi$ also has maximum values at $\psi = 0^{\circ}$ and $\psi = 90^{\circ}$, it would be reasonable to conclude, that as the line shape function for rhombic symmetry $I'(\psi)$, is the product of $I(\psi)$ and $^{1}/\partial H/\partial\psi$, both of which have maxima at $\psi = 0$ and $\psi = 90^{\circ}$, that for $E \sim 80$ Oe, $\theta = 90^{\circ}$ powder peaks are not spread evenly by a rhombic component but concentrated into two components, corresponding to $\psi = 0$ and $\psi = 90^{\circ}$, with the magnitude of the splitting approximately constant for each line. Fig 8.4(b) For axial symmetry we have seen that qualitatively a powder spectrum may be regarded as the sum of $\theta \sim 40^{\circ}$ and $\theta = 90^{\circ}$ single crystal spectra. In a similar manner we may generalize and state that for rhombic symmetry the resultant powder spectrum could be expected to be the sum of the H//OX and H//OY single crystal spectra.

8.4 Interpretation of the $Mg(Mn^{2+})SO_4.7H_2O$ Powder Spectrum.

Single crystal spectra with the applied static field parallel to the OX and OY crystal field axis of one of the ion sites are shown in fig. 8.5, together with a powder spectrum, with an

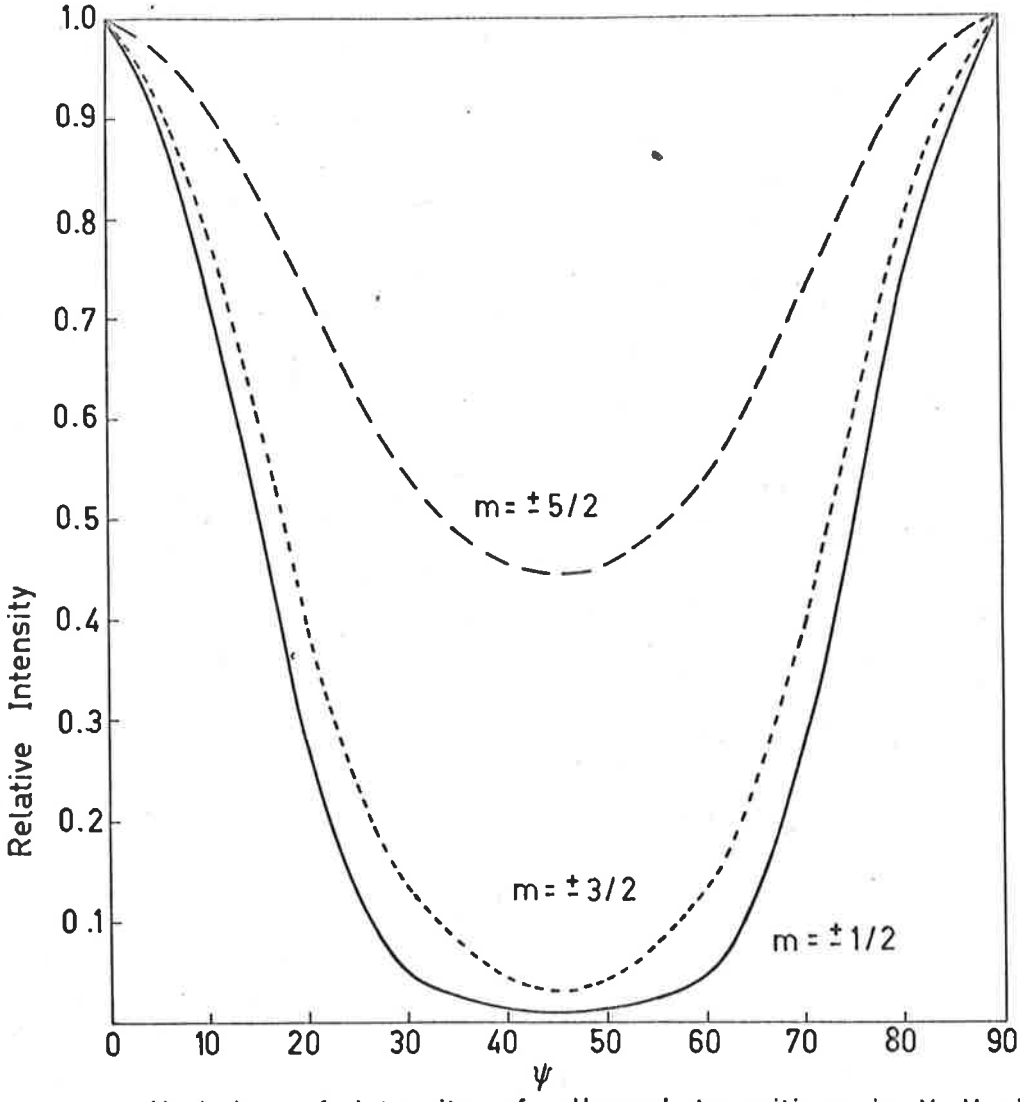

Variation of intensity of allowed transitions in X - Y plane.
($\theta = 90^{\circ}$) E = 80.0 Oe

FIG. 8.4(a)

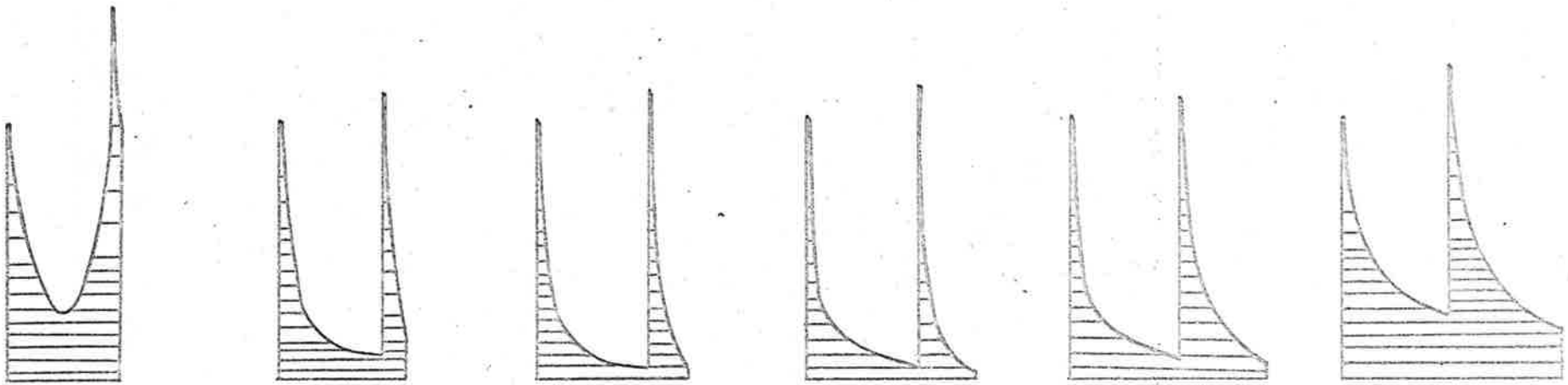

D = 259.4 Oe

E = 106.7 Oe

A = - 97.2 Oe

FIG : 8.4(b)

Splitting of $\theta = 90^{\circ}$ components due to rhombic crystal field.

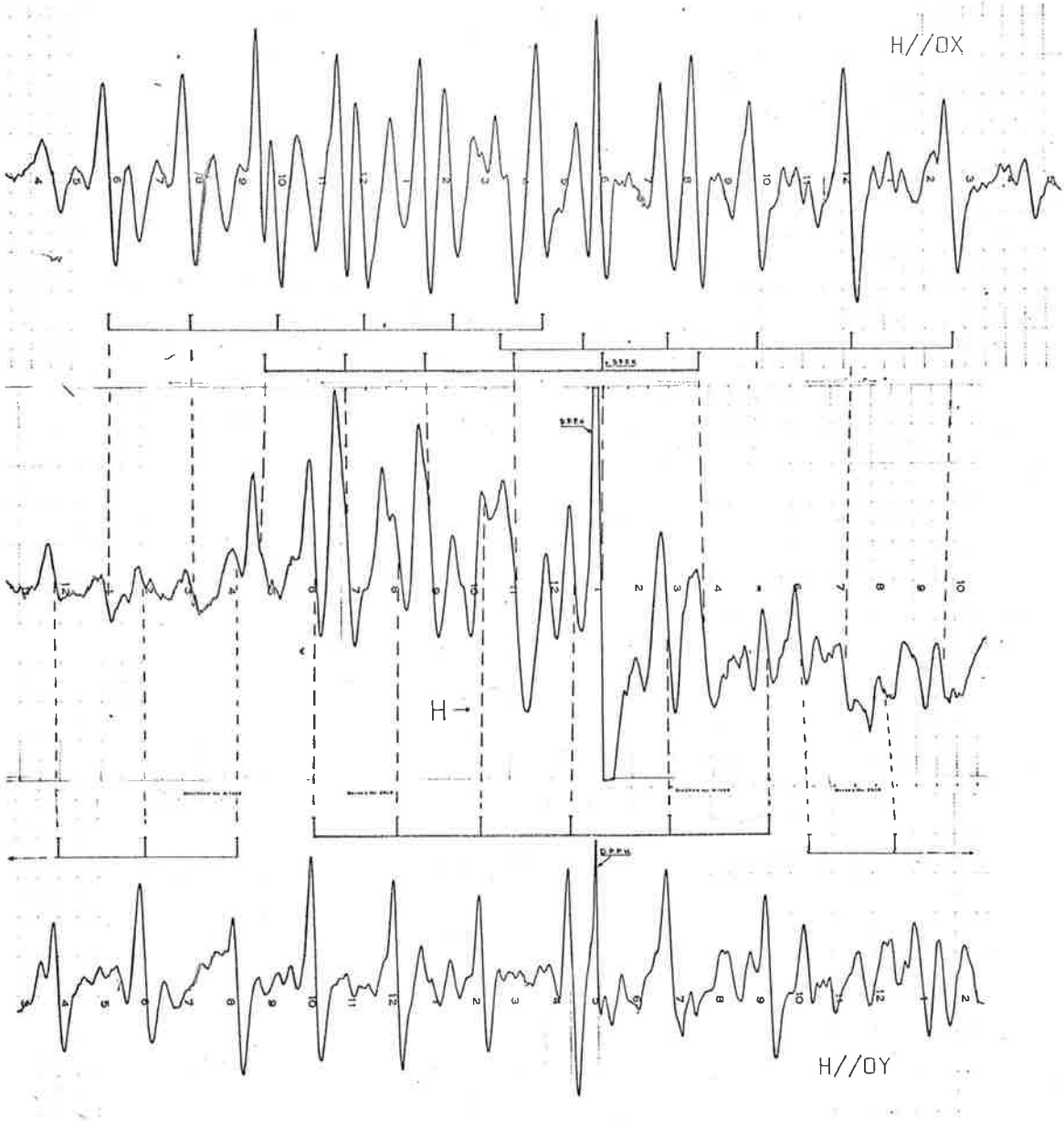

FIG. 8.5

interpretation of the powder lines illustrated bya projection of lines in the single crystal spectra. Reasonable agreement with theory presented, that for rhombic symmetry a powder spectrum may be regarded as the sum of single crystal H//OX and H//OY spectra, is then obtained.

8.5 Mn^{2+} in Tremolite.

The spectrum of Mn^{2+} in tremolite, $H_2Ca_2Mg_5(SiO_3)_8$, has been studied by Manoogian (1968 a, 1969 b). He reported the existence of a single ion site characterized by the parameters:-

g = 1.995, A = -79.9 Oe, D = -442.9 Oe, E = -79.4 Oe.

For the value of the parameter 'E', it could be expected that a complex powder spectrum could be obtained. The powder spectrum observed from the first sample of tremolite obtained by this author (locality : St. Lawrence County, N.Y., U.S.A.) is shown in fig. 8.6. In contrast to the predicted complexity, a relatively simple six-line spectrum is obtained. Because of this, single crystal investigations were carried out to check the parameters given by Manoogian, and an additional Mn^{2+} spectrum was detected. Structurally, tremolite and diopside are similar. (Manoogian 1968 a) Two Mn^{2+} ion sites have been reported for diopside (Vinokurov et al 1964 a) and a second ion site in tremolite could be expected. Fig. 8.7 shows a single crystal spectrum recorded with the applied magnetic field parallel to the Z axis of the site (denoted I) described by Manoogian. Lines of this second spectrum (II) may

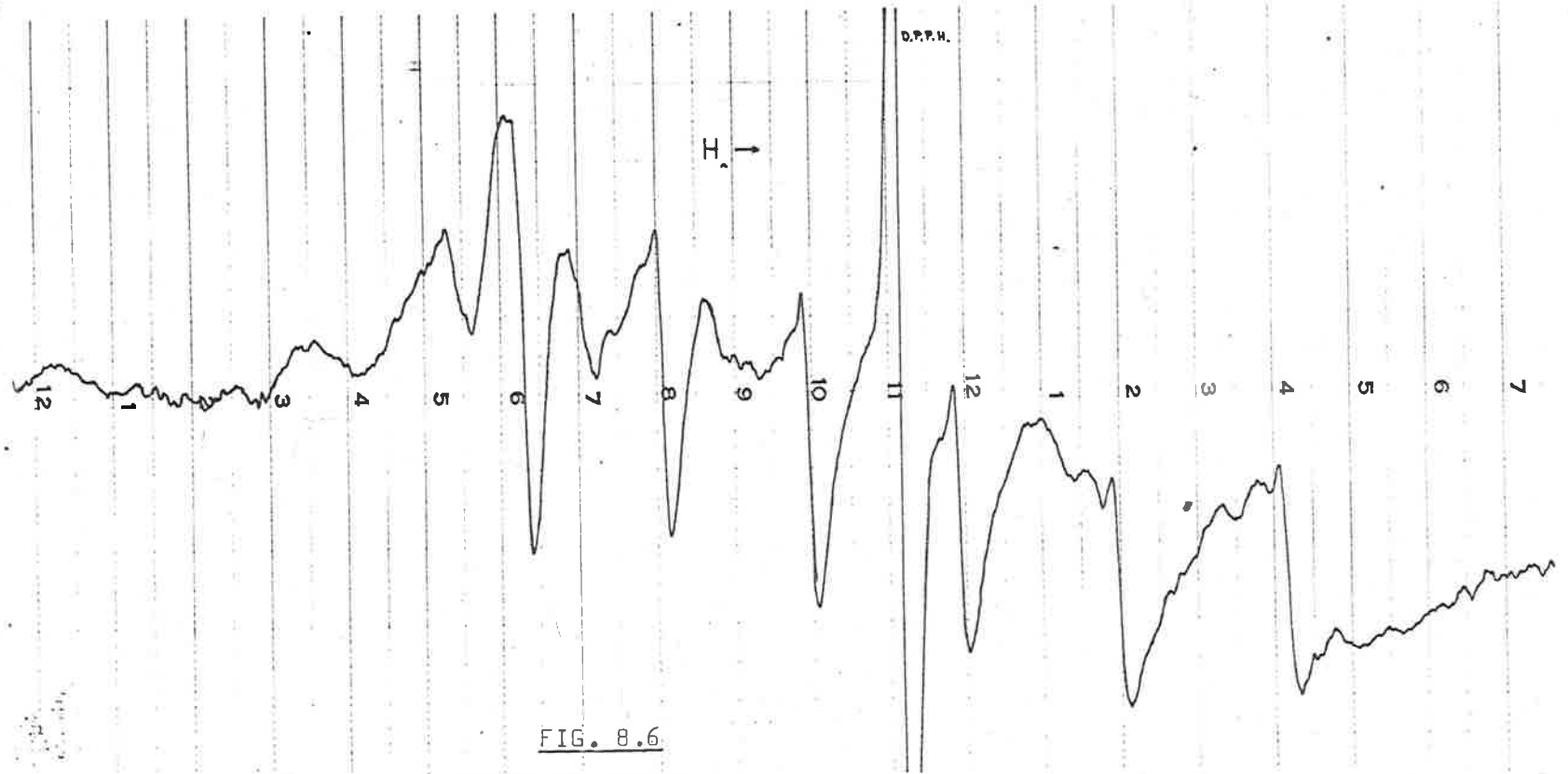

FIG. 8.6

TREMOLITE POWDER

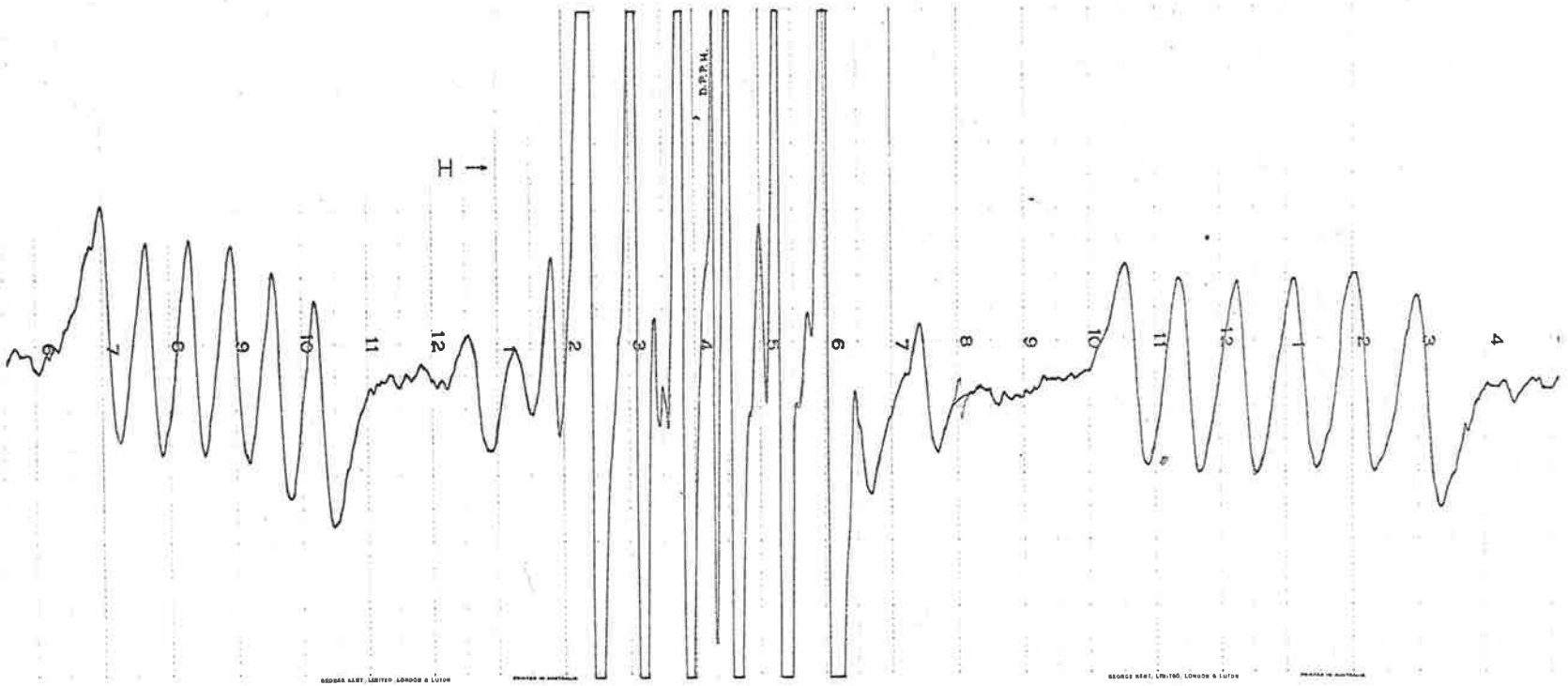

FIG. 8.7

be seen on either side of, and underlying, the central hyperfine sextet of spectrum I. These lines are also observable in the spectrum of white tremolite shown by Manoogian, who has acknowledged the existence of these weaker lines (personal communication, January, 1969), but stated that he could not definitely identify these lines as part of a Mn^{2+} spectrum. In the X-Y plane of the ion-site I, however, the lines of spectrum II almost rival in intensity the lines of spectrum II, for the sample of tremolite used by this author. (The lines of spectrum I are of smaller intensity for H//OX and H//OY than for H//OZ.) This is shown in fig. 8.8, and the additional six line spectra clearly seen in these records may be assigned as originating from Mn^{2+}.

No fine structure could be firmly associated with this second spectrum, and parameters could not therefore be fully determined. From the spectra shown in fig. 8.8, a mean hyperfine splitting of 92.5 Oe was obtained. During rotation of the sample in the applied magnetic field, only relatively small variations of intensity and field position were observed for lines of spectrum II compared with variations for spectrum I indicating a much smaller value of the parameter 'D' compared to that for spectrum I. From fig. 8.6 it is seen that the powder spectrum consists of a reasonably sharp six line spectrum with no large forbidden transitions or splitting of hyperfine lines visible, centred rear the D.P.P.H. resonance.

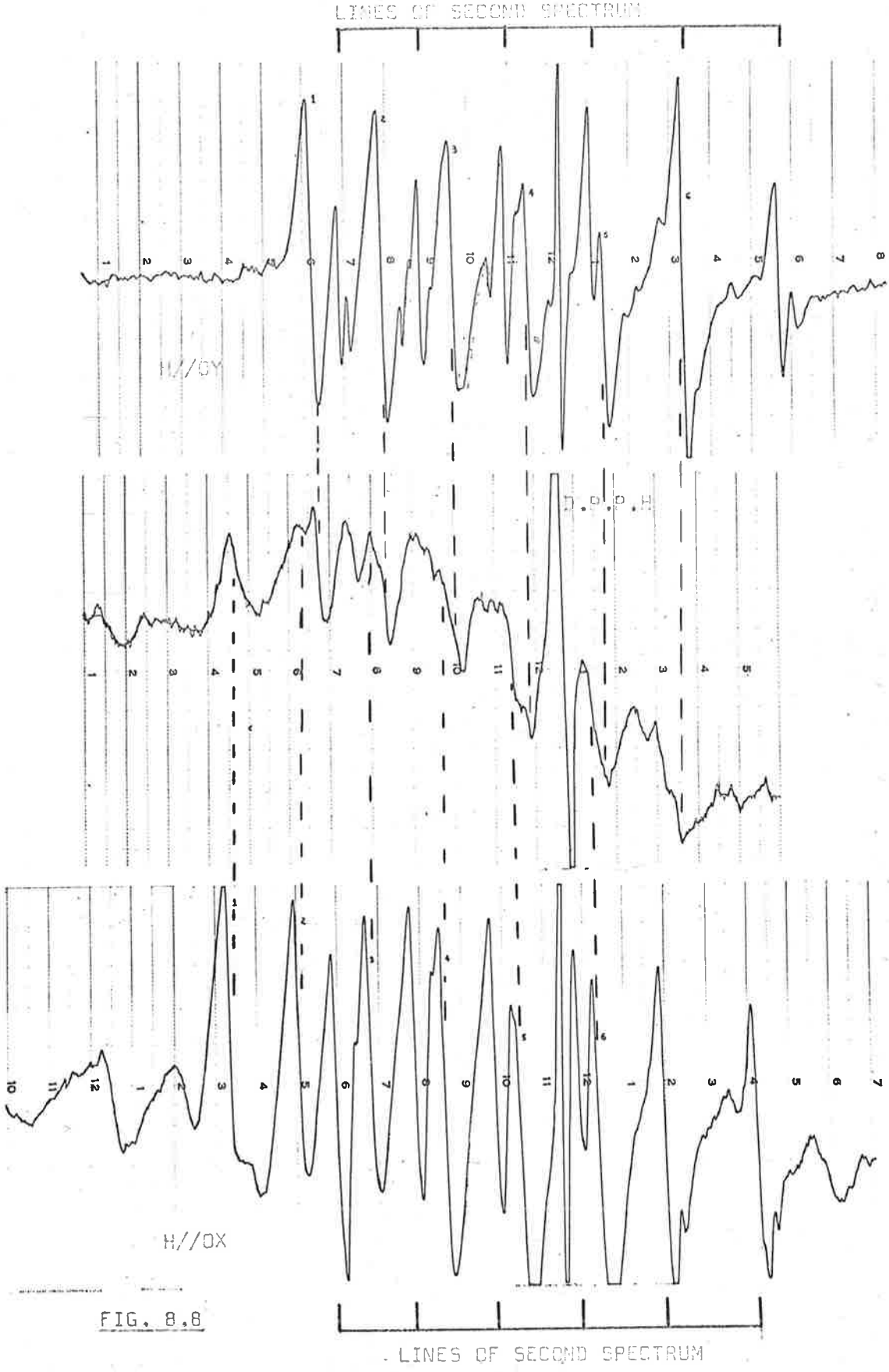
LINES OF SECOND SPECTRUM
H//OY
D. D. D. H
H//OX
LINES OF SECOND SPECTRUM

FIG. 8.8

These features all indicate that the Mn^{2+} ion site mainly responsible for the powder spectrum is characterized by $|D| \sim 50$ Oe, $E \sim 0$, or a slightly larger D value with $|E| \sim 10 - 20$ Oe. It may then be assumed that the powder spectrum shown in fig. 8.6 is due to Mn^{2+} in site II and this spectrum masks the spectrum from site I, for this particular sample of tremolite.

The relative occupation of the two sites, by Mn^{2+} impurities, apparently varies from sample to sample,as the spectrum from pink tremolite shown by Manoogian (1968 a) shows no second spectrum. This was confirmed by single crystal observations using samples of this pink tremolite,which was kindly sent to this author by Dr. A. Manoogian (February, 1969). The powder spectrum from this sample was extremely broadened however, and showed no clear hyperfine structure. The broadening is attributable mainly to dipolar interaction, the Mn^{2+} concentration in this particular sample being $\sim 3\%$. (Manoogian 1968 a).

Another sample of tremolite obtained produced the powder spectrum shown in fig. 8.8. The seven-line spectrum observed,could possibly be interpreted as being due to Mn^{2+} with "OX" and "OY" peaks of spectrum I, overlapping, as shown in this figure. The sample from which this powder spectrum was obtained was polycrystalline,and single crystal studies were not possible. The "OX" and "OY" spectra, shown in this figure, are from the New Jersey sample.

The thermal breakdown of tremolite to a pyroxene of diopside - clinoenstatite type by dehydroxylation, has been studied by Freeman and Taylor (1960). Attempts to follow these changes, by observing changes in the Mn^{2+} spectra, met with no success however. After heat treatment at $1,000^{o}$ - $1,200^{o}$ C for periods up to 24 hours, no hyperfine structure could be observed in the samples. It is known (Wittels, 1952) that iron impurities in tremolite undergo a change of oxidation state at ~ 800^{o} C, and this would probably occur with Mn^{2+} impurities as well.

8.6 Mn^{2+} in Cordierite (Dichroite, Iolite) $Al_3Mg_2(Si_5Al)O_{18}$.

Cordierite, a natural silicate of aluminium and magnesium, is a semi-precious gemstone (water saphire). The spectrum of Mn^{2+} in this mineral has been reported by Hedgecock and Chakravartty (1966), who were however mainly concerned with an investigation of a Fe^{3+} spectrum also observable, and gave no parameters for the Mn^{2+} spectrum. Quoting these authors - "Preliminary observations indicate that manganese occupies a single site, having nearly axial symmetry about the C axis and with a comparitively small crystalline field. (The groups of hyperfine lines overlap at X band.) Presumably manganese is located substitutionally at the Mg sites."

The spectrum obtained from a powdered sample of cordierite was recorded, and is shown in fig. 8.10. It was apparent from the features of this spectrum (six broad lines, no observed splitting

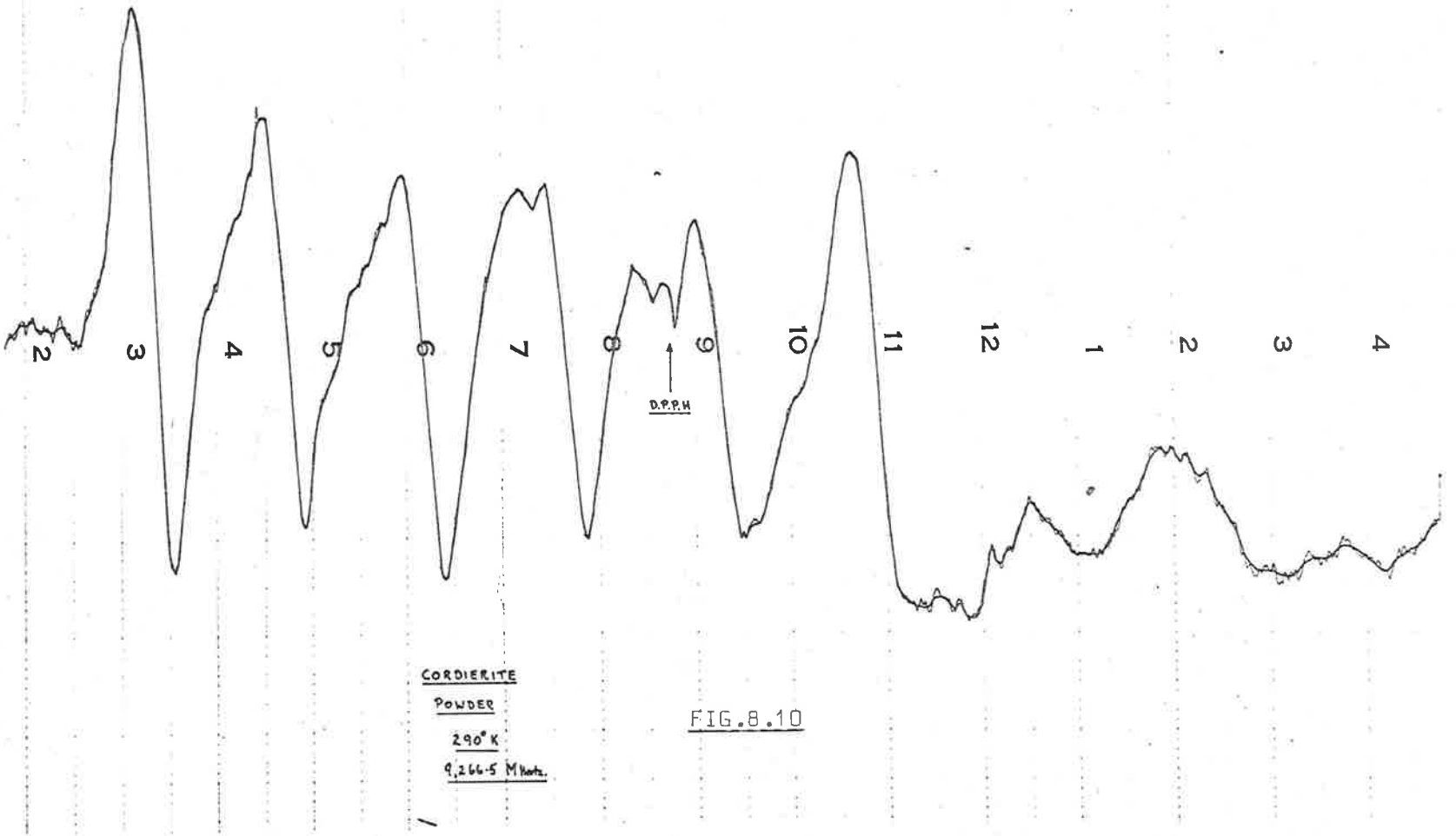

CORDIERITE
POWDER
290°K
9,266·5 M Hertz.

FIG.8.10

of allowed transitions and no large forbidden lines), that the Mn^{2+} ion was not occupying a site of "comparitively small crystalline field" - "having nearly axial symmetry" and single-crystal investigations were therefore carried out.

Samples of cordierite from three localities were obtained (Ceylon, Hart's Range (Australia) and Tsihombe (Madagascar)). These samples had the appearance of a glass with no recognizable crystal faces, and exhibited the intense dichroism characteristic of this material. Viewed in unpolarized white light the samples appeared blue in a direction parallel to the C axis (Miers 1929), and yellow away from this direction, as described for the Madagascar cordierite used by Hedgecock and Chakravartty. The spectrum obtained from the Ceylon sample with the applied static magnetic field parallel to the C axis is shown in fig. 8.11. Identical spectra were obtained for the samples from Hart's Range and Madagascar, and it is readily seen that for this X-band recording, the groups of hyperfine lines do not overlap, in contrast to the observations by Hedgecock and Chakravartty. The parameters obtained from single crystal measurements were -

$g = 2.00 \ (\pm 0.005)$ $\quad \nu_0 = 9.257$ G Hertz

$A = 92.5$ Oe (± 0.5) $\quad T = 290^{\circ}$ K

$D = 430.0$ Oe (± 10)

$E \sim 10$ Oe

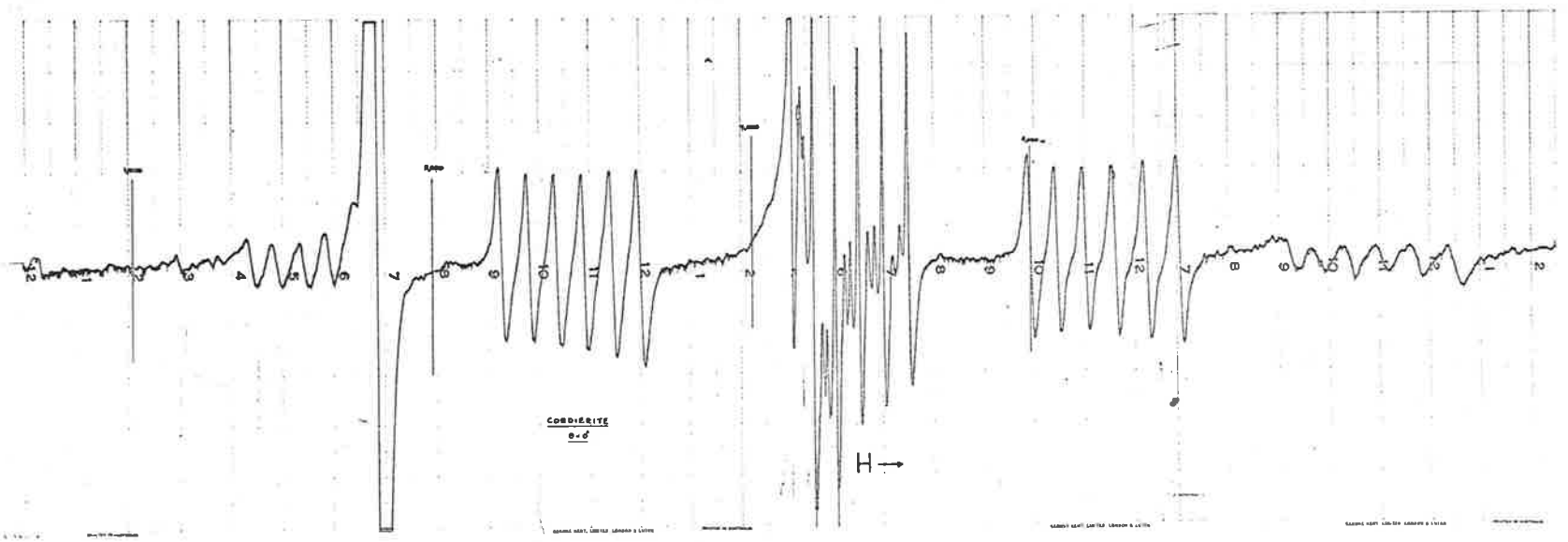

FIG. 8.11

The features of the powder spectrum discussed above, are then in agreement with theory presented previously, for these values of parameters.

It could only be assumed by this author, that the observations by Hedgecock & Chakravartty were made in the X-Y plane of the crystal field. This was confirmed in a letter received from Hedgecock (January, 1969). In this letter Hedgecock has also pointed out that the "comparitively small crystalline field" at the Mn^{2+} ion site, was meant to imply that the field was small compared to the field at the Fe^{3+} site, for which D = 14.6 k Oe.

The following parameters for the Mn^{2+} spectrum in cordierite were also communicated by Hedgecock.

	300^{o} K	77^{o} K	
b_2^o	= 422 ± 2	432 ± 2	b_2^o = D
b_2^2	= 27 ± 3	18 ± 3	b_2^2 = 3E
b_4^o	= - 4 ± 1	- 5 ± 1	
b_4^2	= -13 ± 9	+ 3 ± 9	
b_4^4	= -23 ± 12	-14 ± 12	
g	= 1.997 ± 0.003	} Isotropic within experimental error	
A	= - 90 ± 5		

8.7 Mn^{2+} in Pectolite : $Ca_2Na\ H(SiO_3)_3$.

The spectrum from a powdered sample of pectolite is shown in fig. 8.12. The difficulty of obtaining precise information about the crystal field symmetry and parameters, from certain powder spectra, is illustrated by considering this spectrum as an example. The broadness of the observed allowed transitions could possibly indicate a large D value, if the crystal field symmetry was completely axial. However, the same effect could be produced if the field possessed rhombic symmetry, with E relatively small ($\sim$ 30 Oe), and $|D| < \sim 100 - 200$ Oe. The same choice would apply when considering the lack of any relatively large forbidden doublets in the powder spectrum.

The parameters for the Mn^{2+} spectrum from this naturally occurring silicate have not been published, to this author's knowledge. The normal habit of this mineral is acicular crystals, or, fibrous masses of radiating structure, which are not suitable for single crystal studies. A sample of columnar pectolite (New Jersey, U.S.A.) was, however, obtained from the Adelaide Museum, which produced crystals $\sim$ 1mmx1mmx3mm, and allowed single crystal observations.

Spectra obtained from these crystals are shown in figs. 8.13 and 8.14. The parameters determined from these spectra were:-

$g = 2.001\ (\pm 0.001)$ $\qquad$ $D = 250\ (\pm 10)$ Oe

$A = -93.5(\pm 0.5)$ Oe $\qquad$ $E \sim 25$ Oe

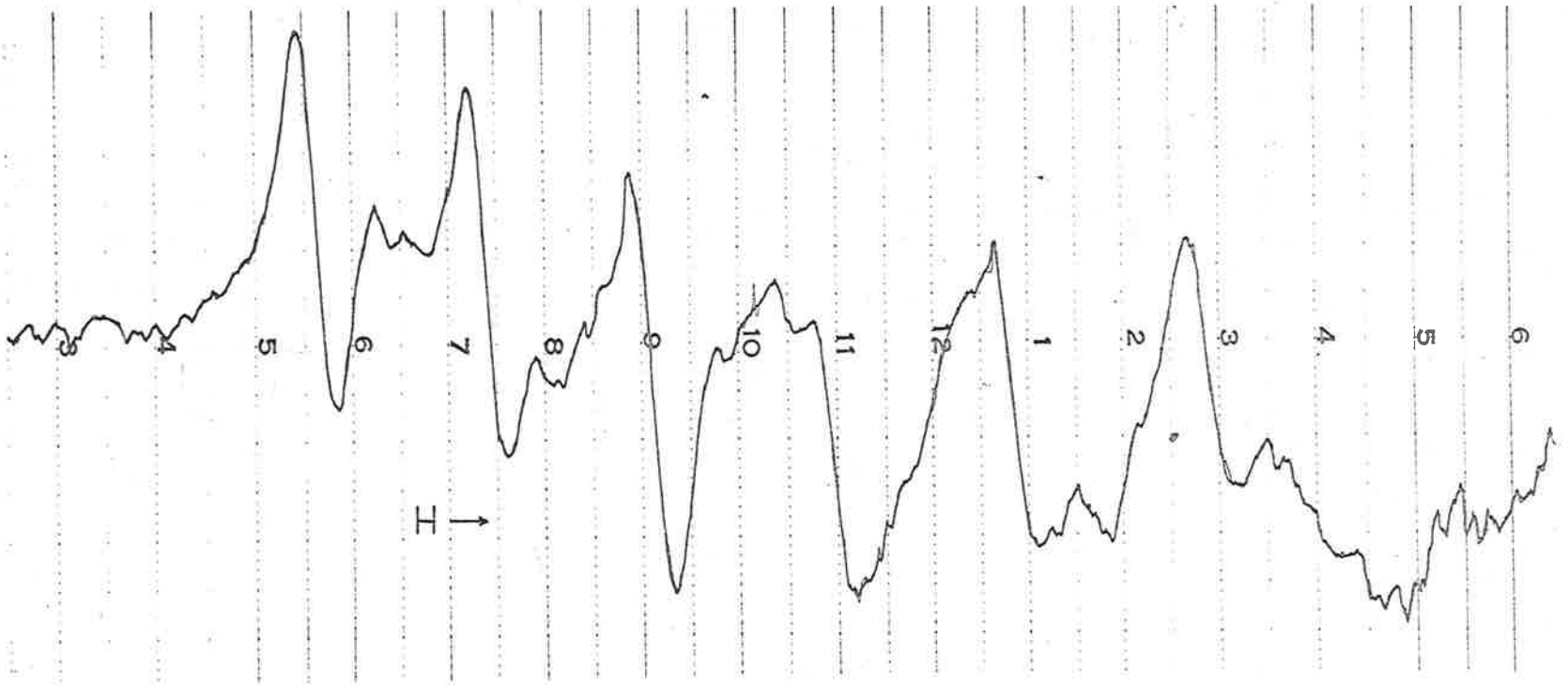

FIG. 8.12

PECTOLITE POWDER

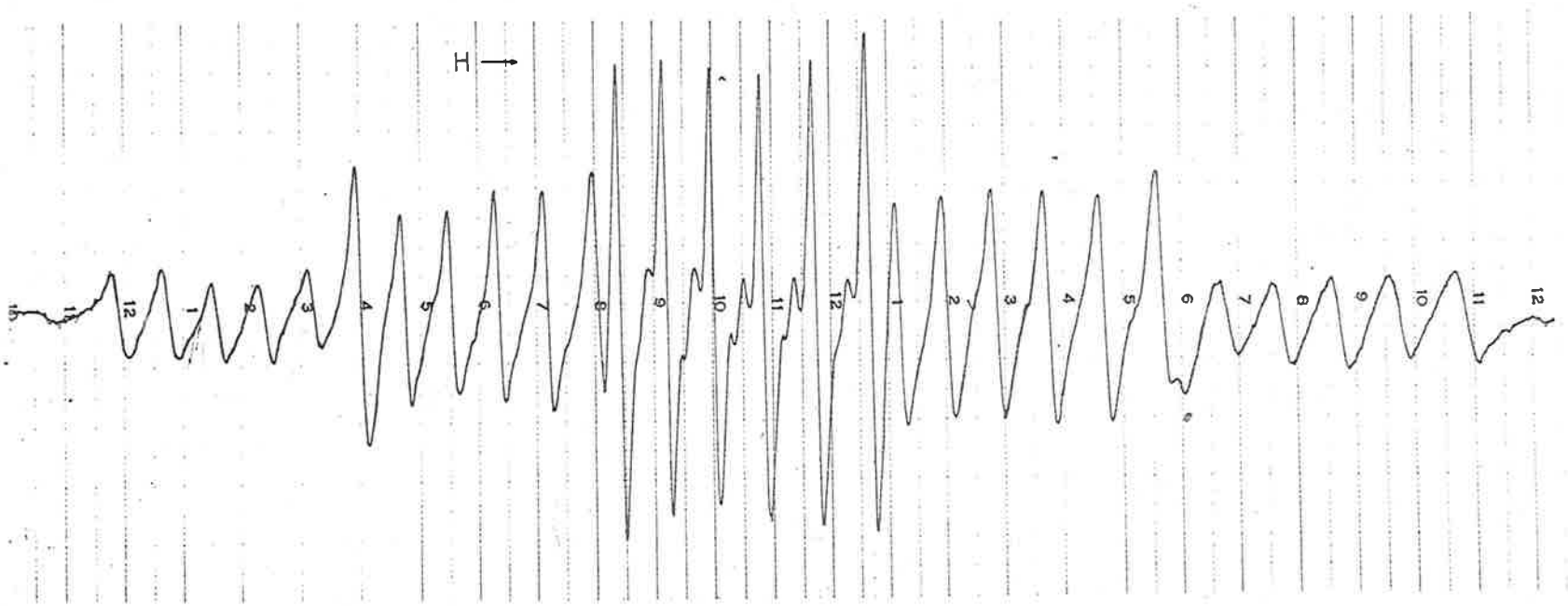

FIG. 8.13

Mn^{2+} SPECTRUM FROM PECTOLITE CRYSTAL , $\theta = 0^{\circ}$

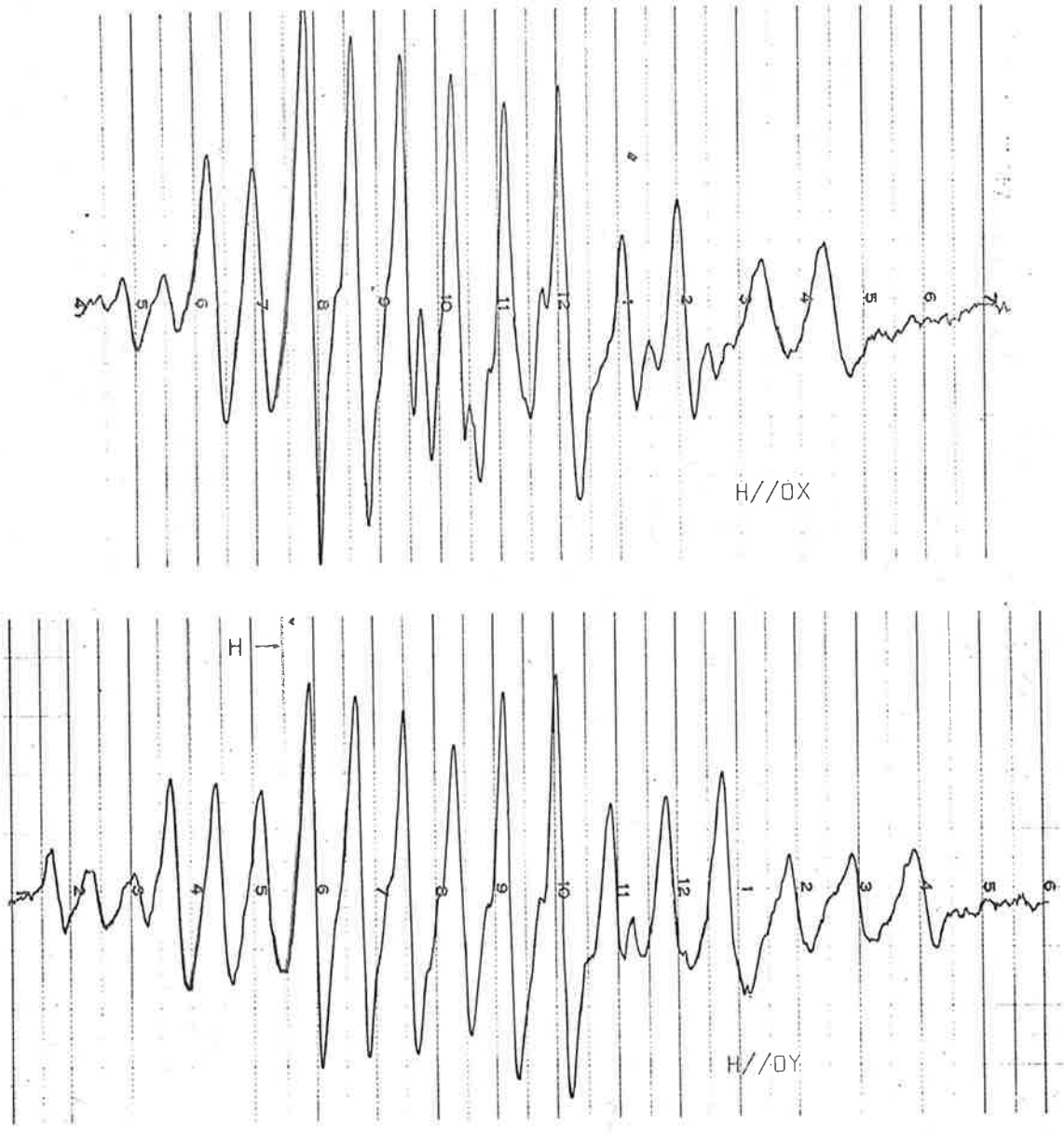

FIG. 8.14

Mn^{2+} SPECTRA FROM PECTOLITE

The features of the powder spectrum discussed earlier, are then explained by the rhombic crystal field symmetry, with E relatively small.

The structure of pectolite has been determined by Buerger (1956) and a projection in the a-b plane, showing only Ca and oxygen sites, is shown in fig. 8.15. The perfect cleavages $\{100\}$ and $\{001\}$, and the relatively large refractive index variations in the a and c directions (Dana 1932), enabled alignment of the crystals in the applied magnetic field. Experimentally, the Z axis of the crystal field was found to lie at an angle of $50^{o}(\pm 2^{o})$ to the b axis, and at an angle of $5^{o}(\pm 2^{o})$ to the a-b plane. This direction is approximately parallel to the directions between the oxygen sites marked '1' and '2', or '3' and '4' in the structure diagram, which are the most distant of the six oxygen sites about the calcium sites.

8.8 The Powder Spectrum of $NH_4\ Mg\ (SO_4)_2\ (Mn^{2+})$.

The hypothesis that a large rhombic component of the crystal field may cause complexity in powder spectra, by splitting of lines, appears to be further verified by a comparison of powder spectra obtained from the Tutton salt, $NH_4\ Mg\ (SO_4)_2\ (Mn^{2+})$, fig. 8.16, and the powder spectrum of pectolite, fig. 8.15. For the Tutton salt (Bleaney & Ingram 1951), the magnitude of the axial parameter 'D' is comparable with that obtained for pectolite, but the rhombic parameter 'E' is much larger at room temperature and T = 90^{o} K for

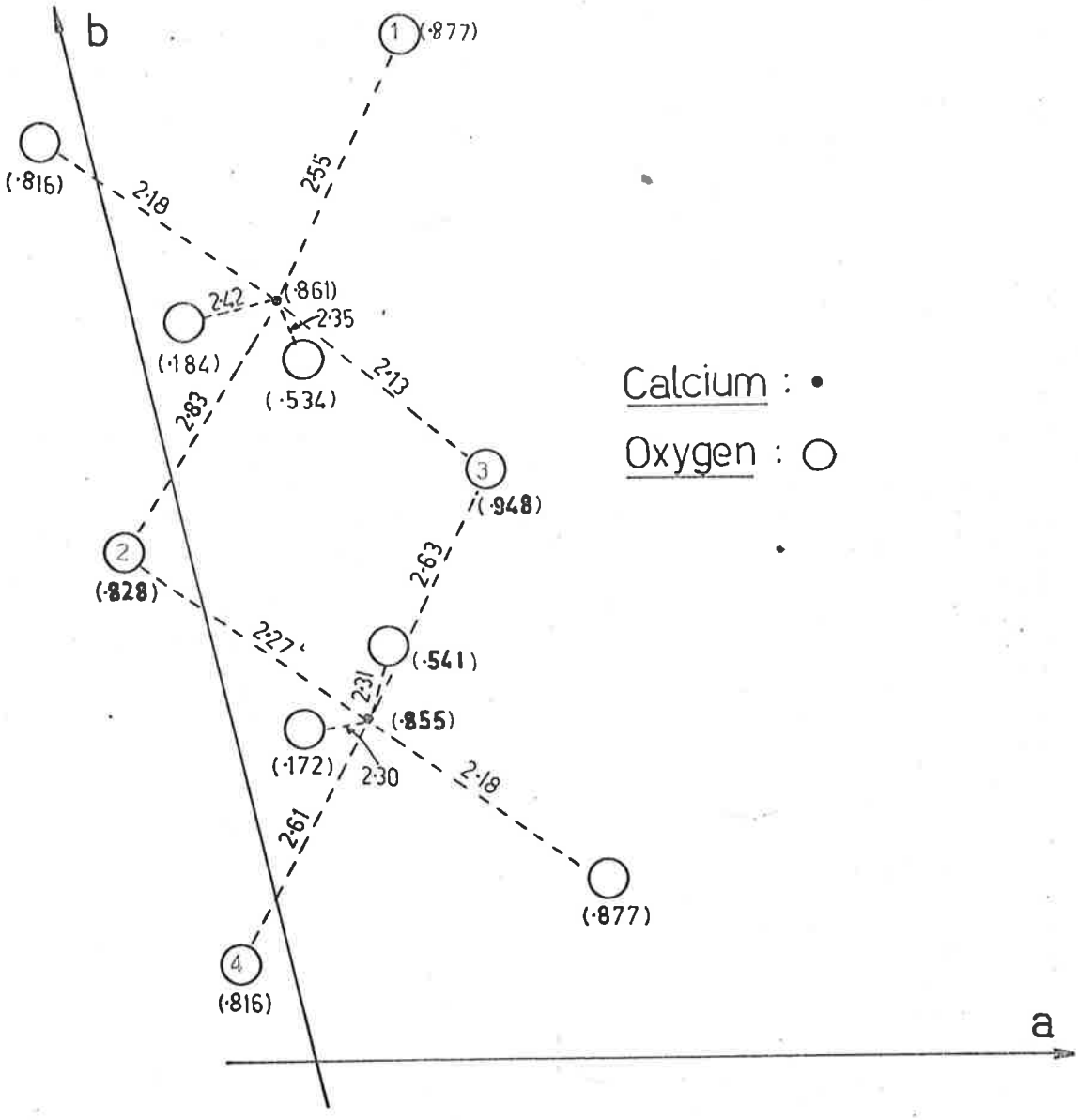

PECTOLITE

FIG. 8.15

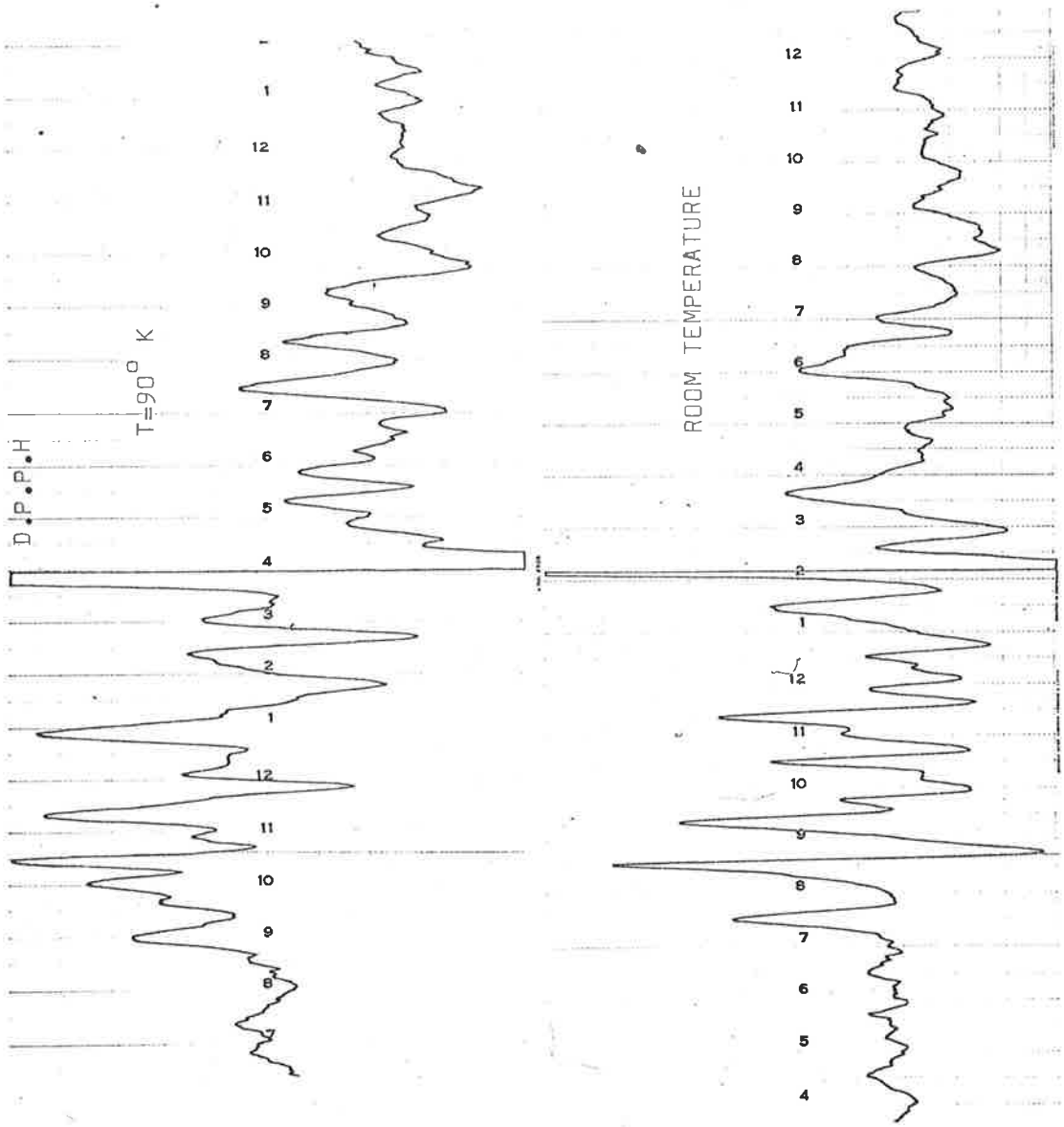

FIG. 8.16

Mn^{2+} SPECTA FROM POWDERED $NH_4Mg(SO_4)_2$

the Tutton salt, than for pectolite. The complexity of the powder spectra from this salt, compared with the powder spectrum of pectolite, may thus be attributed to splitting of allowed $\theta = 90^{o}$ lines, due to the relatively larger rhombic component of the crystal field at the ion sites in this salt.

With a decrease in sample temperature, the magnitudes of the parameters 'D' and 'E', for the Tutton salt, increase and decrease respectively. The value of |D| increases from $\sim$ 260 Oe to $\sim$ 294 Oe, and the value of |E| decreases from $\sim$ 107 Oe to $\sim$ 75 Oe, as the temperature is reduced from room temperature, to $T = 90^{o}$ K. (Bleaney & Ingram 1951.) For these changes of parameters, relatively large changes in the splitting of allowed H//OX and H//OY powder peaks are predicted. The marked differences evident in the powder spectra recorded, and shown in fig. 8.16, may then be attributed to the differences of splitting of these powder peaks, at the two temperatures.

CHAPTER IX

The Spectrum from Cement and Cement Components.

Spectra obtained from two dry cement samples are shown in fig. 9.1. The main features of these spectra are -

1) a six-line powder spectrum attributable to Mn^{2+}

2) A broad signal at g = 4.23, attributable to Fe^{3+} in a site of low crystal field symmetry (Castner 1960).

3) a broad signal underlying the Mn^{2+} spectrum, which may also be attributed to Fe^{3+}

The relative intensities of these three signals, observable in all cement samples examined, varied with the type of cement.

Calcium carbonate is one of the principal ingredients in the preparation of cement, and during the manufacturing process is converted to calcium oxide which then combines with other components to form various calcium-aluminium-iron silicates. Manganese is a common impurity in naturally occurring calcium carbonates, and possibly other ingredients used in the cement industry, and should be incorporated in various silicates formed. As the microwave spectrum from Mn^{2+} ions can indicate the crystal field symmetry at the ion sites, changes in the ionic surroundings of the Mn^{2+} ion may be detected. During the hydration of the various silicates in the cement-setting process, changes in the ionic surroundings of the incorporated Mn^{2+} ions might occur, which would result in changes in the E.S.R. powder spectra, and any observed changes might then

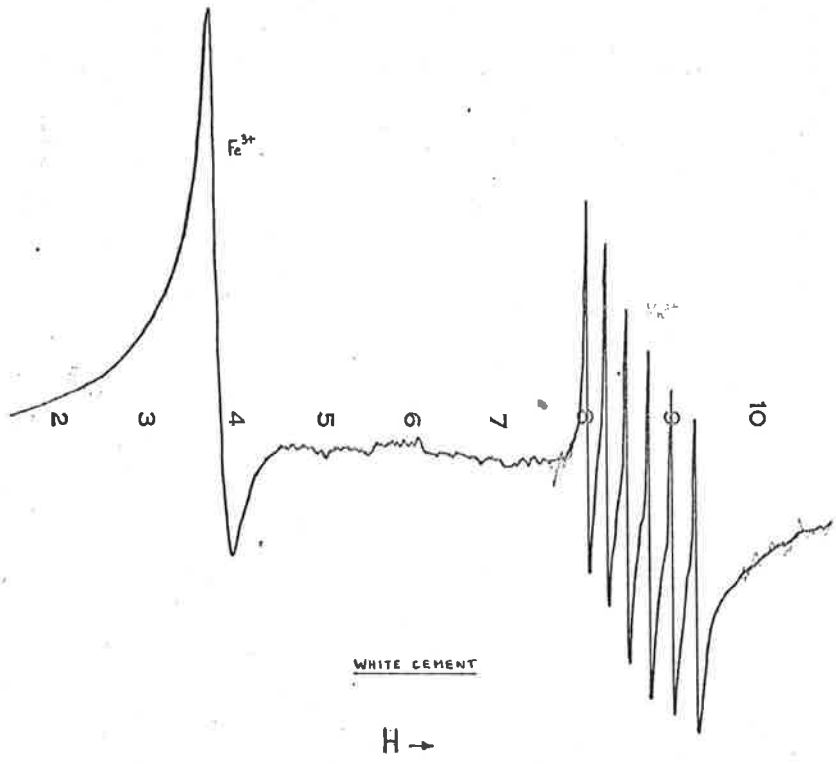
Fe^{3+}
2
3
4
5
6
7
8
9
10
WHITE CEMENT
H →

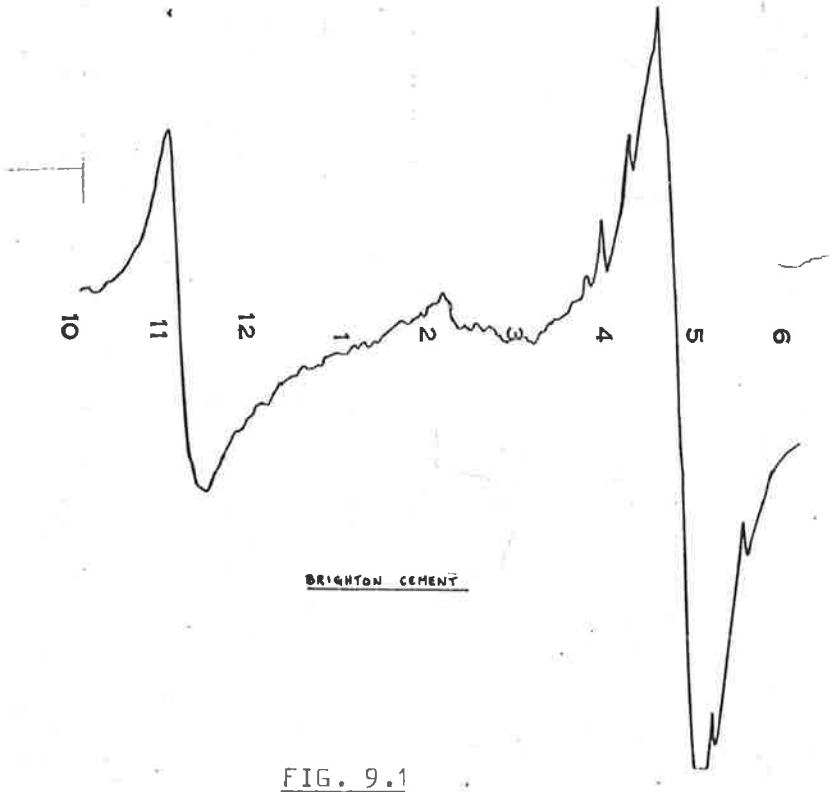
10
11
12
1
2
3
4
5
6
BRIGHTON CEMENT

FIG. 9.1

provide some useful information about the cement setting process. In view of this, a brief investigation was carried out on cement samples, to see whether changes in the manganese powder spectrum could be detected during the setting process.

Samples of various types of cement were mixed with water, allowed to set at room temperature, and periodically examined over a period of six months. Samples were also autoclaved (15 p.s.i.) for 24 hour periods. In all cases, no observable changes in the Mn^{2+} microwave spectra were recorded.

Powder samples of two of the main component silicates, doped with 0.05% Mn^{2+}, were kindly prepared by the Division of Applied Mineralogy, C.S.I.R.O., Fishermen's Bend, Victoria, in an attempt to identify the component(s) containing the Fe^{3+} and Mn^{2+} producing the observed signals. Figs. 9.2 and 9.3 show spectra recorded from dry C_3S (tricalcium aluminium silicate) and C_4AF (tetracalcium-aluminium - Fe phase). The Mn^{2+} spectrum observed from the C_3S sample appears similar to that observed in the various cement samples, and within experimental error possesses the same hyperfine splitting. No changes in this Mn^{2+} spectrum from these components were observed following a 24 hour autoclave.

It can only be concluded that during the setting process, no large changes in the ionic environment of the Mn^{2+} ion occurs.

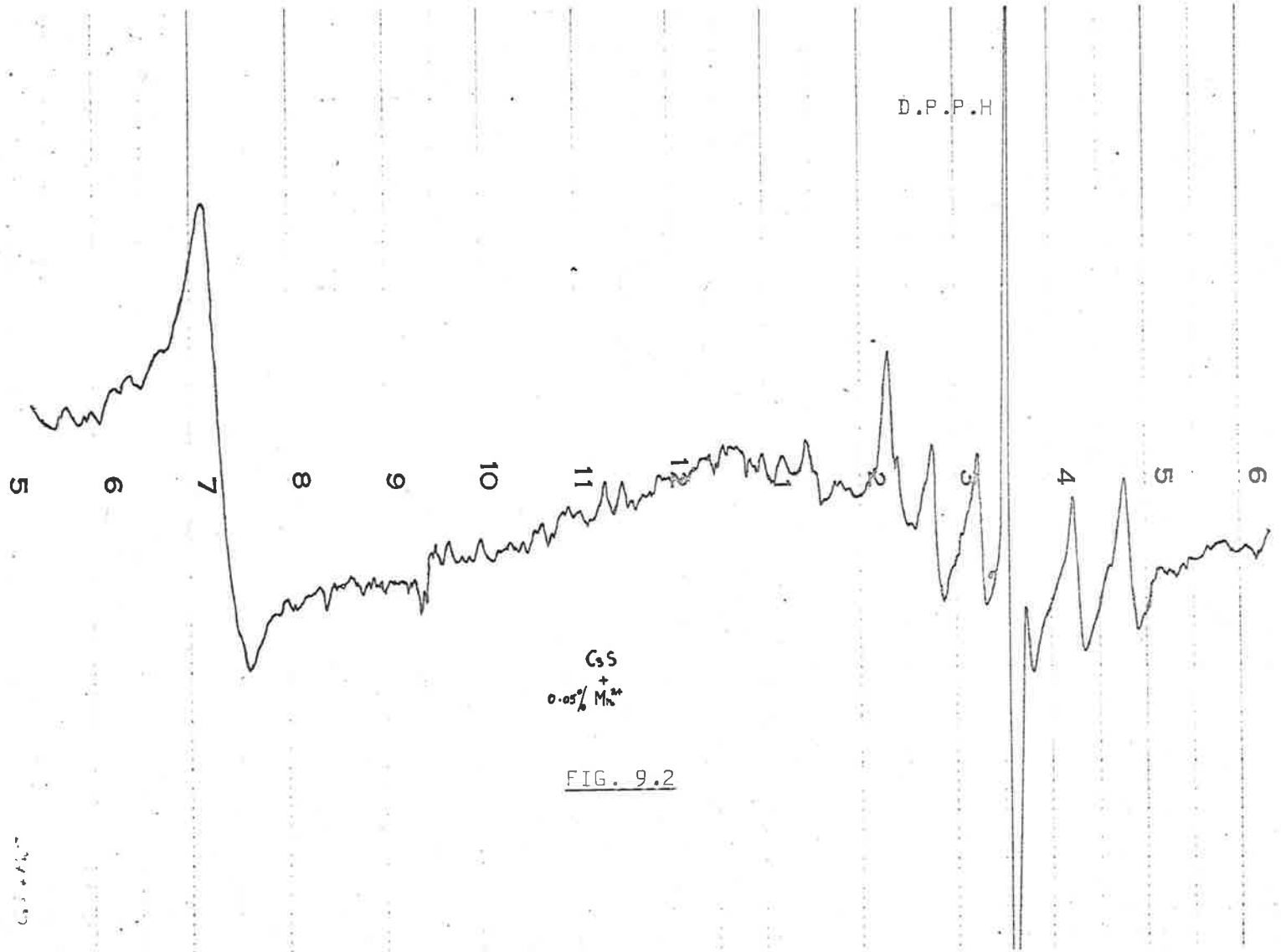

FIG. 9.2

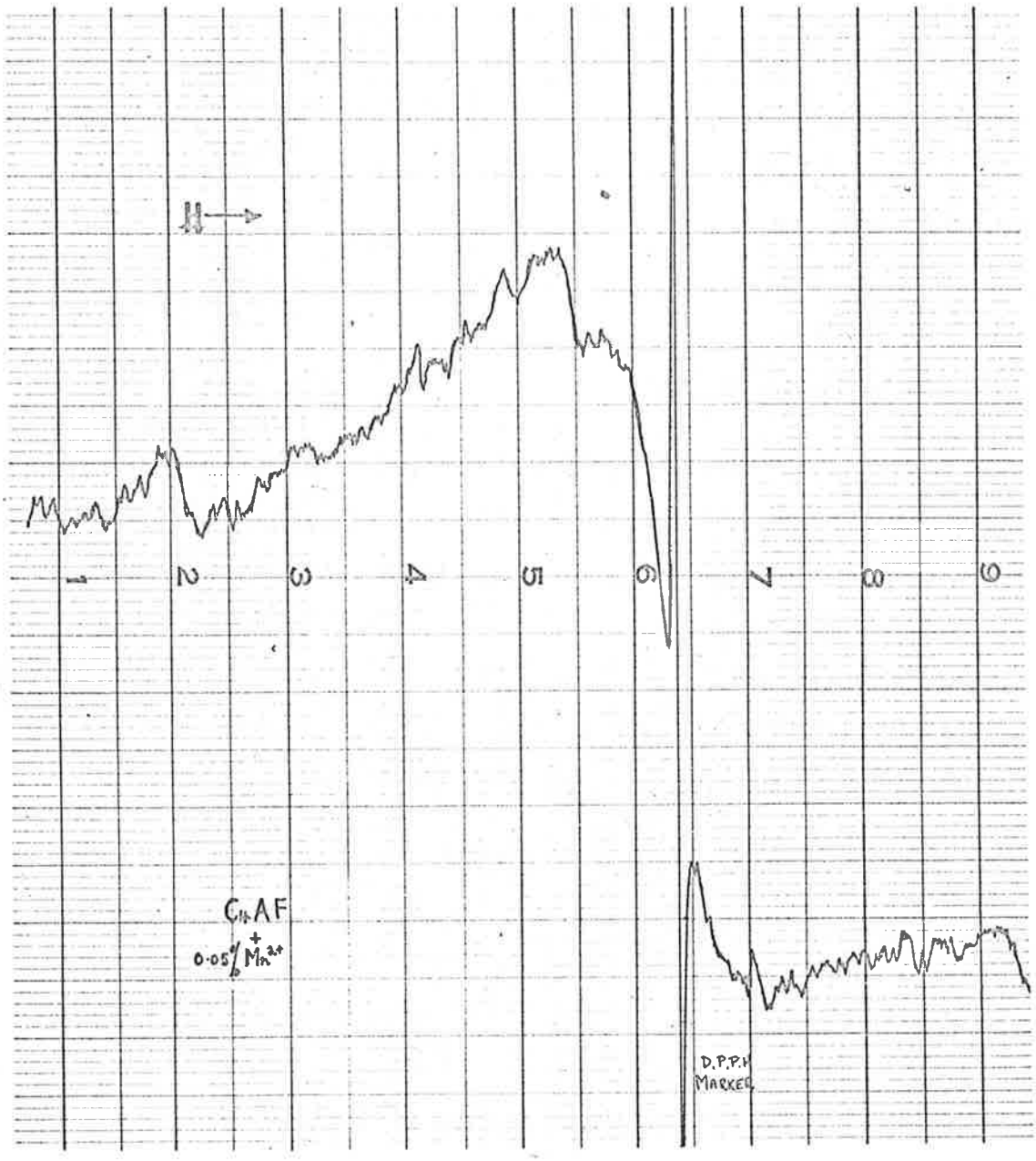

FIG. 9.3

CHAPTER X

A Modulation Technique

10.1 General Theory.

The use of strained crystal to study intensity variations of the central ($M = \frac{1}{2} \rightarrow M = -\frac{1}{2}$) transitions, although convenient, may be criticized because it is known that strain may produce changes in the crystal field parameters (Zaitov 1967). Because of this, some means of observing these central transitions, without the complication of overlapping outer structure ($M = \pm 5/2 \rightleftarrows M = \pm 3/2$, $M = \pm 3/2 \rightleftarrows M = \pm \frac{1}{2}$) was sought. A technique was devised, which in its simplest form showed some promise of achieving the unobscured observation of the central transitions in unstrained crystals, and also enable the identification of component lines in overlapping spectra.

If the angle θ, between the crystal axis and the applied magnetic field is varied periodically with an amplitude θ, the field position at which a resonance occurs will vary periodically, and for a given θ, the amplitude, and hence the velocity, of the variation of field position for a transition to occur, will be generally larger for the more angular dependent outer transitions, than for the central transitions. As the recorded intensity of a resonance depends on the sweep rate through the resonance, it was reasoned that if θ was varied periodically during a sweep of the applied magnetic field (+ a.c. modulation) through a complete spectrum, the transitions

would be broadened, and decreased in peak to peak intensity. This broadening would be larger for the more rapidly varying outer transitions than for the central transitions. The effect may be explained more fully as follows:-

We can imagine that a periodic oscillation of the angle θ about a mean angular position θ_o, is causing an oscillation of an absorption curve. We can also imagine that the applied magnetic field and the small modulation field used for a.c. detection, constitute an 'information probe' which samples the slope of the absorption curve. This information probe is then swept slowly over the field region containing the oscillating resonance. Suppose the resonance for θ_o is centred at H_o, and the information probe is at a field position A, as shown in fig. 10.1(a). During one cycle of the θ variation, the information probe would record the slope of the curve from O-I(A)-O, as shown. For the next cycle the information probe can be imagined to have moved to B, and during this cycle will record the slope from O-I(B)-O, as shown in fig. 10.1(b). If for the next cycle the probe is at C, past the field position corresponding to a point of inflection of the resonance curve, the output will be as shown in fig. 10.1(c). The output as the information probe moves completely through the field region of interest, is then shown diagramatically in fig. 10.2, together with the integrated record which would be obtained. For a small amplitude of oscillation, such as may occur for the central transitions, the output is shown in fig. 10.3.

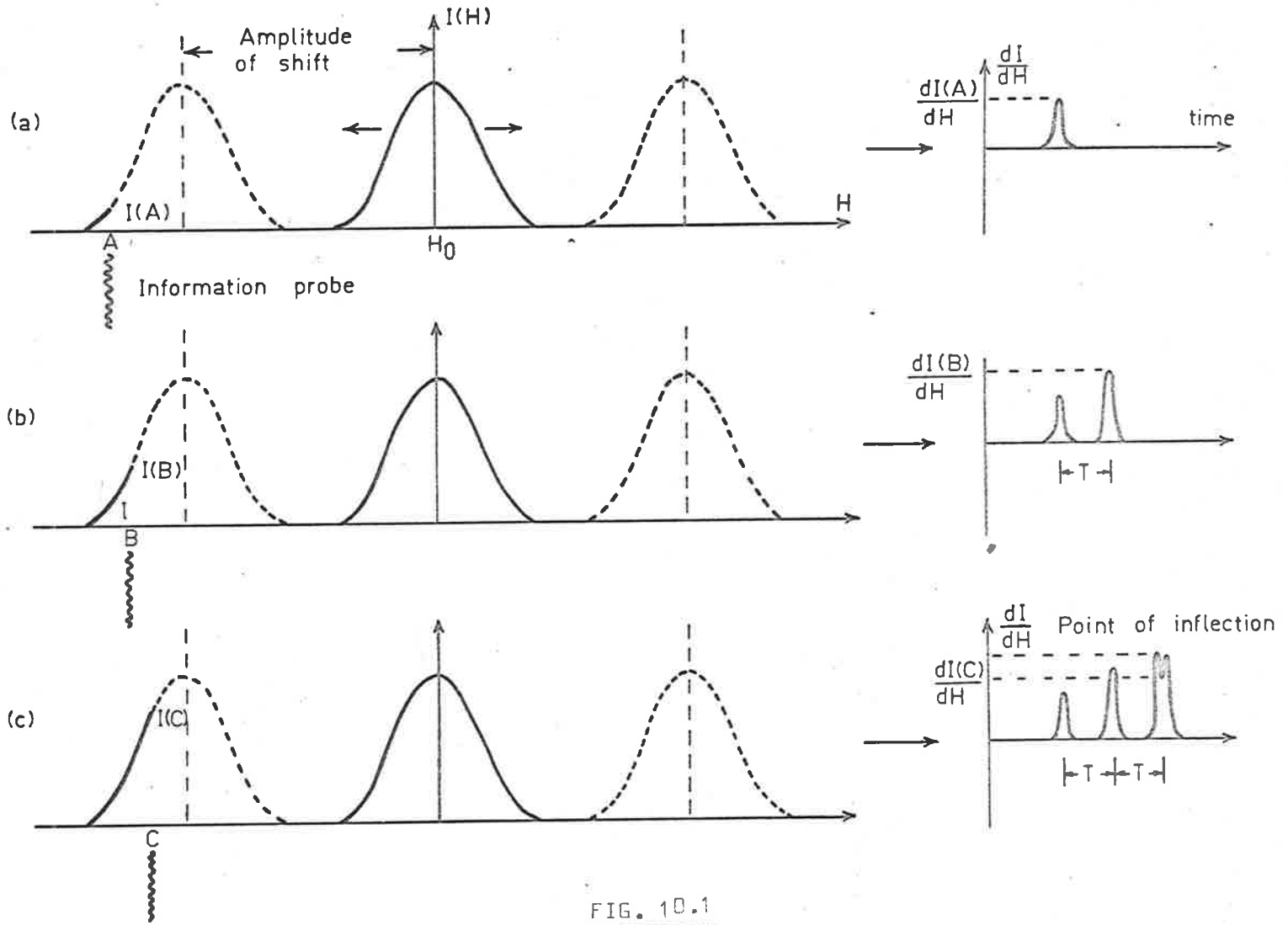
(a)
Amplitude of shift
I(H)
I(A)
A
H
H_0
Information probe
dI/dH
dI(A)/dH
time
(b)
I(B)
B
dI(B)/dH
T
(c)
I(C)
C
dI/dH
Point of inflection
dI(C)/dH
T
T

FIG. 10.1

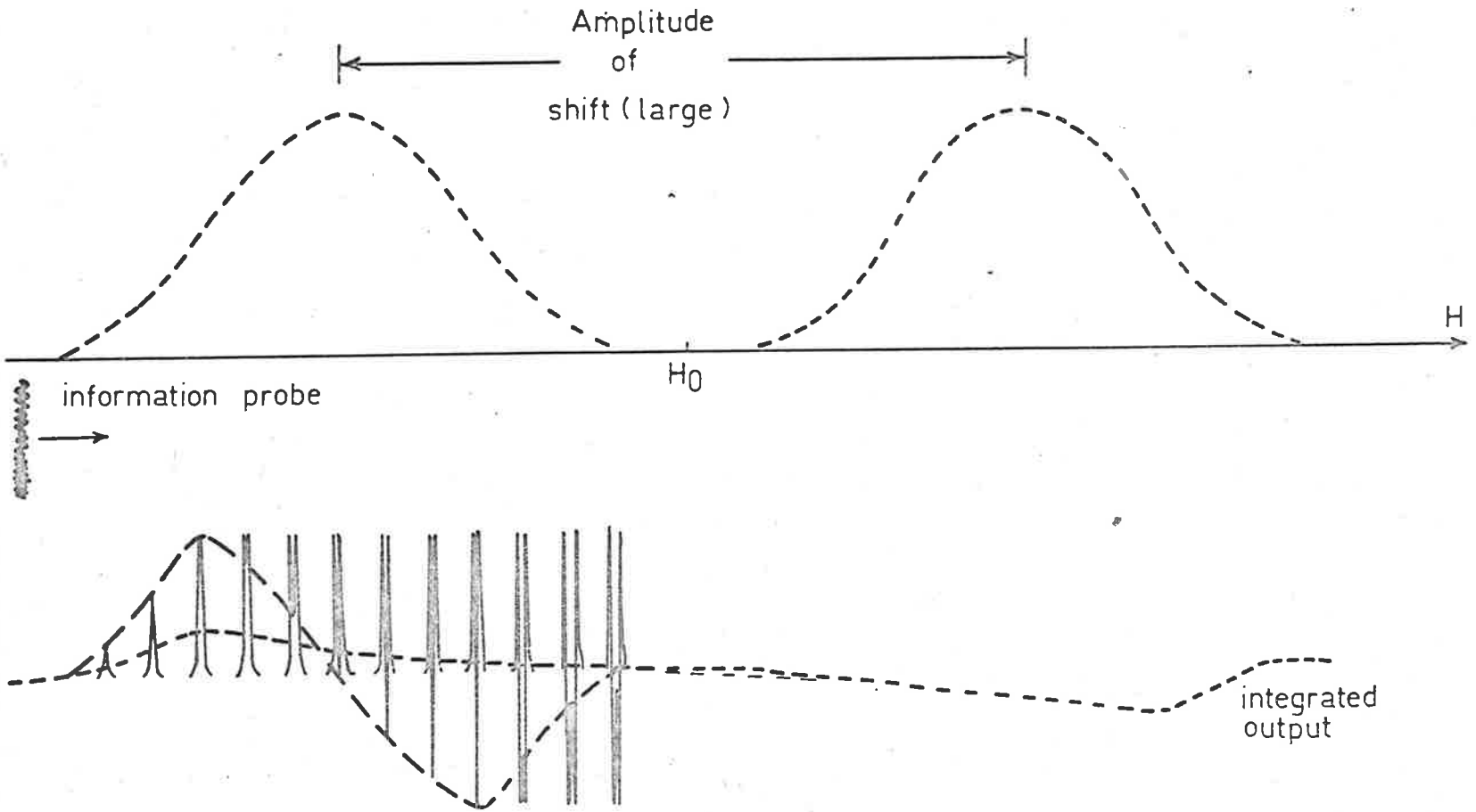
Amplitude
of
shift (large)
H
H0
information probe
integrated
output

FIG.10.2

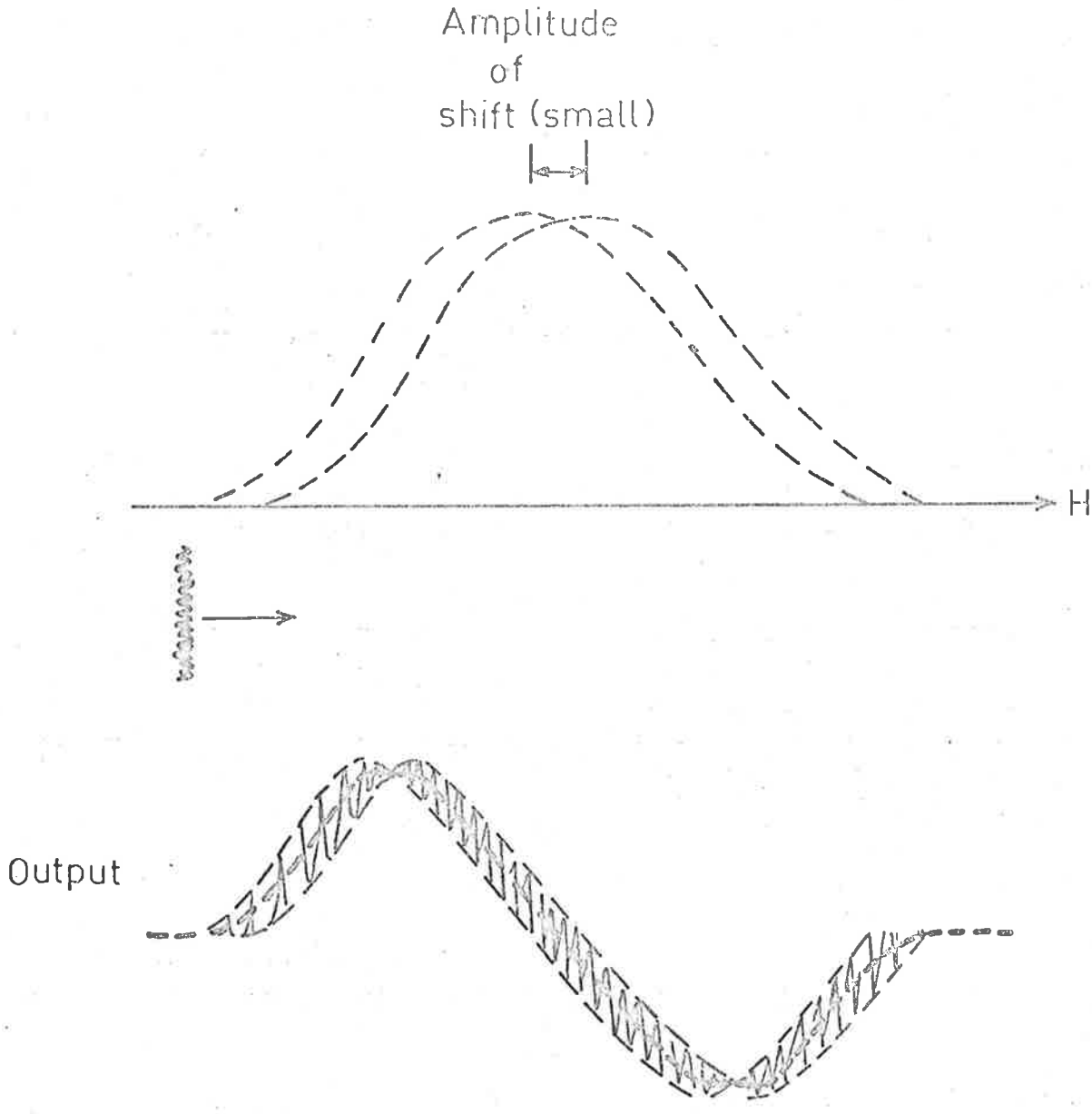

FIG .10.3

To provide the variation in θ, a coil was mounted around the microwave cavity to provide a varying magnetic field ($\sim$200Oe) perpendicular to the applied static field. The resultant field at the sample, being the vector sum of these two fields, could then be periodically varied in direction relative to the sample. To provide the coil current, the output of a Hewlett-Packard low frequency function generator was amplified using a d-c coupled power amplifier. A frequency of 2-3 c.p.s. was found to produce satisfactory results for the spectrometer used.

10.2 Applications.

Fig. 10.4(a) shows part of the normal spectrum of single crystal calcite, near $\theta \sim 45^{o}$. In fig. 10.4(b) the spectrum recorded with the vertical modulation applied is shown. The main (Δm = o) crystal transitions of both spectra are roughly aligned. The dramatic reduction in the intensity of lines in outer hyperfine groups, may then be seen, from a comparison of the two spectra.

The technique even in its present simple form, is capable of removing the overlap of a central forbidden line by one of the outer allowed lines. This is most easily shown using video display of the spectrum, but can also be seen in the chart recordings shown in fig. 10.4. Forbidden lines in the normal spectrum, marked 2' and 3', are partly, or completely overlapped, by outer transitions. This can be seen by considering the relative intensities of the doublets 2 and 2', and 3 and 3'. In the modulated spectrum, the overlapping

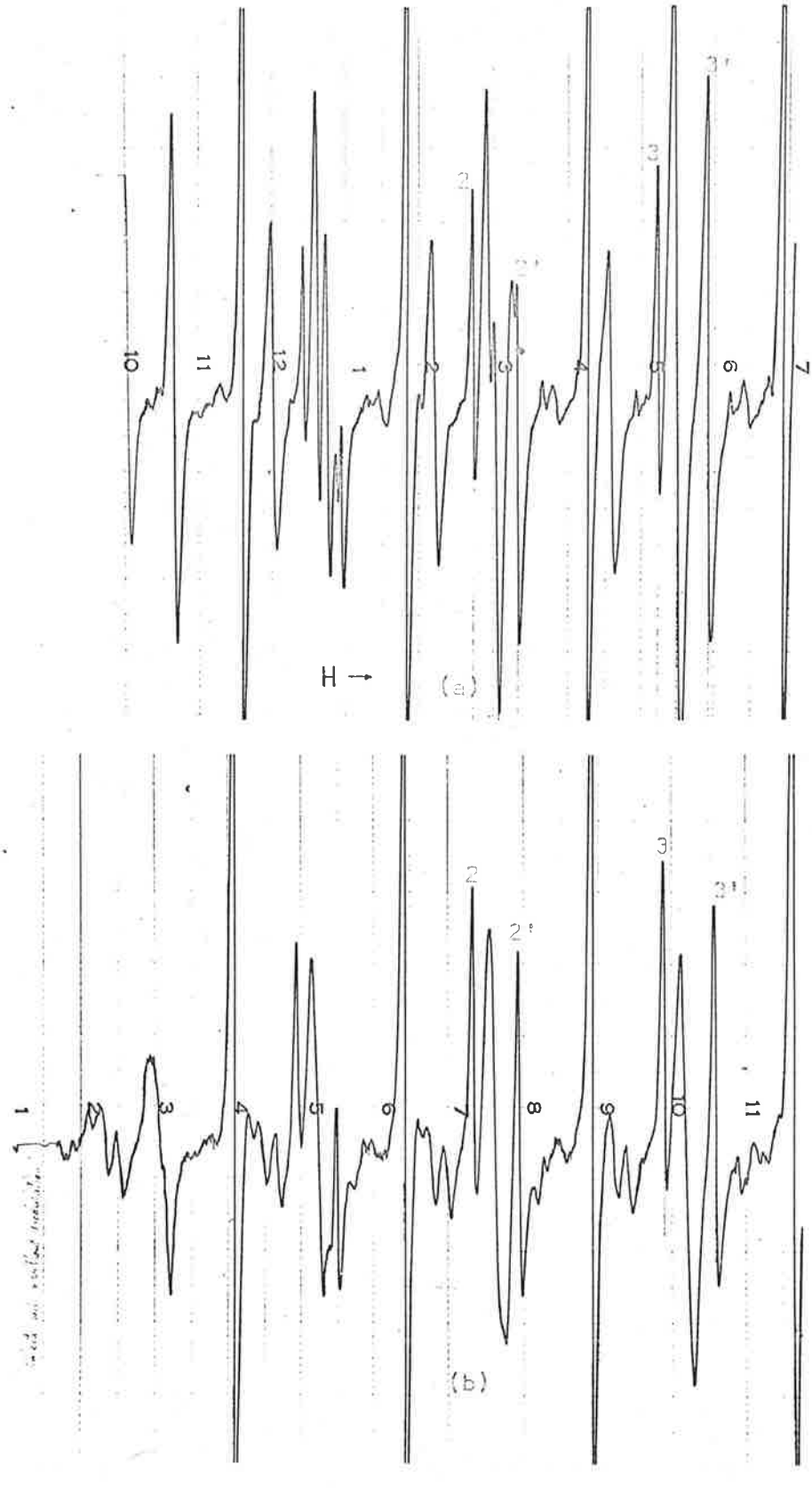

FIG.10.4

lines have almost completely been removed, as can be seen by the relative intensities of 2 and 2', and 3 and 3', in this spectrum.

The use of this modulation technique in identifying components of overlapping spectra is shown in fig. 10.5. The lower record was obtained from a single crystal of the Tutton salt NH_4 Mg $(SO_4)_2(Mn^{2+})$, with the applied magnetic field parallel to the Z axis of the crystal field of one of the two ion sites in this material which may be occupied by Mn^{2+}. (Bleaney & Ingram 1951). The transitions for this $\theta = 0^o$ site are much less angular dependent, for a change θ, than transitions for the other site, for which the Z crystal field axis is not parallel to the applied field. With the vertical modulation applied, lines in the $\theta = 0^o$ spectrum are only slightly broadened compared to lines in the other overlapping spectrum. These latter lines are then broadened out, enabling easy identification of lines in the $\theta = 0^o$ spectrum. The spectra shown in this figure have been roughly aligned using a D.P.P.H. marker to allow a comparison of the reduction of lines. The central ($\Delta m = o$) hyperfine sextet, of the $\theta = 0^o$ spectrum, is easily identifiable when the modulation is applied (marked 1 - 6), whereas without this modulation line identification of this sextet is much more difficult. Of perhaps more importance in the determination of parameters for overlapping spectra, is the firm identification of outer groups of hyperfine lines. In the normal spectrum, shown in fig. 10.5(b), some ambiguity exists as to which lines belong to which spectrum. With the modulation applied,

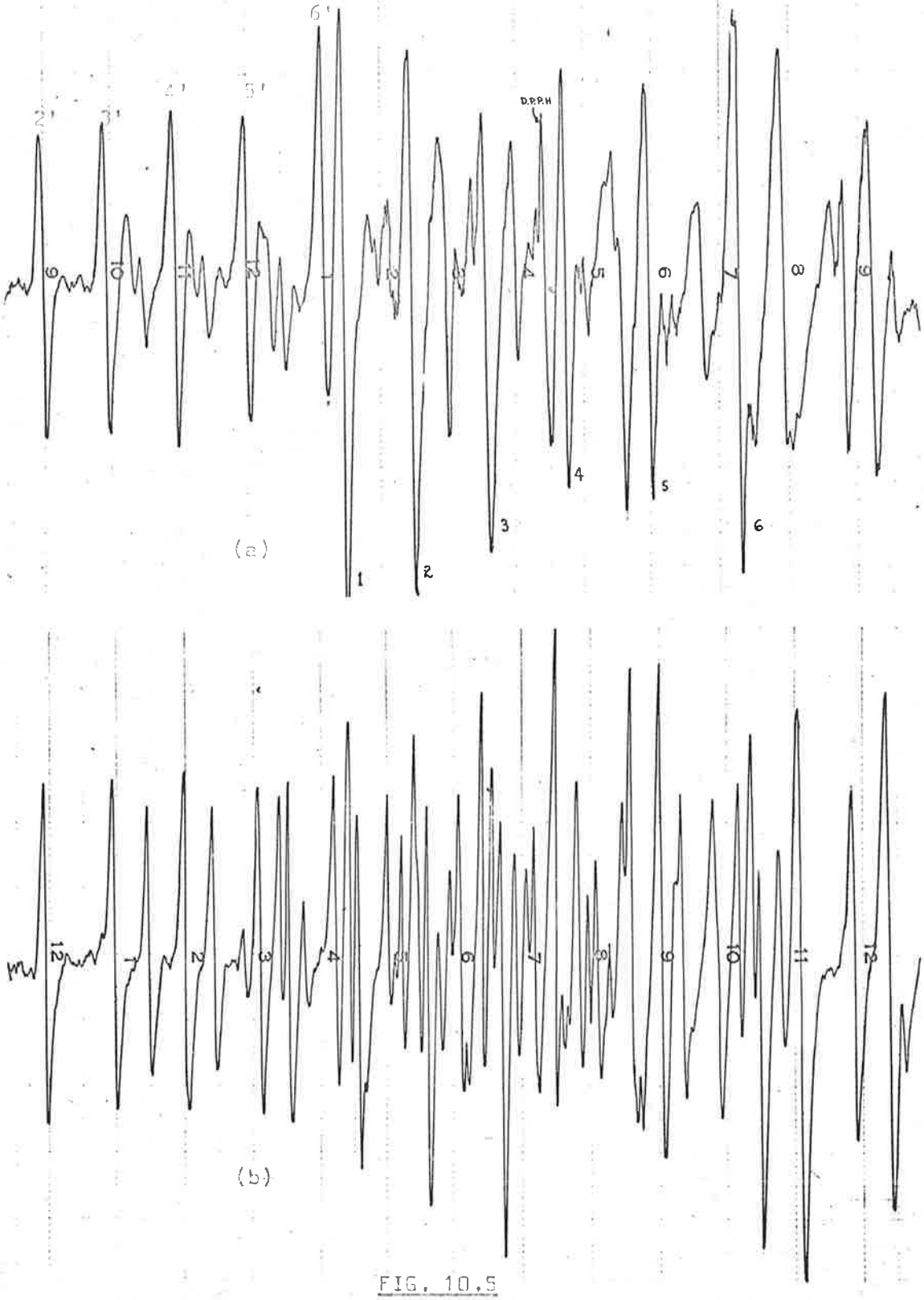

FIG. 10.5

positive identification of the M = 3/2 sextet of the $\theta = 0^{o}$ spectrum (marked 2' - 6') is possible.

This extremely interesting modulation technique was devised near the completion of this thesis, and time did not permit the investigation of any experimental refinements, or relevant theory. One future refinement planned, is the application of an additional varying field in the direction of the static field, at the same frequency as the perpendicular modulation. With the correct amplitude and phase, the information probe could then be kept "in step" with an oscillating line, or lines, of interest, and effectively, no broadening of these lines would then result from the vertical modulation.

CONCLUSIONS.

A general theory of axial and rhombic powder spectra has been presented, which for all powder spectra considered, is in agreement with experimental observations.

It has been shown that for Mn^{2+} ions in sites of axial crystal field symmetry, not only field positions, but relative intensities, of main lines observed in powder spectra, are correlated with line positions and relative intensities observed in single crystal spectra at $\theta = 90^{\circ}$ and $\theta \sim 40^{\circ}$.

It has also been shown that the use of Bir's method to predict intensity variations of both allowed and forbidden transitions, produces agreement with experimentally determined variations for the central ($M = +\frac{1}{2}$) transitions observed in single crystal spectra for axial symmetry.

To this author's knowledge, the expressions derived by Bir have only been tested previously on outer transitions ($M = 5/2, \pm 3/2, -\frac{1}{2}$) for axial and rhombic symmetry (Bir and Sochava 1964, Manoogian 1968 b). Intensity variations obtained using this method have been used to predict features of powder spectra characterized by $|D| \sim 250\text{-}350$ Oe and ~ 850 Oe.

In the case of rhombic spectra, it has been shown that $\theta \sim 40^{\circ}$ components of a Mn^{2+} powder spectrum are preferentially broadened, resulting in $\theta = 90^{\circ}$ components being the dominant feature of these powder spectra. Using the intensity variations predicted by Bir's

method, for rotation in the X-Y plane ($\theta = 90^{o}$), evidence has been presented that splitting of $\theta = 90^{o}$ powder lines may be observed for large rhombic fields ($|E| \sim 80 - 100$ Oe).

For axial powder spectra characterized by $|D| \sim 80$ Oe, it has been shown that an indication of parameters may be obtained by a fit between experimentally determined line positions, and theoretical expressions given in this work, and a determination of parameters for the case of Mn^{2+} adsorbed on an ion-exchange resin has been made using the method.

The theory presented, and spectra shown in this thesis, will be of help to workers engaged in future E.S.R. investigations of materials for which single crystals studies are not possible. For example, splitting of allowed lines for both rhombic and symmetry, and the relative intensity of forbidden lines observed in some axial spectra, are all due to second and higher order effects and all decrease with field. The complexity introduced into powder spectra by these factors would then be expected to be reduced considerably by recording spectra at higher frequencies and fields.

If (say) microwave spectroscopy was to be used by any investigator, as a non-destructive method to determine the presence of Mn^{2+} impurities in powder samples, Q-band, rather than X-band, investigations would then seem to be preferable. If Q-band investigations of a powdered sample of unknown symmetry produced a relatively simple Mn^{2+} spectrum, but X-band spectra from the same sample were complex,

this could be taken as an indication that either a relatively large rhombic field, or an axial field characterized by $|D| \sim 150$ Oe, existed at the Mn^{2+} ion site. Any attempt to obtain quantitative estimates of parameters from such complex X-band powder spectra by line position measurements, could not hope to be successful however, because of the virtual impossibility of identifying powder lines without the aid of single crystal spectra.

The determination of parameters from line position measurements at Q-band may be possible for samples whose spectra at X-band are complex. It was not possible, however, for the author to obtain Q-band spectra of Mn^{2+} in such materials as Scheelite and Tutton salts, at the time of completion of this work, to substantiate or disprove this suggestion.

Correct derivations of (a) third-order corrections to eigenvalues, and (b) intensity variations for cubic crystal field symmetry by perturbation methods (Appendix A), have been given, and finally, it is felt that the modulation technique described in the final chapter, will be of interest to many investigators.

APPENDIX A.

Transition Probabilities for Cubic Crystal Field Symmetry.

A.1. Introduction.

The theory of the intensity variations observed when ions are in a site of cubic crystal field symmetry has been considered by Cavenett (1964a, 1964b), who has derived, using second-order perturbation methods, the following expression for the relative intensity of forbidden transitions.

$$\left[\frac{73a}{8g\beta H_o}\right]^2 \cdot \left[\left\{\sin 2\theta(1-\cos 4\psi) + \sin 2\theta\cos 2\theta(7+\cos 4\psi)\right\}^2 + \left\{4\sin^3\theta\sin 4\psi\right\}^2\right] \cdot \left[I(I+1)-m(m+1)\right] \qquad (A1)$$

The theory has also been considered by Bir et al (1965) who have derived for $\mu_{MM'}$:-

$$\mu_{MM'} = \left\{1 - \frac{1}{8}\left[\frac{a}{6g\beta H}\right]^2\left[\Phi(\psi,\theta)\right]^2\left[\frac{F_M}{M} - \frac{F_{M'}}{M}\right]^2\right\} \cdot \left|\frac{MM'}{MM'}\right| \qquad (A2)$$

where -

$$F_M = 35\,M^4 - 30\,M^2.S(S+1) + 25\,M^2 - 6S(S+1) - 3S^2(S+1)^2$$

$$\left[\Phi(\psi,\theta)\right]^2 = l^2m^2(l^2-m^2)^2 + m^2l^2(m^2-n^2)^2 + n^2l^2(n^2-l^2)^2$$

$$l = \sin\theta\cos\psi,\ m = \sin\theta\sin\psi,\ n = \cos\theta$$

Bir (1964) has shown that for small values of parameters the relative intensity may be approximated by -

$$I \sim \frac{(1+\mu)}{2}\left[I(I+1) - m(m+1)\right] \qquad (A3)$$

Substituting for μ in equation (A3), an expression is obtained which is not in agreement with that derived by Cavenett. Although

spectra from samples containing Mn^{2+} ions in a site of cubic field symmetry are not considered in this thesis, it was felt desirable that this disagreement should be investigated.

The derivation of an expression for the intensity variations using both second-order perturbation methods (as for the case of axial symmetry) and Bir's method was then considered, and it was found that Cavenett had made errors during his derivation. The following derivation, using perturbation methods similar to that used to obtain the Bleaney and Rubins' expression, is now outlined and an expression which is in agreement with that obtained using Bir's method is derived.

A.2. Intensity Variations Using Perturbation Methods.

For a four-fold axis of symmetry, the crystal field potential expressed in operator equivalents is :-

$$V_c = \frac{a}{15}\left(T_4^0 + \sqrt{\frac{5}{14}}\left(T_4^4 + T_4^{-4}\right)\right) \qquad (A4)$$

When this potential is referred to the Zeeman diagonal system, by rotation through the Euler angles $(\psi,\theta,0)$, the expression for the potential contains terms $T_4^{\pm 1}$, which are functions of the spin operators S_+, S_- and S_z, necessary to obtain the expressions for intensity variations. Considering only the terms $T_4^{\pm 1}$, we find on applying the transformation -

$$R_{(\psi,\theta,0)}\ \frac{a}{15}.\left(T_4^0 + \sqrt{\frac{5}{14}}\left(T_4^4 + T_4^{-4}\right)\right)$$

$$\longrightarrow \mp T_4^{\pm 1}.\ \frac{a.\sqrt{20}}{480}\left(7\sin 2\theta\cos 2\theta + \sin 2\theta\right.$$

$$\left. - 4\sin^3\theta\cos\theta\cos 4\psi \pm i4\sin^3\theta\sin 4\psi\right) \qquad (A5)$$

The form of the operators $T_4^{\pm 1}$ is given by Al'tshuler and Kozyrev (1964) and derived from the Spherical Harmonics $Y_4^{\pm 1}$ in Appendix C viz. :-

$$T_4^{\pm 1} = \mp \sqrt{\frac{5}{8}} \left(S_{\pm} f(S_z) + f(S_z) S_{\pm}\right)$$

$$\text{where } f(S_z) = 7S_z^3 - 3S(S+1)S_z - S_z \qquad \text{(A6)}$$

(Cavenett has incorrectly derived $f(S_z) = 7S_z^3 - 3S(S+1)S_z - 59S_z$)

We thus obtain for our perturbation Hamiltonian :-

$$\mathcal{H}' = \frac{a}{384}\left(S_+ f(S_z) + f(S_z) S_+\right) f(\theta,\psi)$$

$$+ \frac{a}{384}\left(S_- f(S_z) + f(S_z) S_-\right) f^*(\theta,\psi)) + \frac{A}{2}(S_+ I_- + S_- I_+) \qquad \text{(A7)}$$

where $f(\theta,\psi) = 7\sin 2\theta\cos 2\theta + \sin 2\theta - 4\sin^3\theta\cos\theta\cos 4\psi + i4\sin^3\theta\sin 4\psi$

and $f^*(\theta,\psi)$ is the complex conjugate.

For forbidden transitions $(M,m) \rightarrow (M+1,m+1)$, we have for our expansions of the perturbed wave functions :-

$$|\Phi_{M,m}) = |M,m) + C_1 |M,m+1) + C_2 |M,m-1)$$

$$|\Phi_{M+1,m+1}) = |M+1, m+1) + C_3 |M+1,m+2) + C_4 |M+1,m)$$

where the coefficients $C_i (i=1,4)$ may be found by using the perturbation method as before.

The intensity is then -

$$I_F \propto \left| (\Phi_{M+1,m+1} | (S_+ + S_-) | \Phi_{M,m}) \right|^2$$

$$I_F \propto \left| F_+(M)(C_1 + C_4^*) \right|^2 \qquad \text{(A8)}$$

where $F_{\pm}(M) = (S(S+1) - M(M\pm1))^{\frac{1}{2}}$

(Cavenett has derived : $I_f \propto |F_+(M)\, C_1|^2$)

$$= \left| F_+(M) \cdot \frac{a}{384} \cdot f(\theta,\psi) \cdot \frac{1}{g\beta H_o} \left\{ \frac{(F_+(M)F_-(M+1)f_+(m)(f(M) + f(M+1))}{M} \right.\right.$$

$$- \frac{F_-(M)F_+(M-1)f_+(m)(f(M) + f(M-1))}{M}$$

$$+ \frac{F_-(M+1)F_+(M)f_-(m+1)(f(M+1) + f(M))}{M+1}$$

$$\left.\left. - \frac{F_+(M+1)F_-(M+2)f_-(m+1)(f(M+1) + f(M+2))}{M+1} \right\}\right|^2$$

where $f_{\pm}(m) = (I(I+1) - m(m\pm1))^{\frac{1}{2}}$

For the central sextet of hyperfine lines in the Mn^{2+} microwave spectrum, $M = \frac{1}{2}$, and on substitution and reduction we obtain :-

$$I_F \propto \left| \frac{5}{4} \cdot \frac{a}{g\beta H_o} \cdot f(\theta,\psi) \cdot F_+(M)\, (I(I+1) - m(m+1))^{\frac{1}{2}} \right|^2 \qquad (A9)$$

For the allowed transitions $I \propto F_+^2(M)$, and for the relative intensity we thus obtain -

$$\left[\frac{5a}{4g\beta H_o}\right]^2 (I(I+1) - m(m+1))((7\sin2\theta\cos2\theta + \sin2\theta$$

$$-4\sin^3\theta\cos\theta\cos4\psi)^2 + (4\sin^3\theta\sin4\psi)^2) \qquad (A10)$$

which may also be written as :-

$$\left[\frac{5a}{4g\beta H_o}\right]^2 \left[I(I+1)-m(m+1)\right] \left[\{\sin2\theta(1-\cos4\psi) + \sin2\theta\cos2\theta.(7+\cos4\psi)\}^2 \right.$$

$$\left. + \{4\sin^3\theta\sin4\psi\}^2\right] \qquad (A11)$$

On comparison with the expression given by Cavenett (1964a) we find that the factor of $\frac{73}{8}$ in Cavenett's expression is replaced by $\frac{5}{4}$.

For the (110) plane, $\psi = 45^{o}$, and we obtain :-

$$\frac{I_F}{I_A} = \left[\frac{5a'}{4H_o}\right]^2 . \left[I(I+1) - m(m+1)\right] . \left[2\sin 2\theta + 3\sin 4\theta\right]^2 \qquad (A12)$$

A.3. Intensity Variations for Cubic Field Symmetry Using Bir's Method.

Using the perturbation Hamiltonian (Equation A5) we obtain for

$M = \frac{1}{2} \rightarrow M = -\frac{1}{2}$, $S = 5/2$,

$$\mu = -\left[1 - \frac{25a^2}{8H_o^2}\left\{(7\sin 2\theta\cos 2\theta + \sin 2\theta - 4\sin^3\theta\cos\theta\cos 4\psi)^2 + (4\sin^3\theta\sin 4\psi)^2\right\}\right]$$

This expression can be shown to be identical with that derived by Bir et al (1965), Equation A2.

Substituting for μ in Equation A3, then produces an expression for the relative intensity which is identical with that derived by second order perturbation theory, Equation A10.

The intensity variation for rotation in the (110) plane, calculated from $I \propto \left| d_I^{mm'}(-\mu) \right|^2$, is shown in figs. A1, and A2.

The experimentally determined intensity ratios for transitions observed by Cavenett (1964b) in the ZnSe : Mn^{2+} spectrum, for $\theta = 31^{o}$ in this plane, are shown in Table (A1), with theoretical ratios shown for comparison. The experimentally observed intensities of the forbidden transitions are smaller than predicted by Cavenett's expression, whereas the observed intensities are larger than predicted by this author's expression (A12).

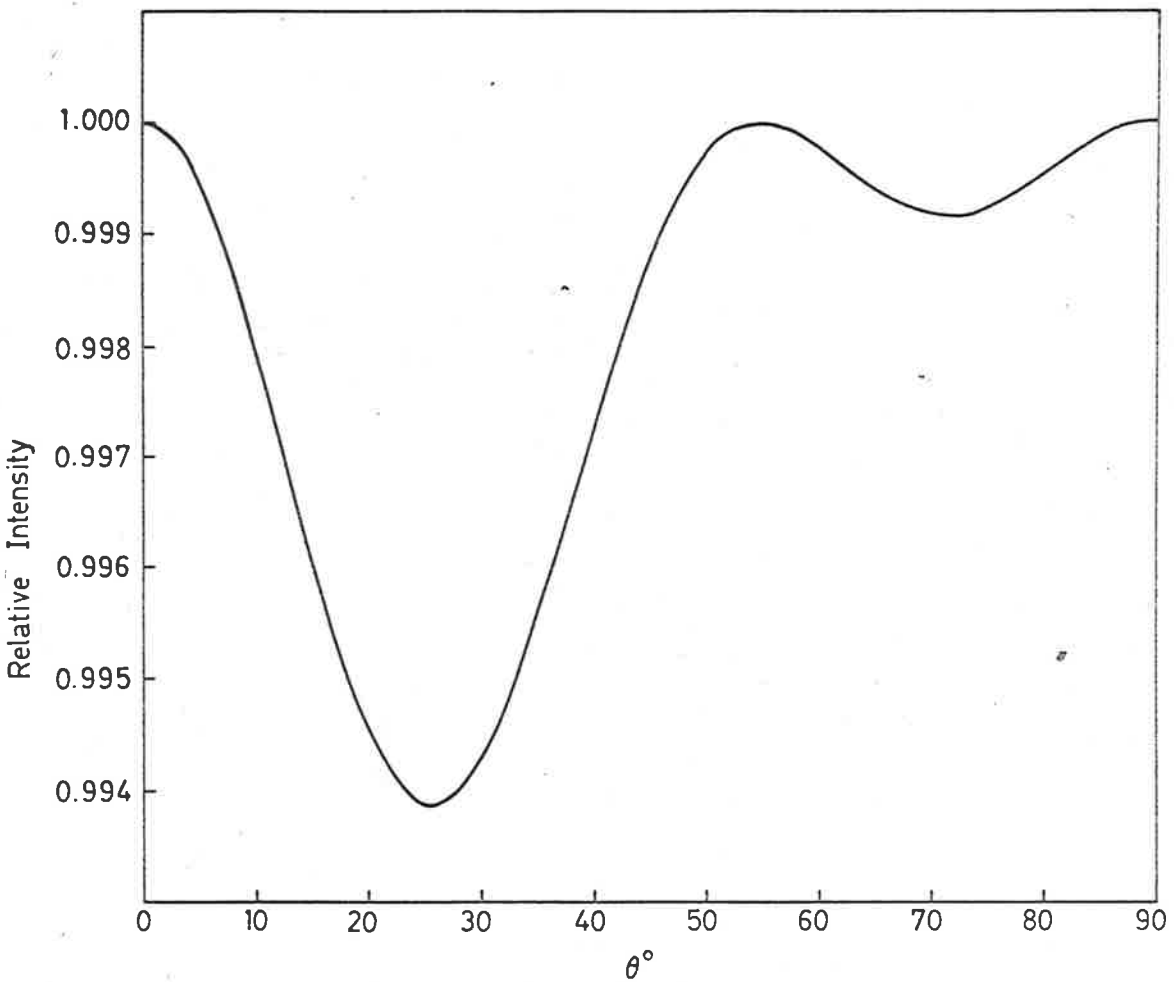

Intensity variation of allowed transition (m = 5/2).
ψ = 45° Cubic field symmetry

FIG. A1

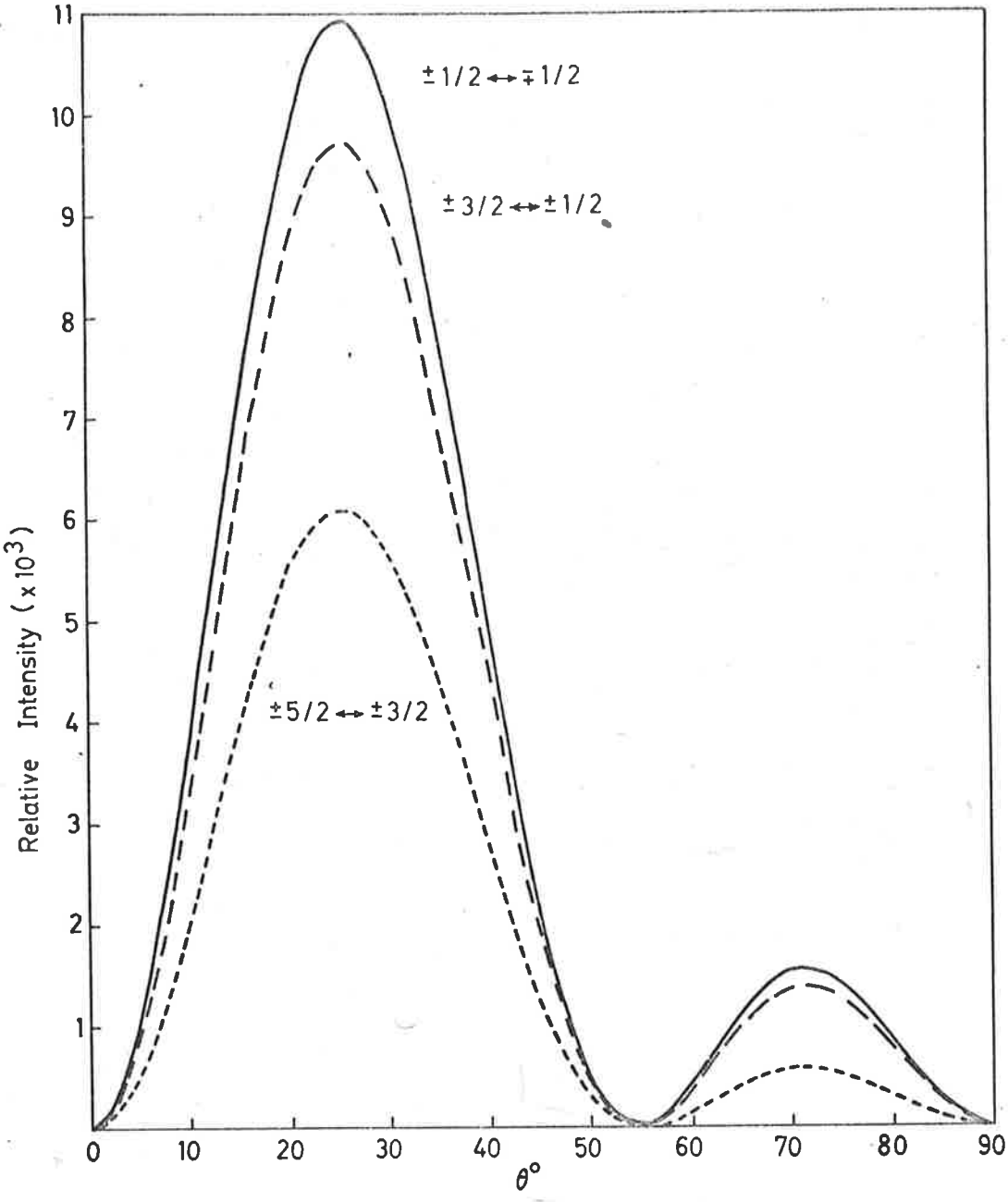

Intensity variation of forbidden transitions. ($\Delta m = \pm 1$)
$\psi = 45°$ Cubic field symmetry

FIG. A2

Table A1.

Intensity Ratios of Allowed and Forbidden Transitions.

ZnSe : Mn^{2+} , a' = 20.6 Oe , H_o = 3310.6 Oe

$\psi = 45^o$, $\theta = 31^o$.

Ratio	Expt. (Cavenett)	Theory (Cavenett)	Theory (Dobney) Second Order Perturbation	Theory (Bir) (From Fig. A1)
$I_A^9 : I_F^9$	30 : 1	17 : 1	100 : 1	101 : 1
$I_A^9 : I_F^8$	50 : 1	20 : 1	112 : 1	114 : 1
$I_A^9 : I_F^5$	80 : 1	30 : 1	180 : 1	182 : 1

APPENDIX B.

Third Order Perturbation Calculations.

As our perturbation Hamiltonian we use:-

$$\mathcal{H}' = \frac{D}{2}(S_z^2 - \frac{1}{3}S(S+1))(3\cos^2\theta - 1) + \frac{D}{4}(S_z(S_+ + S_-) + (S_+ + S_-)S_z)\sin 2\theta$$

$$+ \frac{D}{4}(S_+^2 + S_-^2)\sin^2\theta + AS_zI_z + \frac{A}{2}(S_+I_- + S_-I_+)$$

The possible terms in the single, double and triple summations of equation (3.10) are then:-

$$\underline{\text{1st Term}}:- \quad -\sum_{M'm'}^{M' \neq M} \frac{(Mm|\,H'\,|M'm')(M'm'|\,H'\,|Mm)(Mm\,|\,H'\,|\,Mm)}{(E_{M'} - E_M)^2}$$

	(Mm|	Operator	|M'm')	(M'm'|	Operator	|Mm)	(Mm|	Operator	|Mm)
1.1	M,m	S_-	M+1,m	M+1,m	S_+	M,m	M,m	S_z^2, S_zI_z	M,m
1.2	"	S_+	M−1,m	M−1,m	S_-	"	"	"	"
1.3	"	S_-I_+	M+1,m−1	M+1,m−1	S_+I_-	"	"	"	"
1.4	"	S_+I_-	M−1, m+1	M−1,m+1	S_-I_+	"	"	"	"
1.5	"	S_-^2	M+2,m	M+2,m	S_+^2	"	"	"	"
1.6	"	S_+^2	M−2,m	M−2,m	S_-^2	"	"	"	"

where $S_- = \frac{D}{4}(S_zS_- + S_-S_z)\sin 2\theta$ etc.

2nd Term:- $$-\sum_{M'm'}^{M'\neq M} (Mm|\ H'\ |M'm')$$

$$\cdot\sum_{M''m''}^{M''\neq M} \frac{(M'm'|\ H'\ |M''m'')(M''m''|\ H'\ |Mm)}{(E_{M'}-E_M)(E_M-E_{M''})}$$

	$(Mm\|$	0	$\|M'm')$	$(M'm'\|$	0	$\|M''m'')$	$(M''m''\|$	0	$\|Mm)$
2.1	M,m	S_-	$M+1,m$	$M+1,m$	$S_z^2, S_z I_z$	$M+1,m$	$M+1,m$	S_+	Mm
2.2	"	S_-	"	"	S_+^2	$M-1,m$	$M-1,m$	S_-	"
2.3	"	S_-	"	"	S_-	$M+2,m$	$M+2,m$	S_+^2	"
2.4	"	S_+	$M-1,m$	$M-1,m$	$S_z^2, S_z I_z$	$M-1,m$	$M-1,m$	S_-	"
2.5	"	S_+	"	"	S_+	$M-2,m$	$M-2,m$	S_-^2	"
2.6	"	S_+	"	"	S_-^2	$M+1,m$	$M+1,m$	S_+	"
2.7	"	$S_- I_+$	$M+1,m-1$	$M+1,m-1$	$S_z^2, S_z I_z$	$M+1,m-1$	$M+1,m-1$	$S_+ I_-$	"
2.8	"	$S_+ I_-$	$M-1,m+1$	$M-1,m+1$	$S_z^2, S_z I_z$	$M-1,m+1$	$M-1,m+1$	$S_- I_+$	"
2.9	"	S_-^2	$M+2,m$	$M+2,m$	$S_z^2, S_z I_z$	$M+2,m$	$M+2,m$	S_+^2	"
2.10	"	S_-^2	"	"	S_+	$M+1,m$	$M+1,m$	S_+	"
2.11	"	S_+^2	$M-2,m$	$M-2,m$	$S_z^2 S_z I_z$	$M-2,m$	$M-2,m$	S_-^2	"
2.12	"	S_+^2	"	"	S_-	$M-1,m$	$M-1,m$	S_-	"

$$\underline{\text{3rd Term}}:- \sum_{M'm'}^{M'\neq M} (Mm \mid H' \mid M'm') \cdot \sum_{m''}^{m''\neq m} \frac{(M'm' \mid H' \mid Mm'')}{(E_{M'} - E_{M})}$$

$$\cdot \sum_{M''m''}^{M''\neq M} \frac{(Mm'' \mid H' \mid M''m'')(M''m'' \mid H' \mid Mm)}{(E_{M} - E_{M''})(E_{Mm} - E_{Mm''})}$$

$M' \neq M$ $\qquad$ $m'' \neq m$ $\qquad$ $M'' \neq M$

	$(Mm$	0	$\mid M'm')$	$(M'm'$	0	$\mid Mm'')$	$(Mm''$	0	$\mid M''m'')$	$(M''m''$	0	$\mid Mm)$
3.1	M,m	S_+I_-	M−1,m+1	M−1,m+1	S_-	M,m+1	M,m+1	S_+	M−1,m+1	M−1,m+1	S_-I_+	M,m
3.2	"	S_-	M+1,m	M+1,m	S_+I_-	"	"	S_-I_+	M+1,m	M+1,m	S_+	"
3.3	"	S_+I_-	M−1,m+1	M−1,m+1	S_-	"	"	S_-I_+	"	"	S_+	"
3.4	"	S_-	M+1,m	M+1,m	S_+I_-	"	"	S_+	M+1,m+1	M+1,m+1	S_-I_+	"
3.5	"	S_-I_+	M+1,m−1	M+1,m−1	S_+	M,m−1	M,m−1	S_-	M+1,m−1	M+1,m−1	S_+I_-	"
3.6	"	S_+	M−1,m	M−1,m	S_-I_+	"	"	S_+I_-	M−1,m	M−1,m	S_-	"
3.7	"	S_-I_+	M+1,m−1	M+1,m−1	S_+	"	"	S_+I_-	"	"	S_-	"
3.8	"	S_+	M−1,m	M−1,m	S_-I_+	"	"	S_-	M+1,m−1	M+1,m−1	S_+I_-	"

Approximations Used.

We take :- $E_M = g\beta H_o M$

$E_{M,m} = g\beta H_o M + AMm$

Then - $E_M - E_{M+1} = -g\beta H_o = E_{M-1} - E_M$

$E_{M+1} - E_M = +g\beta H_o = E_M - E_{M-1}$

$E_{M,m} - E_{M,m+1} = -AM = E_{M,m-1} - E_{M,m}$

$E_{M,m+1} - E_{M,m} = +AM = E_{M,m} - E_{M,m-1}$

$E_M - E_{M+2} = -2g\beta H_o$ etc.

Operations on Wave Functions.

Denoting $\left\{S(S+1) - M(M \mp 1)\right\}^{\frac{1}{2}}$ by $F_{\mp}(M)$ and $F_{\mp}$

and $\left\{I(I+1) - m(m \mp 1)\right\}^{\frac{1}{2}}$ by $f_{\mp}(m)$ and $f_{\mp}$

we use :-

$S_+ I_- \mid M,m) = F_+ f_- \mid M+1, m-1)$, $S_+ I_- \mid M,m+1) = F_+ f_+ \mid M+1,m)$

$S_- I_+ \mid M,m) = F_- f_+ \mid M-1, m+1)$, $S_- I_+ \mid M+1,m-1) = F_+ f_- \mid M,m)$

$S_+ I_- \mid M-1,m) = F_- f_- \mid M,m-1)$, $S_- I_+ \mid M+1,m) = F_- f_+ \mid M,m)$

$S_+ I_- \mid M-1,m+1) = F_- f_+ \mid M,m)$, $S_- I_+ \mid M,m-1) = F_- f_- \mid M-1,m)$

$(S_z S_{\mp} + S_{\mp} S_z) \mid M \mp 1) = (2M \mp 3) F_{\mp}(M \mp 1) \mid M \mp 2)$

$(S_z S_- + S_- S_z) \mid M) = (2M-1) F_-(M) \mid M-1)$

$$(S_z S_- + S_- S_z)\ |M+1) = (2M+1)\ F_+(M)\ |M)$$

$$(S_z S_+ + S_+ S_z)\ |M) = (2M+1)\ F_+(M)\ |M+1)$$

$$(S_z S_+ + S_+ S_z)\ |M-1) = (2M-1)\ F_-(M)\ |M)$$

$$(S_z S_\pm + S_\pm S_z)\ |M\mp2) = (2M\mp3)\ F_\pm(M\mp2)\ |M\mp1)$$

$$S_+^2\ |M) = F_+(M)\ F_+(M+1)\ |M+2)$$

$$S_+^2\ |M-2) = F_+(M-2)\ F_+(M-1)\ |M)$$

$$S_-^2\ |M) = F_-(M)\ F_-(M-1)\ |M-2)$$

$$S_-^2\ |M+2) = F_-(M+2)\ F_-(M+1)\ |M)$$

$$S_z^2\ |M) = M^2\ |M)$$

$$S_z^2\ |M\pm1) = (M\pm1)^2\ |M\pm1)$$

$$S_z I_z\ |M,m) = Mm\ |Mm)$$

The Expression in $(D\sin 2\theta)^2$

$$(1.1) \longrightarrow -\left[\frac{D\sin 2\theta}{4g\beta H_o}\right]^2 (2M+1)^2 (S(S+1) - M(M+1)).AMm$$

$$(1.2) \longrightarrow -\left[\frac{D\sin 2\theta}{4g\beta H_o}\right]^2 (2M-1)^2 (S(S+1) - M(M-1)).AMm$$

N.B. The sum of these terms is the expression given by Waldner.

$$(2.1) \longrightarrow \left[\frac{D\sin 2\theta}{4g\beta H_o}\right]^2 (2M+1)^2 (S(S+1) - M(M+1)).A_{(M+1)m}$$

$$(2.4) \longrightarrow \left[\frac{D\sin 2\theta}{4g\beta H_o}\right]^2 (2M-1)^2 (S(S+1) - M(M-1)).A_{(M-1)m}$$

N.B. The sum of the above four terms is the expression given by Nicula, Ursa & Nistor, viz. :-

$$(D\sin 2\theta)^2 Am((2M+1)^2(S(S+1) - M(M+1)) - (2M-1)^2(S(S+1) - M(M-1)))$$

$$\sum_{i=1}^{6} (3,i) \longrightarrow -\left[\frac{D\sin 2\theta}{4g\beta H_o}\right]^2 \frac{A}{4M} ((2M-1)^2 F_-^4 (f_+^2 - f_-^2) + (2M+1)^2 F_+^4 (f_+^2 - f_-^2)$$

$$+ (2M+1)(2M-1) F_+^2 F_-^2 (f_-^2 - f_+^2)) \text{ where } F_{\mp} = F_{\mp}(M) \text{ and } f_{\mp} = f_{\mp}(m)$$

$$= 18 \left[\frac{D\sin 2\theta}{4g\beta H_o}\right]^2 \frac{Am}{M} (M^2 - S(\frac{S+1}{3}))^2$$

which is the term given by Bleaney & Rubins.

The Expression in $\sin^4\theta$.

$$(1.5)\longleftrightarrow \; -\left[\frac{D\sin^2\theta}{4}\right]^2 \frac{AMm}{(2g\beta H_o)^2}\,(F_-(M+2)F_-(M+1)\;F_+(M)F_+(M+1))$$

$$(1.6)\longrightarrow \; -\left[\frac{D\sin^2\theta}{4}\right]^2 \frac{AMm}{(2g\beta H_o)^2}\,(F_+(M-2)F_+(M-1)F_-(M)F_-(M-1))$$

$$(2.9)\longrightarrow \; +\left[\frac{D\sin^2\theta}{4}\right]^2 \frac{A(M+2)m}{(2g\beta H_o)^2}\,(F_-(M+2)F_-(M+1)F_+(M)F_+(M+1))$$

$$(2.11)\longrightarrow \; +\left[\frac{D\sin^2\theta}{4}\right]^2 \frac{A(M-2)m}{(2g\beta H_o)^2}\,(F_+(M-2)F_+(M-1)F_-(M)F_-(M-1))$$

The sum of these terms is then:-

$$\left[\frac{D\sin^2\theta}{4g\beta H_o}\right]^2 2AmM(2M^2+1 - 2S(S+1))$$

The expression in $(3\cos^2\theta-1)$

$$(1.3)\longrightarrow \; -\left(\frac{A}{2}\right)^2\frac{D}{2}\left[M^2 - \frac{1}{3}S(S+1)\right](3\cos^2\theta-1)\cdot\frac{1}{(g\beta H_o)^2}\cdot F_+^2 f_-^2$$

$$(1.4)\longrightarrow \; -\left(\frac{A}{2}\right)^2\frac{D}{2}\left[M^2 - \frac{1}{3}S(S+1)\right](3\cos^2\theta-1)\cdot\frac{1}{(g\beta H_o)^2}\cdot F_-^2 f_+^2$$

$$(2.7)\longrightarrow \; +\left(\frac{A}{2}\right)^2\frac{D}{2}\left[(M+1)^2 - \frac{1}{3}S(S+1)\right](3\cos^2\theta-1)\cdot\frac{1}{(g\beta H_o)^2}\cdot F_+^2 f_-^2$$

$$(2.8)\longrightarrow \; +\left(\frac{A}{2}\right)^2\frac{D}{2}\left[(M-1)^2 - \frac{1}{3}S(S+1)\right](3\cos^2\theta-1)\cdot\frac{1}{(g\beta H_o)^2}\cdot F_-^2 f_+^2$$

The sum of these terms is then:-

$$\frac{DA^2}{8(g\beta H_o)^2}(3\cos^2\theta-1)\,(S(S+1)-M(M+1))(I(I+1)-m(m-1))(2M+1)$$
$$-(S(S+1)-M(M-1))(I(I+1)-m(M+1))(2M-1))$$

The Expression in A^3/H^2 .

$$(1.3)\longrightarrow -\left(\frac{A}{2}\right)^2 \frac{AMm}{(g\beta H)^2}\,(S(S+1)-M(M+1))(I(I+1)-m(m-1))$$

$$(1.4)\longrightarrow -\left(\frac{A}{2}\right)^2 \frac{AMm}{(g\beta H)^2}\,(S(S+1)-M(M-1))(I(I+1)-m(m+1))$$

$$(2.7)\longrightarrow +\left(\frac{A}{2}\right)^2 \frac{A(M+1)(m-1)}{(g\beta H)^2}(S(S+1)-M(M+1))(I(I+1)-m(m-1))$$

$$(2.8)\longrightarrow +\left(\frac{A}{2}\right)^2 \frac{A(M-1)(m+1)}{(g\beta H)^2}(S(S+1)-M(M-1))(I(I+1)-m(m+1))$$

$$\Sigma\longrightarrow \frac{A^3}{(2g\beta H)^2}\,(S(S+1)-M(M+1))(I(I+1)-m(m-1))(m-M-1)$$

$$+(S(S+1)-M(M-1))(I(I+1)-m(m+1))(M-m-1))$$

The Expression in $(D^3/H^2)(3\cos^2\theta-1)\sin^2 2\theta$.

$$(2.1)\longrightarrow +\frac{D^3}{32}\,\frac{(3\cos^2\theta-1)\sin^2 2\theta}{(g\beta H)^2}\,(2M+1)^2(S(S+1)-M(M+1))\,(M+1)^2-\tfrac{1}{3}S(S+1)$$

$$(2.4)\longrightarrow +\frac{D^3}{32}\,\frac{(3\cos^2\theta-1)\sin^2 2\theta}{(g\beta H)^2}\,(2M-1)^2(S(S+1)-M(M-1))\,(M-1)^2-\tfrac{1}{3}S(S+1)$$

$$(1.1)\longrightarrow -\frac{D^3}{32}\,\frac{(3\cos^2\theta-1)\sin^2 2\theta}{(g\beta H)^2}\,(2M+1)^2(S(S+1)-M(M+1))\,M^2-\tfrac{1}{3}S(S+1)$$

$$(1.2)\longrightarrow -\frac{D^3}{32}\,\frac{(3\cos^2\theta-1)\sin^2 2\theta}{(g\beta H)^2}\,(2M-1)^2(S(S+1)-M(M-1))\,M^2-\tfrac{1}{3}S(S+1)$$

$$\Sigma\longrightarrow \frac{D^3(3\cos^2\theta-1)\sin^2 2\theta}{32\,(g\beta H)^2}\,(2M+1)^3(S(S+1)-M(M+1))-(2M-1)^3$$

$$(S(S+1)-M(M-1))$$

The Term in $(D^3/_H 2)(3\cos^2\theta-1)\sin^4\theta$.

(1.5) $\rightarrow -\frac{D^3}{32}\frac{(3\cos^2\theta-1)}{(2g\beta H)^2}(\sin^4\theta)$ $F_-(M+2)F_-(M+1)F_+(M)F_+(M+1)$ $M^2-\frac{1}{3}S(S+1)$

(1.6) $\rightarrow$ " $F_+(M-2)F_+(M-1)F_-(M)F_-(M-1)$ $M^2-\frac{1}{3}S(S+1)$

(2.9) $\rightarrow$ " $F_-(M+2)F_-(M+1)F_+(M)F_+(M+1)$ $(M+2)^2-\frac{1}{3}S(S+1)$

(2.11) $\rightarrow$ " $F_+(M+2)F_+(M-1)F_-(M)F_-(M-1)$ $(M-2)^2-\frac{1}{3}S(S+1)$

$\Sigma \rightarrow +\frac{D^3}{32}\frac{(3\cos^2\theta-1)}{(g\beta H)^2}\sin^4\theta$ $(M+1)(S(S+1)-M(M+1))(S(S+1)-(M+1)(M+2))$
$-(M-1)(S(S+1)-M(M-1))(S(S+1)-(M-1)(M-2))$

The Term in $(D^3/_H 2)\sin^2 2\theta\sin^4\theta$.

(2.2) $\rightarrow -\frac{D^3}{64}\frac{\sin^2 2\theta\sin^4\theta}{(g\beta H)^2}$ $F_-(M+1)F_-(M)F_+(M-1)F_+(M)$ $(2M+1)(2M-1)$

(2.3) $\rightarrow +\frac{D^3}{64}\frac{\sin^2 2\theta\sin^4\theta}{2(g\beta H)^2}$ $F_-(M+1)F_-(M+2)F_+(M)F_+(M+1)$ $(2M+1)(2M+3)$

(2.5) $\rightarrow +\frac{D^3}{64}\frac{\sin^2 2\theta\sin^4\theta}{2(g\beta H)^2}$ $F_+(M-1)F_+(M-2)F_-(M)F_-(M-1)$ $(2M-1)(2M-3)$

(2.6) $\rightarrow -\frac{D^3}{64}\frac{\sin^2 2\theta\sin^4\theta}{(g\beta H)^2}$ $F_+(M-1)F_-(M+1)F_-(M)F_+(M)$ $(2M+1)(2M-1)$

(2.10) $\rightarrow +\frac{D^3}{64}\frac{\sin^2 2\theta\sin^4\theta}{2(g\beta H)^2}$ $F_-(M+2)F_-(M+1)F_+(M+1)F_+(M)$ $(2M+1)(2M+3)$

(2.12) $\rightarrow -\frac{D^3}{64}\frac{\sin^2 2\theta\sin^4\theta}{2(g\beta H)^2}$ $F_+(M-2)F_+(M-1)F_-(M-1)F_-(M)$ $(2M-1)(2M-3)$

$\Sigma \rightarrow \frac{D^3\sin^2 2\theta\sin^4\theta}{64\,(g\beta H)^2}$ $(2M+1)(2M+3)(S(S+1)-M(M+1))(S(S+1)-(M+1)(M+2)$
$+(2M-1)(2M-3)(S(S+1)-M(M-1))(S(S+1)-(M-1)(M-2)$
$-2(2M+1)(2M-1)(S(S+1)-M(M+1))(S(S+1)-M(M-1))$

APPENDIX C.

The Operator Equivalent for $Y_4^1 = -\frac{\sqrt{5}}{4}(x + iy)(7z^3 - 3zr^2)$.

$r^2 = x^2 + y^2 + z^2$, and substituting, we obtain:-

$$Y_4^1 = -\frac{\sqrt{5}}{4}(4xz^3 + i4yz^3 - 3xyx^2 - 3xzy^2 - 3i\,yzx^2 - 3i\,yzy^2) \qquad (C.1)$$

We denote S_x, S_y and S_z by X, Y, Z respectively. With this notation the commutation rules are:-

$$XY - YX = iZ \qquad (C.2a)$$

$$YZ - ZY = iX \qquad (C.2b)$$

$$ZX - XZ = iY \qquad (C.2c)$$

The operator equivalents are found by substituting X, Y and Z for x, y, z with a mean value of all permutations of combinations of x, y and z being considered.

Then -

$$4xz^3 \rightarrow XZ^3 + ZXZ^2 + Z^2XZ + Z^3X$$

$$= XZ^3 + Z^3X + (XZ + iY)Z^2 + Z^2(ZX - iY)$$

$$= 2XZ^3 + 2Z^3X + i(YZ^2 - Z^2Y)$$

$$= 2XZ^3 + 2Z^3X + i\,\{(iX + ZY)Z - Z(-iX + YZ)\}$$

$$= 2XZ^3 + 2Z^3X - XZ - ZX \qquad (C.3)$$

Similarly -

$$i4yz^3 \rightarrow i(2YZ^3 + 2Z^3Y - ZY - YZ) \qquad (C.4)$$

$$3xzx^2 \rightarrow \frac{3}{4}(XZX^2 + ZX^3 + X^3Z + X^2ZX)$$

$$= \frac{3}{4}(2XZX^2 + 2X^22X + ZX + XZ) \qquad (C.5)$$

$$3iyzy^2 \rightarrow \frac{3i}{4}(2YZY^2 + 2Y^2ZY + YZ + ZY) \qquad (C.6)$$

$$3xzy^2 \rightarrow \frac{3}{12}(XZY^2 + ZXY^2 + 2Y^2X + XY^2Z + Y^2ZX + Y^2XZ + YZYX + YXYZ + XYZY + ZYXY + YZXY + YXZY)$$

$$= \frac{3}{12}(6XZY^2 + 6Y^2ZX - 5XZ - 5ZX) \qquad (C.7)$$

$$3iyzx^2 \rightarrow \frac{3i}{12}(6YZX^2 + 6X^2ZY - 5YZ - 5ZY) \qquad (C.8)$$

Then -

$$Y_4^1 \rightarrow -\frac{\sqrt{5}}{4}\Big\{2XZ^3 + 2Z^3X - XZ - ZX + i(2YZ^3 + 2Z^3Y - 2Y - YZ) - \frac{3}{4}(2XZX^2 + 2X^2ZX + ZX + XZ) - \frac{3i}{4}(2YZY^2 + 2Y^2ZY + YZ + ZY) - \frac{1}{4}(6XZY^2 + 6Y^2ZX - 5XZ - 5ZX) - \frac{i}{4}(6YZX^2 + 6X^2ZY - 5YZ - 5ZY)\Big\}$$

$$= \frac{\sqrt{5}}{16}\Big\{8(X+iY)Z^3 + 8Z^3(X+iY) - 4Z(X+iY) - 4(X+iY)Z - 6(X+iY)Z(X^2+Y^2) - 6(X^2+Y^2)Z(X+iY) + 2Z(X+iY) + 2(X+iY)Z\Big\}$$

Putting - $S_+ = X + iY$ and $S(S+1) - S_z^2 = X^2 + Y^2$

we obtain -

$$Y_4^1 \rightarrow -\frac{\sqrt{5}}{8}\Big\{S_+(7S_z^3 - 3S(S+1)S_z - S_z) + (7S_z^3 - 3S(S+1)S_z - S_z)S_+\Big\} = T_4^1$$

APPENDIX D.

The Spin Operators T_2^0, T_2^1, T_2^2.

Spherical Harmonics in rectangular coordinates are given by Ballhausen (1962) -

$$Y_2^0 = \sqrt{\frac{5}{4\pi} \cdot \frac{1}{4}} \cdot \frac{3z^2 - r^2}{r^2} = C \sqrt{\frac{1}{4}} (3z^2 - r^2)$$

$$Y_2^1 = -\sqrt{\frac{5}{4\pi} \cdot \frac{3}{2}} \cdot \frac{z(x + iy)}{r^2} = - C \sqrt{\frac{3}{2}} (z(x + iy))$$

$$Y_2^2 = \sqrt{\frac{5}{4\pi} \cdot \frac{3}{8}} \cdot \frac{(x + iy)^2}{r^2} = C \sqrt{\frac{3}{8}} (x + iy)^2$$

where $C = \sqrt{\frac{5}{4\pi}} \cdot \frac{1}{r^2}$

Then -

$$T_2'^0 \longleftrightarrow C \frac{3}{\sqrt{4}} \left(S_z^2 - \frac{1}{3} S(S + 1)\right) = C^1 \left[S_z^2 - \frac{1}{3} S(S + 1)\right]$$

$$T_2'^1 \longleftrightarrow - C \sqrt{\frac{3}{2}} \cdot \frac{1}{2} (S_z S_+ + S_+ S_z) = - \frac{C^1}{\sqrt{6}} (S_z S_+ + S_+ S_z)$$

$$T_2'^2 \longleftrightarrow C \sqrt{\frac{3}{8}} (S_+^2) = \frac{C^1}{\sqrt{6}} (S_+^2)$$

where $C^1 = \frac{3C}{\sqrt{4}}$

Or -

$$T_2^0 = T_2'^0 / C^1 = S_z^2 - \frac{S(S + 1)}{3}$$

$$T_2^1 = T_2'^1 / C^1 = - \frac{1}{\sqrt{6}} (S_z S_+ + S_+ S_z)$$

$$T_2^2 = T_2'^2 / C^1 = \frac{1}{\sqrt{6}} (S_+^2)$$

APPENDIX E

Experimental Details

The microwave spectrometer used to record the majority of spectra shown in this work has been described by Cavenett (1964a, 1964b), and is shown in fig. E1.

The spectrometer utilizes 135 c.p.s. field modulation for chart recorder output, 50 c.p.s. modulation for video display, superheterdyne detection, and a resonance cavity frequency of approximately 9.2 G c.p.s.

The cavity operated in the TE102 mode, and samples could be rotated in the cavity about a direction parallel to the radio-frequency magnetic field. The static field could be rotated in a horizontal plane.

Magnetic field intensities were measured using proton resonance. The frequency at which proton resonance occurred was obtained by zero beating with a signal generator, the zero beat frequency of the generator was then measured with a Hewlett-Packard counter. At the proton resonance frequency ν_p, the following conversion was used:-

$$H = 2.3487 \times 10^{-4} \nu_p$$

Corrections to line positions measured by proton resonance, were made by placing a small quantity of D.P.P.H. on the sample. The field intensity at which resonance occurred for the D.P.P.H. was calculated using:-

FIG. 51

$$H_{D.P.P.H.} = h\nu_0/\beta\, g_{D.P.P.H.}$$

with $h = 6.62518 \times 10^{-27}$ erg-sec

$\beta = 0.92732 \times 10^{-20}$ emu

$g_{D.P.P.H.} = 2.0037$

and the klystron frequency ν_0 was measured with a Hewlett-Packard transfer oscillator, and counter.

For $\gamma = g_N\beta_N/g\beta$, a value of 3.76×10^{-4} was used.

Line positions of forbidden doublets in the adsorbed Mn^{2+} spectrum, were determined by linear extrapolation between allowed transitions, using chart recordings.

Crystals of $MgSO_4.7H_2O$ were grown from aqueous solutions at room temperature. Dehydration did occur if these crystals were left exposed to air. Investigations of the Mn^{2+} spectra from such samples were always carried out on freshly grown crystals.

APPENDIX F

Mn^{2+} Spectra from Other Minerals

Spectra attributable to Mn^{2+} have also been observed in three other naturally occurring silicates by the author, and are currently being investigated. A preliminary report of these spectra is given below.

Wollastonite ($CaSiO_3$)

Three overlapping spectra have been observed from a sample of Wollastonite from New Jersey, U.S.A. Fig. F1 shows an X-band recording with the applied static field at an angle of $17(\pm 2)^o$ to the c axis in a plane normal to the b axis, and at an angle of $60(\pm 2)^o$ to the negative a axis. This direction appears to be the z crystal field axis of one of the ion sites. The overlap of the spectra and the broadness of lines have prevented any determination of parameters. Specimens are being sought which may produce spectra with narrower line widths.

Olivine ($(Mg,Fe^{2+})\ SiO_4$)

Portion of a spectrum obtained from a small polished sample of the gem-stone peridot (olivine) is shown in fig. F2. The exact composition of the sample used has not as yet been determined. Investigations are planned to determine the crystallographic axes, in an attempt to correlate electrostatic crystal field axes with crystal structure.

The minerals of the olivine group show complete diadochy between the atomic pairs Mg and Fe, i.e. between forsterite, Mg_2SiO_4, and

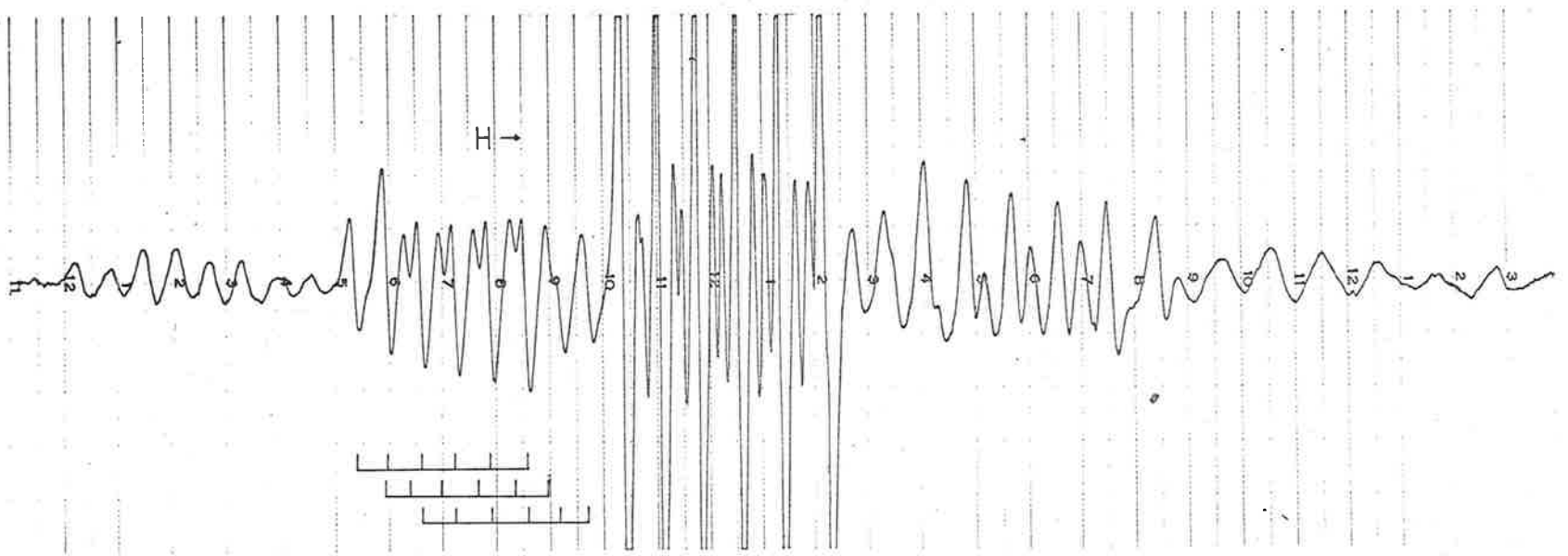

FIG. F1

Mn^{2+} SPECTRUM FROM WOLLASTONITE

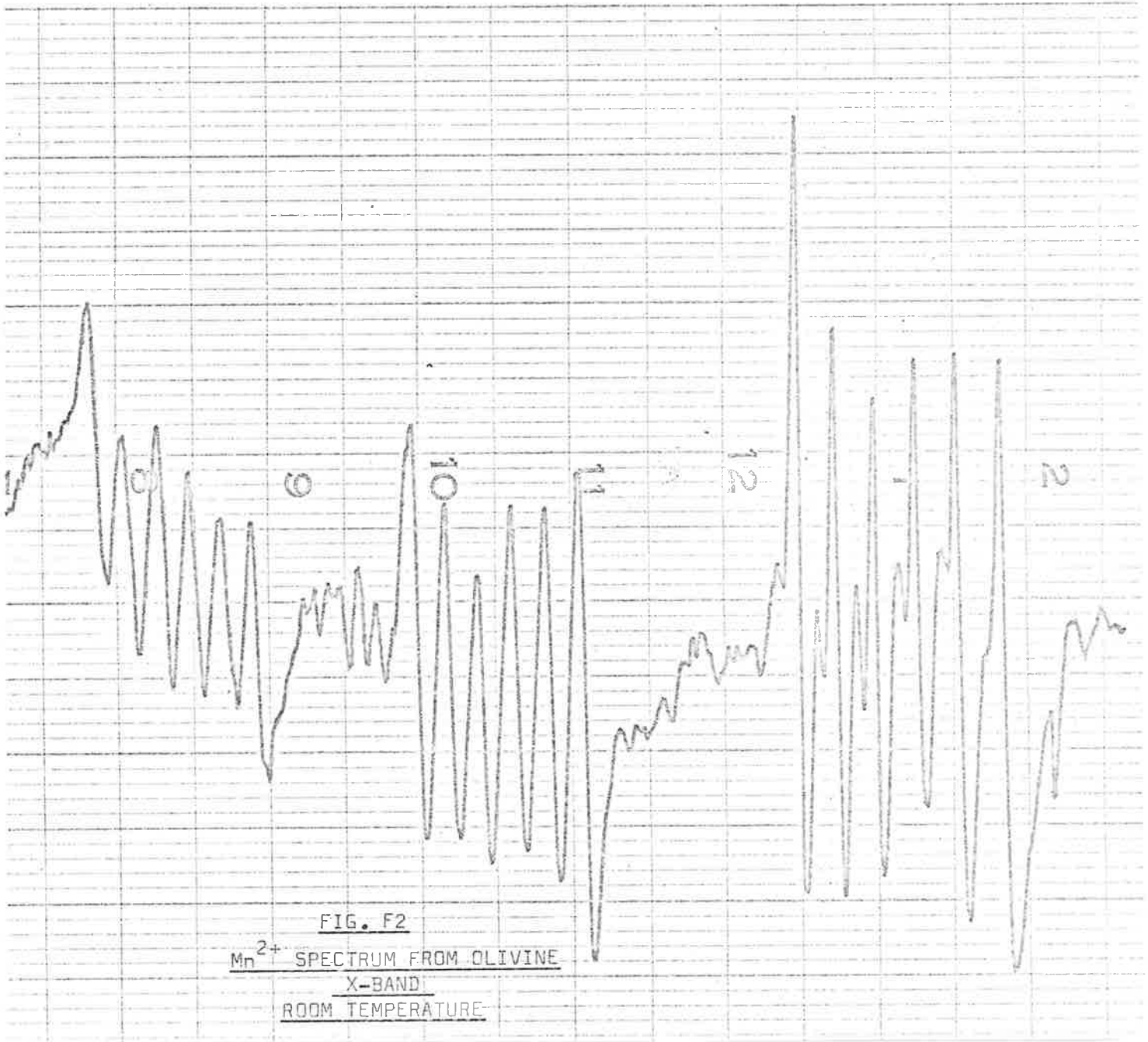

FIG. F2

Mn^{2+} SPECTRUM FROM OLIVINE

X-BAND

ROOM TEMPERATURE

fayalite, Fe_2SiO_4, and other samples of this group are being sought to see what effect, if any, changes in the $Mg:Fe^{2+}$ ratio have on the Mn^{2+} spectrum. It will also be of interest to compare the parameters of the spectrum shown, with those eventually published for Mn^{2+} in monticellite ($CaMgSiO_4$) which is also included in the olivine group. This latter spectrum has been observed independently by Mr. G. Troup of Monash University (personal communication - August, 1968), and by Dr. A. Mannoogian of the University of Ottowa (personal communication - January, 1969, to be published in the Canadian Journal of Physics).

Talc $Mg_3(OH)_2Si_4O_{10}$ (a 5.28, b 9.15, c 10.9 Å, $\beta = 100^{\circ}15'$).

The powder spectrum obtained from a sample of baby powder is shown in fig. F3. The features of this spectrum indicate that the Mn^{2+} ion(s) is in an electrostatic crystal field of axial or rhombic symmetry. Talc usually occurs in massive foliated or fibrous aggregates or in globular stellar groups. Rarer tabular crystals do exist, and the author has recently been able to obtain a sample of this form (locality : Harford County, Maryland, U.S.A.), which has enabled single crystals investigations. The crystals exhibit perfect {001} cleavage, and the a and b axes have been determined from interference figures observed. X-band observations indicate that Mn^{2+} occupies a number of non-equivalent sites in the talc structure. Fig. F4 shows a spectrum recorded with the static field parallel to the c axis. This direction appears to be the Z crystal field axis of one of the ion-sites. Fig. F5 shows another spectrum

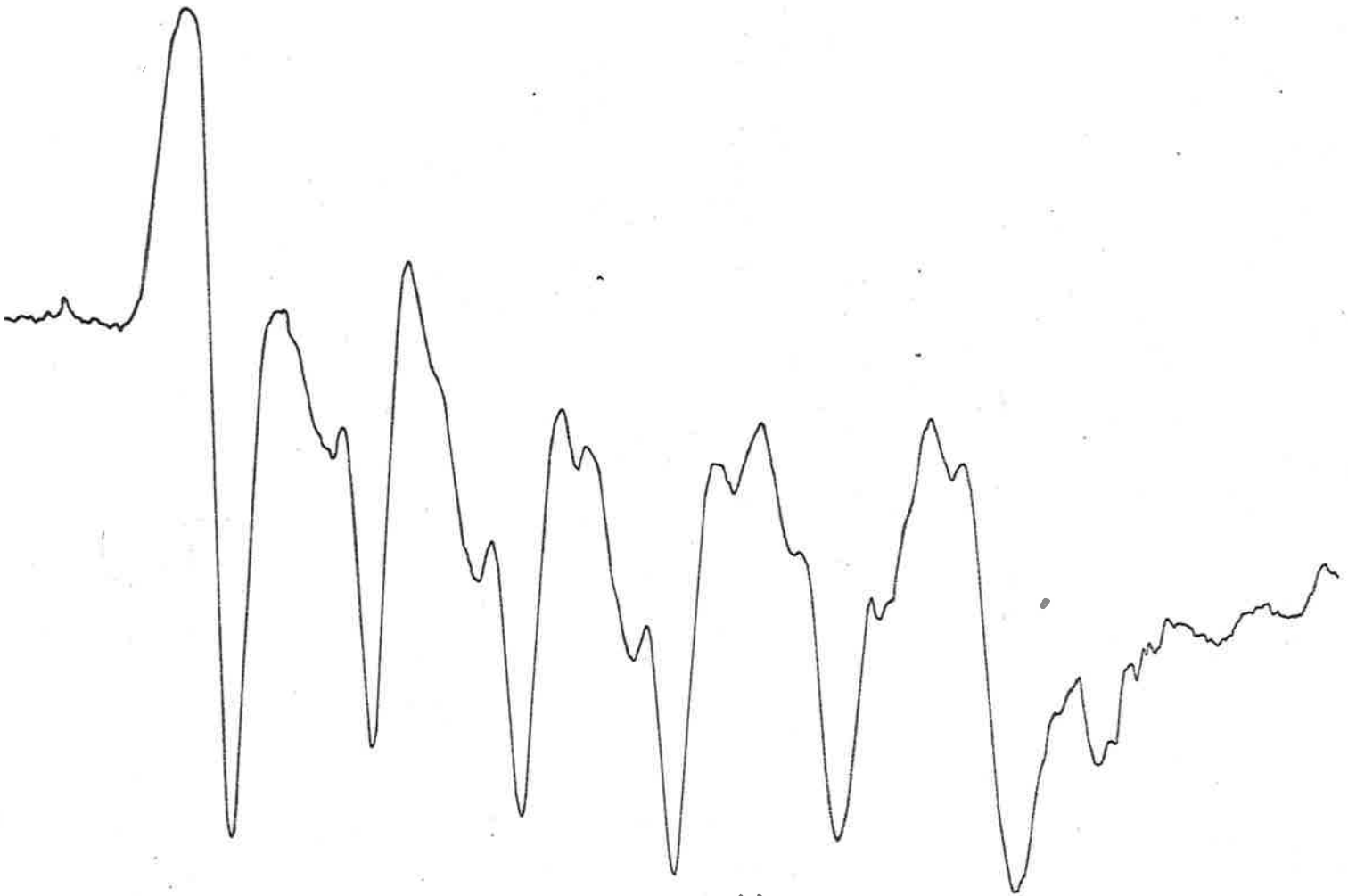

FIG. F3

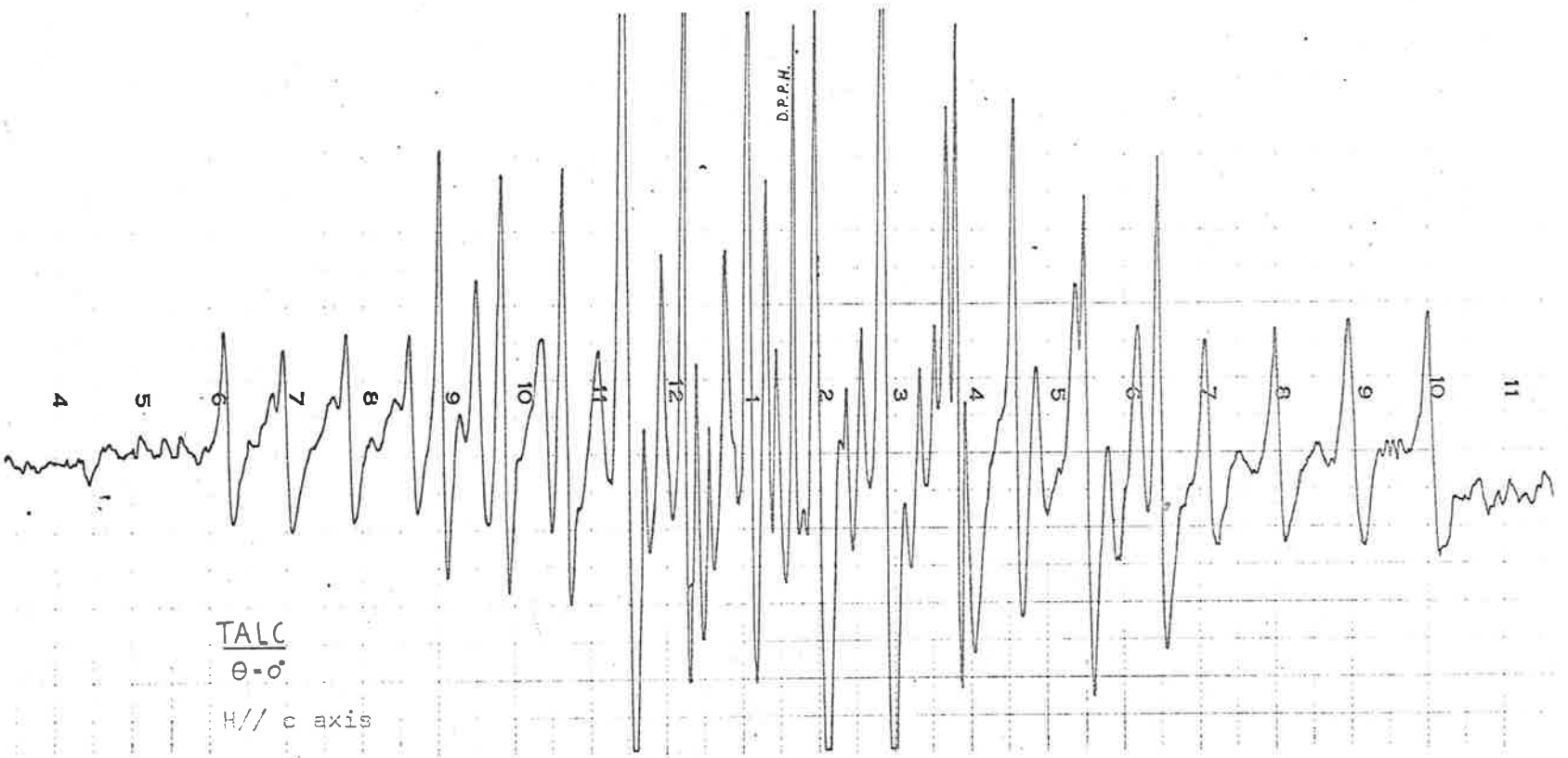

FIG. F4

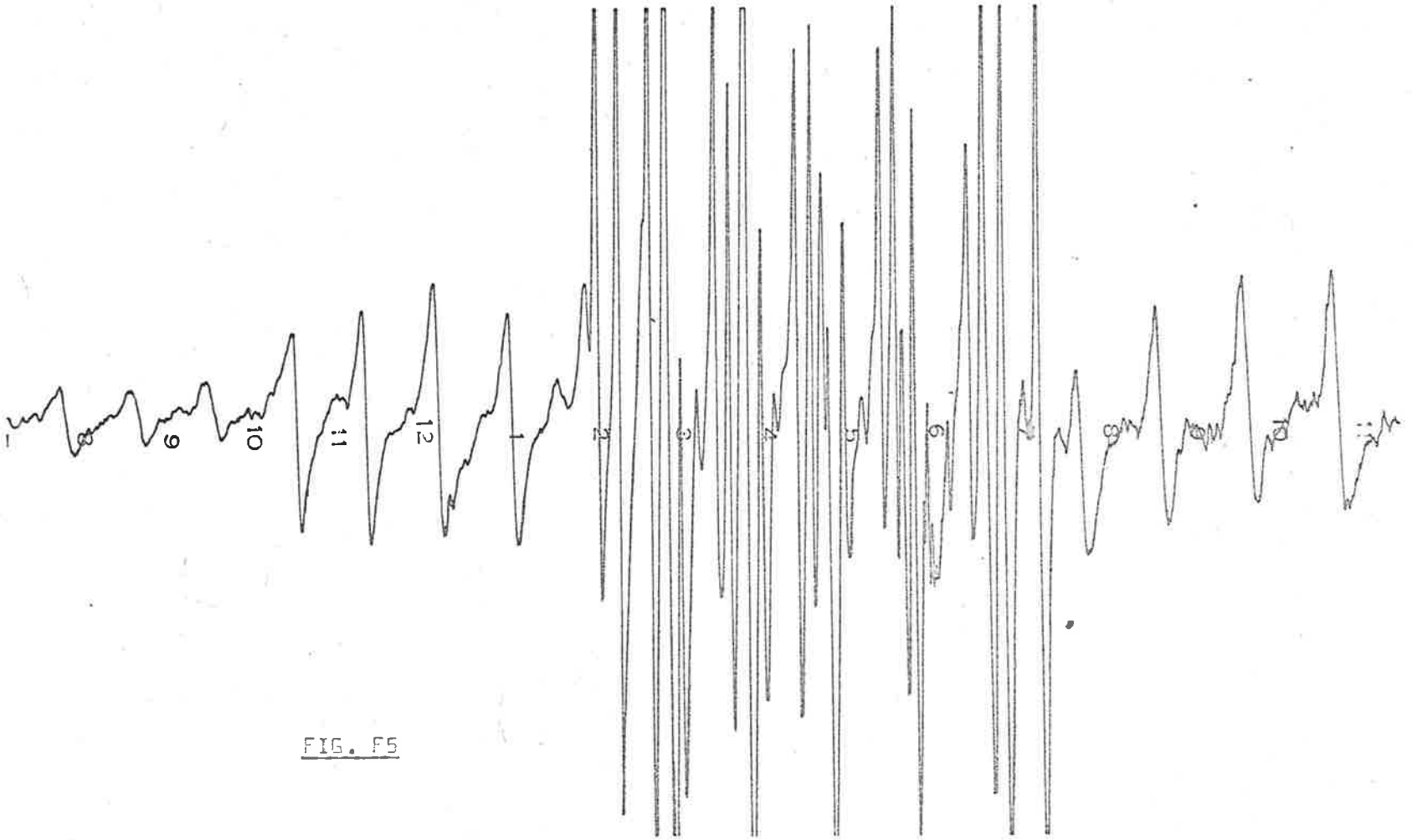

FIG. F5

recorded with the direction of the static field approximately in the (110) plane and at an angle of $\sim 45^{o}$ to the ab plane. This direction appears to be the Z axis of another ion-site or sites.

Insight into the structure of talc was first gained by L. Pauling (Proc. Nat. Acad. Sc. U.S.A. 16 (1930) 123). Lattice parameters have been determined by J. W. Gruner (Z. Krist 88 (1934) 412) and verified by S. B. Hendricks (Z. Krist 99 (1938) 264). The idealized talc structure is shown in fig. F6.

Talc has a layered structure in which a sheet of octahedrally coordinated Mg ions is sandwiched between two sheets of linked SiO_4 tetrahedra. The two possible ways of stacking SiO_4-OH sheets, as discussed by Hendricks, are shown in fig. F7, with coordinating octahedral groups about Mg sites outlined. If the ions surrounding the site of a paramagnetic ion are octahedrally coordinated, the Z axis of the electrostatic crystal field at the paramagnetic ion site might be expected to be approximately parallel to the direction between two of the surrounding ions. The direction between ions marked 1' and 1" in fig. F7 (b) lies approximately in the (1,1,0) plane and is $\sim 45^{o}$ to the ab plane, and it could be expected that the spectrum shown in fig. F5 is due to Mn^{2+} substituting for magnesium at such a site. The octahedral groups of ions surrounding the Mg sites have the same orientation in space for a given stacking of SiO_4-OH sheets, and it does not seem feasible (to this author) that the Mn^{2+} spectrum shown in fig. F4, for which the electrostatic crystal field Z axis is approximately parallel to the c axis, arises

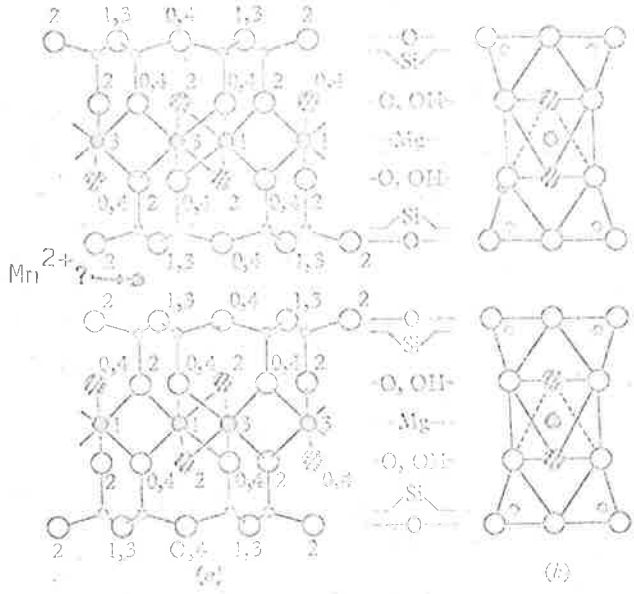

FIG. F6

(a) Plan of the idealized structure of talc, $Mg_3(OH)_2Si_4O_{10}$, projected on a plane perpendicular to the x axis.

(b) Schematic representation of the same structure, showing the co-ordinating octahedra about the magnesium atoms.

The numbers indicate the heights of the various atoms above the plane of projection.

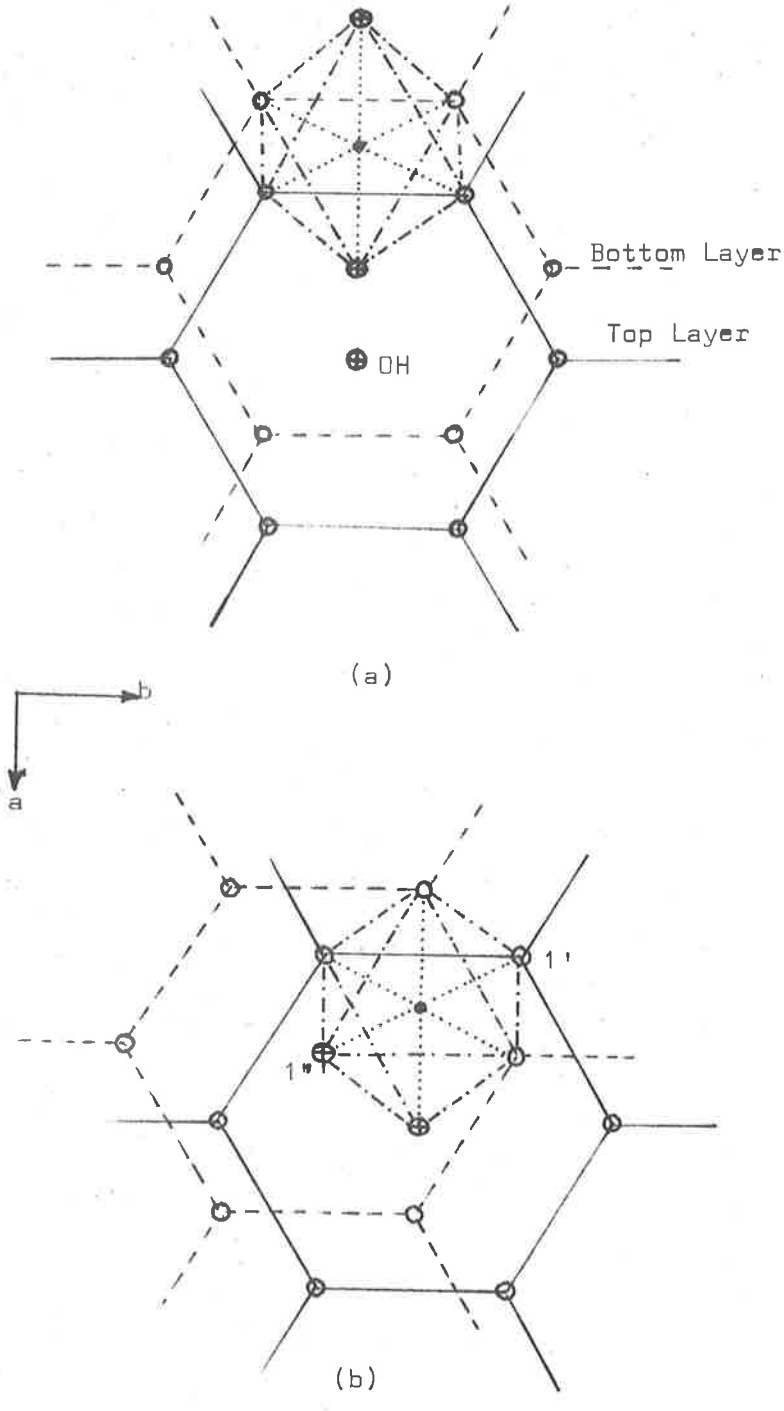

FIG. F7

from Mn^{2+} substituting in such sites as shown in fig. F7. Such a direction for the crystal field Z axis could be expected however if Mn^{2+} was at positions between layers (fig. F6), with surrounding ions at the corners of a triangular prism.

Detailed investigations of the microwave spectra from this mineral are continuing.

BIBLIOGRAPHY AND REFERENCES.

ALGER, R.S. (1968) "Electron Paramagnetic Resonance". (Wiley-Interscience)

AL'TSHULER, S.A. and KOZYREV, B.M. (1964) "Electron Paramagnetic Resonance". (Academic Press)

AYSCOUGH, P.B. (1967) "Electron Spin Resonance in Chemistry". (Methuen)

APPLE, E.F. and ISHLER, W.E. (1962) "Luminescence of Organic and Inorganic Materials". (Wiley)

BALLHAUSEN, C.J. (1962) "Introduction to Ligand Field Theory". (McGraw-Hill)

BERSOHN, M. and BAIRD, J.C. (1966) "An Introduction to E.P.R.". (Benjamin)

BIR, G.L. (1964) Soviet Physics - Solid State 5(8), 1628.

BIR, G.L., BUTIKOV, E.I. and SOCHAVA, L.S. (1965) Soviet Physics - Solid State 6(8), 1966.

BIR, G.L. and SOCHAVA, L.S. (1964) Soviet Physics - Solid State 5(12), 2637.

BLEANEY, B. and INGRAM, D.J.E. (1951) Proc. Roy Soc. A205, 336.

BLEANEY, B. and RUBINS, R.S. (1961) Proc. Phys. Soc. (London) 77, 103.

BROVETTO, P., CINI, G. and FERRONI, S. (1953) Nuovo Cimento 10(9) 1325.

BUERGER, M.J. (1956) Zeit. Krist, 108, 248.

BUERGER, M.J. and PREWITT, C.T. (1961) Proc. Nat. Acad. Sc. 47, 1884.

BURLEY, S.P. (1964) Australian J. Phys. 17, 537.

BUTLER, K. and JEROME, C.W. (1950) J. Electrochem Soc. 97, 265.

CASTNER, T.G. (1960) J. Chem. Phys. 32, 668.

CAVENETT, B.C. (1964A) Proc. Phys. Soc. (London) 84, 1.

CAVENETT, B.C. (1964B) Ph.D. Thesis, Adelaide University.

CONDON, E.U. and SHORTLEY, G.H. (1951) "The Theory of Atomic Spectra". (Cambridge Uni. Press)

DANA, E.S. (1932) "A Textbook of Mineralogy". 4th Ed. (Wiley)

DE WIJN, H.W. and VAN BALDEREN, R.F. (1967) J. Chem. Phys. 46, 1381.

DUBOS, R.J. (1949) "The Bacterial Cell". (Harvard University Press)

DORAIN, P. (1958) Phys. Rev. 112, 1058.

FABER, R.J. and ROGERS, M.T. (1959) J. Amer. Chem. Soc. 81, 1849.

FOLEN, V.J. (1962) Phys. Rev. 125, 1581.

FREEMAN, A.G. and TAYLOR, H.J.W. (1960) Silikat. Tech. 11, 490.

FRIEDMAN, E. and LOW, W. (1960) Phys. Rev. 120, 408.

GEL'FAND, I.M., MINLOS, R.A. and SHAPIRO, Z.Ya. (1963) "Representations of the Rotation and Lorentz Groups and Their Applications". (Pergamon Press, English Translation)

GORTER, C.J. (1932) Phys. Rev. 42, 437.

HAMERMESH, M. (1962) "Group Theory". (Addison-Wesley)

HAYASHI, I. and ONO, K. (1953) J. Phys. Soc. Japan 8, 270.

HECHT, H.G. (1967) "Magnetic Resonance Spectroscopy". (Wiley)

HEDGECOCK, N.E. and CHAKRAVARTTY, S.C. (1966) Canadian J. Phys. 44, 2749.

HENDRICKS, St. B. (1938) Zeit. Krist. 99, 264.

HURD, F.K., SACHS, M. and HERSHBERGER, W.D. (1954) Phys. Rev. 93, 373.

INGRAM, D.J.E. (1967) "Spectroscopy at Radio and Microwave Frequencies". (2nd Edition) (Butterworths)

JOHNSON, P.D. (1962) "Luminescence of Organic and Inorganic Materials". (Wiley)

KASAI, P.H. (1962) J. Phys. Chem. 66, 674.

KIKUCHI, C. and MATARRESE, L.M. (1960) J. Chem. Phys. 33(2), 601.

LOW, W. (1957) Phys. Rev. 105, 793.

LOW, W. (1960) "Paramagnetic Resonance in Solids", in Solid State Physics - Suppl. 2.

LYONS, D.H. and KEDZIE, R.W. (1966) Phys. Rev. 145, 148.

MANOOGIAN, A. (1968a) Canadian J. Phys., 46, 129.

MANOOGIAN, A. (1968b) " " " 46, 1029.

MARRIAGE, A.J. (1965) Aust. J. Chem. 18, 463.

MATARESSE, L.M. (1961) J. Chem. Phys. 34, 336.

MIERS, H.A. "Mineralogy". (Macmillan Press) (1929)

MORIGAKI, K., FUJIMOTO, M. and ITOH, J. (1958) Journal Phys. Soc. Japan 13, 1174.

NARITA, K. (1961) J. Phys. Soc. Japan 16, 99.

NICULA, A., URSU, I. and NISTOR, S. (1965) Rev. Roumaine. Phys. 10(2), 229.

ODENHAL, M. (1963) Czech. J. Phys. B13, 566.

OHKUBO (1963) J. Phys. Soc. Japan 18, 916.

OUWELTJES, J.L. (1951) Philips Tech. Rev., 13, 346.

PEACOR, D.R. and PREWITT, C.T. (1963) Amer. Min. 48, 588.

PIPER, W.W., KRAVITZ, L.C. and SWANK, R.K. (1965) Phys. Rev. 138, A1802.

SCHNEIDER, J. and SIRCAR, S.R. (1962) 17a, 651.

SCHULZ - DUBOIS (1959), Bell System Tech. J., 38, 271.

ST. NARAY-SZABO (1930), Zeit. Krist 75, 387.

STEVENS, K.W.H. (1952) Proc. Phys. Soc. A65, 209.

TAKEDA, T. (1967) J. Phys. Soc. Japan 23, 1314.

TITLE, R.S. (1963) Phys. Rev. 131, 623.

URSU, I., LUPEI, V. and LUPEI, A. (1966) Rev. Roum. Phys. 11(9), 875.

URSU, I. and NICULA, A. (1964) Rev. Roumaine Phys. 9(4), 343.

VINOKUROV, V.M., ZARIPOV, M.M. and STEPANOV, V.G. (1961) Soviet Phys.- Crystallography 6, 83.

VINOKUROV, V.M., ZARIPOV, M.M. and STEPANOV, V.G. (1964a) Soviet Phys. - Solid State 6, 866.

VINOKUROV, V.M., ZARIPOV, M.M. and STEPANOV, V.G. (1964b) Ibid, 6, 870.

WALDNER, F. (1962) Helv. Phys. Acta 35, 756.

WIJN, H.W. de and BALDEREN, R.F. Van (1967) J. Chem. Phys. 46, 1381.

WITTELS, M. (1952) Amer. Min. 37, 28.

WOLGA, G.J. and TSENG, R. (1964) Phys. Rev. 113, A1563.

ZAITOV, M.M. (1967) Fiz. Tverdoga Tela (U.S.S.R.) 9(2), 453. English Translation : Soviet Phys. - Solid State 9(2), 346.